

9

# Phosphorus Cycling in the Gulf of Maine: A Multi-Tracer Approach

By

Claudia R. Benitez-Nelson

B. S., University of Washington  
(1992)

SUBMITTED IN PARTIAL FULFILLMENT OF THE REQUIREMENTS FOR THE  
DEGREE OF

DOCTOR OF PHILOSOPHY

at the

MASSACHUSETTS INSTITUTE OF TECHNOLOGY

and the

WOODS HOLE OCEANOGRAPHIC INSTITUTION

September 1998

© Claudia Benitez-Nelson 1998  
All rights reserved.

The author hereby grants to MIT and WHOI permission to reproduce paper and electronic copies of this thesis in whole or in part, and to distribute them publicly.

Signature of Author \_\_\_\_\_  
Joint Program in Oceanography  
Massachusetts Institute of Technology/Woods Hole Oceanographic Institution

Certified by \_\_\_\_\_  
Ken O. Buesseler  
Thesis Supervisor

Accepted by \_\_\_\_\_  
Edward A. Boyle  
Chair, Joint Committee for Chemical Oceanography  
Massachusetts Institute of Technology/Woods Hole Oceanographic Institution

WITHDRAWN  
FROM 7 1998  
MIT LIBRARIES  
LIBRARIES

Ludgren  
\_\_\_\_\_



# Phosphorus Cycling in the Gulf of Maine: A Multi-Tracer Approach

by

Claudia R. Benitez-Nelson

Submitted in September 1998 in partial fulfillment of the requirements for the degree of Doctor of Philosophy in Oceanography at the Massachusetts Institute of Technology and the Woods Hole Oceanographic Institution

## ABSTRACT

Knowledge of temporal and spatial nutrient turnover and export rates is of great importance for a variety of investigations, ranging from nutrient limitation to contamination uptake and removal. However, there are few methods which allow for the *in situ* elucidation of these processes. In this thesis research, *in situ* phosphorus turnover rates and upper ocean export were determined within the southwestern Gulf of Maine using the naturally occurring radionuclides phosphorus-32 ( $t_{1/2} = 14.3$  d), phosphorus-33 ( $t_{1/2} = 25.3$  d), thorium-234 ( $t_{1/2} = 24.1$ ) and beryllium-7 ( $t_{1/2} = 53.3$  d).

New techniques were developed for the extraction, purification and measurement of  $^{32}\text{P}$  and  $^{33}\text{P}$  in rainwater and in inorganic, organic and particulate pools in seawater. In order to constrain the input ratio of  $^{33}\text{P}/^{32}\text{P}$ , rain samples were collected and measured continuously for  $^{32}\text{P}$  and  $^{33}\text{P}$ , as well as  $^7\text{Be}$  and  $^{210}\text{Pb}$ , from March 1996 to March 1998 at Woods Hole, MA, and from March 1997 to October 1997 at Portsmouth, NH. The average  $^{33}\text{P}/^{32}\text{P}$  ratio was  $0.88 \pm 0.20$ .  $^{32}\text{P}$ ,  $^{33}\text{P}$ ,  $^7\text{Be}$  and  $^{210}\text{Pb}$  were further used to determine aerosol residence times and as possible tracers of stratospheric/tropospheric exchange, during severe storm events.

Four cruises were conducted in Wilkinson Basin, in the Gulf of Maine, during the spring and summer of 1997.  $^{234}\text{Th}$  was used to estimate advection and diffusion using 1D steady state and multi-dimensional non-steady state models. Export ratios (export/primary production) were found to range between 0.11 and 0.37. Vertical eddy diffusivity found using  $^7\text{Be}$  varied from 0.5 to 1.5  $\text{cm}^2 \text{sec}^{-1}$ .

Significant changes in phosphorus turnover rates within the reservoirs which contained  $^{32}\text{P}$  and  $^{33}\text{P}$  activity were found between the spring and summer months. In late summer, bacterial activity was substantial, significantly affecting the residence times of dissolved inorganic and organic phosphorus pools. Our results clearly show that  $^{32}\text{P}$  and  $^{33}\text{P}$  can provide much needed information regarding the biogeochemical cycling of P in marine systems and can be of use in the development of ecosystem models which seek to address mechanisms which affect primary production in the ocean.

Thesis Supervisor: Kenneth O. Buesseler

Title: Associate Scientist, Department of Maine Chemistry and Geochemistry  
Woods Hole Oceanographic Institution



## Acknowledgements

This thesis could never have been completed without the guidance of a very special group: Café Thorium. My thesis advisor, Ken Buesseler, never hesitated to quickly respond to my multitude of emails, faxes, and phone calls. His insight, integrity and zen-like personality have greatly shaped my perspective as a young scientist. John Andrews and Lary Ball, the wonder-twins of our lab, assisted me daily with assorted research questions ranging from chemistry to electronics. They have taught me how to make even the most monotonous of tasks enjoyable. Glenn Crossin, where would I be without your help in cruise preparation and post cruise sample chemistry. Who else would have accompanied me on not one but four cruises in the Gulf of Maine. I also would like to thank Minhan Dai for showing me how to have quiet confidence in the face of adversity, Carly Tarr for always being there when I needed some last minute help in the lab, and Becky Belastock for never minding the clutter I always seemed to leave on her desk. May the coffee gods grace you all with caffeine forever.

I would also very much like to thank my secondary thesis advisor, Dave Glover, for always being there to give me his perspective and advice on everything from research to life in general. Special thanks are also due to Bill Jenkins and my other thesis committee members, Mike Bacon, Dave Caron, John Edmond, and Kathleen Ruttenburg for their contributions and insight. I would like to express my gratitude to Carolyn Jordan, a fellow graduate student, who went beyond the call of duty in collecting rain samples for me at Portsmouth, NH and the crew of *R/V Cape Hatteras*, who taught a fledgling Chief Scientist how to achieve a successful research cruise.

I also would like to acknowledge all those people who made my stay in Falmouth and at WHOI enjoyable. The soccer at lunch and in the evenings, the gab sessions in the halls of Clark and Fye, and those nighttime gatherings kept my spirits high.

This thesis is dedicated to my family, who supported me through all of the good and bad and taught me to never lose perspective on the important things in life. Most especially, it is dedicated to my husband Bryan, who brought me dinner when I worked

late, who stayed with me through the night when I had to do chemistry, and who never hesitated to join me in the lab on the weekends.

Funding for this work was provided by the Office of Naval Research Fellowship Program, The Environmental Protection Agency Science to Achieve Results (STAR) Fellowship Program, the National Science Foundation (Grant no. OCE-9633240) and the Woods Hole Oceanographic Institution (unrestricted funds).

## Table of Contents

	<u>Page</u>
Abstract .....	3
Acknowledgements .....	5
List of Tables .....	10
List of Figures .....	11
Chapter 1. Introduction .....	15
Chapter 2. Sensitive techniques for the measurement of $^{32}\text{P}$ and $^{33}\text{P}$ in rain and seawater	
Abstract .....	25
Introduction .....	26
Sample Collection .....	28
Sample Processing .....	32
Instrumentation .....	39
Data Analysis, Sources of Error and Reproducibility .....	47
Results .....	49
Conclusions .....	52
Acknowledgements .....	53
Chapter 3. $^{32}\text{P}$ , $^{33}\text{P}$ , $^7\text{Be}$ and $^{210}\text{Pb}$ as tracers of aerosol residence times and stratosphere/troposphere exchange.	
Abstract .....	55
Introduction .....	56
Materials and Methods .....	58
Results and Discussion	
Radionuclide activities and flux measurements.....	63
Relationship between specific activities and fluxes with rainfall ....	68

Tropospheric aerosol residence times .....	70
Tropospheric irradiation periods of an airmass .....	75
Radionuclide ratios as an indicator of airmass source .....	79
Conclusions .....	89
Acknowledgements .....	91

**Chapter 4. In situ temporal variability of inorganic and organic phosphorus cycling  
in the coastal ocean**

Abstract .....	105
Introduction .....	106
Study Area .....	106
Methods .....	109
Results .....	112
Discussion .....	116
Conclusions .....	135

**Chapter 5. Carbon export, eddy diffusivity and horizontal transport in the  
southwestern Gulf of Maine.**

Abstract .....	141
Introduction .....	142
Methods .....	145
Results .....	148
Discussion	
<sup>234</sup> Th derived particle export .....	155
Steady state and non-steady state 1D <sup>234</sup> Th flux model .....	156
Non-steady state 3D <sup>234</sup> Th flux model .....	159
Particulate organic carbon export derived from <sup>234</sup> Th .....	166
Vertical eddy diffusivity (K <sub>z</sub> ) .....	171



Conclusions .....	175
Acknowledgements .....	176
<b>Chapter 6. Application of <math>^{32}\text{P}</math> and <math>^{33}\text{P}</math> in numerical modelling studies</b>	
Abstract .....	191
Introduction .....	192
The Data .....	194
The Models	
Inverse models .....	197
Prognostic model .....	199
Results and Discussion	
Inverse models .....	203
Prognostic model .....	208
Future Modelling Efforts .....	219
Conclusions .....	220
<b>Chapter 7. Summary .....</b>	<b>229</b>
Future Work .....	233
<b>Biographical Note .....</b>	<b>238</b>

## List of Tables

	<u>Page</u>
<b>Chapter 2</b>	
Table 2.1 $^{32}\text{P}$ and $^{33}\text{P}$ activities in individual rain events at Woods Hole .....	50
Table 2.2 $^{32}\text{P}$ and $^{33}\text{P}$ activities in selected seawater samples .....	51
<b>Chapter 3</b>	
Table 3.1 $^{32}\text{P}$ , $^{33}\text{P}$ , $^7\text{Be}$ and $^{210}\text{Pb}$ activities in individual rain events collected at Woods Hole .....	95
Table 3.2 $^{32}\text{P}$ , $^{33}\text{P}$ , $^7\text{Be}$ and $^{210}\text{Pb}$ activities in individual rain events collected at Portsmouth, NH .....	102
Table 3.3 $^{32}\text{P}$ , $^{33}\text{P}$ , $^7\text{Be}$ and $^{210}\text{Pb}$ activities measured sequentially during single rainfall events at Woods Hole .....	103
<b>Chapter 4</b>	
Table 4.1 Ancillary measurements taken at Wilkinson Basin .....	111
Table 4.2 $^{32}\text{P}$ and $^{33}\text{P}$ activities in dissolved and particulate seawater samples .....	113
Table 4.3 Particulate organic carbon fluxes derived from $^{32}\text{P}$ , $^{33}\text{P}$ , and $^{234}\text{Th}$ radionuclide inventories .....	132
<b>Chapter 5</b>	
Table 5.1 Radionuclide data collected in the southwestern Gulf of Maine ..	182
Table 5.2 Steady state and non-steady state surface model results .....	186
Table 5.3 Depth integrated steady state and non-steady state model results .....	188
Table 5.4 Steady state, non-steady state, and advection/diffusion model results .....	189
Table 5.5 Comparison of ThE ratios found in the Gulf of Maine with those of other regimes .....	190

**Chapter 6**

<b>Table 6.1 Radioactive and stable phosphorus data from surface waters of Wilkinson Basin in the Gulf of Maine .....</b>	<b>195</b>
<b>Table 6.2 Biological parameter values .....</b>	<b>203</b>
<b>Table 6.3 Stable phosphorus residence times derived from the inversion and two-box models of the <sup>32</sup>P and <sup>33</sup>P data .....</b>	<b>204</b>

## List of Figures

	<u>Page</u>
<b>Chapter 1</b>	
Figure 1.1 Biogeochemical cycling of $^{32}\text{P}$ , $^{33}\text{P}$ , $^7\text{Be}$ and $^{210}\text{Pb}$ .....	18
<b>Chapter 2</b>	
Figure 2.1 Collection efficiency for DIP and DOP using a) Iron coated polypropylene and b) Iron coated acrilan .....	31
Figure 2.2 Chemical purification scheme .....	33
Figure 2.3 Decay curve analysis for $^{32}\text{P}$ in a rain sample collected April 2, 1996 at WHOI; Evidence of sample contamination .....	37
Figure 2.4 Quench curves for a) $^{32}\text{P}$ and b) $^{33}\text{P}$ , over the last 6 months .....	42
Figure 2.5 Liquid scinitillation spectra of a rain sample collected at WHOI ..	45
Figure 2.6 Activity of $^{32}\text{P}$ and $^{33}\text{P}$ for two rain samples collected 5/9/97 and 5/10/97 and split into three unequal portions: a) $^{32}\text{P}$ , b) $^{33}\text{P}$ .....	48
<b>Chapter 3</b>	
Figure 3.1 Map of rain collection stations .....	59
Figure 3.2 Daily $^{33}\text{P}$ flux measured at Woods Hole and Portsmouth .....	64
Figure 3.3 Daily $^7\text{Be}$ flux measured at Woods Hole and Portsmouth .....	66
Figure 3.4 Daily $^{210}\text{Pb}$ depositional flux versus the time period between precipitation events .....	67
Figure 3.5 Specific activity of $^{33}\text{P}$ , $^7\text{Be}$ , and $^{210}\text{Pb}$ versus rainfall .....	69
Figure 3.6 Specific activity of $^{32}\text{P}$ , $^{33}\text{P}$ , $^7\text{Be}$ and $^{210}\text{Pb}$ in sequential samples taken during an 8-12 hour continuous rainfall period .....	71
Figure 3.7 Daily flux of $^{33}\text{P}$ , $^7\text{Be}$ , and $^{210}\text{Pb}$ versus rainfall .....	72
Figure 3.8 Activity ratio of $^{33}\text{P}/^{32}\text{P}$ in precipitation samples measured at Woods Hole and at Portsmouth .....	77
Figure 3.9 Activity ratio of $^7\text{Be}/^{32}\text{P}$ in precipitation samples measured at Woods Hole and at Portsmouth .....	78

Figure 3.10 Schematic of possible mechanisms which can increase the theoretical equilibrium ratio, $R_e$ , greater than 1.15 for the ratio of $^{33}\text{P}/^{32}\text{P}$	82
Figure 3.11 Model results of instantaneously mixing 10% higher activity air with 90% lower activity air, 25% with 75%, and 50% with 50%	84
<b>Chapter 4</b>	
Figure 4.1 Map of rain collection and Wilkinson Basin stations	108
Figure 4.2 Schematic of a) continuous and b) non-continuous uptake models	118
Figure 4.3 Phosphorus ages and radionuclide derived carbon export	121
Figure 4.4 Ratio of $^{33}\text{P}/^{32}\text{P}$ in dissolved and in small and large particulate pools for March, 1997	123
Figure 4.5 Ratio of $^{33}\text{P}/^{32}\text{P}$ in dissolved and in small and large particulate pools for April, 1997	124
Figure 4.6 Ratio of $^{33}\text{P}/^{32}\text{P}$ in dissolved and in small and large particulate pools for July, 1997	125
Figure 4.7 Ratio of $^{33}\text{P}/^{32}\text{P}$ in dissolved and in small and large particulate pools for August, 1997	126
Figure 4.8 Relative distribution of $^{32}\text{P}$ activity found among the measured size classes at that water depth	127
<b>Chapter 5</b>	
Figure 5.1 Station locations for all four cruises conducted in 1997	144
Figure 5.2a-d Contour plots of total $^{234}\text{Th}$ surface activities in d.p.m. $\text{L}^{-1}$ from all four cruises	149
Figure 5.3a-d Contour plots of total $^7\text{Be}$ surface activities in d.p.m. $\text{m}^{-3}$ from all four cruises	150
Figure 5.4 Depth profiles of salinity, $\text{NO}_3 + \text{NO}_2$ , particulate organic carbon and chl $a$	151
Figure 5.5 Particulate, dissolved, and total $^{234}\text{Th}$ activities with depth	153
Figure 5.6 Particulate, dissolved, and total $^7\text{Be}$ activities with depth	154

Figure 5.7a-d Contour plots of steady state determinations of the upper 10 m particulate $^{234}\text{Th}$ flux in d.p.m. $\text{m}^{-2} \text{day}^{-1}$ .....	157
Figure 5.8 Schematic of box model .....	163
Figure 5.9a-c $^{234}\text{Th}$ model flux results for the April, July and August cruises	164
<b>Chapter 6</b>	
Figure 6.1 Schematic of inverse box model .....	198
Figure 6.2 Schematic of prognostic model .....	199
Figure 6.3 Doney's model for stable phosphorus using original parameters	209
Figure 6.4 Doney's model for $^{32}\text{P}$ using original parameters .....	210
Figure 6.5 Doney's model for $^{33}\text{P}$ using original parameters .....	211
Figure 6.6 Doney's model for stable phosphorus using 'tuned' parameters derived from $^{32}\text{P}$ and $^{33}\text{P}$ .....	215
Figure 6.7 Doney's model for $^{32}\text{P}$ using 'tuned' parameters derived from $^{32}\text{P}$ and $^{33}\text{P}$ .....	216
Figure 6.8 Doney's model for $^{33}\text{P}$ using 'tuned' parameters derived from $^{32}\text{P}$ and $^{33}\text{P}$ .....	217

## Chapter 1

### Introduction

The purpose of this thesis work was to further current understanding of phosphorus uptake, remineralization and export within the southwestern Gulf of Maine using naturally occurring short-lived radionuclides. Nutrients such as phosphorus can play an essential role in the temporal and spatial variability of primary production. Numerous studies have shown that variations in primary productivity are closely mirrored by particulate matter fluxes (Deuser and Ross, 1980; Martin *et al.*, 1987; Lohrenz *et al.*, 1992). Further research has demonstrated that one of the major removal pathways of organic carbon, nutrients and many associated minor and trace elements is biologically controlled, occurring with sinking plankton fecal matter, marine snow, and organic particle aggregation (e.g. Fowler and Knauer, 1986). Many man-made contaminants, such as anthropogenically produced CO<sub>2</sub>, xenobiotic organic compounds, and heavy metals, are also predominantly removed by the same pathway, i.e. onto settling particulate matter (Larsen *et al.*, 1985; Barrick and Prahl, 1987; Kennicutt, 1994; Gustaffson *et al.*, 1998). Thus, it is of the utmost importance to understand the mechanisms which govern or enhance biologically driven particle fluxes to sediments.

Traditionally, studies of upper ocean primary production have been made using incubation experiments with radiolabeled C or  $^{15}\text{N}$ . Unfortunately, these methods may be compromised due to bottle related artifacts. Bottle incubations will, at best, miss sporadic bloom events and provide rate estimates that are valid only for discrete depths and times. Sediment traps have been typically used to estimate particulate export and remineralization with depth (Eppley and Peterson, 1979). However, sediment traps have been found to suffer from both hydrodynamic effects and "swimmer" related artifacts, which are likely to be particularly detrimental to trap studies in coastal environments (Buesseler, 1991; Buesseler *et al.*, 1994; Michaels *et al.*, 1994).

More recently, measurements of seasonal changes in oxygen, nutrients or carbon have been used to estimate total and 'new' production (Jenkins, 1984; Schlitz and Cohen, 1984; Townsend, 1992; Emerson *et al.*, 1997), where new production is defined as the amount of primary production supported by nutrients supplied from outside the euphotic zone, e.g. from upwelling or atmospheric deposition (Eppley and Peterson, 1979; Buesseler, 1998). These techniques have been infrequently applied, especially in the dynamic coastal ocean. As a result, there is little consensus regarding the magnitude or temporal and spatial variability of new production in the oceans (see review by Ducklow, 1995). One of the major obstacles to understanding upper ocean biogeochemical cycles is the inability to accurately decipher nutrient uptake and export rates. There is currently open debate as to the extent to which and under what conditions primary production is limited by nitrogen, phosphorus, or trace elements (Codispoti, 1989; Hecky and Kilham, 1988; Martin *et al.*, 1994; Hutchins and Bruland, 1998; Takeda, 1998).

Coastal zones have been recognized as playing an important role in the global carbon cycle (Falkowski *et al.*, 1988; Jahnke *et al.*, 1990; Walsh, 1991). However, a lack of reliable export rates has placed limits on recent efforts to understand how these regimes fit into the global oceanic realm. In addition, many of these coastal regions are vulnerable to anthropogenic impacts caused by enhanced nutrient loading and elevated pollutant inputs. The Gulf of Maine, in particular, sustains one of the most productive fisheries in



North America (O'Reilly and Busch, 1984). However, while the Gulf of Maine is pristine relative to other eastern coastal sites (Larsen, 1992), it is difficult to predict the effect man's activities will have on the environmental quality of this region (Hecky and Kilham, 1988; Smayda, 1991; Gulf of Maine Research Plan, 1992). Unfortunately, it is not yet clear as to what causes these blooms to occur.

The Gulf of Maine is an enclosed basin which exhibits strong temporal and spatial variability in primary productivity and particulate matter export (Proceedings of the Gulf of Maine Scientific Workshop 1991; Moran and Buesseler, 1993; Charrette et al., 1996; Pilskaln et al., 1996). There is currently a wide range of new and export production estimates (O'Reilly and Busch, 1984; Campbell, 1986; Schlitz and Cohen, 1984; Townsend, 1991; Christensen *et al.*, 1991; Charrette et al., 1996; Pilskaln et al., 1996) due to the limited set of integrated time-series measurements. One vital piece of information which is needed is a characterization of the role that phytoplankton play in both the uptake and removal of particle reactive chemicals and as a food source for zooplankton and larger grazers. This requires an understanding of the relative rates of zooplankton grazing, nutrient uptake and recycling, as well as how these processes vary temporally and vertically in the Gulf of Maine.

In this thesis work, the naturally occurring radioisotopes phosphorus-32 ( $t_{1/2} = 14.3$  d), phosphorus-33 ( $t_{1/2} = 25.3$  d), beryllium-7 ( $t_{1/2} = 53.3$  d) and thorium-234 ( $t_{1/2} = 24.1$  d) were used to determine seasonal variations in the biogeochemical cycling of phosphorus in Wilkinson Basin, in the southwestern Gulf of Maine. The cosmogenic radionuclides  $^{32}\text{P}$ ,  $^{33}\text{P}$  and  $^7\text{Be}$  are naturally produced in the atmosphere from spallation reactions with Ar ( $^{32}\text{P}$ ,  $^{33}\text{P}$ ), or O and N ( $^7\text{Be}$ ) nuclei (Lal and Peters, 1967).  $^{234}\text{Th}$  is a particle reactive radionuclide which is produced at a constant rate from the decay of its soluble parent  $^{238}\text{U}$  in seawater. When used in conjunction, these isotopes can be used to study phosphorus uptake and regeneration rates as well as particulate and nutrient export from the euphotic zone (Fig. 1).

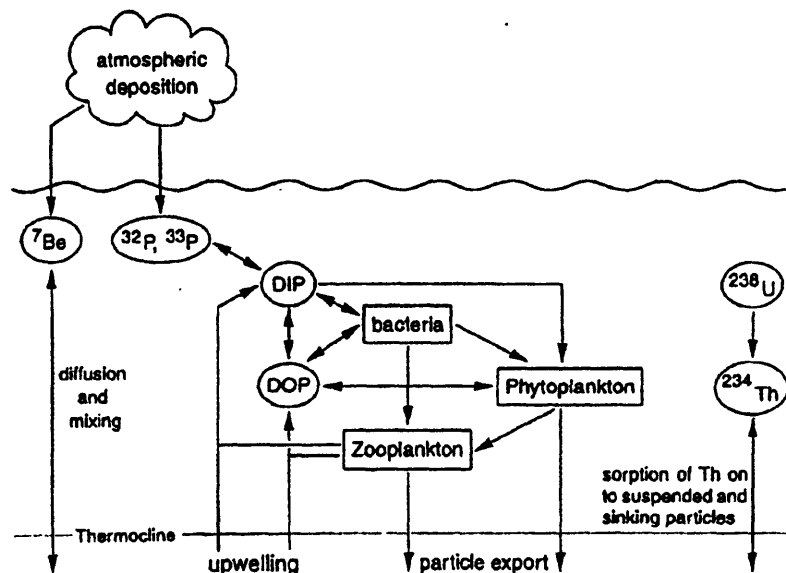


**Figure 1.1** Biogeochemical cycling of  $^{32}\text{P}$  ( $t_{1/2} = 14.3$  d),  $^{33}\text{P}$  ( $t_{1/2} = 25.3$  d),  $^7\text{Be}$  ( $t_{1/2} = 53.3$  d), and  $^{234}\text{Th}$  ( $t_{1/2} = 24.1$  d) in the upper ocean.

In essence, if the atmospheric input of the cosmogenic  $^{32}\text{P}$  and  $^{33}\text{P}$  tracers is known then the ratio of  $^{32}\text{P}$  and  $^{33}\text{P}$  can be used to determine the *in situ* uptake and turnover rates of P into various dissolved and biological pools. In other words, by measurement of  $^{32}\text{P}$  and  $^{33}\text{P}$  the net transfer of P can be detected by the "age" of cosmogenic P in any particular reservoir, be it dissolved, bacterial or planktonic pools.  $^7\text{Be}$  is used as a tracer of upper ocean mixing. Additionally, since  $^{234}\text{Th}$  is measured, estimates of particle export can be obtained for organic C and the major nutrients (e.g. Buesseler, 1998). As such, the  $^{234}\text{Th}$  based particulate P flux can be directly compared to P export deduced from the upper ocean  $^{32}\text{P}$  and  $^{33}\text{P}$  activity. Thus, the information gained from these tracers is highly complementary.

Phosphorus isotopes have advantages over previously used techniques in that phosphorus is not only a nutrient directly utilized by organisms, but  $^{32}\text{P}$  and  $^{33}\text{P}$  have half-lives short enough to follow biologically driven processes. Furthermore, utilization of an *in situ* tracer allows for temporal and spatial integration over the mean-life of the

radionuclide. As a result, these *in situ* isotopic measurements escape many of the difficulties associated with incubation methods.

Only two groups of researchers have successfully measured  $^{32}\text{P}$  or  $^{33}\text{P}$  in at least one component of the upper ocean P cycle. Lee *et al.* (1991, 1992 - lab of Dr. D. Lal at Scripps) simultaneously measured  $^{32}\text{P}$ ,  $^7\text{Be}$  and  $^{234}\text{Th}$  in nearshore waters of the California Current, and Waser *et al.* (1994; 1995) measured both  $^{32}\text{P}$  and  $^{33}\text{P}$  in rain, suspended particulate matter and plankton tows near Bermuda. Unfortunately, both groups were severely restricted by the use of traditional low level beta counting for measuring  $^{33}\text{P}$  activities.

The limited data gathered by these previous investigations suggest a number of important features in the cycling of P in surface waters. Both groups found generally higher  $^{33}\text{P}/^{32}\text{P}$  ratios as one moved up the food chain. Using this progressive change, Waser (1993) determined an average turnover time of phosphorus in zooplankton to be 60-70 days of Bermuda. In contrast, off the coast of California, Lal and Lee (1988) and Lal *et al.* (1988) found net turnover times to be substantially lower, 30-40 days. In addition, Waser (1993) also theorized that most of the  $^{32}\text{P}$  and  $^{33}\text{P}$  activity was in particles, implying rapid turnover within the dissolved P pool. Lee *et al.* (1992), however, measured equal activities of  $^{32}\text{P}$  in total dissolved phosphorus (TDP) and dissolved inorganic phosphorus (DIP) pools, suggesting that the residence time of P in the dissolved organic phosphorus (DOP) pool exceeded 6 weeks. Thus, it was further interpreted that the ecosystem was N rather than P limited. Using the measured or calculated  $^{32}\text{P}$  and  $^{33}\text{P}$  rain input, both groups were able to determine an estimate of POP export. While Lee *et al.* (1992) employed a simple mass balance approach, Waser (1993) utilized a more complicated model of zooplankton grazing, assimilation, and fecal pellet formation. In addition to the limited data sets obtained, these studies suffer in that in the first case, Lee *et al.* (1992), were only able to assume an input rate, and in the second case, Waser (1993) was unable to measure P activities in the dissolved phase.

This thesis work substantially furthers the initial phosphorus radioisotope studies conducted by Lee and Waser in the early 1990's. In **Chapter 2**, new techniques for the extraction, purification, and measurement of  $^{32}\text{P}$  and  $^{33}\text{P}$  in rainwater and seawater are discussed in detail. The most important development is the utilization of an ultra low level liquid scintillation counter, which significantly decreases the detection limit of  $^{33}\text{P}$ . **Chapter 3** details the  $^{32}\text{P}$ ,  $^{33}\text{P}$ ,  $^7\text{Be}$ , and  $^{210}\text{Pb}$  measurements made in individual rain samples at Woods Hole, MA, and Portsmouth, NH. Results suggest that  $^{32}\text{P}$  and  $^{33}\text{P}$  can be used to trace aerosol residence times and stratospheric/tropospheric exchange. In **chapter 4**, the  $^{32}\text{P}$  and  $^{33}\text{P}$  activity data are presented. For the first time the in situ temporal variability in the residence time of soluble reactive (inorganic) and dissolved organic phosphorus has been demonstrated. In addition, our results show that bacterial activity is not only prevalent within Wilkinson Basin, but very important in the uptake and remineralization of phosphorus during the summer. **Chapters 5** discusses the temporal and spatial variability in  $^{234}\text{Th}$  derived organic carbon export as well as estimates of vertical eddy diffusivity. Results indicate that within the coastal ocean, physical processes such as advection and diffusion need to be considered when using  $^{234}\text{Th}$  to determine particulate organic carbon export. **Chapter 6** discusses the utilization of  $^{32}\text{P}$  and  $^{33}\text{P}$  in numerical modelling efforts. The radioactive phosphorus data was employed in two different types of steady state models. Results demonstrate that  $^{32}\text{P}$  and  $^{33}\text{P}$  can help pinpoint weaknesses within model formulations. Furthermore, these isotopes have the potential to possibly 'tune' specific model parameters. The work is summarized in **Chapter 7** and avenues of future research using  $^{32}\text{P}$  and  $^{33}\text{P}$  to solve both atmospheric and oceanic problems are discussed.

## References

- Barrick, R. C and F. G. Prahl (1987). Hydrocarbon geochemistry of the Puget Sound Region-III. Polycyclic aromatic hydrocarbons in sediments. *Estuarine Coastal and Shelf Science*, **25**, 175-191.
- Buesseler, K. O. (1991). Do upper-ocean sediment trap studies provide an accurate estimate of sediment trap flux? *Nature*, **353**, 420-423.
- Buesseler, K. O., A. F. Michaels, D. A. Siegel, and Anthony H. Knap (1994). A three dimensional time-dependent approach to calibrating sediment trap fluxes. *Global Biogeochemical Cycles*, **8**, 179-193.
- Buesseler, K. O., (1998) The decoupling of production and particle export in the surface ocean. *Global Biogeochemical Cycles*, **12**, 297-310.
- Campbell, D. E. (1986). Process variability in the Gulf of Maine - a macroestuarine environment. In: *Estuarine Variability*, D. A. Wolfe, Ed., Academic Press., pp. 261-275.
- Charette, M. A., S. B. Moran and C. H. Pilskaln (1996) Particulate organic carbon export fluxes in the central Gulf of Maine estimated from <sup>234</sup>Th/<sup>238</sup>U disequilibria. Poster presented at the Gulf of Maine Ecosystem Dynamics: A Scientific Symposium and Workshop, St. Andrews, NB, September, 1996.
- Christensen, J. P., D. B. Smith and L. M. Mayer (1991). The nitrogen budget of the Gulf of Maine and climate change. In: *Proceedings of the Gulf Of Maine Scientific Workshop*, T. Wigger and C. N. K. Mooers (Eds.), Woods Hole, MA, 75-90.
- Codispoti, L.A. (1989). Phosphorus vs. Nitrogen Limitation of New and Export Production. In: *Productivity of the Ocean: Present and Past*, W. H. Berger, V. S. Smetacek, G. Wefer (Eds.), John Wiley & Sons Limited, 377-394.
- Deuser, W. G. and E. H. Ross (1980). Seasonal change in the flux of organic carbon to the deep Sargasso Sea. *Nature*, **283**, 364-365.
- Ducklow, H. W. (1995). Ocean biogeochemical fluxes: New production and export of organic matter from the upper ocean. *Review of Geophysics*, **33**, 1271-1276.
- Emerson, S., Quay, ., Karl, D., Winn, C., Tupas, L., and Landry, M. (1997) Experimental determination of the organic carbon flux from open-ocean surface waters. *Nature*, **389**, 951-954.
- Eppley, R. W. and B. J. Peterson (1979) Particulate organic matter flux and planktonic new production in the deep ocean. *Nature*, **282**, 677-680.
- Falkowski, P. G., C. N. Flagg, G. T. Rowe, S. L. Smith, T. E. Whittedge, and C. D. Wirick (1988) The fate of a spring phytoplankton bloom: Export or oxidation? *Continental Shelf Research*, **8**, 457-484.
- Fowler, S. W. and G. A. Knauer (1986). Role of large particles in the transport of elements and organic compounds through the oceanic water column. *Progress in Oceanography*, **16**, 147-194.
- Gulf of Maine Research Plan (1992). Prepared by: The Gulf of Maine Regional Marine Research Program, Orono, ME, 35 pp.

- Gustafsson, Ö., P.M. Gschwend, and K. O. Buesseler (in press). Using  $^{234}\text{Th}$  disequilibria to estimate the vertical removal rates of polycyclic aromatic hydrocarbons from the surface ocean. *Marine Chemistry*.
- Hecky, R. E. and P. Kilham (1988). Nutrient limitation of phytoplankton in freshwater and marine environments: A review of recent evidence on the effects of enrichment. *Limnology Oceanography*, **33**, 796-822.
- Hutchins, D. A. and K. W. Bruland (1998) Iron-limited diatom growth and Si:N ratios in a coastal upwelling regime. *Nature*, **393**, 561-564.
- Jahnke, R. A., C. E. Reimers, and D. B. Craven (1990). Intensification of recycling of organic matter at the seafloor near ocean margins. *Nature*, **348**, 50-54.
- Jenkins, W. J. (1984) The use of tracers and water masses to estimate rates of respiration. In: *Heterotrophic Activity in the Sea*, J. E. Hobbie and P. J. LeB. Williams (Eds.), Plenum Publishing Corp., pp. 391-403.
- Kennicutt II, M. C., T. R. Wade, B. J. Presley, A. G. Requejo, J. M. Brooks and G. J. Denoux, (1994) Sediment contaminants in Casco Bay, Maine: Inventories, sources, and potential for biological impact. *Environmental Science Technology*, **28**, 1-15.
- Lal, D., and B. Peters (1967). Cosmic ray produced radioactivity in the Earth. In: *Handbuch der Physik 46/2*, S. Flugge (Ed.), Springer-Verlag, Berlin, pp. 551-612.
- Lal, D. and T. Lee, 1988. Cosmogenic  $^{33}\text{P}$  and  $^{32}\text{P}$  Used as Tracers to Study Phosphorus Recycling in the Upper Ocean. *Nature*, **333**, 752-754.
- Lal, D., Y. Chung, T. Platt and T. Lee, 1988. Twin Cosmogenic Radiotracer Studies of Phosphorus Recycling and Chemical Fluxes in the Upper Ocean. *Limnology and Oceanography*, **33(6, part 2)**, 1559-1567.
- Larsen, P.F., D. F. Gadbois and A.C. Johnson (1985). Observations on the distribution of PCBs in the deepwater sediments of the Gulf of Maine. *Marine Pollution Bulletin*, **16**, 439-442.
- Larson, P. F. (1992) An overview of the environmental quality of the Gulf of Maine. The Gulf of Maine, *NOAA Coastal Ocean Program Regional Synthesis Series*, **1**, 71-95.
- Lee, T., E. Barg, and D. Lal (1991). Studies of vertical mixing in the Southern California Bight with cosmogenic radionuclides  $^{32}\text{P}$  and  $^7\text{Be}$ . *Limnology Oceanography*, **36(5)**, 1044-1053.
- Lee, T., E. Barg, and D. Lal (1992). Techniques for extraction of dissolved inorganic and organic phosphorus from large volumes of sea water. *Analytica Chimica Acta*, **260**, 113-121.
- Lohrenz, S. E., G. A. Knauer, V. L. Asper, M. Tuel, A. F. Micheals, and A. H. Knap (1992) Seasonal variability in primary production and particle flux in the northwestern Sargasso Sea: U.S. JGOFS Bermuda Atlantic Time-Series Study. *Deep-Sea Research*, **39**, 1373-1391.
- Martin, J. H., G. A. Knauer, D. M. Karl, and W. W. Broenkow (1987) VERTEX: Carbon cycling in the northeast Pacific. *Deep-Sea Research*, **34**, 267-285.

- Martin, J.H., K.H. Coale, K.S. Johnson, S.E. Fitzwater, R.M. Gordon, S.J. Tanner, C.N. Hunter, V.A. Elrod, J.L. Nowicki, T.L. Coley, R.T. Barber, S. Lindley, A.J. Watson, K.V. Scoy, C.S. Law, M.I. Liddicoat, R. Ling, T. Stanton, J. Stockel, C. Collins, A. Anderson, R. Bidigare, M. Ondrusek, M. Latasa, F.J. Millero, K. Lee, W. Yao, J.Z. Zhang, G. Friederich, C. Sakamoto, F. Chavez, K. Buck, Z. Kolber, R. Greene, P. Falkowski, S.W. Chisholm, F. Hoge, R. Swift, J. Yungel, S. Turner, P. Nightingale, A. Hatton, P. Liss and N.W. Tindale (1994). Testing the Iron Hypothesis in Ecosystems of the Equatorial Pacific Ocean. *Nature*, **371**,123-129.
- Michaels, A. F., N. R. Bates, K. O. Buesseler, C. A. Carlson and A. H. Knap (1994). Carbon-cycle imbalances in the Sargasso Sea. *Nature*, **372**, 537-540.
- Moran, S.B. and K.O. Buesseler, (1993) Size-Fractionated <sup>234</sup>Th in Continental Shelf Waters off New England: Implications for the Role of Colloids in Oceanic Trace Metal Scavenging. *Journal of Marine Research*, **51**, 893-922.
- O'Reilly, J. E. and D. A. Busch, (1984) Phytoplankton primary production on the northwestern Atlantic Shelf. *Rapport P.-v. Reun. Cons. Int. Explor. Mer.*, **183**, 255-268.
- Pilskaln, C. H., W. Arnold, C. Lehmann and L. E. Watling (1996) Particulate flux dynamics in Jordan and Wilkinson Basins: Seasonal POC export and particle resuspension. Poster presented at the Gulf of Maine Ecosystem Dynamics: A Scientific Symposium and Workshop, St. Andrews, NB, September, 1996.
- Proceedings of the Gulf of Maine Scientific Workshop (1991) *Gulf of Maine Council on the Marine Environment*, J. Wiggin and C. N.K. Mooers (Eds.), Urban Harbors Inst., 394 pp.
- Schlitz, R. J. and E. B. Cohen (1984) A nitrogen budget for the Gulf of Maine and Georges Bank. *Biological Oceanography*, **3**, 203-221.
- Smayda, T. J. (1991). Global epidemic of noxious phytoplankton blooms and food chain consequences. In: Food Chains, Yields, Models and Management of Large Marine Ecosystems. AAAS Symp. Vol., K. Sherman and V. Alexander (Eds.).
- Takeda, S. (1998) Influence of diatom availability on nutrient consumption ratio of diatoms in oceanic waters. *Nature*, **393**, 774-777.
- Townsend, D. W., (1991) Influences of oceanographic processes on the biological productivity of the Gulf of Maine. *Review of Aquatic Sciences*. **4**,1-20.
- Townsend, D. W. (1992). An overview of oceanography and biological productivity in the Gulf of Maine. *The Gulf of Maine, NOAA Coastal Ocean Program Regional Synthesis Series*, **1**, 5-26.
- Walsh, J. J. (1991). Importance of continental margins in the marine biogeochemical cycling of carbon and nitrogen. *Nature*, **350**, 53-55.
- Waser, N. A. D (1993). Cosmogenic <sup>32</sup>P and <sup>33</sup>P in the atmosphere and oligotrophic ocean and applications to the study of phosphorus cycling, Ph.D. Thesis, MIT/WHOI, Woods Hole, MA, 153 pp.

- Waser, N. A. D., A. P. Fleer, T. R. Hammer, K. O. Buesseler and M. P. Bacon (1994). Determination of natural  $^{32}\text{P}$  and  $^{33}\text{P}$  in rainwater, marine particles and plankton by low-level beta counting. *Nuclear Instruments and Methods. in Physics*, **A388**, 560-567.
- Waser, N.A.D., M. P. Bacon and A. F. Michaels (1995). Natural Activities of  $^{32}\text{P}$  and  $^{33}\text{P}$  and the  $^{33}\text{P}/^{32}\text{P}$  Ratio in Suspended Particulate Matter and Plankton in the Sargasso Sea. *Deep-Sea Research II*, **43**, 421-436.



Reprinted with permission from  
*Analytical Chemistry* 70, 64-72, 1998.  
Copyright 1998 American Chemical Society

## Chapter 2

### **Sensitive techniques for the measurement of cosmogenic $^{32}\text{P}$ and $^{33}\text{P}$ activities in rain and seawater**

#### **ABSTRACT**

We have developed a new method for the collection, purification, and measurement of natural levels of  $^{32}\text{P}$  and  $^{33}\text{P}$  in rain, marine particulates, and dissolved constituents of seawater.  $^{32}\text{P}$  and  $^{33}\text{P}$  activities were measured using a recently developed ultra low level liquid scintillation counter. Measurement by liquid scintillation counting allows, for the first time, simultaneous measurement of both  $^{32}\text{P}$  and  $^{33}\text{P}$ . Furthermore,  $^{33}\text{P}$  activities are measured with high efficiency ( $> 50\%$ ), regardless of the amount of stable phosphorus in the sample. Liquid scintillation also produces energy specific beta spectra, which have enabled us to identify previously unrecognized beta emitting contaminants in natural samples. In order to remove these contaminants, new methods of purification have been developed which utilize a series of precipitations and anion and cation ion exchange columns. Phosphorus was extracted from large volumes of rain and seawater, 5- 20 and  $> 5000$  l, respectively, using iron hydroxide impregnated polypropylene filters. On these filters, it was possible to load 25-30%  $\text{Fe}(\text{OH})_3$  by weight, over twice that loaded on previously utilized materials. Using our collection, purification, and liquid scintillation counting techniques, it was possible to obtain specific  $^{32}\text{P}$  and  $^{33}\text{P}$  activities with less than 10% error ( $2\sigma$ ) in rain, and 20% error ( $2\sigma$ ) in seawater.

## INTRODUCTION

A new technique was developed for the extraction, purification, and measurement of  $^{32}\text{P}$  (half-life: 14.28 days) and  $^{33}\text{P}$  (half-life: 25.3 days) in rain, marine particulates, including plankton, and dissolved inorganic and organic phosphorus. These two cosmogenic radioisotopes are removed from the atmosphere predominantly via wet precipitation<sup>1-3</sup>. Due to their short half-lives and reactivity towards atmospheric aerosols,  $^{32}\text{P}$  and  $^{33}\text{P}$  have shown great utility in the determination of stratospheric/tropospheric air mass exchange and tropospheric air mass and aerosol residence times<sup>1-2,4-6</sup>.

More recently,  $^{32}\text{P}$  and  $^{33}\text{P}$  have been used in an attempt to elucidate the short term biogeochemical cycling of P within the upper ocean by measuring the activities of these isotopes in various dissolved and particulate biological pools<sup>7-12</sup>. Phosphorus is an essential nutrient, and one of the main obstacles in furthering our understanding of upper ocean biogeochemical cycling is the lack of reliable nutrient uptake and export rate data. Thus, any direct measurements of nutrient turnover within the marine biological cycle are of great importance. However, both atmospheric and marine investigations which utilize  $^{32}\text{P}$  and  $^{33}\text{P}$  have been hampered by the extremely low levels found in natural environments. Average concentrations of  $^{32}\text{P}$  and  $^{33}\text{P}$  in rainwater range from 0.2 - 6 dpm/L, whereas in seawater, dissolved  $^{32}\text{P}$  and  $^{33}\text{P}$  concentrations are 1000 times lower<sup>7-12</sup>. Hence, preconcentration from several thousand liters of seawater and ultra low level counting techniques are needed.

$^{32}\text{P}$  and  $^{33}\text{P}$  both decay via beta emission with maximum energies ( $E_{\text{max}}$ ) occurring at 1.71 MeV and 0.249 MeV, respectively. Until now,  $^{32}\text{P}$  and  $^{33}\text{P}$  activities have been determined by counting a hygroscopic precipitate,  $\text{NH}_4\text{MgPO}_4 \cdot 6\text{H}_2\text{O}$ , on an anticoincidence low level beta counter<sup>4,7-13</sup>. The combined  $^{32}\text{P}$  and  $^{33}\text{P}$  activities have been separated by taking advantage of the differences in the relative  $E_{\text{max}}$  intensity of the two isotopes<sup>7,11,14</sup>. Briefly, because  $^{33}\text{P}$  is a low energy beta emitter, its beta emission is easily blocked by increasing sample thickness and/or by the presence of an external absorber. In contrast,  $^{32}\text{P}$ , due to its relatively high  $E_{\text{max}}$  is only minimally affected by absorption.

Thus, for measurement of both isotopes, P samples are counted twice: once with an external absorber to block  $^{33}\text{P}$  activity and only measure  $^{32}\text{P}$ , and again without the absorber to measure the total activity. The  $^{33}\text{P}$  activity is then found by the difference between the two count rates.

The efficiency of beta detection for  $^{32}\text{P}$  is often between 25-50% using anticoincidence low level beta counting<sup>2</sup>. The efficiency of  $^{33}\text{P}$  for beta detection via traditional beta counting, on the other hand, is highly dependent on the thickness of the  $\text{NH}_4\text{MgPO}_4 \cdot 6\text{H}_2\text{O}$  precipitate to be counted, and is much less than 20% using low level beta counting. Thus, measurement of  $^{33}\text{P}$  requires low levels of stable P (i.e. less precipitate) within the sample. This makes  $^{33}\text{P}$  measurement in eutrophic environments very difficult. In addition, changes in sample geometry caused by the nature of the hygroscopic precipitate will alter the  $^{33}\text{P}$  detection efficiency. Also, the low level beta counters provide only gross counts. Thus, any interference due to other short-lived beta emitters present in the sample are not easily distinguished from the relatively small sample signal. Samples must be counted repeatedly to allow for time and half live comparisons between sample and expected values in order to verify that the sample is free of other beta emitters. This only works if the half-lives of the two isotopes of interest are considerably different and the activities are large. Depending on the efficiency and background of the low level beta detectors, and assuming high purity and reasonably low counting errors, between 1-2 liters ( $^{33}\text{P}$  activity  $\geq 0.3$  dpm) of rainwater and  $\geq 1000$  l of low stable P seawater ( $\leq 0.3$   $\mu\text{M}$ ) are needed for measurement of both  $^{33}\text{P}$  and  $^{32}\text{P}$ .

An alternative approach is to use low level background liquid scintillation spectrometry (LSS). LSS produce energy specific beta spectra and recent developments in LSS technology have reduced background levels to less than 3 cpm over the entire energy spectrum. Background can be further reduced to less than 1.5 cpm by defining specific  $^{33}\text{P}$  and  $^{32}\text{P}$  regions of interest. As a result, it is now possible to measure low levels of  $^{33}\text{P}$  and  $^{32}\text{P}$  activity ( $^{33}\text{P}$  activity  $\geq 0.5$  dpm) with LSS. The advantages of using LSS over low level beta counters are numerous. Both  $^{32}\text{P}$  and  $^{33}\text{P}$  can be counted

*simultaneously*, and with significantly *higher* efficiencies (> 50% for both  $^{32}\text{P}$  and  $^{33}\text{P}$ ). In addition, samples with low amounts of stable P are not required in order to achieve such high efficiencies. Evidence of contamination by other beta emitters can be determined by analyzing spectra for evidence of anomalous peaks that are not readily apparent when using traditional beta counters.

In the following, a new technique is described for the collection, purification, and, separate determination of  $^{33}\text{P}$  and  $^{32}\text{P}$  in rain and seawater using LSS. In each section, we describe a detailed procedure and discuss how each differs from previous work. Results from rain and seawater measurements are shown thereafter.

### **Sample Collection**

The measurement of  $^{32}\text{P}$  and  $^{33}\text{P}$  in rain and in seawater requires the extraction of these isotopes from relatively large amounts water. In this study, we have utilized the strong affinity of phosphorus in all forms onto iron impregnated filters in order to achieve this goal. However, numerous tests had to be conducted in order to first ensure good extraction efficiency of P over the course of sample collection. In rain water, there is typically little to no stable phosphorus<sup>15</sup>. In contrast, in seawater, dissolved P is divided into two main pools: dissolved inorganic (DIP) and dissolved organic (DOP) phosphorus. Both are comprised of a wide range of chemical compounds, which have yet to be fully quantified and most likely have large variations in chemical reactivity (see **Chapter 4**). Traditional measurements of P in the ocean sciences as well as in this study, define DIP as that fraction which reacts to form a molybdenum blue complex in the presence of ascorbic acid<sup>16</sup>. DOP is calculated as the difference between total dissolved phosphorus (TDP) and DIP. TDP is measured here using the acid persulfate method<sup>16</sup>.

**Iron filter preparation.** Previous researchers utilized the impregnation of acrilan fibers with  $\text{Fe}(\text{OH})_3$ <sup>8-10</sup>. However, in this study, 25  $\mu\text{m}$  pore size polypropylene sheets (MWM Company, 1 Newbury St., Quincy, MA 02171) are impregnated with iron instead of acrilan fibers. Filters were first impregnated with 6.25N NaOH at 85-90°C for 10-15

minutes, allowed to cool, and rinsed with distilled water. The filters were then impregnated with a 50%  $\text{FeCl}_3$  solution at 85-90°C for 15 minutes, allowed to cool, and placed in a 3N  $\text{NH}_4\text{OH}$  bath for several hours<sup>17</sup>. Filters were subsequently rinsed and stored in a plastic bag. Certified ACS  $\text{FeCl}_3$  used in the impregnation of the polypropylene sheets was first extracted with di-isopropyl ether in order to reduce levels of stable P in the  $\text{FeCl}_3$  solution to less than 0.1  $\mu\text{Mol P/gm Fe(OH)}_3$ .

Using this technique, it was possible to load between 25-30%  $\text{Fe(OH)}_3$  by weight onto the polypropylene sheets, twice the estimated load of  $\text{Fe(OH)}_3$  on acrilan fibers<sup>8</sup>. We found that the polypropylene was much easier to impregnate with Fe in a consistent and uniform manner. Furthermore, it was possible to obtain much better water flow through the polypropylene sheets.

**Extraction experiments.** We checked the extraction efficiency of DIP from fresh water and both DIP and DOP from seawater on these new adsorbers. As expected, extraction efficiency increased with increased loading of  $\text{Fe(OH)}_3$  and care was taken to ensure a relatively consistent maximum loading of between 25-30%  $\text{Fe(OH)}_3$  by weight on the polypropylene filters. Initial extraction efficiency tests were conducted with pH 7 distilled water spiked with 4.1  $\mu\text{M}$  DIP and 1.9  $\mu\text{M}$  DOP (0.5  $\mu\text{M}$  adenosine triphosphate (ATP) + 1.4  $\mu\text{M}$  1-glucose phosphate). The sample was then passed through a 30.5 cm long, 1.9 cm diameter (vol. = .087 L) PVC pipe packed with iron filters. Extraction was maintained at greater than 95%, with a flow rate as high as 440 mL/min over the course of 280 column volumes (25 liters) of flow.

In seawater experiments, it was expected that the efficiency of extraction would be significantly altered due to differences in ion association between fresh and salt water and the high scavenging efficiency of  $\text{Fe(OH)}_3$  for a variety of other elements. In particular, it was expected that dissolved silica, which can be up to 10 times higher in concentration than TDP, would be the main chemical species to absorb and saturate the  $\text{Fe(OH)}_3$  column<sup>8</sup>. Large scale TDP extraction tests were conducted by passing 4000 L of 0.2  $\mu\text{M}$  filtered seawater (DIP = 0.2-0.3  $\mu\text{M}$ ; DOP = 0.45-0.5  $\mu\text{M}$ ; silicate = 2- 4  $\mu\text{M}$ ) through a

1.4 l volume collection tube packed with Fe coated polypropylene at a flow rate 4-6 liters/min. Extraction was maintained at greater than 95% for both DIP and DOP over the first 700 column volumes or 980 L of seawater. Extraction efficiencies decreased for both DIP and DOP to 90% and 60%, respectively, by 2850 column volumes (Fig. 1a). This compares favorably with similar experiments utilizing acrilan fibers tested in this lab (Fig. 1b) and by previous investigators<sup>9</sup>. More interestingly, the extraction efficiency differs between the DOP and DIP fraction. There is a more rapid decrease in collection efficiency for DOP relative to DIP. This is true for acrilan fibers as well (Fig. 1b). This is not surprising given the wide range in reactivity expected from the known chemical species of DOP<sup>19</sup>. The observed difference in absorption between DIP and DOP necessitates that little or no P should be allowed to pass through (breakthrough) the iron absorbers during sample collection. Otherwise, fractionation of the two reservoirs would result in <sup>32</sup>P and <sup>33</sup>P measurements which would be difficult to interpret within the context of biological cycling in the system. Therefore, the size of the iron extraction cartridge utilized in extracting dissolved <sup>32</sup>P and <sup>33</sup>P must be varied in accordance with the seawater volume to be sampled in order to maintain 95% TDP extraction efficiency.

**Field Sampling: Rain.** Rainwater was collected from the roof of Clark Laboratory, at the Woods Hole Oceanographic Institution (WHOI) in Woods Hole, MA (41°32.11'N, 70°38.89'W). The extraction of <sup>32</sup>P and <sup>33</sup>P from rainwater was modified so that <sup>7</sup>Be and <sup>210</sup>Pb activities could be measured separately via gamma counting. Rain samples were spiked with 100 μmoles of stable P (as Na<sub>3</sub>PO<sub>4</sub>·12H<sub>2</sub>O), stable Pb (as PbNO<sub>3</sub>), and stable Be (as Be<sub>4</sub>O(C<sub>2</sub>H<sub>3</sub>O<sub>2</sub>)<sub>6</sub>) as yield monitors and passed through a 30.5 cm long, 1.9 cm diameter (vol.= .087 L) PVC pipe packed with iron filters. It was found that by adjusting the pH of the rain sample to less than 1.5, TDP was still collected with an efficiency greater than 70%, while less than 10% of the <sup>7</sup>Be and 50% of the <sup>210</sup>Pb, were absorbed. This allowed for two separate samples: one containing <sup>32</sup>P and <sup>33</sup>P, the other, <sup>7</sup>Be and <sup>210</sup>Pb. The filtrate was then prepared for <sup>7</sup>Be and <sup>210</sup>Pb measurement via gamma detection<sup>18</sup>.

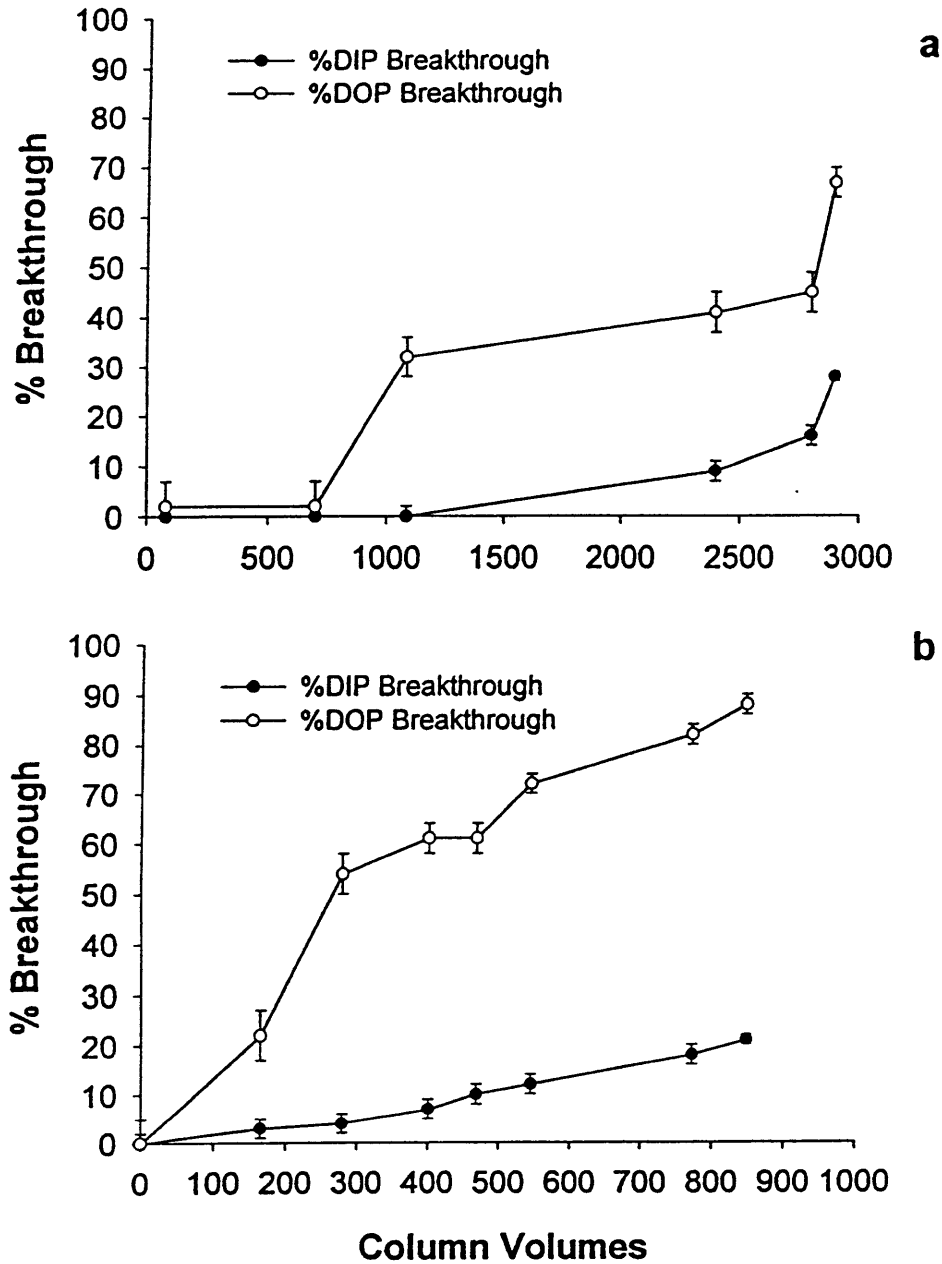


**Figure 2.1** Collection efficiency for DIP (black diamonds) and DOP (white circles) versus column volume for a 1.4 liter collection tube. % Breakthrough is defined by the measured DIP and DOP concentrations in the pipe effluent relative to that entering. Errors are  $2\sigma$  as determined by replicate analysis. (A) Iron coated polypropylene, (B) Iron coated acrilan.

**Field Sampling: Seawater.** Seawater samples were collected in Wilkinson Basin in the Gulf of Maine. Between 4000 and 6000 liters of seawater were passed sequentially through two parallel 10 and 1  $\mu\text{m}$  polypropylene HYTREX prefilters, and a 0.2  $\mu\text{m}$  pleated polypropylene membrane cartridge (25.4 cm long, 7.6 cm diameter) before passing through three parallel 61 cm long, 7.6 cm diameter PVC pipes (vol.= 2.7 L) packed with  $\text{Fe}(\text{OH})_3$  impregnated polypropylene filters. Sample volumes were maximized in order to obtain the largest possible dissolved  $^{32}\text{P}$  and  $^{33}\text{P}$  activities. PVC pipe sizes were chosen in order to maintain DIP and DOP extraction efficiencies at greater than 95% based on our earlier smaller scale experiments. Prefilters were selected so as to obtain different size classes of suspended particulate matter. A one inch inside diameter pool hose was attached to the ship's weighted hydrowire, placed over the side, and lowered to variable depths between the sea surface and 110 m. Water was then pumped using a 0.75 horsepower bronze gear pump (Teel, 1B416). Flow meters were placed at the end of each pipe to monitor variations in flow due to packing; flow rates averaged between 3 - 4 L/min through each pipe. Pressure gauges were also placed between the pump and 10  $\mu\text{m}$  prefilter and between the 0.2  $\mu\text{m}$  prefilter and  $\text{Fe}(\text{OH})_3$  cartridges. The pressure varied from 15-20 psi at the first gauge to 40-45 psi at the second. The 20 psi increase in pressure was due to the  $\text{Fe}(\text{OH})_3$  columns rather than the 0.2  $\mu\text{m}$  prefilter. In order to check for TDP break-through, additional samples were taken from the filtrate and analyzed for both DIP and DOP (see Results).

## **SAMPLE PROCESSING**

The chemical purification techniques utilized here are similar to those employed in earlier studies and involve a series of P specific precipitations and ion exchange chromatography<sup>10-12</sup> (Fig. 2). Modifications have been made, however, to effect complete removal of beta emitting contaminants such as  $^{210}\text{Pb}$  and its radioactive daughter  $^{210}\text{Bi}$ . Based upon these modifications, we conclude that both potential contaminants were not efficiently removed by previous purification methods<sup>4,8,10-13</sup> (see following).



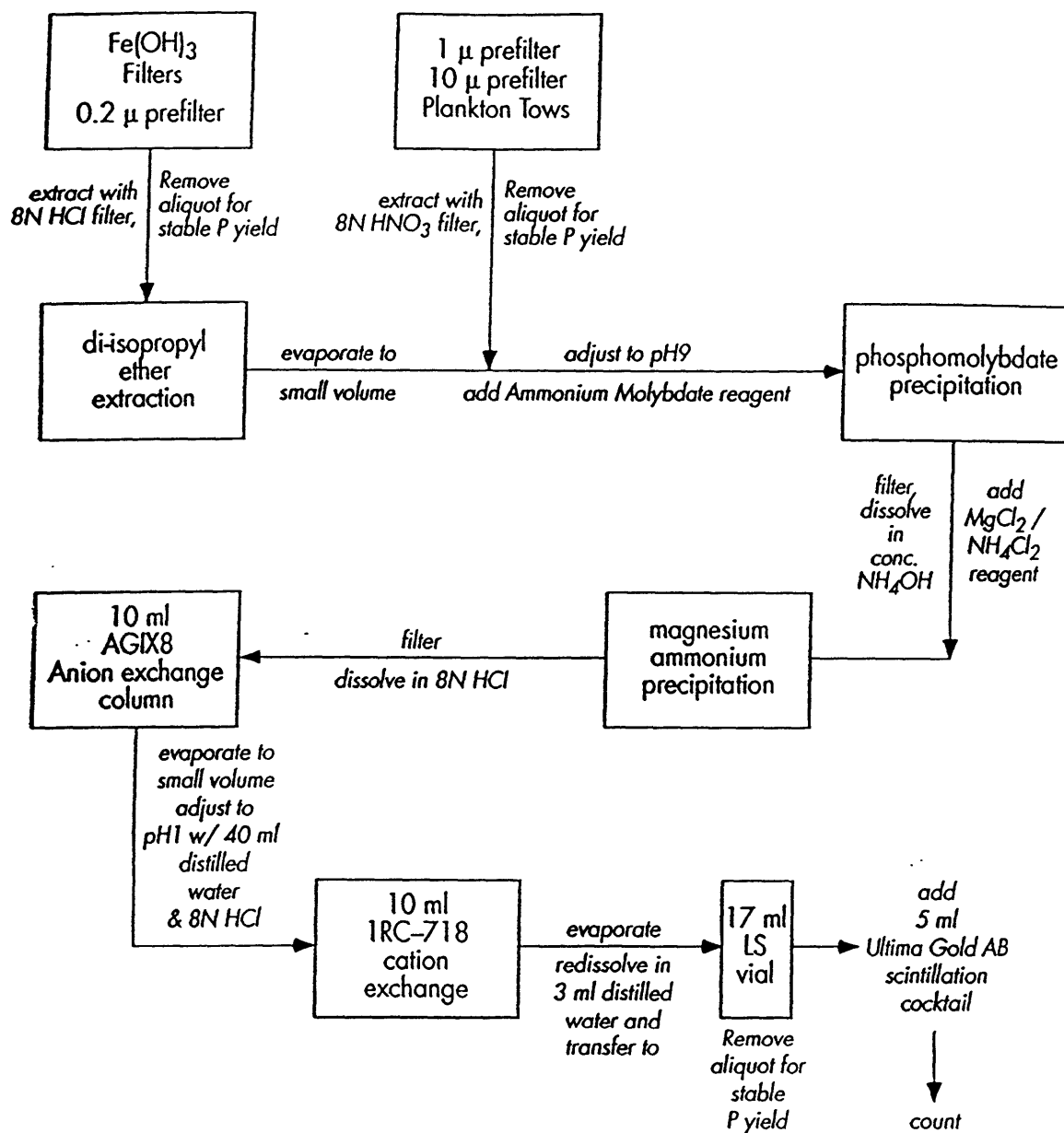


Figure 2.2 Chemical purification scheme.

**Ashing and dissolution.** The 10, 1, and 0.2  $\mu\text{m}$  HYTREX prefilters and the  $\text{Fe}(\text{OH})_3$  filters utilized for both rain and seawater were ashed in a muffle furnace at  $500^\circ\text{C}$  for four hours to reduce the volume of the sample and to convert all of the phosphorus to inorganic forms. It was found that the polypropylene material combusted much more cleanly to  $\text{CO}_2$  at high temperatures than the previously used acrilan fibers. The 10 and 1  $\mu\text{m}$  prefilters were then extracted with a mixed solution of 8N  $\text{HNO}_3$  and 30%  $\text{H}_2\text{O}_2$  on low heat for at least 12 hours, while the 0.2  $\mu\text{m}$  and  $\text{Fe}(\text{OH})_3$  filters were extracted with a mixed solution of 8N  $\text{HCl}$ , and 30%  $\text{H}_2\text{O}_2$ .  $\text{HNO}_3$  acid was used when possible in order to achieve more rapid extraction of DIP and better precipitation of ammonium phosphomolybdate (see below).  $\text{HCl}$  was used to achieve optimal removal of  $\text{Fe}(\text{III})$  into di-isopropyl ether. All of the samples were allowed to cool, filtered using a 934 AH GF/F filter, and an aliquot removed to monitor the chemical yield of stable P during purification.

**Chemical purification.** The 0.2  $\mu\text{m}$  prefilter and  $\text{Fe}(\text{OH})_3$  rain and seawater samples were repeatedly extracted with di-isopropyl ether until the water phase turned from brown to a pale yellow color. These samples, along with the 10 and 1  $\mu\text{m}$  prefilters, were then reduced to a small volume (50 ml for the prefilters, 200 ml for the iron filters) via evaporation on a hot plate. Preliminary purification of the samples was achieved using an ammonium phosphomolybdate precipitation<sup>21</sup>. This acid insoluble precipitate separates P from almost all other anions and cations with the exception of lead, bismuth, tin, and zirconium<sup>20</sup>.

Samples were heated to  $45^\circ\text{C}$  and 60 mL of the ammonium molybdate reagent was added for every 0.1 grams of  $\text{P}_2\text{O}_5$  present in the sample. Sample pH was adjusted prior to the addition of reagent such that the final pH of the sample with the added ammonium molybdate solution was between 0.6 and 0.8. Heating samples to temperatures greater than  $50^\circ\text{C}$  caused precipitation of molybdic acid and contaminated the precipitate with metals such as Si, As, and V. Samples were stirred until the yellow ammonium molybdate precipitate appeared, at which point, samples were removed from the stir plate, and allowed to settle for at least one hour. After settling, the ammonium molybdate

precipitate was vacuum filtered using a 934 AH GF/F filter and dissolved in concentrated  $\text{NH}_4\text{OH}$ . Samples were then prepared for magnesium ammonium orthophosphate hexahydrate precipitation.

The magnesium ammonium molybdate precipitation, while not a purification step, is necessary in order to dissolve the sample in an acidic medium for ion exchange chromatography. After dissolution of the precipitate in  $\text{NH}_4\text{OH}$ , the samples were cooled in an ice bath and the pH lowered to 3 - 4 with 8N HCl. Approximately 10 mL of the  $\text{MgCl}_2/\text{NH}_4\text{Cl}_2$  reagent<sup>21</sup> was added for every 0.1 grams of  $\text{P}_2\text{O}_5$  in the sample solution. Concentrated  $\text{NH}_4\text{OH}$  was then added slowly to the sample, with stirring, until a white precipitate formed. Excess  $\text{NH}_4\text{OH}$  was added, and the precipitate allowed to settle for at least an hour. The magnesium ammonium orthophosphate hexahydrate was vacuum filtered through a 934 AH GF/F filter and dissolved in 8N HCl with low heat.

Further purification of the samples is accomplished using ion exchange chromatography. The sample solution in 8N HCl was first passed through a 10 mL anion exchange column packed with AG1x8 100 -200 mesh resin (Bio-rad laboratories) in order to remove any residual Fe (III) in sample, and other elements such as Cu, Cd and Zn. This step was necessary as it was found that in the subsequent cation exchange separation steps, phosphate would be retained from dilute acid media as a result of coabsorption when Fe (III) is present. The sample was then evaporated to a small volume ( $\leq 1$  mL) and the pH adjusted to between 0.8 and 1 with slightly basic distilled water (total vol.= 40 mL). The solution was then passed through a 10 ml column packed with a weakly acidic cation exchange resin, Amberlite IRC-718 (iminodiacetate group, Rohm and Haas Company) to remove any residual  $^{210}\text{Pb}$  and  $^{210}\text{Bi}$  in the sample.

Once the sample had been purified using the IRC cation exchange resin, solutions were carefully evaporated to dryness, taking care not to over-heat the sample. After evaporation, the sample was dissolved in 1 ml of distilled water and transferred via a glass pipette to a preweighed 17 mL non-static liquid scintillation vial (available from Packard Industries). The beaker was then carefully rinsed twice with exactly 1 mL portions of

distilled water and transferred to the LS vial. The vial was weighed, a 50  $\mu\text{L}$  aliquot removed to track chemical recovery, and 5 mL of Ultima Gold AB (Packard) scintillation cocktail added. The Ultima Gold AB cocktail is an organic solvent containing a blend of alkylnaphthalene and PPO and bis-MSB scintillators. This cocktail was chosen because it is biodegradable, able to incorporate higher acidity samples at relatively high sample to cocktail ratios, and has low associated background. No other cocktails were tested.

**Contaminant identification.** Evidence of  $^{210}\text{Pb}$  and  $^{210}\text{Bi}$  contamination was first apparent in initial rain measurements when the Amberlite IRC column was not utilized. Samples were counted repeatedly on the LSS. Measured half-lives and region of interest backgrounds were compared with the expected backgrounds and known half-lives of  $^{32}\text{P}$  and  $^{33}\text{P}$  using a non-weighted linear least squares fitting curve fitting routine. Sample counts were first curve fitted using the known half-lives of  $^{32}\text{P}$  and  $^{33}\text{P}$  and the backgrounds calculated. It was found that the calculated sample background counts were significantly higher than those determined from chemistry blanks (i.e. distilled water samples processed identically to the rain samples) for both the  $^{32}\text{P}$  and  $^{33}\text{P}$  regions. Furthermore, there was significant disagreement between the measured  $^{32}\text{P}$  and  $^{33}\text{P}$  signals and their known half-lives when the background was fixed at the expected chemical blank background of 1.0 cpm and the  $^{32}\text{P}$  and  $^{33}\text{P}$  half-lives allowed to vary (Fig. 3). Upon closer analysis of the LSS beta spectra, it became apparent that during decay of  $^{32}\text{P}$  and  $^{33}\text{P}$ , a small peak emerged beneath the two. All of these factors pointed to a significant contaminant in the sample. Analysis of radioactive nuclides commonly found in rain, coupled with LSS spectral analysis indicated that the contaminant was due to decay of  $^{210}\text{Pb}$  to  $^{210}\text{Bi}$  and that both the beta decay of  $^{210}\text{Pb}$  and  $^{210}\text{Bi}$  were contaminating the sample. Due to the chemical manipulation of the samples,  $^{210}\text{Pb}$  and  $^{210}\text{Bi}$  were being removed to different, unknown extents. In effect, once 'purified',  $^{210}\text{Bi}$  was either growing in or decaying into secular equilibrium with its parent  $^{210}\text{Pb}$ .

After testing a number of ion exchange resins at various pH and carrier medium, the IRC-718 cation exchange resin proved to be the most efficient in fully removing any

### Rain Collected 4/2/96

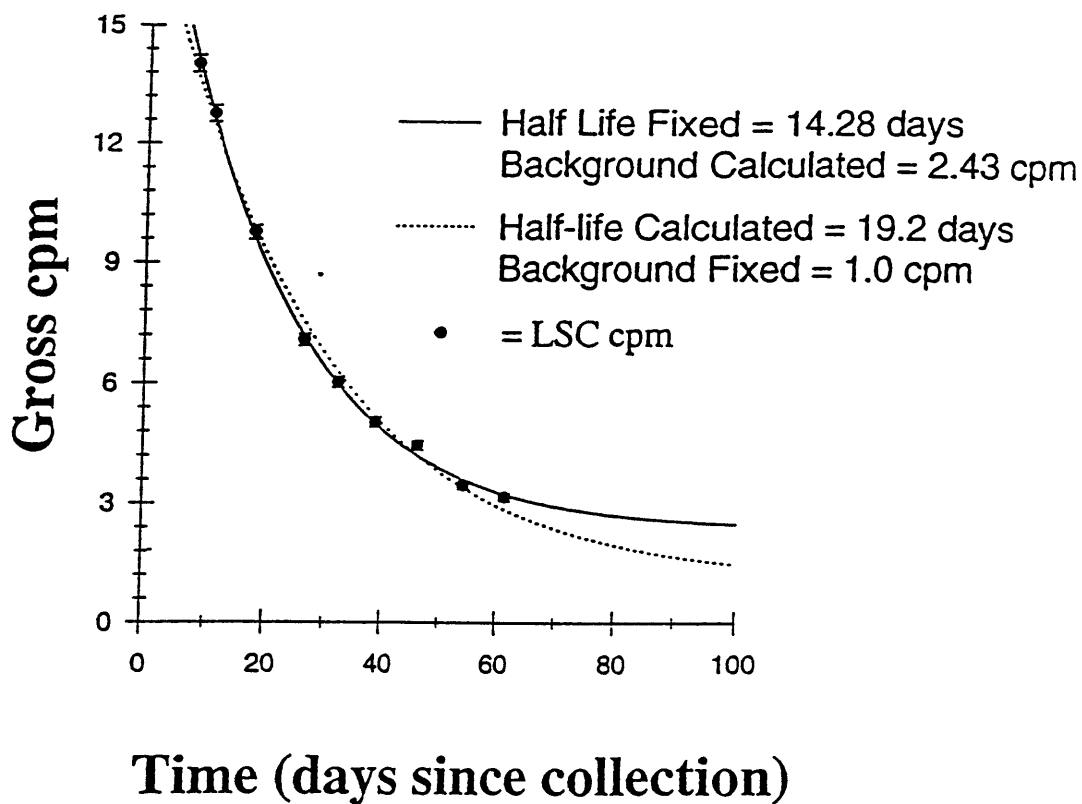


**Figure 2.3** Decay curve analysis for  $^{32}\text{P}$  in a rain sample collected April 2, 1996 at WHOI; Evidence of sample contamination. Circles are gross  $^{32}\text{P}$  cpm data points, the solid line is with the half-life fixed and a calculated background, the dotted line is with the background fixed, and the half-life calculated.

residual  $^{210}\text{Pb}$  and  $^{210}\text{Bi}$  from the sample without loss of P. Previous investigations used 10 ml columns packed with a strongly acidic cation exchange resin Dowex 50 (sulfonic acid group, Bio-Rad Industries), in acidic media ranging from 9N to 0.1N HCl. At both 0.1N and 9N, tests conducted in this laboratory indicated that a small fraction of the  $^{210}\text{Pb}$  and  $^{210}\text{Bi}$ , was still present in the sample (0.1 - 0.5% of initial or 1-3 dpms each).

It is not clear what effect  $^{210}\text{Pb}$  and  $^{210}\text{Bi}$  has had on earlier investigations using previously published ion exchange methods and low level beta counting involving adsorbers to separate  $^{32}\text{P}$  and  $^{33}\text{P}$ . Our experience in rain collected at the Woods Hole Oceanographic Institution is that the  $^{210}\text{Pb}$  and  $^{210}\text{Bi}$  contaminants would cause an underestimation of 10% of the  $^{32}\text{P}$  activity ( $^{210}\text{Bi}$  ingrowth), and a 10% overestimate in the  $^{33}\text{P}$  activities (higher background due to  $^{210}\text{Pb}$ ) when samples were counted repeatedly with time and curve fitted (see below). Those studies which counted  $^{32}\text{P}$  and  $^{33}\text{P}$  samples only once and maintained fixed detector backgrounds, would be expected to have even larger contributions from  $^{210}\text{Pb}$  and  $^{210}\text{Bi}$  contamination in the  $^{32}\text{P}$  and  $^{33}\text{P}$  signal. It should be noted that in samples counted with the LSS, it was possible to remove the contaminants  $^{210}\text{Pb}$  and  $^{210}\text{Bi}$  by restricting the regions of interest, although this restriction resulted in loss of counting efficiency.

**Chemical purification yields and blanks:** Yields of chemical purification ranged from 50-100%, but were typically greater than 80%. Most of the phosphorus lost in the chemical purification procedure occurred during the di-isopropyl ether extractions, where some phosphate partitioned into the ether phase with the iron. Further P loss occurred due to absorption onto the walls of the glass beaker if samples were allowed to go dry and bake during the evaporation steps. Iron impregnated filters were chemically processed and counted on the liquid scintillation counter to determine both stable and  $^{32}\text{P}$  and  $^{33}\text{P}$  backgrounds. Radioactive phosphorus activities were below detection and background counts were, within counting statistics, the same as the Ultima Gold AB scintillation cocktail.

Stable P blanks, while less than 1  $\mu\text{M}$  for the chemicals used in purification, were significant, although reproducible, ( $7.51 \pm 1.18 \mu\text{Mol P/g Fe(OH)}_3$ ) for the iron impregnated polypropylene filters. This P blank was equivalent to < 10% of the total stable P spike added to rain, but close to 25% of the total measured natural stable P levels in high TDP ( $\approx 1.25 \mu\text{M}$ ) seawater samples. This would pose a problem for tracking total yields of samples retrieved from oligotrophic marine environments, as the blank stable P could be considerably greater than the actual P in the sample. Most of the stable P contamination appeared to come from the polypropylene filters. Repeated extraction of the polypropylene filters with hot 8N HCl did not reduce stable P levels to any extent. However, extraction with 6.25N NaOH at high temperatures and the utilization of  $\text{FeCl}_3$  extracted with di-isopropyl ether, reduced the stable P on the iron coated polypropylene filters to  $2.50 \pm 0.27 \mu\text{Mol P/gm Fe(OH)}_3$ .

## INSTRUMENTATION

**Background.** As stated previously, liquid scintillation counting has tremendous advantages over conventional beta counting because it allows for higher efficiencies in counting and the ability to count both isotopes simultaneously. All of our samples were counted using a Packard Tri-Carb 2770 TR/SL LSS (Packard Instrument Company). This particular instrument has been specifically designed for counting low level radioactive samples by utilizing both burst counting circuitry (BCC) in and a newly developed high density, high  $\gamma$  cross section detector guard consisting of bismuth germanate,  $\text{Bi}_4\text{Ge}_3\text{O}_{12}$  (BGO), to reduce background<sup>22</sup>. In liquid scintillation counting, background consists of both quenchable (32%) and unquenchable (68%) events. Quenchable background is caused by the interaction of high energy cosmic rays interacting directly with the scintillation cocktail to produce photons similar those produced by radioactive sample decay. Unquenchable background events, principally Cerenkov events, are caused by cosmic ray interactions with the vial wall and photomultiplier tubes.

Cosmic rays interact with the BGO guard to produce scintillations which primarily consist of a single burst followed by a number of after-pulses which can last up to 5  $\mu$ s. In general, a larger number of after-pulses will occur after an unquenchable event, than after a true scintillation event, especially for low energy beta events. The Packard 2770 TR/SL reduces background via burst counting circuitry which discriminates against unquenchable background by rejecting those events with after-pulses which exceed a user determined, delay before burst (DBB), preset threshold. This threshold has a preset range between 75 and 800 ns. Thus, after-pulses resulting from the interaction of cosmic rays with the BGO guard can be eliminated by adjusting the DBB. Furthermore, the BGO guard passively reduces background by preventing some cosmic rays from reaching the sample.

**Instrument Optimization.** Optimization of the LSS was conducted using known amounts of  $^{32}\text{P}$  and  $^{33}\text{P}$  tracer. Both radioisotopes are commercially available from New England Nuclear Life Sciences Products and are certified to within 1% at the  $\mu$ curie level ( $2.22 \times 10^6$  dpm). However, because our laboratory was interested in measuring much lower activities, a more precise measurement of  $^{32}\text{P}$  and  $^{33}\text{P}$  activity was necessary. Briefly, known aliquots of  $^{32}\text{P}$  and  $^{33}\text{P}$  ranging between 30 to 100 dpm were evaporated on stainless steel planchettes and counted on  $2\pi$  Riso anticoincidence low level beta detectors<sup>11</sup>. Measurement of  $^{32}\text{P}$  was conducted with an external Al foil ( $18 \text{ mg/cm}^2$ ), in order to block beta emission from any longer lived  $^{33}\text{P}$  impurities contained within the  $^{32}\text{P}$  solution. Efficiencies of  $^{32}\text{P}$  and  $^{33}\text{P}$  were then determined by using calibrated beta emitting analogs,  $^{147}\text{Pm}$  ( $E_{\text{max}} = 0.224$ ) for  $^{33}\text{P}$ , and  $^{234}\text{Pa}$  ( $E_{\text{max}} = 1.13$ ) for  $^{32}\text{P}$  counted under similar geometries. Efficiencies were  $28.5 \pm 0.3\%$  and  $55 \pm 0.4\%$  respectively, very similar to those found previously<sup>11</sup>.

Once the  $^{32}\text{P}$  and  $^{33}\text{P}$  activities were determined, it was possible to maximize the LSS settings for simultaneous measurement of  $^{32}\text{P}$  and  $^{33}\text{P}$ . High activity, 30 - 50 dpm, samples were counted on the LSS in low level count mode with the static controller on, over a range of DBB settings. The goal was to maintain the lowest possible background (B) while still maintaining high efficiency (E), such that the figure of merit ( $E^2/B$ )<sup>22</sup> was



maximized for both the low energy beta emitter  $^{33}\text{P}$  and the high energy beta emitter  $^{32}\text{P}$ . Based on this parameter, a DBB of 450 ns was chosen.

**Quench Correction.** During evaporation and transfer of the sample to a LS vial, it was found that small amounts of residual acid caused variable levels of quench. Sample size did not appear to be as significant. Simply put, quench is a measure of the photon production within the sample system, such that the higher quench, the fewer photons are produced, and hence the lower the counting efficiency. Quench further causes the  $^{32}\text{P}$  and  $^{33}\text{P}$  LS peaks to shift to lower energies within the chosen energy regions of interest. In the Tri-Carb 2770 TR/SL the degree to which sample quenching occurs is parameterized by the tSIE value, or the transformed spectral index of an external standard,  $^{133}\text{Ba}$ . This parameter is a function of the endpoint of the external standard and varies from 1000, no sample quenching, to 0, for a fully quenched sample<sup>22</sup>. Because of the variances in quench and its effect on efficiency, it is critical to generate quench curves, i.e. standards of similar activity, but quenched to different degrees. We utilized both 8N  $\text{HNO}_3$  and 8N  $\text{HCl}$  as quenching agents in all of our quench curves. Separate curves were made with Ultima Gold AB Cocktail spiked with either  $^{32}\text{P}$  or  $^{33}\text{P}$ .

Our samples also tended to be of very low activity. Thus, an additional 'blank' quench correction curve, Ultima Gold AB with quenching agent only, was necessary. As expected, efficiencies changed relative to the given quench level and chosen region of interest (Fig. 4a,b). It should be noted that changing these regions will influence the efficiency curve. Thus, care must be taken to choose regions appropriate for differing sample quenches. In rain samples, tSIE values ranged from 100 - 480, while in seawater samples, tSIE values ranged from 90 - 350, primarily due to variations in acidity and, in the case of seawater, substantially higher concentrations of trace constituents, such as  $\text{Fe(II)}$ . Quench values between repeat counts normally did not vary by more than 10 tSIE units. If larger variations in tSIE occurred, individual counts were converted to activities prior to decay curve analysis.  $^{32}\text{P}$  and  $^{33}\text{P}$  efficiencies ranged between 50 - 70% and rarely

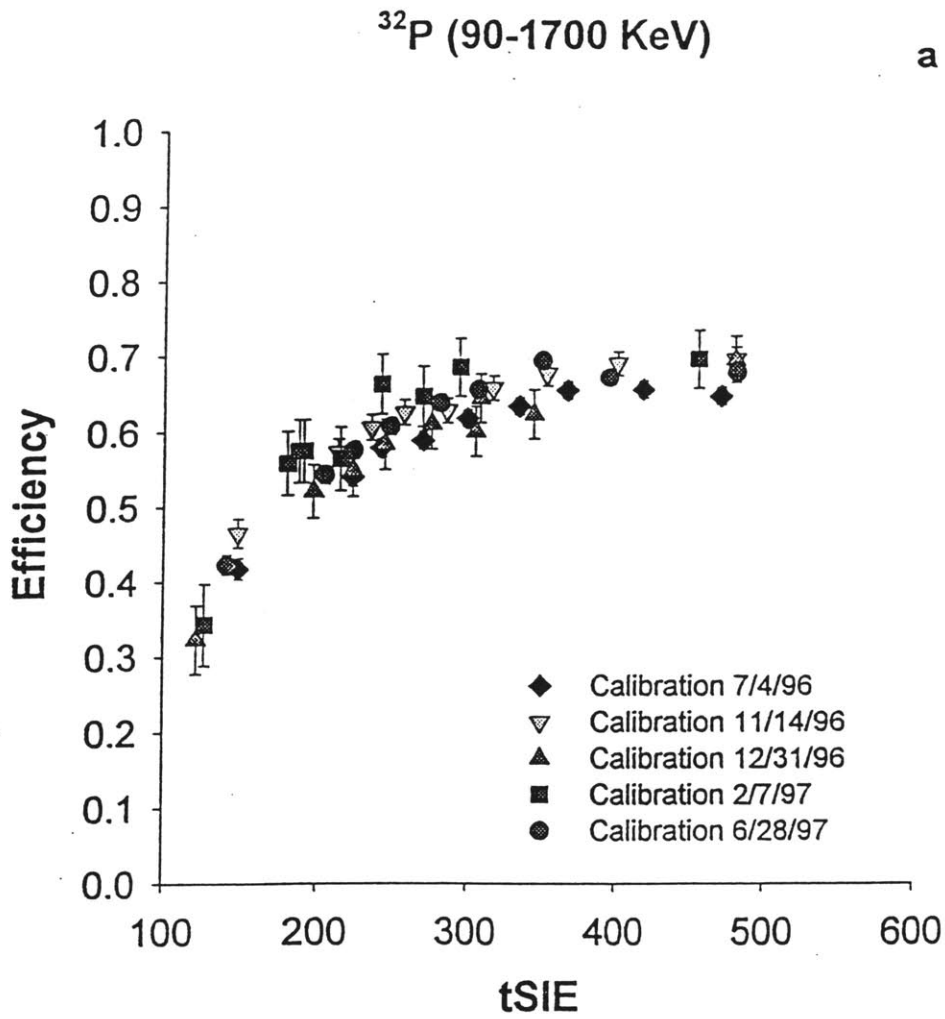
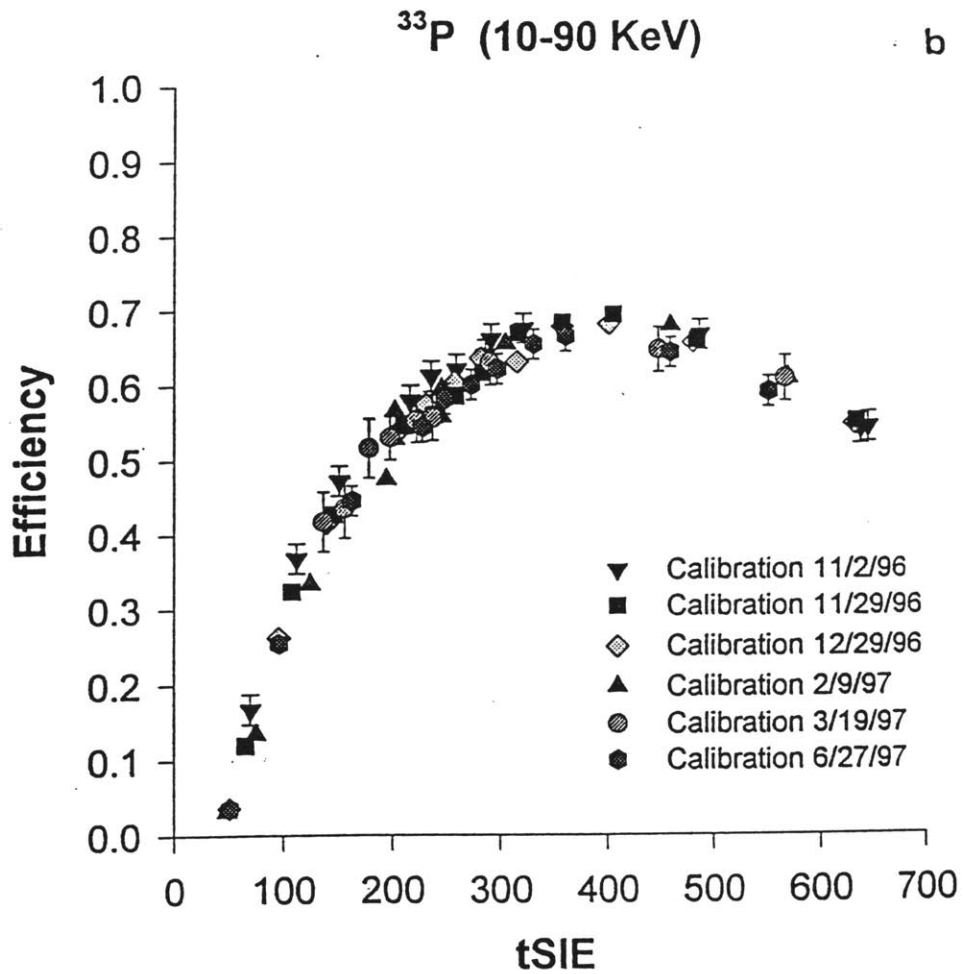


**Figure 2.4** Quench curves for a)  $^{32}\text{P}$  (90-1600 KeV) and b)  $^{33}\text{P}$  (10-90 KeV), over the last 6 months. Error bars are determined from counting statistics.



varied by more than 2.5% ( $2\sigma$ ) between counts. Regions of interest were selected so as to maintain both  $^{32}\text{P}$  and  $^{33}\text{P}$  efficiencies greater than 50% in all samples.

The  $^{32}\text{P}$  and  $^{33}\text{P}$  quench correction curves further allowed for determination of the amount of  $^{32}\text{P}$  in the  $^{33}\text{P}$  region of interest. Because of the asymmetrical nature of LSS peaks, the amount of activity of  $^{32}\text{P}$  falling in the  $^{33}\text{P}$  region (10-90 keV), needed to be determined (Fig. 5). In most of our samples, the contribution of  $^{32}\text{P}$  in the  $^{33}\text{P}$  window normally did not exceed 10% of the corrected  $^{33}\text{P}$  activity. This correction was determined by analyzing the distribution of  $^{32}\text{P}$  and  $^{33}\text{P}$  counts within each region of interest over the range of sample quench values. In essence, the activity of  $^{32}\text{P}$  and  $^{33}\text{P}$  can be described by the following two equations<sup>23</sup>:

$$^{32}\text{P (dpm/L)} = (A \ ^{33}\text{E}_{(90-1700\text{keV})} - B \ ^{33}\text{E}_{(10-90 \text{KeV})}) / ( \ ^{33}\text{E}_{(10-90 \text{KeV})} \ ^{32}\text{E}_{(90-1700 \text{KeV})} - \ ^{33}\text{E}_{(90-1700\text{keV})} \ ^{32}\text{E}_{(10-90 \text{KeV})} ) \quad (1)$$

$$^{33}\text{P (dpm/L)} = (A \ ^{32}\text{E}_{(90-1700\text{keV})} - B \ ^{32}\text{E}_{(10-90 \text{KeV})}) / ( \ ^{33}\text{E}_{(10-90 \text{KeV})} \ ^{32}\text{E}_{(90-1700 \text{KeV})} - \ ^{33}\text{E}_{(90-1700\text{keV})} \ ^{32}\text{E}_{(10-90 \text{KeV})} ) \quad (2)$$

where A is the net cpm (total - blank) in the 10-90 KeV region, B is the net cpm in the 90-1700 KeV region and  $^{32}\text{E}$  and  $^{33}\text{E}$  are the  $^{32}\text{P}$  and  $^{33}\text{P}$  counting efficiencies in either the specified 10-90 or the 90-1700 KeV regions. Equations 1 and 2 are significantly simplified in our analyses since the  $^{32}\text{P}$  window is set to exclude the majority of decay events from  $^{33}\text{P}$ . The simplified versions of the  $^{32}\text{P}$  and  $^{33}\text{P}$  activity equations are as follows:

$$^{32}\text{P (dpm/L)} = (A \ ^{33}\text{E}_{(90-1700\text{keV})} - B \ ^{33}\text{E}_{(10-90 \text{KeV})}) / ( \ ^{33}\text{E}_{(10-90 \text{KeV})} \ ^{32}\text{E}_{(90-1700 \text{KeV})} ) \quad (3)$$

$$^{33}\text{P (dpm/L)} = B / \ ^{32}\text{E}_{(90-1700 \text{KeV})} \quad (4)$$

Rain Collected 6/17/97

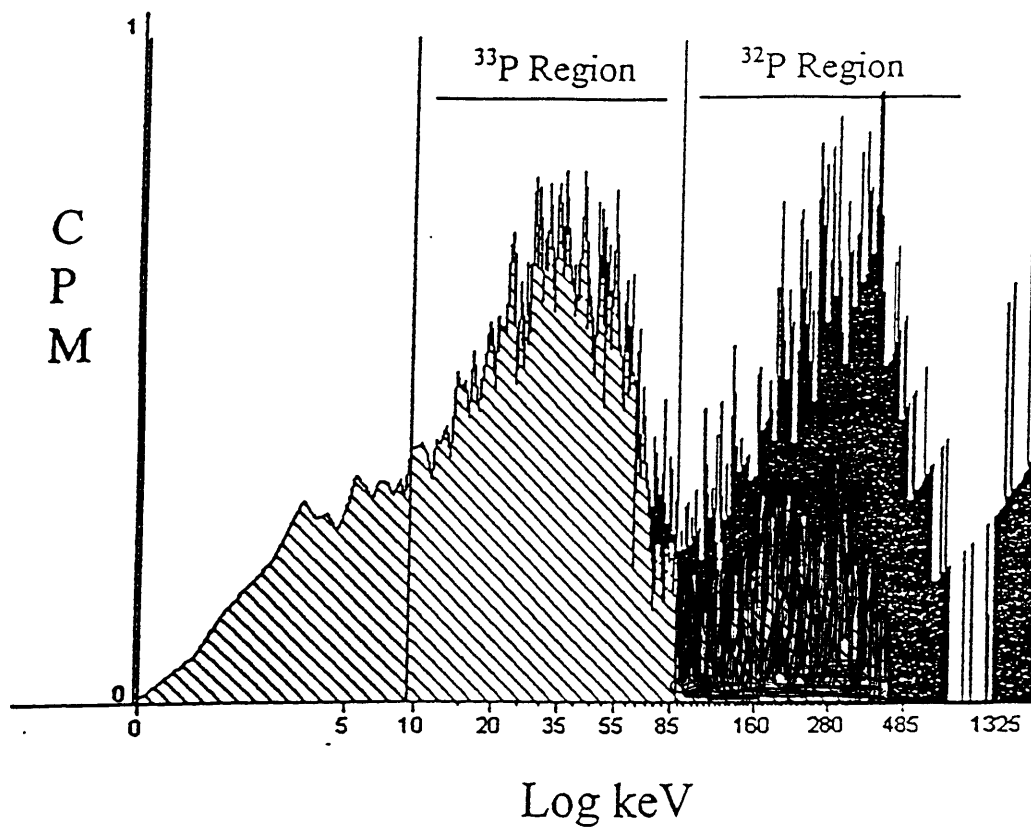


**Figure 2.5** Liquid scintillation spectra of a rain sample collected at WHOI. Spectra is shown in cpm versus log KeV in order to better show the separation of the two P isotopes.

**Instrument Stability.** Quench curves and Ultima Gold AB blanks were run repeatedly over the course of one year. Efficiencies for both  $^{32}\text{P}$  and  $^{33}\text{P}$  changed by less than 5% with tSIE (Fig. 4). Small variations were probably more likely due to the use of different stock solutions, which were each calibrated separately, and to slight variances in pipetting and LSS vials, rather than to the actual instrument variability. Instrument blanks varied between regions of interest, but remained very stable within a given region. For example, over the course of 6 months, 5 ml of Ultima Gold AB scintillation cocktail (tSIE  $\approx 645$ ) was counted for 300 minutes once a week. Blank cpm in the 10-90 keV window averaged  $0.95 \pm 0.05$  cpm, while blank cpm in the 90-1700 keV window averaged  $0.89 \pm 0.09$  cpm.

**Counting Procedure and Limit of Detection.** Rain and seawater samples were counted with the low level mode and static controller on, and a DBB of 450 ns. Samples were dark adapted for six hours, allowed to cool to ambient LSS temperature, and counted repeatedly (5-10 times) over the course of one to two months for a period of 300 minutes. In this manner, it was possible to compare known and measured half-lives. Count times were shorter than optimal due to the large number of samples which needed to be counted over the relatively short decay period of time. As a result, the minimum detectable count rate at the 95% confidence limit,  $L_d$ , was limited to 0.3 cpm for both  $^{32}\text{P}$  and  $^{33}\text{P}$  in our samples<sup>24</sup>. In this scenario,  $L_d$  is defined by the following:

$$L_d = (2.71 + 4.65 * \mu_b^{0.5}) / T$$

where  $T$  is the total count time in minutes and  $\mu_b$  is the mean number of total background counts registered within the region of interest during the same counting period. For our samples, increasing counting times to 1440 min (24 hours) reduces the limit of detection by 50%, but does not allow for adequate half-life resolution. Assuming total purity of  $^{32}\text{P}$  and  $^{33}\text{P}$ , the ultimate detection limit of  $^{32}\text{P}$  and  $^{33}\text{P}$  by ultra low level liquid scintillation counting is 0.1 and 0.18 cpm, or twice the standard deviation of the background cpm within the  $^{33}\text{P}$  and  $^{32}\text{P}$  regions of interest (10-90 keV, 90-1700 keV), respectively.

## DATA ANALYSIS, SOURCES OF ERROR, AND REPRODUCIBILITY

Each sample was counted 5-10 times and the counts corrected for  $^{32}\text{P}/^{33}\text{P}$  overlap. The activity of  $^{32}\text{P}$  and  $^{33}\text{P}$  at sample collection was then determined using the characteristic half-life of each isotope and a weighted nonlinear least squares curve fitting routine. Calculated backgrounds were then compared with that of the known scintillation cocktail blank at a given quench. Use of the curve fitting procedure significantly improved precision and reduced the uncertainty associated with the sample and detector background. Furthermore, it enabled us to determine if there were any other beta emitting isotopes in the sample which would interfere with the background and/or the half-life fit.

All of the  $^{32}\text{P}$  and  $^{33}\text{P}$  data are decay corrected to the midpoint of the collection period. The error on each  $^{32}\text{P}$  and  $^{33}\text{P}$  activity measurement is produced from the propagation of uncertainties from the nonlinear least squares curve fit, detector calibration, and chemical recoveries. Overall errors for  $^{32}\text{P}$  and  $^{33}\text{P}$  activities measured in rain samples are between 3-10%. Larger errors are associated with those rain samples having low chemical recoveries (< 10%), incomplete removal of  $^{210}\text{Pb}$  and  $^{210}\text{Bi}$  (earliest collected rain samples), or low number of repeat counts (< 3). Seawater samples, generally had larger errors between 8-25%, predominantly due to the extremely low natural  $^{32}\text{P}$  and  $^{33}\text{P}$  activities (0.89-32.08 cpm) and our inability to count samples for a longer length of time.

In order to confirm the reproducibility of our  $^{32}\text{P}$  and  $^{33}\text{P}$  activity measurements, two rain samples, one with high total P activity (collected 5/9/97), the other with relatively low total P activity (collected 5/10/97), were spiked with stable phosphorus and split into three unequal fractions. Each fraction was then passed through a set of iron filters, purified, and counted on the LSS. tSIE values in the three 5/9/97 rain fractions varied (200-280), such that the chosen  $^{32}\text{P}$  and  $^{33}\text{P}$  regions, efficiency, and background, were different between each fraction. Results of both rain samples are shown in Figure 6. There is no difference in the calculated  $^{32}\text{P}$  or  $^{33}\text{P}$  activity regardless of volume, chemical blank, or efficiency correction.

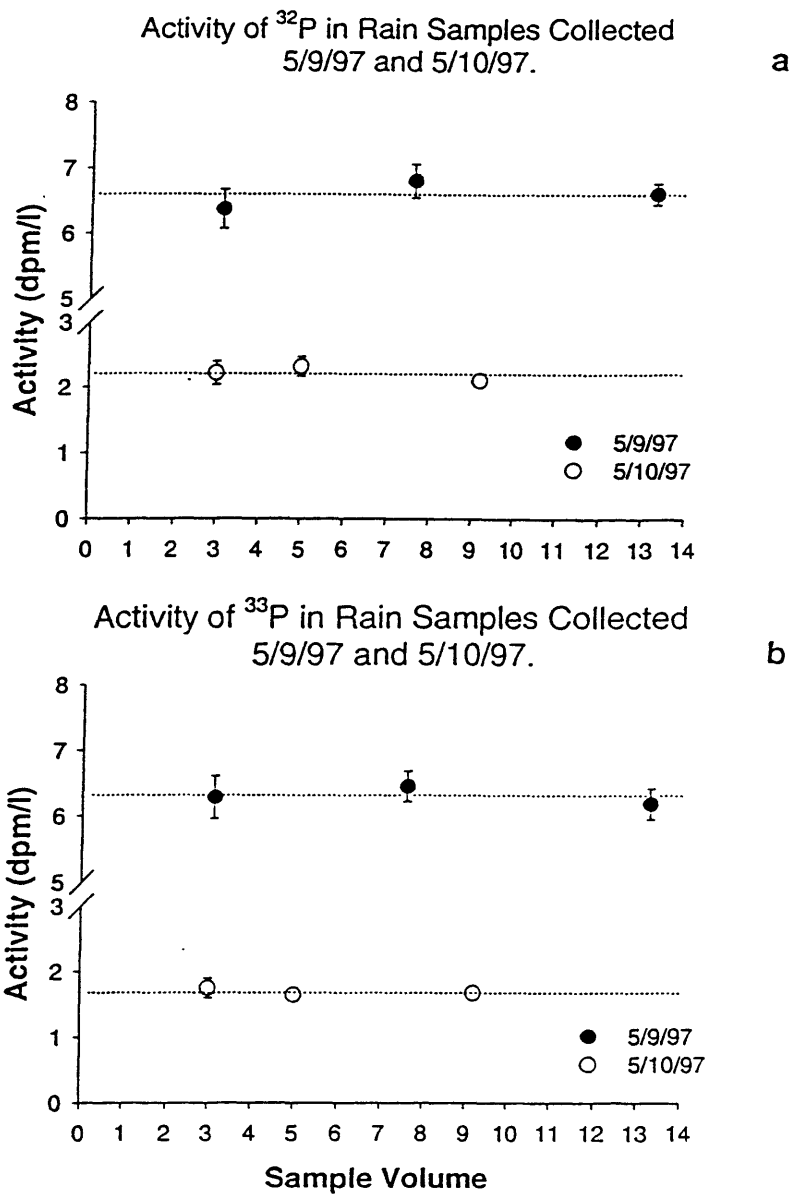


**Figure 2.6** Activity of  $^{32}\text{P}$  and  $^{33}\text{P}$  for two rain samples collected 5/9/97 (filled circles) and 5/10/97 (open circles) and split into three unequal portions (Sample Volume). Dashed lines represent average values. A)  $^{32}\text{P}$  (dpm/L), B)  $^{33}\text{P}$  (dpm/L).



## RESULTS

**Rain.** Results of several rain samples collected during single rain events in June and July of 1996 from the roof of Clark Laboratory at the Woods Hole Oceanographic Institution are shown in Table 1. These rain samples were chosen to help illustrate the variation in chemical yield and the tSIE values encountered. In our rain samples, chemical recoveries were typically greater than 80%, with tSIE values averaging  $310 \pm 75$ . Specific activities of  $^{32}\text{P}$  and  $^{33}\text{P}$  ranged from 0.5 to 4.1 dpm/L, in *single* rain events, slightly higher than the average range of activities measured previously<sup>1,2,4-6</sup>. This is most likely due to both the higher  $^{33}\text{P}$  efficiency achieved in LSS and the identification and removal of contaminants. Ingrowth of the contaminant  $^{210}\text{Bi}$  will decrease the rate of the 'apparent' decay of  $^{32}\text{P}$ . The average ratio of  $^{33}\text{P}/^{32}\text{P}$  was fairly constant over the 1 month period averaging  $0.80 \pm 0.09$ , quite similar to the  $0.82 \pm 0.13$  measured previously in a combined two week sample by GM-C at WHOI in April of 1991<sup>2</sup>. Our rain data again indicate the higher precision and accuracy capable with LSS.

**Marine Samples.** Results are also given for some measurements of marine particulates and dissolved phases of seawater, collected in Wilkinson Basin in the Gulf of Maine during two cruises conducted in March and April of 1997 (Table 2). Chemical recoveries were typically greater than 80%. These samples represent the first  $^{32}\text{P}$  and  $^{33}\text{P}$  activities to be measured in a coastal, high P environment. The marine particulate and dissolved samples resulted from filtration of 4300-6500 L of seawater. In these surface TDP samples, no breakthrough of P occurred. However, in one of the deep TDP samples (not shown here), breakthrough did occur in one of the three, 2 l extraction tubes, most likely due to higher deep silicate concentrations. Regardless, breakthrough of DIP (< 20% of the total), and DOP (< 35% of the total) in the tube, occurred towards the end of the filtration period, such that less than 20% of the *total* sample volume was affected. Slightly larger collection tubes will alleviate this small problem in the future. Dissolved surface activities of  $^{32}\text{P}$  and  $^{33}\text{P}$  ranged from 1.5 to 5.6 dpm/m<sup>3</sup>.

**Table 1.**  $^{32}\text{P}$  and  $^{33}\text{P}$  activities in individual rain events collected during June and July of 1996 at the Woods Hole Oceanographic Institution (WHOI, 41°32.11'N, 70°38.89'W). Absolute errors are  $2\sigma$ .

Sample	tSIE	Chemical	$^{33}\text{P}$	$^{32}\text{P}$		$^{33}\text{P}/^{32}\text{P}$	$\pm$ Error	
		Yield (%)	dpm /L	$\pm$ Error	dpm/L			
6/17/96	312	78.5	3.27	0.17	3.86	0.12	0.84	0.05
6/20/96	305	84.0	1.12	0.11	1.63	0.08	0.69	0.08
6/22/96	320	85.7	3.87	0.10	4.10	0.18	0.94	0.05
7/1/96	275	43.8	2.42	0.12	3.09	0.10	0.78	0.05
7/12/96	477	31.6	0.54	0.05	0.61	0.06	0.88	0.12
7/15/96	452	66.0	0.58	0.05	0.74	0.04	0.79	0.08
7/19/96	158	90.8	1.38	0.05	2.01	0.09	0.69	0.04

**Table 2.**  $^{32}\text{P}$  and  $^{33}\text{P}$  activities in selected samples collected during March and April of 1997 from Wilkinson Basin, the Gulf of Maine (42°29.41'N 69°45.02'W). Absolute errors are  $2\sigma$ .

Sample	Volume liters	Chemical Yield (%)	$^{33}\text{P}$ dpm/m <sup>3</sup>	$\pm$ Error	$^{32}\text{P}$ dpm/m <sup>3</sup>	$\pm$ Error	$^{33}\text{P}/^{32}\text{P}$	$\pm$ Error
March, 5m, TDP	4334	90.2	4.56	0.79	5.60	0.97	0.82	0.20
April, 5m, TDP	6492	82.1	3.11	0.47	3.61	0.57	0.86	0.19
March, 5m, Suspended Matter (10-102 $\mu\text{m}$ )	4334	99.0	0.51	0.13	0.70	0.18	0.73	0.26
			dpm/mg P		dpm/mg P			
April, 0-110 m, Integrated Plankton Tow (> 335 $\mu\text{m}$ )		86.8	0.28	0.02	0.23	0.01	1.23	0.12

These activities are similar in magnitude, but higher than the surface  $^{32}\text{P}$  activities of 0.2 to 2.0 dpm/m<sup>3</sup> found off the coast of California<sup>7,8,10</sup>. This is easily explained by the higher input fluxes of  $^{32}\text{P}$  and  $^{33}\text{P}$  activity found in rain at the Gulf of Maine site and the ability to measure  $^{33}\text{P}$  with better efficiency. The measured ratio of  $^{33}\text{P}/^{32}\text{P}$  found in the dissolved constituent of seawater and in the in the  $>10\ \mu\text{m}$  particulate fraction are similar to that found in rain, indicating rapid turnover of P on the order of a few days. The activities of  $^{32}\text{P}$  and  $^{33}\text{P}$  and the ratio of  $^{33}\text{P}/^{32}\text{P}$  found in the  $> 335\ \mu\text{m}$  plankton sample are also within the range of activities found previously<sup>7,8,11,12</sup>.

The ratio of  $^{33}\text{P}/^{32}\text{P}$  found in the  $> 335\ \mu\text{m}$  plankton sample was significantly higher,  $1.23 \pm 0.12$ , than that found in the dissolved and particulate seawater fractions. This difference in activity ratio provides a powerful tool for determining the relative *in situ* turnover times of P between plankton and dissolved seawater. Using a simple continuous uptake model, described in detail by a previous researcher<sup>2</sup>, the average residence time of P in the  $> 335\ \mu\text{m}$  plankton is 46 days. In contrast, if plankton ingest P early during their life time, and then stop feeding, the residence time of P, described by a simple age decay equation<sup>2</sup>, is 17 days. More intensive models which include the speciation or life cycles of the collected plankton, and the cycling of P within the smaller size fractions, i.e. bacterial pools, will substantially increase our knowledge of P cycling in coastal marine environments.

## CONCLUSIONS

A new technique for the collection, purification, and measurement of  $^{32}\text{P}$  and  $^{33}\text{P}$  in rain and in various phases of marine systems is described. For the first time, it is now possible to measure  $^{33}\text{P}$  and  $^{32}\text{P}$  in *single* rain events and in coastal marine environments with *high* stable P concentrations. We have demonstrated that it is now possible to measure these isotopes with significantly higher accuracy than prior work. Ultra low level liquid scintillation counting is a substantial improvement over low level beta counters, since it allows for the simultaneous measurement of  $^{32}\text{P}$  and  $^{33}\text{P}$ , and high counting efficiency of  $^{33}\text{P}$ , regardless of the amount of stable P. It has enabled us to quantify and remove previously unidentified beta emitting contaminants from our samples. The use of

iron-coated polypropylene is also an improvement over previously used extraction methods in that it is possible to load twice the amount of  $\text{Fe}(\text{OH})_3$  on the filters. Furthermore, this material combusts cleanly to  $\text{CO}_2$  at high temperatures, reducing sample processing and increasing chemical recovery.

The ability to easily measure  $^{32}\text{P}$  and  $^{33}\text{P}$  in single rain events with high precision and accuracy will enable these isotopes to be used much more successfully in atmospheric chemistry studies, especially those characterizing tropospheric air mass and/or aerosol residence times, and the extent of stratospheric intrusion. The application of this newly developed technique in marine studies, however, is even more significant. The biogeochemical cycling of phosphorus within the euphotic zone can now be elucidated to a much higher degree with the additional measurement of  $^{33}\text{P}$ , especially in coastal environments where nutrient uptake and export are greatest.

## **ACKNOWLEDGEMENTS**

The authors wish to thank J. E. Andrews, III and Lary A. Ball for their help and insightful comments in the development of the phosphorus isotope method. The authors would also like to thank Dr. D. Glover, Dr. K. C. Ruttenburg, and B. Benitez-Nelson for comments pertaining to the manuscript. This work was funded in part by the Office of Naval Research Fellowship Program, STAR Environmental Protection Agency Fellowship Program, National Science Foundation (Grant no. OCE-9633240), and the Woods Hole Oceanographic Institution (unrestricted funds).

## REFERENCES

- (1) Lal, D.; Peters, B. In *Handbuch der Physik* 46/2, Flugge, S., Ed.; Springer Verlag, New York, 1967; pp. 551-612.
- (2) Waser, N. A. D. Ph.D. Thesis, MIT/WHOI, 1993.
- (3) Waser, N. A. D.; Bacon M. P. *Geophys. Res. Lett.* 1994, 21, 991-994.
- (4) Goel, P.S.; Rama Thor; Zutshi, P. K. *Tellus.* 1959, XI, 91-100.
- (5) Bhandari, N.; Lal, D.; Rama Thor *J. of Geophys. Res.* 1970, 75(15), 2974-2980.
- (6) Walton, A; Fried, R. E. *J. of Geophys. Res.* 1962, 67(13), 5335-5340.
- (7) Lal, D.; Lee, T. *Nature* 1988, 333, 752-754.
- (8) Lal, D.; Chung, Y.; T. Platt, T.; Lee, T. *Limnol. Oceanogr.* 1988, 33(6, part 2), 1559-1567.
- (9) Lee, T.; Barg, E.; Lal, D. *Limnol. Oceanogr.* 1991, 36(5), 1044-1053.
- (10) Lee, T; Barg, E.; Lal D. *Anal. Chim. Acta* 1992, 260, 113-121.
- (11) Waser, N. A. D.; Fleer, A. P.; Hammer, T. R.; Buesseler, K. O.; Bacon, M. P. *Nucl. Instr. and Meth. in Phys.* 1994, A388, 560-567.
- (12) Waser, N. A. D.; Bacon, M. P.; Michaels, A. P. *Deep-Sea Res.* 1996, 43(2-3), 421-436.
- (13) Lal, D.; Rama Thor; Zutshi, P. K. *J. of Geophys. Res.* 1960, 65(2), 669-673.
- (14) Lal, D.; Schink, D. *Rev. Sci. Instru.* 1960, 31, 395-398.
- (15) Duce, R. A. In: *The Role of Air-Sea Exchange in Geochemical Cycling*; Buat-Menard, P., Ed.; D. Reidal Publishing Co.; 1986, pp. 497-529.
- (16) Koroleff, F. In: *Methods of Seawater Analysis*; Grasshoff, K., Ehrherd, M., Kremling, K. Eds.; Verlag Chemie, Weinheim, 1983; 2<sup>nd</sup> edition, pp. 125-135.
- (17) Krishnaswami, S.; Lal, D.; Somayajulu, B. L. K.; Dixon, F. S.; Stonecipher, S. A; Craig, H. *Earth and Planet. Sci. Lett.* 1972, 16, 84-90.
- (18) Dibb, J. E. *J. of Geophys Res.* 1989, 94, 2261-2265.
- (19) Strickland, J. D. H.; Parsons, T. R. In: *A Practical Handbook of Seawater Analysis*; Fisheries Research Board of Canada, Ottawa, 1972; 2<sup>nd</sup> edition, 310 pp.
- (20) Karl-Kroupa, E.; Van Wazer, J. R.; Russell, C. H. In: *Scott's Standard Methods of chemical analysis*; Furman, N. H. Ed.; D. Van Nostrand Co., Inc., Princeton, New Jersey; 1961; Vol. 1, pp.809-813.
- (21) Whaley, T. P.; Ferrara, L. W. In: *Environmental Phosphorus Handbook*; Griffith, E. J., Beeton, A., Spencer, J. M., Mitchell, D. T., Eds.; Wiley, New York, 1973; 313 pp.
- (22) Passo, C. J.; G. T. Cook *Handbook of environmental liquid scintillation spectrometry. A compilation of theory and methods* Packard Instruments, Meriden, CT, 1992; pp 1-1 - 1-15.
- (23) Klein, P. D.; Eisler, W. J. *Analytical Chemistry* 1966, 38, 1453-1460.
- (24) Currie, L. A. *Analytical Chemistry* 1968, 40(3), 586-593.

## Chapter 3

### **$^{32}\text{P}$ , $^{33}\text{P}$ , $^7\text{Be}$ , and $^{210}\text{Pb}$ as Tracers of Aerosol Residence Times and Stratosphere/Troposphere Exchange**

#### **ABSTRACT**

The deposition of  $^{32}\text{P}$ ,  $^{33}\text{P}$ ,  $^7\text{Be}$ , and  $^{210}\text{Pb}$  was measured in individual rain events at Woods Hole, MA from March, 1996 to February, 1998 and in bi-monthly integrated samples from Portsmouth, NH, from March to November, 1997. Annual depositional fluxes of  $^{32}\text{P}$  and  $^{33}\text{P}$  were 1781 and 1653 disintegrations per minute (dpm)  $\text{m}^{-2} \text{yr}^{-1}$ , respectively, at Woods Hole and 2123 and 1752 dpm  $\text{m}^{-2} \text{yr}^{-1}$  at Portsmouth.  $^7\text{Be}$  and  $^{210}\text{Pb}$  fluxes averaged 12.8 and 1.43 dpm  $\text{cm}^{-2} \text{yr}^{-1}$ , respectively, at Woods Hole and 16.6 and 0.95 dpm  $\text{cm}^{-2} \text{yr}^{-1}$ , at Portsmouth. Absolute activities and radionuclide ratios indicate that simple models of cosmogenic production and removal from a single airmass are insufficient to describe tropospheric aerosol residence times; mixing of airmasses containing different activities need to be included. In addition, fractionation appears to be occurring among phosphorus, beryllium and lead between time of production and atmospheric removal via precipitation. High ratios of  $^{33}\text{P}/^{32}\text{P}$  in our samples suggest that these isotopes can trace stratosphere/troposphere exchange, especially during severe storms, such as hurricanes.

## INTRODUCTION

Naturally produced radionuclides have proven to be useful tracers of a wide range of atmospheric processes (Bhandari *et al.*, 1966, 1970; Luyanus *et al.*, 1970; Viezee and Singh, 1980; Dibb *et al.*, 1992). These elements are particularly powerful in that they enable one to estimate mean in situ rates of processes which vary in space and time. In many cases, the radionuclide production rates are known and they are generally impervious to analytical contamination. Beryllium-7 ( $t_{1/2} = 53.3$  days) and Lead-210 ( $t_{1/2} = 22.3$  years), are two radionuclides which have been used to study aerosol residence times and air mass sources (Lal, 1958; Lal *et al.*, 1960; Bhandari *et al.*, 1966, 1970; Luyanas *et al.*, 1970; Dutkiewicz and Hussain, 1978, 1985; Dibb *et al.*, 1992; Baskaran *et al.*, 1993; Baskaran, 1995). In this investigation, we have included the additional measurement of phosphorus-32 ( $t_{1/2} = 14.3$  days), and phosphorus-33 ( $t_{1/2} = 25.3$  days). Our study encompasses, for the first time, the simultaneous measurement of  $^{32}\text{P}$ ,  $^{33}\text{P}$ ,  $^7\text{Be}$ , and  $^{210}\text{Pb}$  in individual rain events in order to determine day-to-day variability in radionuclide fluxes, and the feasibility of using these isotopes to determine aerosol scavenging and air mass mixing over short time scales.

The residence time of aerosols and the processes which control air mass mixing events, such as stratosphere/troposphere exchange (STE), are of significant interest for elucidating the atmospheric cycling of many natural and anthropogenically produced trace elements. Many of these elements may play a significant role in controlling radiative forcing, and thus, provide a mechanism for inducing global climate change (Ramaswamy *et al.*, 1992; Toumi *et al.*, 1994). In addition, upward transport of anthropogenic trace chemical species, such as CFC's and other halocarbons, from the troposphere into the stratosphere, is one of the major causes of stratospheric ozone depletion (*World Meteorological Organization (WMO)*, 1995). Downward transport from the stratosphere into the troposphere is a major removal pathway for many stratospheric components, including ozone and other reactive constituents.



$^{32}\text{P}$ ,  $^{33}\text{P}$ , and  $^7\text{Be}$  are formed by cosmic ray spallation of atmospheric argon ( $^{32}\text{P}$  and  $^{33}\text{P}$ ), oxygen and nitrogen ( $^7\text{Be}$ ) (Lal and Peters, 1967). Production rates, while highest in the stratosphere (between 15-20 km), decrease with decreasing altitude (Lal and Peters, 1967) such that in the troposphere, the rate of  $^{32}\text{P}$ ,  $^{33}\text{P}$ , and  $^7\text{Be}$  production is an order of magnitude lower. Short aerosol residence times (<100 days), coupled with strong and rapidly varying tropospheric wind patterns, essentially mask most of the altitude dependence of tropospheric  $^{32}\text{P}$ ,  $^{33}\text{P}$ , and  $^7\text{Be}$  production (Goel *et al.*, 1959; Lal and Peters, 1967; Bhandari *et al.*, 1970). Because the half lives of  $^{32}\text{P}$ ,  $^{33}\text{P}$ , and  $^7\text{Be}$  are short relative to the residence time of stratospheric air (12-14 months), the majority of the activity measured in the troposphere is from tropospheric production only (Lal and Peters, 1967; Bhandari *et al.*, 1970; Reiter, 1975; Turekian *et al.*, 1983; Baskaran *et al.*, 1993). Only during STE events does the stratosphere affect tropospheric radionuclide inventories (Goel *et al.*, 1959; Lal *et al.*, 1960; Walton and Fried, 1962; Viezee and Singh, 1980; Waser and Bacon, 1995).

In contrast,  $^{210}\text{Pb}$  is produced by the decay of Radon-222, an inert gas which enters the troposphere predominantly from continental crust. As a result,  $^{210}\text{Pb}$  concentrations are typically higher at lower altitudes and over continental regions (Moore *et al.*, 1973; Turekian *et al.*, 1977).  $^{32}\text{P}$ ,  $^{33}\text{P}$ ,  $^7\text{Be}$ , and  $^{210}\text{Pb}$  are all particle-reactive radionuclides which become quickly associated with aerosols and are predominantly removed from the atmosphere via wet precipitation (Maenhaut *et al.*, 1979; Bondietti *et al.*, 1988; Baskaran *et al.*, 1993; Waser and Bacon, 1995). Thus, when used in concert, these isotopes may be ideal tracers of the temporal and spatial magnitude of STE.

Until recently, poor  $^{33}\text{P}$  counting efficiencies limited the number of measurements made. Unlike  $^{32}\text{P}$  ( $E_{\text{max}} = 1711 \text{ KeV}$ ),  $^{33}\text{P}$  is a low energy beta emitter, having a maximum energy of only 249 KeV. Previous  $^{33}\text{P}$  measurements were limited by self adsorption, which effectively reduced  $^{33}\text{P}$  counting efficiencies to less than 4%. Atmospheric filter measurements regularly had associated errors greater than 30%, and rain samples often required greater than 20 L of rainwater. As a result, rain samples were generally collected

over two to four week intervals, substantially reducing most STE signals (Goel *et al.*, 1959, Lal *et al.*, 1960, Walton and Fried, 1962, Waser and Bacon, 1995). Additionally, it also appears that many of the previous  $^{33}\text{P}$  and  $^{32}\text{P}$  measurements were contaminated due to incomplete removal of two other decaying radioisotopes,  $^{210}\text{Pb}$  and  $^{210}\text{Bi}$  (Benitez-Nelson and Buesseler, 1998). Recent developments in the collection, purification, and measurement of  $^{33}\text{P}$  and  $^{32}\text{P}$  have substantially improved the ability to accurately measure  $^{32}\text{P}$  and  $^{33}\text{P}$  activities (Benitez-Nelson and Buesseler, 1998).  $^{33}\text{P}$  and  $^{32}\text{P}$  activities can now be determined routinely in single rainfall events.

From March, 1996 to February, 1998 the radionuclides,  $^{32}\text{P}$ ,  $^{33}\text{P}$ ,  $^7\text{Be}$ , and  $^{210}\text{Pb}$  were measured in individual rain events at Woods Hole, MA. Additional samples, integrated over 1-2 week periods, were also measured from March to October 1997 at Portsmouth Harbor, NH. Our results indicate that simple models of cosmogenic production and removal are not sufficient to accurately quantify tropospheric aerosol residence times. Furthermore, fractionation between elements appears to be significant. Of the four isotopes utilized, only the  $^{32}\text{P}$  and  $^{33}\text{P}$  pair can be effectively used to trace STE events, especially during severe storms.

## **MATERIALS AND METHODS**

Bulk precipitation samples, consisting of 3 to 25 L of rainwater, were collected from the roof of Clark Laboratory (height above sea level ~23 m) at the Woods Hole Oceanographic Institution (WHOI), Woods Hole, MA (41°32' N, 70°39'W) and at ground level at the U.S. Coast Guard Station at Portsmouth Harbor, New Hampshire (43°04' N, 70°42' W) (Fig. 1). Both sites are located less than 0.25 miles from the New England coast and are free of surrounding vegetation. No attempt was made to separate wet and dry deposition as both rain collectors were open to the atmosphere at all times. At Woods Hole, the rain collector consisted of 2 x 5 meters of plywood coated by a thin polyethylene sheeting. At Portsmouth, a circular, one meter diameter stainless steel dish was used for collection. At Woods Hole, samples were immediately collected into acid

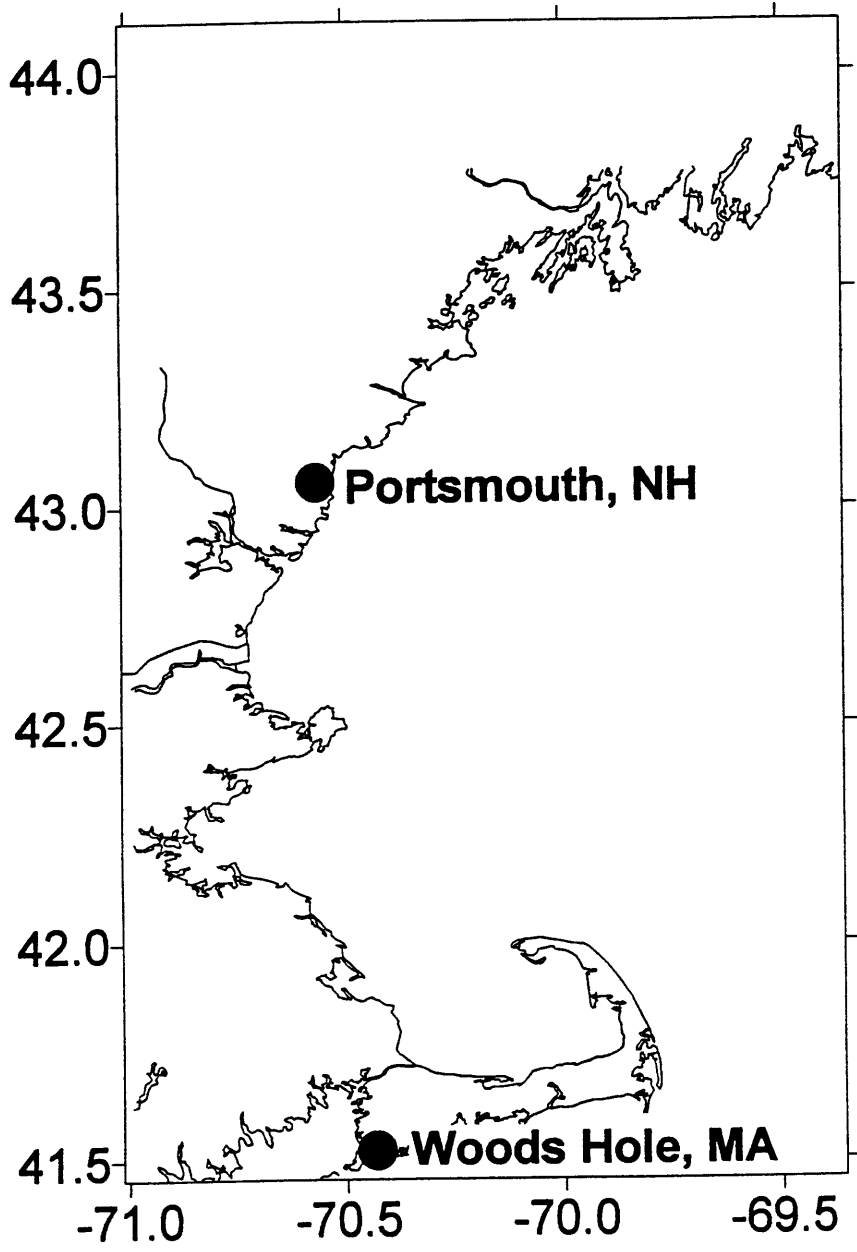


Figure 3.1 Map of rain collection stations.

cleaned cubitainers following individual rain events, while Portsmouth rain samples were collected over 1-2 week intervals.

Precipitation was measured daily at both Woods Hole and Portsmouth using a standard rain gauge, consisting of a 10.5 cm diameter funnel leading to a graduated plastic cylinder (Cole Palmer Model No. 03319-00). At the Woods Hole site, additional precipitation measurements were made at Long Pond, a site approximately 3 miles north, and 1.5 miles inland of Buzzards Bay. These rain measurements were recorded by the Falmouth Water Department. Comparisons between precipitation measured at WHOI and at Long Pond were within 10% with the exception of large rain events (>0.75 inches), where the Long Pond estimates tended to be over 20% greater. It is possible that, in addition to differences in local rain patterns, hydrodynamic effects may play a role in our rain gauge measurements, causing either an over- or under-determination of precipitation at our sites. The precipitation measured at WHOI was used to determine radionuclide flux estimates at the Woods Hole site, and precipitation measured at Portsmouth for the New Hampshire site.

Once collected, rain sample cubitainers were first acidified with concentrated  $\text{HNO}_3$  to adjust the pH to <1. 1 mg of stable Pb (as  $\text{PbNO}_3$ ), 1 mg of stable Be (as  $\text{BeO}_4(\text{C}_2\text{H}_3\text{O}_2)_6$ ), and 100  $\mu\text{mol}$ s of stable  $\text{PO}_4$  (as  $\text{Na}_3\text{PO}_4 \cdot 12\text{H}_2\text{O}$ ) were added as yield monitors. Natural levels of phosphorus in rain water were also monitored and found to be less than 0.2  $\mu\text{mol}$ s  $\text{L}^{-1}$ , except during the spring/early summer pollen season. The acidified cubitainers were allowed to equilibrate at least 5 hours, and often more than 12 hours. After equilibration, Woods Hole samples were passed through a 30.5 cm long, 1.9 cm diameter PVC pipe packed with iron impregnated filters (Benitez-Nelson and Buesseler, 1998). It was found that while greater than 70% of the  $\text{PO}_4$  was collected, less than 10% of the Be and 40% of the Pb, were adsorbed onto the filters. This allowed for two separate samples; the filters containing most of the  $^{32}\text{P}$  and  $^{33}\text{P}$ , and the filtrate containing most of the  $^7\text{Be}$  and  $^{210}\text{Pb}$ .

$^7\text{Be}$  and  $^{210}\text{Pb}$  were measured via gamma spectroscopy after coprecipitation with  $\text{Fe}(\text{OH})_3$  under basic conditions. During the initial collection on the iron impregnated filters, a small fraction of iron (~10%) was released into the filtrate. This iron was utilized to form an  $\text{Fe}(\text{OH})_3$  precipitate after the filtrate was allowed to equilibrate for 3-4 hours. The sample filtrate pH was adjusted to 9 with concentrated  $\text{NH}_4\text{OH}$ , and an  $\text{Fe}(\text{OH})_3$  precipitate allowed to form and settle overnight. The precipitate was then filtered onto a 147 mm GF/F and dried in an oven at  $80^\circ\text{C}$ . Once dry, the iron precipitates were ground with a mortar and pestle and  $^{210}\text{Pb}$  and  $^7\text{Be}$  measured via gamma detection in 1 oz polyethylene jars. Rain samples collected at Portsmouth did not undergo separation of  $^{32}\text{P}$  and  $^{33}\text{P}$  using the iron impregnated filters prior to  $\text{Fe}(\text{OH})_3$  precipitation. Rather, 250 mg of iron was added during initial equilibration of the rain sample and the iron precipitate sent to Woods Hole for immediate measurement of  $^{32}\text{P}$ ,  $^{33}\text{P}$ ,  $^{210}\text{Pb}$  and  $^7\text{Be}$ .

High purity germanium gamma detectors (Canberra 2000  $\text{mm}^2$  LEGe style) were calibrated for  $^7\text{Be}$  and  $^{210}\text{Pb}$  using standards of known activity (EPA Standard Pitchblend Ore). Standards of similar geometry and of differing heights were placed in the same 1 oz. (31 mL) jars used for our samples.  $^{210}\text{Pb}$  efficiencies and self absorption factors were directly calibrated, while  $^7\text{Be}$  efficiencies and self absorption were determined by interpolating between the gamma emissions of  $^{214}\text{Pb}$  (242, 295, 352 KeV) and  $^{214}\text{Bi}$  (609 KeV). An additional check of this interpolation procedure was conducted by directly comparing the interpolated efficiencies found for  $^{137}\text{Cs}$  (661 KeV) with those derived from counting a known activity  $^{137}\text{Cs}$  standard. Interpolated and measured  $^{137}\text{Cs}$  efficiencies were within 5%.

After counting, samples were dissolved in 8N HCl, and stable Pb and Be yields determined by ICPES. Typical recoveries for Be were greater than 85%, while Pb recoveries averaged close to 50%. Most of the Pb loss occurred via adsorption onto the iron filters during the initial separation.  $^{210}\text{Pb}$  and  $^7\text{Be}$  activities were decay corrected to the midpoint of collection and  $1\sigma$  errors were determined from counting statistics.

The iron oxide filters and the gamma counted iron precipitate from Portsmouth were purified and measured for  $^{32}\text{P}$  and  $^{33}\text{P}$  according to the methods described by Benitez-Nelson and Buessler (1998). Briefly, rain samples were purified from other beta emitting radionuclides, such as residual  $^{210}\text{Pb}$ , by utilizing a series of phosphorus specific precipitates followed by anion and cation exchange chromatography. The resulting solution was then analyzed using a new technique involving an ultra-low level liquid scintillation counter (Packard 2770TR/LL). This new method has the advantage of allowing simultaneous measurement of both  $^{32}\text{P}$  and  $^{33}\text{P}$  with much greater efficiencies than previously employed methods. Efficiencies in counting varied between samples, but were all greater than 50% for both  $^{32}\text{P}$  and  $^{33}\text{P}$ . Radioactive phosphorus samples were counted repeatedly over time (3-8 times) in order to ensure that all other  $\beta$ -emitting isotopes were completely removed. The activities of  $^{32}\text{P}$  and  $^{33}\text{P}$ , decay corrected to the midpoint of sample collection, were then determined using the half-life of each isotope and a weighted non-linear least-squares curve-fitting routine. Recoveries of stable  $\text{PO}_4$ , as measured by the molybdenum blue method of Koroleff (1983), were typically greater than 75% (Benitez-Nelson and Buessler, 1998). Overall errors are  $2\sigma$  and are derived from the propagation of uncertainties associated with the non-linear least-squares curve fit, detector calibration, and chemical recoveries (Benitez-Nelson and Buessler, 1998).

A simple test was conducted to ensure that these particle reactive radionuclides were not lost to the polyethylene sheeting of the rain collector during collection at Woods Hole. The rain collector was first rinsed with distilled water ( $\text{pH} = 7$ ) to remove any particles that may have been collected since the previous rain event. The collector was then rinsed with 0.2N HCl, which was collected into an acid cleaned cubitainer, and the sample treated similarly to the Portsmouth rain samples. The activity removed during this process was equivalent to  $0.057 \text{ dpm cm}^{-2} \text{ yr}^{-1}$  for  $^7\text{Be}$  and  $0.030 \text{ dpm cm}^{-2} \text{ yr}^{-1}$  for  $^{210}\text{Pb}$ , calculated assuming constant input and irreversible adsorption prior to removal by the acid rinse. This is less than 3% of the annual bulk deposition of  $^{210}\text{Pb}$  and  $^7\text{Be}$  measured at the Wood Hole site (see below).

## RESULTS AND DISCUSSION

### *Radionuclide Activities and Flux estimates*

The absolute activity of  $^{32}\text{P}$ ,  $^{33}\text{P}$ ,  $^7\text{Be}$ , and  $^{210}\text{Pb}$  in disintegrations per minute per liter ( $\text{dpm L}^{-1}$ ) was measured in individual rain events at Clark Laboratory in Woods Hole, MA beginning in March of 1996 and in 1-2 week integrated samples at the U.S. Coast Guard Station in Portsmouth, NH, beginning in March of 1997. It should be noted that each rain event collected at Woods Hole also includes the preceding days of dry fallout (0-17 days).  $^{32}\text{P}$  and  $^{33}\text{P}$  activities were similar and ranged from 0.27 to 13.61  $\text{dpm L}^{-1}$  (Tables 1 and 2). This activity range was significantly higher than the 0.06 to 3.78  $\text{dpm L}^{-1}$  found previously (Goel *et al.*, 1959; Lal *et al.*, 1960; Walton and Fried, 1962; Waser and Bacon, 1995). This is most likely due to the fact that prior sampling was often integrated over one to three week periods.

The average yearly flux of  $^{32}\text{P}$  and  $^{33}\text{P}$  at Woods Hole was  $1781 \pm 41$  and  $1653 \pm 37$   $\text{dpm m}^{-2} \text{yr}^{-1}$ , respectively, while the  $^{32}\text{P}$  and  $^{33}\text{P}$  flux at Portsmouth was  $2123 \pm 41$  and  $1752 \pm 32$   $\text{dpm m}^{-2} \text{yr}^{-1}$  (e.g. Fig. 2). The  $^{32}\text{P}$  and  $^{33}\text{P}$  fluxes measured at Portsmouth were slightly higher than the  $^{32}\text{P}$  and  $^{33}\text{P}$  flux of 1806 and 1662  $\text{dpm m}^{-2} \text{yr}^{-1}$  measured at Woods Hole during the same time period. The difference in flux between the two sites was most likely due to differences in air mass source, since the rainfall amounts were indistinguishable over the period of comparison (64.7 versus 64.5 cm). The annual measured  $^{32}\text{P}$  and  $^{33}\text{P}$  fluxes at Woods Hole and Portsmouth were substantially higher than the annual  $^{32}\text{P}$  flux of  $860 \pm 150$   $\text{dpm m}^{-2} \text{yr}^{-1}$ , and the  $^{33}\text{P}$  flux of  $820 \pm 210$   $\text{dpm m}^{-2} \text{yr}^{-1}$  measured previously at Bermuda (Waser and Bacon, 1995). Elevated fluxes are most likely related to differences in the source and precipitation rate (47  $\text{cm yr}^{-1}$  at Bermuda, versus 84.8  $\text{cm yr}^{-1}$  at Woods Hole).

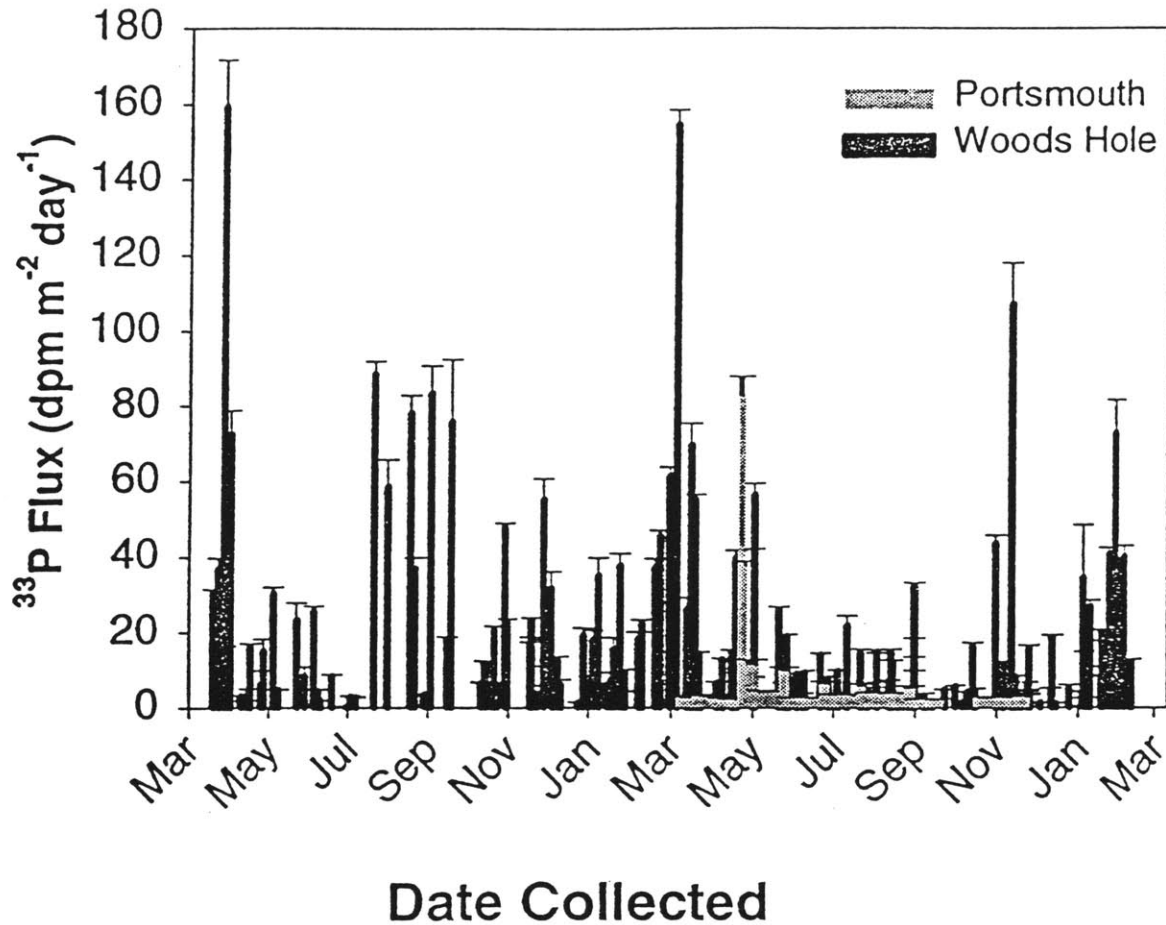


**Figure 3.2** Daily  $^{33}\text{P}$  flux measured at Woods Hole (dark bars) and Portsmouth (light bars). Daily fluxes at Woods Hole are derived by multiplying the rainfall in the individual rain event by the specific activity of the sample. Fluxes at Portsmouth are derived by multiplying the cumulative rainfall by the specific activity found in the sample and dividing by the number of days in the collection period. Errors are derived from counting statistics and assuming a 5% error in rainfall measurements. The magnitude of  $^{32}\text{P}$  fluxes varies in the same manner.



$^7\text{Be}$  and  $^{210}\text{Pb}$  activities also had a wide range in specific activity, 21 to 1442 dpm  $\text{L}^{-1}$ , and 2 to 160 dpm  $\text{L}^{-1}$ , respectively (Tables 1 and 2). These activities are similar to those found in other areas (Turekian *et al.*, 1983; Olsen *et al.*, 1985; Dibb, 1989; Todd *et al.*, 1989; Baskaran *et al.*, 1993; Kim *et al.*, 1998). The yearly flux of  $^7\text{Be}$  and  $^{210}\text{Pb}$  at Woods Hole was  $12.8 \pm 0.2$  and  $1.43 \pm 0.03$  dpm  $\text{cm}^{-2} \text{yr}^{-1}$ , respectively, while the flux of  $^7\text{Be}$  and  $^{210}\text{Pb}$  at Portsmouth was  $16.6 \pm 0.05$  and  $0.95 \pm 0.01$  dpm  $\text{cm}^{-2} \text{yr}^{-1}$ , respectively (e.g. Fig. 3). The flux of  $^7\text{Be}$  at Portsmouth was again higher than the  $12.07$  dpm  $\text{cm}^{-2} \text{yr}^{-1}$  measured at Woods Hole (over the same summer time period) similar to  $^{32}\text{P}$  and  $^{33}\text{P}$ . In contrast, the  $^{210}\text{Pb}$  flux at Woods Hole over the same time period was substantially higher,  $1.36$  dpm  $\text{cm}^{-2} \text{yr}^{-1}$ . While the difference in  $^7\text{Be}$  flux was again most likely due to differences in precipitation, the dissimilarity in  $^{210}\text{Pb}$  fluxes must be due either to differences in precipitation source (i.e. continental versus marine) and/or dry deposition rates.

It is unlikely that differences in dry deposition could account for the variation in total fluxes between Portsmouth and Woods Hole. Previous studies of dry deposition of  $^{210}\text{Pb}$  and  $^7\text{Be}$  have been found, in general, to be less than 15% of the total flux (Brown *et al.*, 1989; Todd *et al.*, 1989; Koch *et al.*, 1996). However, the relative importance of dry versus wet deposition has been shown to increase during periods of low rainfall. Baskaran *et al.* (1993) found that dry deposition could account for as much as 41% of the total fallout measured at several stations in Texas.

A single dry deposition sample was taken during 7 days in July, 1997, in order to evaluate the relative importance of dry deposition at our Woods Hole site. Our results, collected during a low rainfall period, indicated that dry deposition accounts for less than 1% of the  $^7\text{Be}$  flux, but accounted for 12% of the  $^{210}\text{Pb}$  flux. The effect of dry deposition on the flux of  $^{210}\text{Pb}$  and  $^7\text{Be}$  can be further evaluated by examining the relationship between bulk depositional fluxes and the period between individual rain events, as the collector always remained open to the atmosphere. If dry deposition was a major

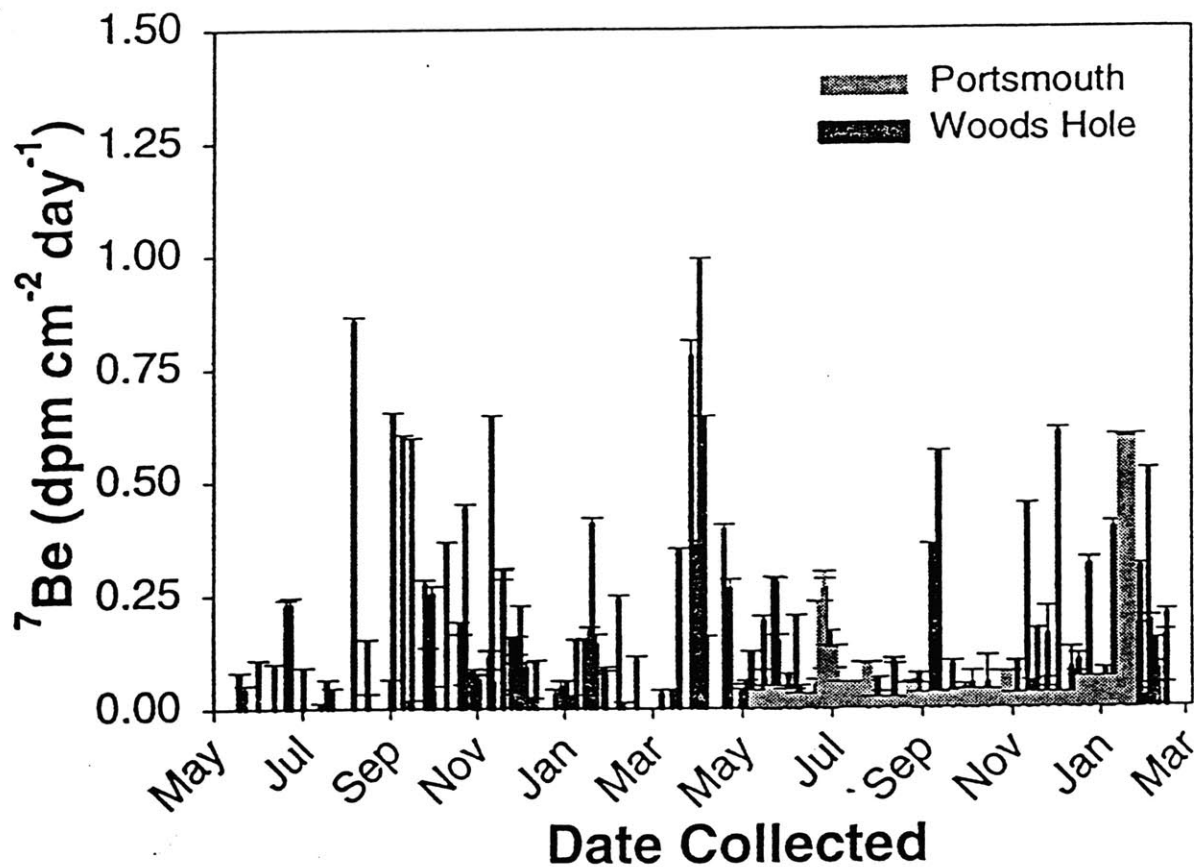


**Figure 3.3** Daily  ${}^7\text{Be}$  flux measured at Woods Hole (dark bars) and Portsmouth (light bars). Daily fluxes at Woods Hole are derived by multiplying the rainfall in the individual rain event by the specific activity of the sample. Fluxes at Portsmouth are derived by multiplying the cumulative rainfall by the specific activity found in the sample and dividing by the number of days in the collection period. Errors are derived from counting statistics and assuming a 5% error in rainfall measurements.

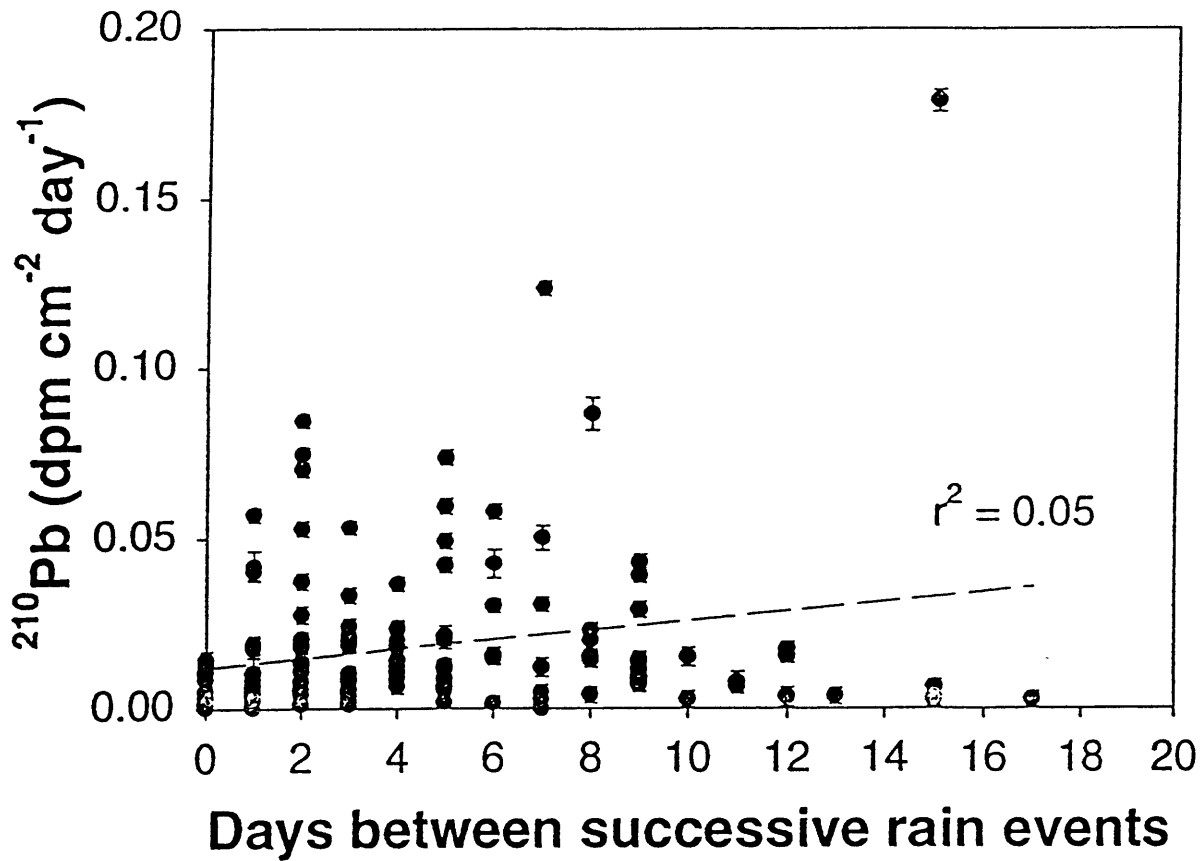


**Figure 3.4** Daily  $^{210}\text{Pb}$  depositional flux versus the time period (in whole days) between precipitation events. The regression line is determined by a linear least squares fit through the data.

contributor to flux, then the time between rain events should be positively correlated with the bulk flux. However, no relationship was found (Fig. 4).

Fluxes of  $^7\text{Be}$  measured at Woods Hole are very similar to the  $^7\text{Be}$  fluxes (4.3 to 22.7 dpm cm<sup>-2</sup> yr<sup>-1</sup>) found previously on the northeastern coast. Our Woods Hole  $^{210}\text{Pb}$  fluxes, on the other hand, are 1.2 to 1.8 times higher than prior estimates of 1.20 dpm cm<sup>-2</sup> yr<sup>-1</sup> at New Haven, Connecticut and 0.79 and 0.85 dpm cm<sup>-2</sup> yr<sup>-1</sup> at Norfolk, Virginia (Turekian *et al.*, 1983; Todd *et al.*, 1989). Emission of  $^{222}\text{Rn}$  from the continents has been found to range from 0.7 to 4.45 dpm cm<sup>-2</sup> yr<sup>-1</sup>, with an average value of 0.9 dpm cm<sup>-2</sup> yr<sup>-1</sup> (Wilkening and Clements, 1975; Turekian *et al.*, 1977; Polian *et al.*, 1986). Thus, continental sources can easily support our measured Woods Hole  $^{210}\text{Pb}$  fluxes. The most likely explanation for the difference between the Woods Hole and Portsmouth stations was that our Woods Hole station must collect precipitation from continental air masses at a higher relative rate than other stations. The other explanation was that the rain gauge at the Woods Hole site is over-collecting. However, this is unlikely given the similarities in rain collector design and the measured precipitation rates between the Woods Hole and Long Pond stations.

#### *Relationship between absolute activities and fluxes with rainfall*

There was no significant correlation between the absolute activity of  $^{32}\text{P}$ ,  $^{33}\text{P}$ ,  $^7\text{Be}$ , or  $^{210}\text{Pb}$  in individual rain events and rainfall at Woods Hole or at Portsmouth (e.g. Fig. 5,  $r^2 < 0.05$ ). Nevertheless, higher activity rain samples tended to occur with low rainfall and vice versa. A lack of correlation between the absolute activity of  $^{32}\text{P}$  and  $^{33}\text{P}$  and rainfall was also found in measurements of  $^{32}\text{P}$  and  $^{33}\text{P}$  at Bermuda (Waser and Bacon, 1995). In contrast, several investigations have found relationships between rainfall amount and the absolute activity  $^7\text{Be}$  and  $^{210}\text{Pb}$  in rainfall samples integrated over longer time scales (Olsen *et al.*, 1985; Todd *et al.*, 1983; Turekian *et al.*, 1983; Baskaran *et al.*, 1993; Kim *et al.*, 1998). The lack of a linear relationship found in this study suggests that radionuclide activities at our site are not controlled by dilution alone, but rather by other processes,

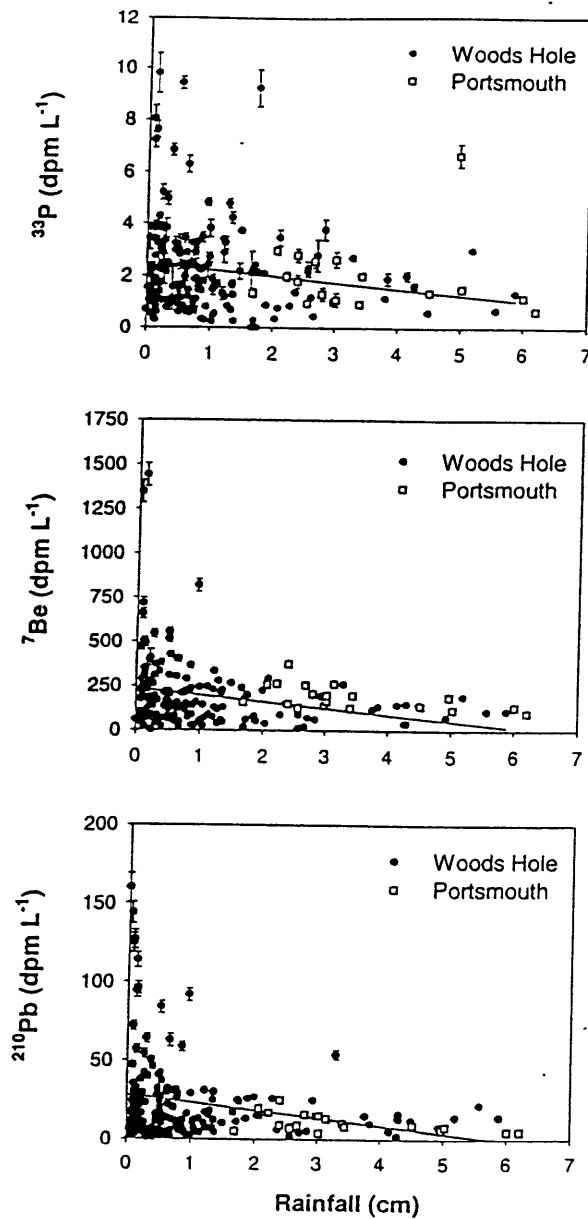


**Figure 3.5** Specific activity of  $^{33}\text{P}$ ,  $^7\text{Be}$ , and  $^{210}\text{Pb}$  versus rainfall. The regression line is determined by a linear least squares fit through the data. The relationship between  $^{32}\text{P}$  and rainfall is similar to that of  $^{33}\text{P}$ .

such as source and scavenging intensity.

A further test of dilution effects on absolute radionuclide activities can be conducted by measuring changes in the absolute activity of  $^{32}\text{P}$ ,  $^{33}\text{P}$ ,  $^7\text{Be}$ , and  $^{210}\text{Pb}$  during a single rain event. Between 4 and 6 rain samples were taken sequentially during individual rain events which occurred over a 12 hour period in December, 1996, and in July, August, November, and December of 1997. Our results showed no evidence of a decrease in absolute activity with time during single rain events. Such an occurrence would be expected if dilution was a dominating factor controlling absolute activities (Table 3, Fig. 6). Again, these results differ from previous investigations which did find decreases in the absolute activity of  $^7\text{Be}$  during a single rain event (Olsen *et al.*, 1985; Dibb, 1989; Baskaran *et al.*, 1993). However, it should be noted that these previous investigations characterized single rain events as spanning several days, whereas this study limited investigations to those rain events which occurred over less than a 12 hour period.

In contrast to absolute activity, all four isotopes do show a correlation between flux and rainfall (e.g. Fig. 7). This indicates that rain rate does play an important part in the removal of these isotopes from the troposphere. Similar relationships for  $^7\text{Be}$  and  $^{210}\text{Pb}$  have also been found (Turekian *et al.*, 1983; Dibb, 1989; Baskaran *et al.*, 1993; Kim *et al.*, 1998). Deviations in the relationships between flux and rainfall among the radionuclides can arise from differences in air mass sources, scavenging rates, and radioactive decay.

#### *Tropospheric aerosol residence times*

The radioisotopes,  $^{32}\text{P}$ ,  $^{33}\text{P}$ , and  $^7\text{Be}$  may provide insight into the residence time of tropospheric aerosols given the relatively short half-lives of the three nuclides. Although the tropospheric reservoir is often considered to be relatively well mixed, there is an altitude dependence associated with the residence time of aerosols in the troposphere. In the upper troposphere, the residence time of aerosols has been found to range from 4-60 days (Martell and Moore, 1974; Balkanski *et al.*, 1993). In contrast, in the lower 2 km of

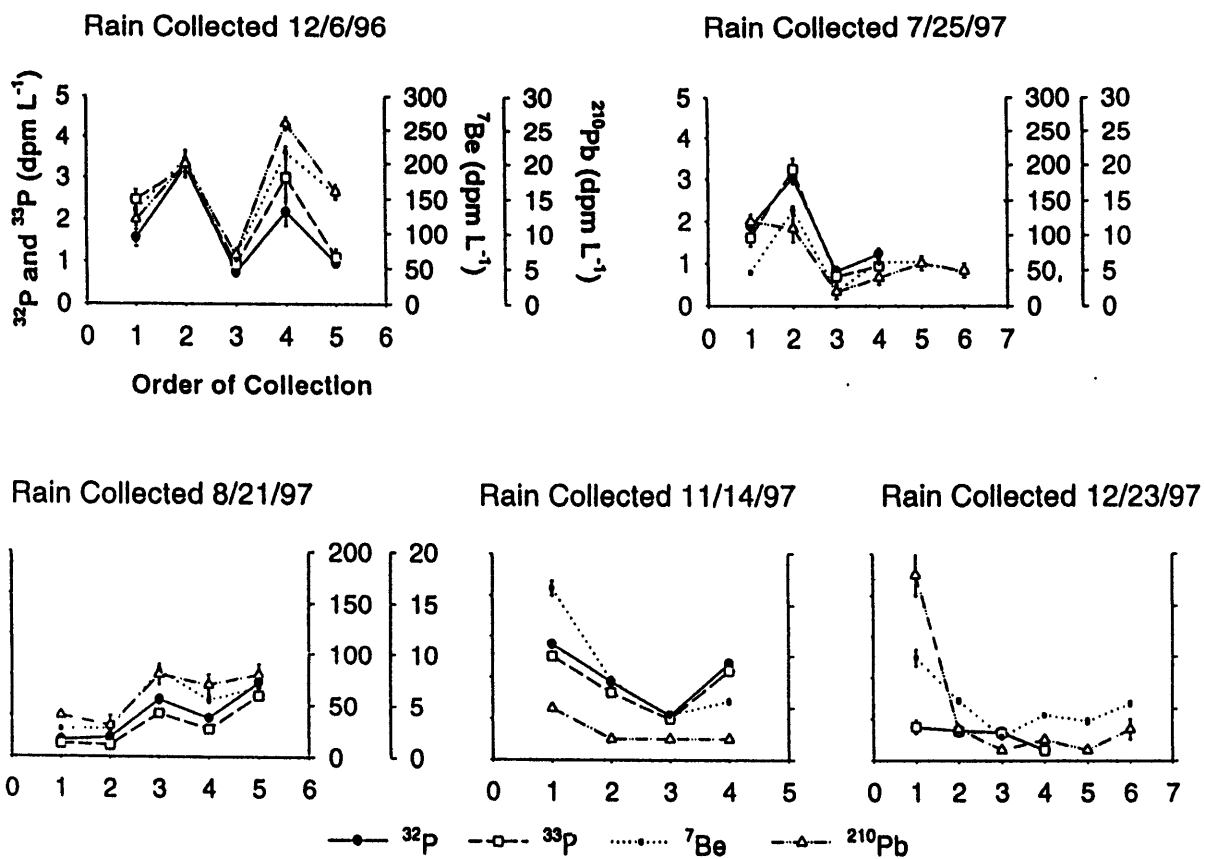


**Figure 3.6** Specific activity of  $^{32}\text{P}$  (filled circles),  $^{33}\text{P}$  (unfilled squares),  $^7\text{Be}$  (filled triangles), and  $^{210}\text{Pb}$  (unfilled triangles) in sequential samples taken during an 8-12 hour continuous rainfall period.

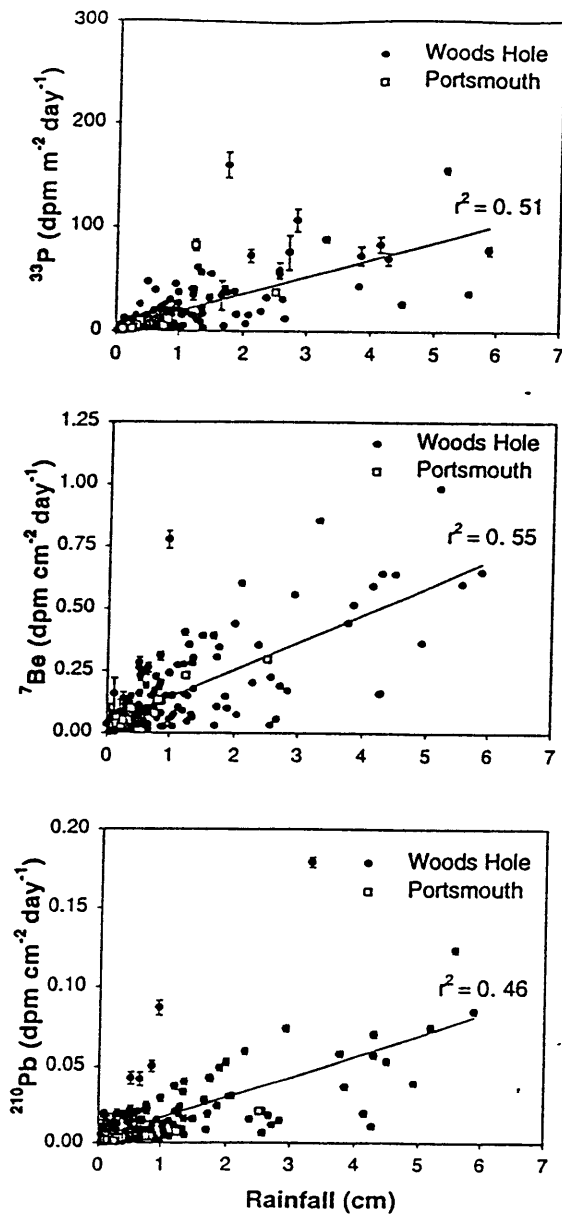


**Figure 3.7** Daily flux of  $^{33}\text{P}$ ,  $^7\text{Be}$ , and  $^{210}\text{Pb}$  versus rainfall. The regression line is determined by a linear least squares fit through the data. The relationship between  $^{32}\text{P}$  and rainfall is again similar to that of  $^{33}\text{P}$ .



the troposphere, the residence time of aerosols is often less than a week (Poet *et al.*, 1972; Moore *et al.*, 1973; Martell and Moore, 1974). Mixing between the upper and lower troposphere can therefore produce a large range in observed aerosol residence times.

The average residence time of an aerosol in the troposphere can be determined using a mass balance approach by comparing the expected and measured fallout rates of  $^{32}\text{P}$ ,  $^{33}\text{P}$ , and  $^7\text{Be}$  (Goel *et al.*, 1959; Lal *et al.*, 1960; Waser and Bacon, 1995). Simply stated, the residence time of an aerosol is related to the balance between the removal flux measured in rain and the mean tropospheric production rate, such that:

$$\tau = \Lambda [P/W-1] \quad (1)$$

where  $\tau$  is the residence time of the aerosol,  $\Lambda$  is the mean life of the radionuclide,  $P$  is the average tropospheric radionuclide production rate, and  $W$  is the removal flux. In practice this model is inappropriate in that: 1) production rates are averaged latitudinally, thus local variations in precipitation rates may offset the signal, and 2) there is most likely a strong stratospheric influence in some of our samples. Regardless, it is possible to achieve an estimate of the average residence time of a tropospheric aerosol by attempting to remove some of these effects. In order to remove effects caused by local variations in precipitation, a zonally averaged precipitation rate of  $93.7 \text{ cm yr}^{-1}$  was assumed for the  $42^\circ\text{N}$  latitudinal belt. This precipitation rate is the annual average rainfall at  $42^\circ\text{N}$  determined from a 30 year study of precipitation samples measured globally from 1950 to 1979 (Shea, 1986). The zonal precipitation number was then multiplied by an average activity of  $^{32}\text{P}$ ,  $^{33}\text{P}$ , and  $^7\text{Be}$  in the Woods Hole and Portsmouth samples. The average activity used in the calculation was determined by multiplying the annual radionuclide flux calculated at Woods Hole by the annual measured rain rate. Average activities were  $2.08 \pm 0.05$ ,  $1.94 \pm 0.05$ , and  $112.6 \pm 0.9 \text{ dpm L}^{-1}$  for  $^{32}\text{P}$ ,  $^{33}\text{P}$ , and  $^7\text{Be}$ , respectively.

The estimated production rate of  $^{32}\text{P}$ ,  $^{33}\text{P}$ , and  $^7\text{Be}$ , in the troposphere is  $2869 \text{ dpm m}^{-2} \text{ yr}^{-1}$ ,  $1320 \text{ dpm m}^{-2} \text{ yr}^{-1}$ , and  $7.69 \text{ dpm cm}^{-2} \text{ yr}^{-1}$ , respectively (Lal and Peters, 1967). Given these estimates, the production ratio of  $^{33}\text{P}/^{32}\text{P}$  is 0.45. Recent measurements by Waser and Bacon (1995), and in this study, suggest that the  $^{33}\text{P}/^{32}\text{P}$  ratio is closer to 0.65

$\pm 0.05$  (see below). Thus, it should be noted that the  $^{32}\text{P}$  production rate is lower, or the  $^{33}\text{P}$  production rate higher than the estimates of Lal and Peters (1967). Our measured  $^{33}\text{P}$  fluxes at Woods Hole and Portsmouth are substantially higher than the production rate estimates of Lal and Peters (1967). This suggests that the  $^{33}\text{P}$  production rate estimates are too low. Assuming the  $^{32}\text{P}$  production rate estimate is correct and multiplying by the  $^{33}\text{P}/^{32}\text{P}$  ratio of 0.65, results in a new  $^{33}\text{P}$  production rate estimate of  $1865 \text{ dpm m}^{-2} \text{ yr}^{-1}$ . Using equation (1), the corrected estimates of  $^{32}\text{P}$  and  $^{33}\text{P}$  production rates, and the zonally averaged precipitation rate, gives an aerosol residence time of 9.7 and 0.9 days for  $^{32}\text{P}$  and  $^{33}\text{P}$ , respectively. This is similar to the 12.6 and 4.7 day aerosol residence times determined for  $^{32}\text{P}$  and  $^{33}\text{P}$  using the WHOI precipitation estimates.

A similar aerosol residence time determination for  $^7\text{Be}$  is not feasible, given that the zonally averaged fallout flux of  $^7\text{Be}$  is  $10.9 \text{ dpm cm}^{-2} \text{ yr}^{-1}$ , over 30% higher than the calculated production rate, and over 50% higher than that expected given an aerosol residence time of 30 days. It is possible that the discrepancy results from stratospheric intrusions, which have been estimated to contribute as much as 25% to the annual  $^7\text{Be}$  flux (see below; Dutkiewicz and Hussain, 1985).

If stratospheric intrusion is substantial, then one would also expect a similar increase in the annual  $^{32}\text{P}$  and  $^{33}\text{P}$  depositional flux, given the similarity in the production mechanisms of the three nuclides. However, differences between the half lives of  $^{32}\text{P}$  ( $t_{1/2} = 14.3$  days) versus  $^{33}\text{P}$  ( $t_{1/2} = 25.3$  days) and  $^7\text{Be}$  ( $t_{1/2} = 53.3$  days), coupled with the relatively long average residence time of aerosols in the uppermost troposphere, minimize the stratospheric influence over annual time scales in the  $^{32}\text{P}$  flux. If it is assumed that the precipitation corrected  $^{33}\text{P}$  flux is overestimated by 20 to 30%, based on estimates of stratospheric intrusion by Dutkiewicz and Hussain (1985), an increased aerosol residence time of 12.4 and 16.5 days is determined.

The large range in annual mean aerosol residence times (2-17 days) predicted using the mass balance approach points to the sensitivity of the model to stratospheric influences and production rates. Unfortunately, both are poorly constrained. More data is needed in

order to use these isotopes to investigate aerosol related processes. Nonetheless, our results are similar to those found previously (4-60 days) using  $^{32}\text{P}$ ,  $^{33}\text{P}$ , and  $^7\text{Be}$  and other radioactive tracers (Lal 1958, Lal *et al.*, 1960; Goel *et al.*, 1959; Poet *et al.*, 1972; Martell and Moore, 1974; Balkanski *et al.*, 1993; Waser and Bacon, 1995). That our estimates fall towards the shorter residence time estimates indicates that our precipitation measurements are dominated by removal from the lower troposphere, in addition to other such regional factors as the origin of the aerosol, size distribution and frequency of precipitation.

#### *Tropospheric irradiation periods of an airmass*

A second method used to quantify the residence time of aerosols in the troposphere is the determination of the average cosmic ray irradiance period of an airmass. The irradiation period of an airmass is similar to the airmass 'age' in that it is also a balance between radionuclide production, decay, and, in this formulation, removal by precipitation. Determination of the irradiance period of a tropospheric airmass involves the utilization of a simple non steady state model and the following assumptions: 1) tropospheric production rates can be approximated by an average value, 2) the tropospheric air is instantaneously cleansed of all radioactivity following a precipitation event, and 3) there is no stratospheric input (Lal, 1958, Lal *et al.*, 1960; Waser and Bacon, 1995). In this formulation the activity of a radionuclide can be described by the following equation:

$$dN/dt = P - \lambda_a N \quad (2)$$

where  $N$  is the radionuclide concentration in atoms,  $dN/dt$  is the change in radionuclide concentration with time, and  $\lambda_a$  is the radionuclide decay constant. Assuming non-steady state, this equation can be solved to give the following:

$$A = P / \lambda_a [1 - \exp(-\lambda_a \tau_i)] \quad (3)$$

where  $A$  is the activity of the nuclide in the tropospheric airmass, and  $\tau_i$  is the time period between successive precipitation events. While the absolute activities of a  $^{32}\text{P}$ ,  $^{33}\text{P}$ , and

$^7\text{Be}$  can vary by as much as a factor of 100, the ratio of  $^{33}\text{P}/^{32}\text{P}$ ,  $^7\text{Be}/^{32}\text{P}$ ,  $^7\text{Be}/^{33}\text{P}$  has been shown to vary to a much lesser extent (Lal *et al.*, 1960; Walton and Fried, 1962; Waser and Bacon, 1995). Thus, we use ratios instead of absolute activities of a single radionuclide.

Assuming that there is no fractionation of the radionuclides during condensation and precipitation, the irradiation period can be found by using the ratio of one radionuclide to another, such that:

$$^a\text{A} / ^b\text{A} = (^a\text{P} \lambda_b / ^b\text{P} \lambda_a) (1 - \exp(-\lambda_a \tau_i)) / (1 - \exp(-\lambda_b \tau_i)) \quad (4)$$

where  $^a\text{A}$  and  $^b\text{A}$  are the activities of the longer lived and shorter lived radionuclide, respectively;  $^a\text{P} / ^b\text{P}$  refers to the production ratio of nuclide a to b, and  $\lambda_a$  and  $\lambda_b$  are the half lives of the respective nuclides (Lal and Peters, 1967). At steady state, the time between successive precipitation events increases to infinity, such that the  $^{33}\text{P}/^{32}\text{P}$  ratio at equilibrium,  $R_e = ^a\text{P} \lambda_b / ^b\text{P} \lambda_a$ .

The above non-steady state model (equation 4) predicts that the ratio in rainwater can only vary between an initial production ratio  $R_0$ , and an equilibrium value,  $R_e$ , of  $1.77R_0$ ,  $3.7R_0$  and  $2.1R_0$ , for  $^{33}\text{P}/^{32}\text{P}$ ,  $^7\text{Be}/^{32}\text{P}$ , and  $^7\text{Be}/^{33}\text{P}$ , respectively (e.g. Fig. 4 in Waser and Bacon, 1995). The time period necessary to achieve 95% equilibrium for the ratio of  $^{33}\text{P}/^{32}\text{P}$ ,  $^7\text{Be}/^{32}\text{P}$ , and  $^7\text{Be}/^{33}\text{P}$ , is greater than 100 days. Thus, given that the average aerosol residence time is much shorter, tropospheric airmasses rarely reach equilibrium. The activity ratio of  $^{33}\text{P}/^{32}\text{P}$  measured in samples collected at Woods Hole and Portsmouth range from  $0.55 \pm 0.14$  to  $1.59 \pm 0.26$  (Fig. 8). The activity ratio of  $^7\text{Be}/^{32}\text{P}$  and  $^7\text{Be}/^{33}\text{P}$  ranged from  $22 \pm 2$  to  $423 \pm 52$ , and  $22 \pm 2$  to  $501 \pm 69$ , respectively (e.g. Fig 9). Only the  $^{33}\text{P}/^{32}\text{P}$  ratios stay, within error, relatively close to the expected range. Thus, the above model assumptions must not hold for  $^7\text{Be}/^{32}\text{P}$  and  $^7\text{Be}/^{33}\text{P}$  ratios, and are the result of either stratospheric influences, and/or fractionation processes between the different radioisotopes.

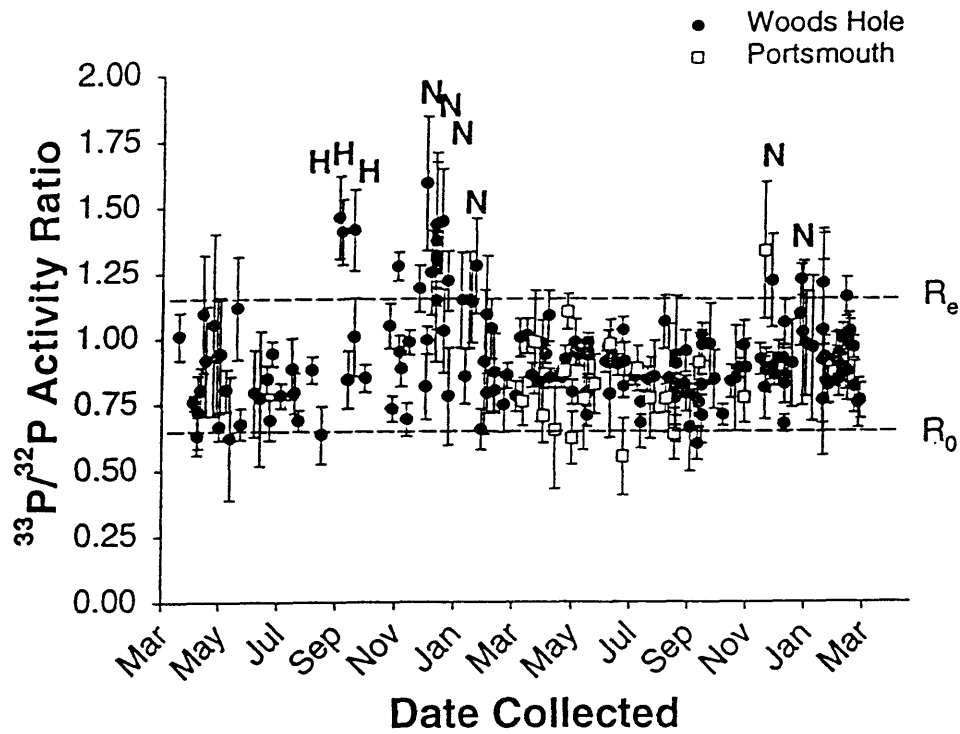


**Figure 3.8** Activity ratio of  $^{33}\text{P}/^{32}\text{P}$  in precipitation samples measured at Woods Hole (filled circles) and at Portsmouth (unfilled squares).  $R_0$  is the tropospheric production ratio of 0.65.  $R_e$  is the theoretical tropospheric steady state ratio of 1.15. H's signify Hurricanes Edourd, Fran, and Hortense, and N's, Nor'easters.

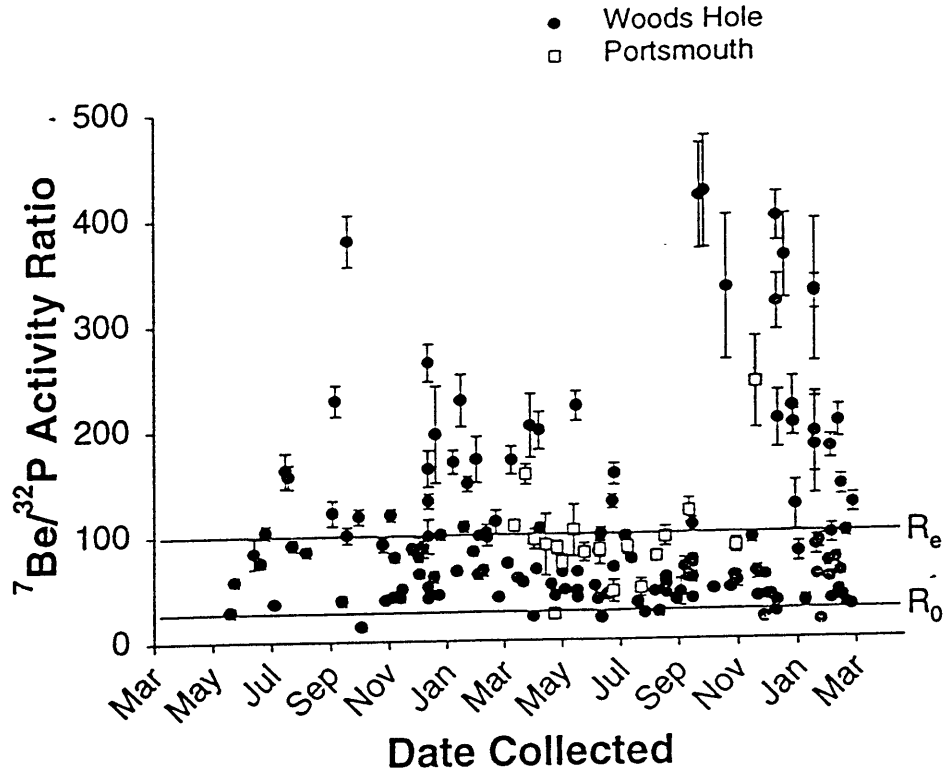


**Figure 3.9** Activity ratio of  ${}^7\text{Be}/{}^{32}\text{P}$  in precipitation samples measured at Woods Hole (filled circles) and at Portsmouth (unfilled squares).  $R_0$  is the tropospheric production ratio of 25.  $R_e$  is the theoretical tropospheric steady state ratio of 99. Ratios greater than 250, all occur during low rainfall periods (<0.3 cm).

As a result, a cosmic ray irradiance period can only be calculated using the ratio of  $^{33}\text{P}/^{32}\text{P}$ . With the exception of specific rain events in September, 1996, and in the winters of 1997, and 1998, the average  $^{33}\text{P}/^{32}\text{P}$  activity ratio measured in samples collected at Woods Hole and at Portsmouth was surprisingly consistent and averaged  $0.88 \pm 0.14$ . The tropospheric production rate of  $^{33}\text{P}/^{32}\text{P}$  has been estimated to be 0.46 by Lal and Peters (1967) and 0.70 by Waser and Bacon (1995). Both values are within the range of the lowest  $^{33}\text{P}/^{32}\text{P}$  ratio sample,  $0.55 \pm 0.15$ , observed at Woods Hole and Portsmouth. However, a production ratio of 0.46 would indicate that well over 50% of our rain measurements fall outside of equilibrium, ( $1.77R_0$ ), an occurrence which is highly unlikely. Thus, we have chosen a  $^{33}\text{P}/^{32}\text{P}$  production ratio of  $0.65 \pm 0.05$ , similar to that chosen by Waser and Bacon, because this value best represents the range in  $^{33}\text{P}/^{32}\text{P}$  ratios observed in our data set. Using the non steady state equation above, a  $\tau_i$  of  $39 \pm 7$  days is calculated, a value consistent with previous irradiance period estimates of 40-50 days (Lal *et al.*, 1960; Waser and Bacon, 1995).

The above non steady state model is very dependent on tropospheric production rates and, more importantly, the assumption of no stratospheric influences in our samples. However, it has already been shown that both processes are not well constrained. More information concerning STE and radionuclide production rates are necessary in order to quantify aerosol residence times.

#### *Radionuclide Ratios as an indicator of Airmass Source*

It should be obvious from the previous discussions of tropospheric aerosol residence times and irradiance periods that stratospheric intrusion plays a significant role in our  $^{32}\text{P}$ ,  $^{33}\text{P}$ , and  $^7\text{Be}$  data. Many prior investigations have noted an increase in the flux of  $^7\text{Be}$  during the spring months of March, April, and May (Olsen *et al.*, 1985, Todd *et al.*, 1989; Viezee and Singh, 1980). This variation has been largely attributed to the spring injection of  $^7\text{Be}$  enriched stratospheric air into the troposphere during isentropic mixing at mid-latitudes (Dutkiewicz and Husain 1978, 1985; Todd *et al.*, 1989). In this study,

increases in the fluxes of  $^{32}\text{P}$ ,  $^{33}\text{P}$ , and  $^7\text{Be}$  during the spring are also apparent. However, the use of absolute activities does not allow for an evaluation of what fraction is due to stratospheric influences, seasonal increases in rainfall, and/or increases in mixing between the upper and lower troposphere (Baskaran, 1995). The use of radionuclide ratios instead of absolute activity concentrations should depress any effects associated with variations in seasonal rainfall, and thus allow for better elucidation of the above mechanisms.

It has already been shown that in the troposphere the ratio of  $^{33}\text{P}/^{32}\text{P}$ ,  $^7\text{Be}/^{32}\text{P}$ , and  $^7\text{Be}/^{33}\text{P}$ , should vary between an estimated production ratio,  $R_0$ , and an equilibrium value  $R_e$ , using equation (4). Deviations from this range suggest that other processes, such as STE, are affecting the ratios. Further evaluation of the variations found in  $^{33}\text{P}/^{32}\text{P}$ ,  $^7\text{Be}/^{32}\text{P}$ ,  $^7\text{Be}/^{33}\text{P}$ , and  $^7\text{Be}/^{210}\text{Pb}$  ratios may provide insight into the timing and magnitude of atmospheric mixing mechanisms. This study is the first to examine the relationship of all four isotopes in individual rain events.

**$^{33}\text{P}/^{32}\text{P}$ .** Significantly elevated  $^{33}\text{P}/^{32}\text{P}$  ratios of 1.1-1.5 were observed during specific rain events in September, 1996 and in the winter (Dec.-Feb.) of 1997 and 1998. The elevated ratios in September, 1996 all correspond with rain collected during hurricanes: Edouard, Fran, and Hortense (Fig 8). These hurricanes were all ranked as Category Three Hurricanes on the Saffir-Simpson Hurricane Scale (winds 111-130 mph) during their life history. The additional higher ratios measured in Winter of 1997 and 1998 also correspond to a series of events called Nor'easters, intense storms from the North East containing rain, sleet, snow, and hail. In contrast, lower ratios ( $<1.0$ ) were almost always found between storm episodes.

Our rain measurements suggest that severe storms, such as hurricanes and Nor'easters were tapping higher  $^{33}\text{P}/^{32}\text{P}$  ratio air. The production ratio of  $^{33}\text{P}/^{32}\text{P}$  in the troposphere has been estimated to be  $0.65 \pm 0.05$ . If the higher measured ratios (storm events) are assumed to have no other source, calculated aerosol residence times increase to greater 3 months, much longer than that the average aerosol residence time found in this study and by other investigators (Lal and Peters, 1967; Bleichrodt, 1978; Waser and



Bacon, 1995). The measured  $^{33}\text{P}/^{32}\text{P}$  ratios greater than  $1.15 \pm 0.08$  are higher than the model derived equilibrium values from equation (4). Consequently, there is most likely another source of  $^{33}\text{P}$  and  $^{32}\text{P}$  contributing to the storm signal. This source air appears to have a  $^{33}\text{P}/^{32}\text{P}$  ratio of at least 1.5, the highest value measured in our rain samples.

Previous measurements of  $^{33}\text{P}/^{32}\text{P}$  ratios suggest that the high ratio signal is predominantly of stratospheric origin. Waser and Bacon (1995) observed an increase in the ratio of  $^{33}\text{P}/^{32}\text{P}$  in integrated rain samples at Bermuda to values as high as 1.20 during March, April and July of 1991, and January and February of 1992. Increases in  $^{90}\text{Sr}$  and ozone, two components predominantly derived from stratospheric air masses, were also noted to occur during the same months, although in previous years (Waser and Bacon, 1995).

There are several mechanisms by which the  $^{33}\text{P}/^{32}\text{P}$  ratio could be increased beyond equilibrium. One mechanism is that the production ratio could be significantly higher in the stratosphere than in the troposphere (Fig. 10a, mechanism 1). The other mechanisms all require intermittent mixing between higher activity stratospheric air and lower stratospheric air. This mixing could periodically increase the ratio in the lower stratosphere beyond equilibrium values (Figs. 10b and 10c, mechanisms 2-5).

It is unlikely that the production ratio of  $^{33}\text{P}/^{32}\text{P}$  is substantially different between the stratosphere and troposphere given our knowledge of spallation reactions in the atmosphere (Lal and Peters, 1967). Furthermore, actual measurements of stratospheric air conducted in the early 1960's, while few in number, reported that the average  $^{33}\text{P}/^{32}\text{P}$  activity ratio was  $0.9 \pm 0.2$  (Friend *et al.*, 1961; Rama and Honda, 1961; Drevinsky *et al.*, 1964). This value is similar to the expected equilibrium  $^{33}\text{P}/^{32}\text{P}$  ratio,  $R_e$ , of 1.15 (derived from equation (4)).

Another method of achieving an air mass with a higher  $^{33}\text{P}/^{32}\text{P}$  ratio is to invoke periodic mixing between higher activity and lower activity air masses. Theoretically, the absolute activity of  $^{32}\text{P}$  and  $^{33}\text{P}$  increases with increasing altitude and latitude, such that the

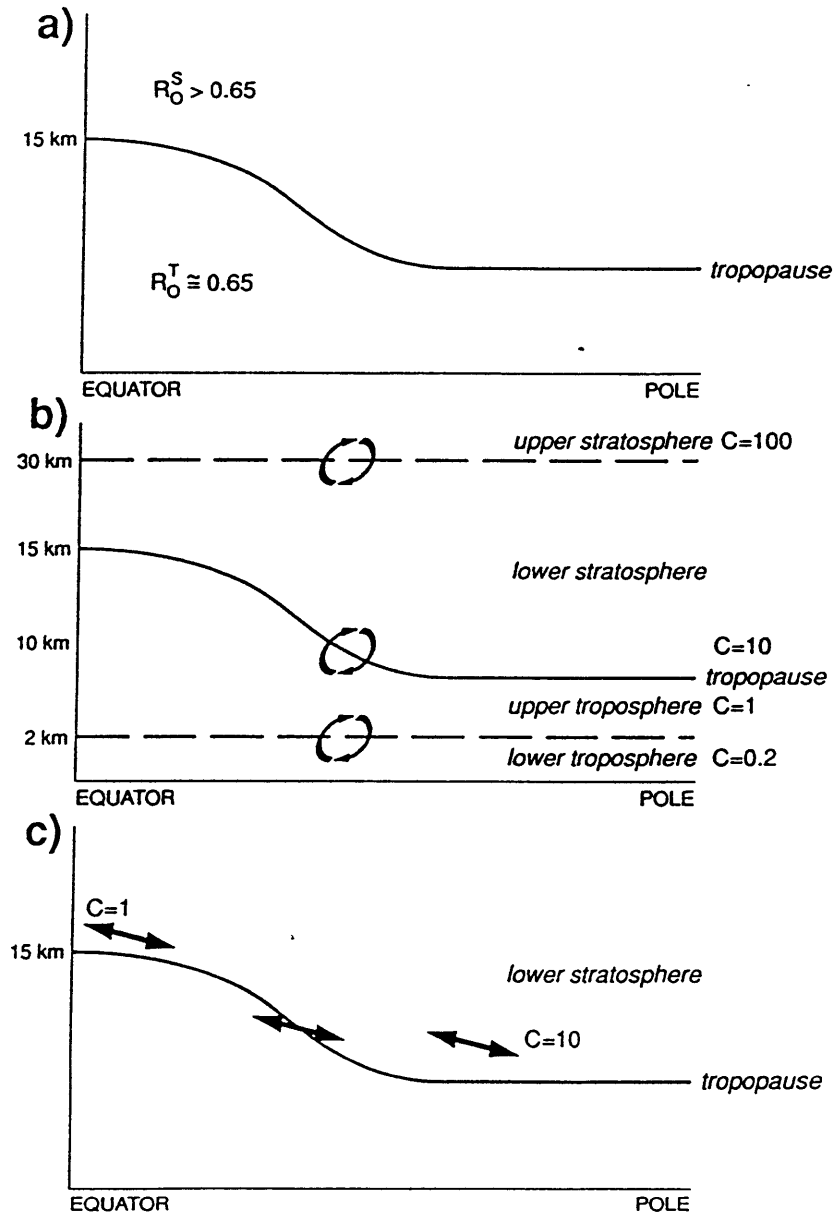


**Figure 3.10** Schematic of possible mechanisms which can increase the theoretical equilibrium ratio,  $R_e$ , greater than 1.15 for the ratio of  $^{33}\text{P}/^{32}\text{P}$ .  $C$  is the specific activity of a the radionuclide in each region. a) Stratospheric production ( $R_0^S$ ) rates greater than that in the troposphere ( $R_0^T$ ); b) Vertical mixing between atmospheric regions; and c) Horizontal or isentropic mixing between polar and mid-latitudes.

highest absolute activities are found in the upper stratosphere and at the poles (Lal and Peters, 1967). If it is assumed that the average stratospheric  $^{33}\text{P}/^{32}\text{P}$  ratio is 0.9 (based on actual measurements), and that the difference in absolute activity of an air mass between specified regions is an order of magnitude (Rama and Honda, 1961; Lal and Peters, 1967), simply mixing an air mass containing higher activity air with lower activity air will reproduce the high ratios observed in our rain samples (Fig. 11; 25%). Simply put, once the higher activity air mass is sequestered from its source and mixed, it will decay with time, increasing the ratio of  $^{33}\text{P}/^{32}\text{P}$ . After some time period the concentrations of the mixed air mass will have decayed to the point that the ratio will begin to decrease back to pre-mixing levels. If the air masses are at the hypothesized equilibrium value of 1.15 then even less decay and intermittent mixing between higher and lower activity air masses is required. This higher ratio air could then be tapped by severe storm events and quickly scavenged by precipitation.

There are several processes by which the above mechanism can occur: 1) local mixing between the upper and lower stratosphere (mechanism 2), 2) local mixing between the lower stratosphere and upper troposphere (mechanism 3), 3) local mixing between the upper and lower troposphere (mechanism 4), and 4) isentropic mixing between polar and mid-latitude lower stratospheric air (mechanism 5). Sporadic mixing between the upper and lower stratosphere at mid-latitudes is unlikely, given that the stratosphere has a large static stability resulting from an increase in temperature with height.

In contrast, mixing between the lower stratosphere and upper troposphere occurs relatively often and fairly rapidly (Fig. 10b, mechanism 3) (e.g. Reiter, 1975; Holten *et al.*, 1995). High  $^{33}\text{P}/^{32}\text{P}$  ratios would be derived from periodic mixing with the lower stratosphere followed by precipitation scavenging after a given time period. This scenario does not explain the rarity of the observed higher  $^{33}\text{P}/^{32}\text{P}$  ratios in our precipitation data. If higher ratios exist in the upper troposphere one would expect to see a greater number of precipitation samples with high  $^{33}\text{P}/^{32}\text{P}$  ratios rather than only during specific storm events. In addition, tropopause folding and injection of stratospheric air at the midlatitudes has

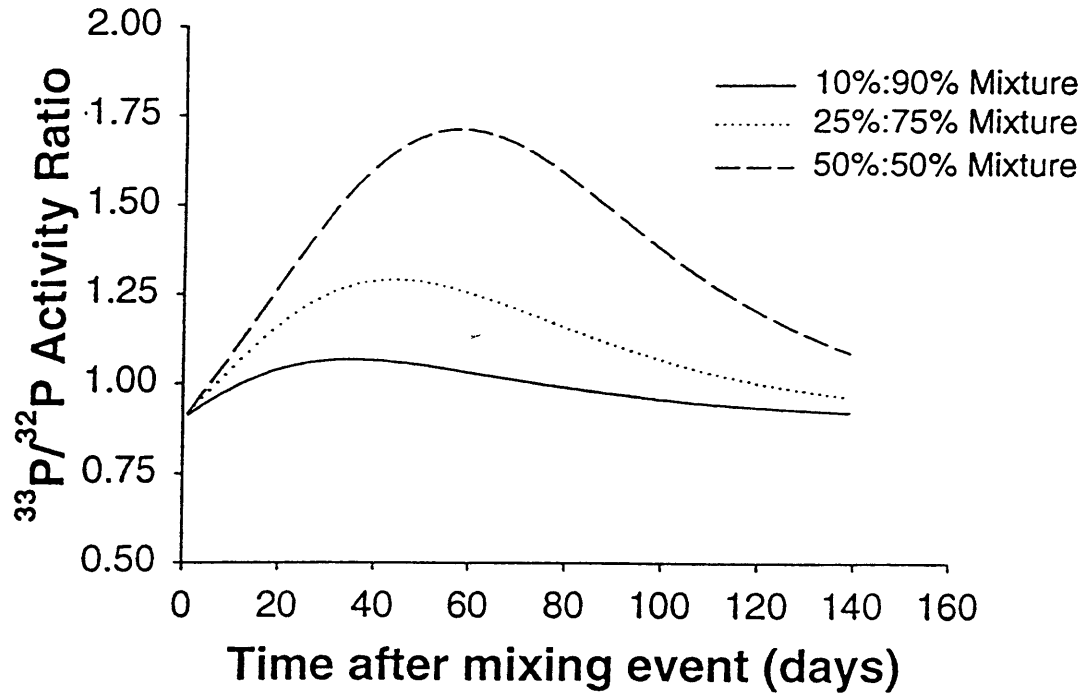


**Figure 3.11** Model results of instantaneously mixing 10% higher activity air with 90% lower activity air, 25% with 75%, and 50% with 50%. Model assumed no further mixing after the initial event.

been found to occur during the early spring months of February, March, and April (Reiter, 1975; Viezee and Singh, 1980). If the ratio measured in our precipitation samples stems from such a process, one would expect to observe a time lag between the STE event and high  $^{33}\text{P}/^{32}\text{P}$  ratios. However, this time lag is not apparent and higher ratios are observed earlier than expected, in December, January and February.

A fourth mechanism is the sequestering of a higher activity airmass from the upper troposphere into the lower troposphere (Fig. 10b). Assuming that this higher tropospheric airmass has an average activity ratio of 0.88, decay of the resulting higher activity airmass alone could produce the observed higher ratios after several weeks. However, lower tropospheric air has been found to have a residence time of several days, too short to produce the highest ratios ( $>1.15$ ) observed in our data.  $^{33}\text{P}/^{32}\text{P}$  ratios less than 1.15 cannot be ruled out as being produced by this pathway.

The last mechanism which can produce  $^{33}\text{P}/^{32}\text{P}$  ratios which exceed equilibrium values invokes intermittent isentropic mixing within the lower stratosphere between higher activity polar regions and the lower activity mid-latitudes (mechanism 5, Fig. 10c). The production rate of  $^{32}\text{P}$  and  $^{33}\text{P}$  increases with increasing latitude (Lal and Peters, 1967). Because the half-lives of  $^{32}\text{P}$  and  $^{33}\text{P}$  are short relative to the residence time of air in the lower stratosphere localized differences in radionuclide concentrations can develop. These regional airmasses may then be rapidly mixed between the polar and mid-latitudes via breaking planetary waves. The zonal mean isentropic mixing times in the lower stratosphere/tropopause boundary are on the order of one year (Hall and Waugh, 1997a/b). However, in the mid-latitude to polar regions, isentropic mixing can occur on much more rapid timescales (McIntyre and Palmer, 1983). Higher ratio  $^{33}\text{P}/^{32}\text{P}$  air could then be mixed into the troposphere during STE events caused by intense storms.

It is obvious from our measurements of  $^{33}\text{P}/^{32}\text{P}$  that these radionuclides can provide powerful insight into the spatial and temporal magnitude of STE processes. However, one must first know the ratio of  $^{33}\text{P}/^{32}\text{P}$  in the source air contributing to our precipitation samples. The mechanisms which produce higher  $^{33}\text{P}/^{32}\text{P}$  ratio air is unclear

but is most likely the result of isopycnal mixing between latitude regions, followed by STE (mechanism 5), and/or STE followed by decay (mechanism 3). There is currently not enough information regarding the distribution of  $^{33}\text{P}$  and  $^{32}\text{P}$  in the upper troposphere and stratosphere to answer which process is the most dominant.

**$^7\text{Be}/^{32}\text{P}$  and  $^7\text{Be}/^{33}\text{P}$ .** Another indication of STE events is found in the large range of activity ratios of  $^7\text{Be}/^{32}\text{P}$ , and  $^7\text{Be}/^{33}\text{P}$  (e.g. Fig. 9). The activity ratios of  $^7\text{Be}/^{32}\text{P}$  and  $^7\text{Be}/^{33}\text{P}$  varied dramatically between precipitation events, over a factor of 10 higher than the non steady-state model estimated range of  $3.7R_0$  and  $2.1R_0$ , respectively. Similar large variations in  $^7\text{Be}/^{32}\text{P}$  and  $^7\text{Be}/^{33}\text{P}$  ratios have been previously reported (Lal *et al.*, 1960; Walton and Fried, 1962) and are probably more pronounced in this study due to the greater number of measurements and the sampling of individual rather than integrated rain events.

One possible explanation for the large range in  $^7\text{Be}/^{32}\text{P}$  and  $^7\text{Be}/^{33}\text{P}$  is a source of higher ratio air being scavenged by some of our precipitation samples. This air must be produced in the same manner as that hypothesized for  $^{33}\text{P}/^{32}\text{P}$ ; either upper/lower stratospheric mixing and/or simple STE alone (Fig. 10). As a result, one would expect to see a relationship between  $^7\text{Be}/^{32}\text{P}$  or  $^7\text{Be}/^{33}\text{P}$  and  $^{33}\text{P}/^{32}\text{P}$ , however this is not found ( $r^2 < 0.5$ ). Previous measurements of  $^{33}\text{P}/^{32}\text{P}$  and  $^7\text{Be}/^{32}\text{P}$  in precipitation (Goel *et al.*, 1959) and in ground air (Luyanus *et al.*, 1970) also showed no correlation. In contrast, upper tropospheric ( $> 3$  km) and stratospheric air measured by Rama and Honda (1961) showed a significant correlation for  $^{33}\text{P}/^{32}\text{P}$  versus  $^7\text{Be}/^{32}\text{P}$  ( $r^2 = 0.61$ ).

Airmass mixing in the various atmospheric regions can occur on varying timescales. As a result, differences in decay may mask any ratio relationship. For this to be true, there should be little or no correlation between  $^7\text{Be}/^{32}\text{P}$  and  $^7\text{Be}/^{33}\text{P}$  ratios, given the differences in half-lives. Yet, the correlation between the ratios is substantial, having an  $r^2 = 0.87$ . This is not surprising, given that the difference between the half-lives of  $^{32}\text{P}$  and  $^{33}\text{P}$  is small (10 days) relative to the difference in half-life between  $^7\text{Be}$  and  $^{32}\text{P}$  and  $^{33}\text{P}$  (28 and 39 days, respectively).

Thus, there must be a process other than STE which affects the observed  ${}^7\text{Be}/{}^{32}\text{P}$  and  ${}^7\text{Be}/{}^{33}\text{P}$  ratios in our study. One of the assumptions in the non-steady state model given by equation (4) is that there is no fractionation of the radionuclides during condensation and precipitation. While fractionation is highly unlikely between  ${}^{32}\text{P}$  and  ${}^{33}\text{P}$ , it is entirely possible that it could be significant for the ratio of  ${}^7\text{Be}/{}^{32}\text{P}$  and  ${}^7\text{Be}/{}^{33}\text{P}$ . Beryllium and phosphorus may be expected to behave differently under certain processes, i.e. differences in scavenging may occur among various aerosol size classes. Evidence of fractionation is further demonstrated in that the correlation between  ${}^7\text{Be}/{}^{32}\text{P}$  and  ${}^{33}\text{P}/{}^{32}\text{P}$  in upper tropospheric and stratospheric *air* is significant, whereas in ground level air and in precipitation, it is not (Rama and Honda, 1961; Goel *et al.*, 1959; Luyanus *et al.*, 1970). Fractionation processes would be expected to be minimized in upper atmospheric air samples, where filter samples efficiently collect aerosols of all types and sizes greater than the filter pore size ( $\sim 0.7 \mu\text{m}$ , Rama and Honda, 1961; Gandrud *et al.*, 1989). In the lower atmosphere and in rain, fractionation would be expected to be significantly greater, given differences in condensation and in the regional frequency of aerosol scavenging by precipitation. The lack of correlation found in our rain data suggests that  ${}^7\text{Be}$ ,  ${}^{32}\text{P}$ , and  ${}^{33}\text{P}$  are scavenging onto different aerosol particle types and/or size classes which can have different origins, transport mechanisms and/or residence times. It should also be noted that all of the high  ${}^7\text{Be}/{}^{32}\text{P}$  and  ${}^7\text{Be}/{}^{33}\text{P}$  ratios ( $> 250$ ) occur during low precipitation periods ( $< 0.3 \text{ cm}$ ), which tend to scavenge aerosols from the lower troposphere.

It appears that the ratios of  ${}^7\text{Be}/{}^{32}\text{P}$ , and  ${}^7\text{Be}/{}^{33}\text{P}$  cannot be used to trace STE. Only isotopes of the same element are appropriate, at least when used in conjunction with the simple non steady state model given in equation (3). However, further measurements of  ${}^7\text{Be}/{}^{32}\text{P}$  and  ${}^7\text{Be}/{}^{33}\text{P}$  in upper tropospheric and stratospheric air and in different aerosol particle sizes and types may provide information into the residence time and transport of various aerosol classes. For example, if the distribution of these radionuclides on various aerosol size classes and types is better constrained then these isotopes could be used to describe atmospheric mixing processes over short time scales.

**${}^7\text{Be}/{}^{210}\text{Pb}$ .** It is obvious that if the ratio of  ${}^7\text{Be}/{}^{32}\text{P}$  and  ${}^7\text{Be}/{}^{33}\text{P}$  suffers from fractionation affects, so should the ratio of  ${}^7\text{Be}/{}^{210}\text{Pb}$ . Nonetheless, further evaluation of how the ratio of  ${}^7\text{Be}/{}^{210}\text{Pb}$  varies in relationship to the other radionuclides may be useful. In previous studies, the ratio of  ${}^7\text{Be}/{}^{210}\text{Pb}$  has been used to determine whether the source of a scavenged air mass is oceanic versus continental and/or upper versus lower tropospheric (Baskaran *et al.*, 1993; Koch *et al.*, 1996; Kim *et al.*, 1998). The major source of  ${}^{210}\text{Pb}$  to the atmosphere is via decay of  ${}^{222}\text{Rn}$ , a gas predominantly emitted from continental material. Therefore, the concentration of  ${}^{210}\text{Pb}$  should decrease with increasing altitude and over the open ocean.  ${}^7\text{Be}$  concentrations should increase with altitude, and remain uniform at constant altitude over land versus sea. Thus, an increase in the  ${}^7\text{Be}/{}^{210}\text{Pb}$  ratio can indicate either STE events or changes in the extent of continental versus oceanic air masses.

The average activity ratio of  ${}^7\text{Be}/{}^{210}\text{Pb}$  measured in rain collected at Woods Hole and at Portsmouth was 12.6 and 20.1, respectively. This is within the range of 11.3 to 25 observed by other investigators (Turekian *et al.*, 1983; Todd *et al.*, 1989, Baskaran *et al.*, 1993; Kim *et al.*, 1998). Lower ratios in previous studies tended to correspond with continental sites, whereas the highest ratio, 25, was measured at Bermuda. The difference in the  ${}^7\text{Be}/{}^{210}\text{Pb}$  ratio between Woods Hole and Portsmouth, suggests that the Woods Hole station measures precipitation derived from more continental air masses, whereas the Portsmouth station measures precipitation from more oceanic air. This is also evident in the higher  ${}^{210}\text{Pb}$  fluxes measured at Woods Hole.

If high  ${}^7\text{Be}/{}^{210}\text{Pb}$  ratios are also indicators of upper/lower tropospheric mixing, and increased ratios of  ${}^7\text{Be}/{}^{32}\text{P}$ ,  ${}^7\text{Be}/{}^{33}\text{P}$  and  ${}^{33}\text{P}/{}^{32}\text{P}$  are predominantly caused by STE, then one would expect to see a relationship. However, no such correlation is apparent in our data. Previous data which include measurements of all four isotopes is limited. Nonetheless, no correlations between  ${}^7\text{Be}/{}^{32}\text{P}$  and  ${}^7\text{Be}/{}^{210}\text{Pb}$  were found in precipitation or between  ${}^{33}\text{P}/{}^{32}\text{P}$  and  ${}^7\text{Be}/{}^{210}\text{Pb}$  in stratospheric *air* samples (Rama and Honda, 1961;



Bhandari *et al.*, 1970). Although a weak correlation ( $r^2 = 0.49$ ,  $n=12$ ) was found between  $^7\text{Be}/^{32}\text{P}$  and  $^7\text{Be}/^{210}\text{Pb}$  in stratospheric air samples.

The lack of correlation between the various radionuclide ratios suggests a difference in chemical reactivity among beryllium, lead and phosphorus. In addition, any relationship between upper and lower tropospheric mixing is probably diminished due to the additional dependence of  $^7\text{Be}$  and  $^{210}\text{Pb}$  on continental versus oceanic air mass sources. Thus, the ratio of  $^7\text{Be}/^{210}\text{Pb}$  may be a qualitative indicator of continental air masses, but it cannot be used to trace tropospheric mixing directly unless used in conjunction with regional atmospheric transport and mixing process models.

## CONCLUSIONS

Elucidating stratosphere/troposphere exchange events and aerosol residence times are important for understanding the cycling of many natural and anthropogenically produced elements. Radioisotopes are unique tools with which to further investigate these processes over temporal scales. Our measurements of  $^{32}\text{P}$ ,  $^{33}\text{P}$ ,  $^7\text{Be}$ , and  $^{210}\text{Pb}$  are the first to be conducted in individual rain events over a seasonal cycle.

Absolute activities of  $^{32}\text{P}$ ,  $^{33}\text{P}$ ,  $^7\text{Be}$ , and  $^{210}\text{Pb}$  were found to vary over a wide range at both at Woods Hole, MA and Portsmouth, NH. No correlations were found between absolute radionuclide activities and rainfall, suggesting that dilution is not a major factor controlling radionuclide activities in rainfall. This theory was tested by serial sampling during large rain events which also showed no decrease in absolute activity with time.

Annual depositional fluxes of  $^{32}\text{P}$ ,  $^{33}\text{P}$ , and  $^7\text{Be}$  measured at both Woods Hole and Portsmouth were similar in magnitude.  $^{32}\text{P}$  and  $^{33}\text{P}$  fluxes, however, were significantly higher than those found previously, while  $^7\text{Be}$  fluxes were similar to those found along the Northeastern coast.  $^{210}\text{Pb}$  fluxes measured at Woods Hole were 25% higher than those measured at Portsmouth, indicating that continental air masses were more prevalent at the Woods Hole site. Significant correlations were found between radionuclide fluxes and

rainfall. This indicates that rainfall is an important removal pathway of these isotopes from the troposphere.

Our results further suggest that simple models which balance cosmogenic production and removal from a single air mass are not sufficient to accurately quantify residence times and cosmic ray irradiance periods of atmospheric aerosols. Stratospheric influences must be considered. Only the ratio of  $^{33}\text{P}/^{32}\text{P}$  measured in precipitation appears to give reasonable estimates for irradiance periods when the effects of STE events are removed from the data. It appears that  $^7\text{Be}/^{32}\text{P}$ ,  $^7\text{Be}/^{33}\text{P}$ ,  $^7\text{Be}/^{210}\text{Pb}$  ratios all suffer from fractionation associated with differences in scavenging among beryllium, lead, and phosphorus.  $^7\text{Be}/^{210}\text{Pb}$  ratios are especially difficult to interpret given the differences in production between the two radionuclides. The ratio of  $^7\text{Be}/^{32}\text{P}$  and  $^7\text{Be}/^{33}\text{P}$ , however, may prove useful in investigating differences in aerosol residence times within various particle size classes and types.

In order to utilize any of the above radionuclide ratios to describe atmospheric mixing and/or aerosol scavenging a more detailed analysis of the distribution of  $^{32}\text{P}$ ,  $^{33}\text{P}$ , and  $^7\text{Be}$  in the upper atmosphere will be necessary. Our measurements of  $^{33}\text{P}/^{32}\text{P}$  ratios have enabled the development of several hypotheses whereby elevated  $^{33}\text{P}/^{32}\text{P}$  ratios can be produced in the upper troposphere and lower stratosphere. The two most likely mechanisms for the origin of high  $^{33}\text{P}/^{32}\text{P}$  ratios are: 1) STE followed by decay, and/or 2) lower stratospheric isentropic mixing followed by STE. Once the distribution of these radionuclides is better constrained, these isotopes can provide powerful insight into the timing and magnitude of STE.

## **ACKNOWLEDGEMENTS**

The authors wish to thank Carolyn Jordan at the University of New Hampshire for collecting and performing the initial processing of samples retrieved from Portsmouth, NH. We would also like to thank the U.S. Coast Guard Station for allowing the collection of samples from their base of operations at Portsmouth Harbor, L. A. Ball for ICPES analyses, J. E. Andrews for rain collector construction, and J. MacFarlane for the map of the Gulf of Maine. The authors further to wish thank G. Crossin for help in collecting and processing samples retrieved from Woods Hole, MA, and Drs. D. Glover, W. Jenkins, M. Kurz and M. Follows and B. Benitez-Nelson for insightful comments pertaining to the manuscript. This work was funded in part by the Office of Naval Research Fellowship Program, STAR Environmental Protection Agency Fellowship Program, National Science Foundation (Grant OCE-9633240), and the Woods Hole Oceanographic Institution (unrestricted funds). This is Contribution 9705 from the Woods Hole oceanographic Institution.

## REFERENCES

- Baskaran, M., A search for the seasonal variability on the depositional fluxes of  $^7\text{Be}$  and  $^{210}\text{Pb}$ , *J. of Geophys. Res.*, 100, 2833-2840, 1995.
- Baskaran, M., C. H. Coleman, and P. H. Santschi, Atmospheric depositional fluxes of  $^7\text{Be}$  and  $^{210}\text{Pb}$  at Gavelston and College Station, Texas, *J. of Geophys. Res.*, 98, 20,555-20,571, 1993.
- Balkanski, Y. J., D. J. Jacob, G. M. Gardner, W. C. Graustein, and K. K. Turekian, Transport and residence times of aerosols inferred from a global three-dimensional simulation of  $^{210}\text{Pb}$ , *J. of Geophys. Res.*, 98, 20,573-20,586, 1993.
- Benitez-Nelson, C. R. and K. O. Buesseler, Measurement of cosmogenic  $^{32}\text{P}$  and  $^{33}\text{P}$  activities in rainwater and seawater, *Anal. Chem.*, 70, 64-72, 1998.
- Bleichrodt, J. F., Mean residence time of cosmic-ray-produced beryllium 7 in the environment, *J. of Geophys. Res.*, 83, 3058-3062, 1978.
- Bhandari, N., D. Lal, and Rama, Vertical structure of the troposphere as revealed by radioactive tracer studies, *J. of Geophys. Res.*, 75(15), 2974-2980, 1970.
- Bhandari, N., D. Lal, and Rama, Stratospheric circulation studies based on natural and artificial radioactive tracer elements, *Tellus*, XVIII, 391-405, 1966.
- Bondietti, E. A., J. N. Brantley, and C. Rangarajan, Size distributions and growth of natural and Chernobyl-derived submicron aerosols in Tennessee, *J. of Environ. Radioact.*, 6, 99-120, 1988.
- Brown, L., G. L. Stensland, J. Klein, and R. Middleton, Atmospheric deposition of  $^7\text{Be}$  and  $^{210}\text{Pb}$ , *Geochem. Cosmochem. Acta*, 3, 135-142, 1989.
- Dibb, J. E., Atmospheric Deposition of beryllium 7 in the Chesapeake Bay region, *J. of Geophys. Res.*, 94(D2), 2261-2265, 1989.
- Dibb, J. E., R. W. Talbot, and G. L. Gregory, Beryllium 7 and lead 210 in the western hemisphere Arctic atmosphere; Observations from three recent aircraft-based sampling programs, *J. of Geophys. Res.*, 97, 16,709-16,715, 1992.
- Drevinsky, P.J.; Wasson, J. T.; Couble, E. C.; Dimond, N. A.,  $^7\text{Be}$ ,  $^{32}\text{P}$ ,  $^{33}\text{P}$ , and  $^{35}\text{S}$ : Stratospheric concentrations and artificial production, *J. of Geophys. Res.*, 69(8), 1457-1467, 1964.
- Dutkiewicz, V. A., and L. Hussain, Stratospheric and tropospheric components of Be in surface air, *J. of Geophys. Res.*, 99, 5783-5788, 1985.
- Dutkiewicz, V. A., and L. Hussain, Determination of stratospheric ozone at ground level using  $^7\text{Be}$ /ozone ratios, *Geophys. Res. Lett.*, 6, 171-174, 1978.
- Koch, D. M., D. J. Jacob, W. C. Graustein, Vertical transport of tropospheric aerosols as indicated by  $^7\text{Be}$  and  $^{210}\text{Pb}$  in a chemical tracer model, *J. of Geophys. Res.*, 101(D13), 18,651-18,666, 1996.
- Koroleff, F., Determination of nutrients, in *Methods of seawater analysis*, 2<sup>nd</sup> ed., edited by K. Grasshoff, M. Ehrherd, and K. Kremling, pp. 125-135, Verlag Chemie, Weinheim, 1983.
- Friend, J. P., H. W. Feely, P.W. Krey, J. Spar, and A. Walton, High altitude sampling program, *Defense Atomic Support Agency Rept. 1300*, August 31, 1961.

- Gandrud, B. W., P. D. Sperry, L. Sanford, K. Kelly, G. V. Ferry, K. R. Chan, filter measurement results from the airborne Antarctic ozone experiment, *J. of Geophys. Res.*, 94(D9), 11,285-11, 297, 1989.
- Goel, P.S., N. Narsappaya, C. Prabhakara, Rama, and P. K. Zutshi, Study of cosmic ray produced short-lived isotopes  $^{32}\text{P}$ ,  $^{33}\text{P}$ ,  $^7\text{Be}$ , and  $^{35}\text{S}$  in tropical latitudes, *Tellus*, XI, 91-100, 1959.
- Hall, T. M. and D. Waugh, Timescales for the stratospheric circulation derived from tracers, *J. of Geophys. Res.*, 102, 9881-9001, 1997.
- Hall, T. M. and D. Waugh, Tracer transport in the tropical stratosphere due to vertical diffusion and horizontal mixing, *Geophys. Res. Lett.*, 24, 1383-1386, 1997.
- Holton, J. R., P. H. Haynes, M. E. McIntyre, A. R., Douglass, R. B. Rood, L. Pfister, Stratosphere-troposphere exchange, *Rev. of Geophys.*, 33(4), 403-439, 1995.
- Kim, G., T. M. Church, N. Hussain, and J. Scudlark, Seasonal variability in atmospheric depositional fluxes of stable Pb,  $^{210}\text{Pb}$ , and  $^7\text{Be}$  into Chesapeake Bay, *Science*, submitted, 1998.
- Lal, D. Cosmic ray produced radioisotopes for studying the general circulation in the atmosphere, *Indian J. Meteor. and Geophys.*, 10, 147-154, 1959.
- Lal, D., Rama Thor, P. K. Zutshi, P., Radioisotopes  $^{32}\text{P}$ ,  $^7\text{Be}$ , and  $^{35}\text{S}$  in the atmosphere, *J. of Geophys. Res.*, 65(2), 669-673, 1960.
- Lal, D., and B. Peters, Cosmic ray produced radioactivity on the Earth, in *Handbuch der Physik* 46/2, edited by K. Sitte, pp. 551-612, Springer Verlag, New York, 1967.
- Luyanus, V., R. Y. Yasyulynis, D. A. Shopanskiene, and B. I. Styra, Cosmogenic  $^{22}\text{Na}$ ,  $^7\text{Be}$ ,  $^{32}\text{P}$ , and  $^{33}\text{P}$  in atmospheric dynamics research, *J. of Geophys. Res.*, 75, 3665-3667, 1970.
- Maenhaut, W., W. H. Zoller, and D. G. Coles, Radionuclides in the South Pole atmosphere, *J. of Geophys. Res.*, 84, 3131-3138, 1979.
- Martell, E. A. and H. E. Moore, Tropospheric aerosol residence times: A critical review, *J. Rech. Atmos.*, 8, 903-910, 1974.
- McIntyre, M. E., and T. N. Palmer, Breaking planetary waves in the stratosphere, *Nature*, 305, 593-594, 1983.
- Moore, H. E., S. E. Poet, E. A. Martell,  $^{222}\text{Rn}$ ,  $^{210}\text{Pb}$ ,  $^{210}\text{Bi}$ , and  $^{210}\text{Po}$  profiles and aerosol residence times versus altitude, *J. of Geophys. Res.*, 78(30), 7065-7075, 1973.
- Poet, S. E., H. E. Moore, and E. A. Martell, Lead 210, Bismuth 210, and Polonium 210 in the atmosphere: Accurate ratio measurement and application to aerosol residence time determination, *J. of Geophys. Res.*, 77, 6,515-6,527, 1972.
- Olsen, C. R., I. L. Larsen, P. D. Lowry, and n. H. Cutshal, J. F. Todd, G. T. F. Wong, and W. H. Casey, Atmospheric fluxes and marsh-soil inventories of  $^7\text{Be}$  and  $^{210}\text{Pb}$ , *J. of Geophys. Res.*, 90, 10,487-10,495, 1985.
- Polian, D. H., G. Lambert, B. Ardouin, and A. Jegou, Long-range transport of continental radon in Subantarctic areas, *Tellus*, 38B, 178-189, 1986.
- Rama, T. and M. Honda, Natural Radioactivity in the atmosphere, *J. of Geophys. Res.*, 66(10), 3227-3231, 1961.

- Ramaswamy, V., M. D. Schwarzkopf, K. P. Shine, Radiative forcing of climate from halocarbon-induced global stratospheric ozone loss, *Nature*, 355, 810-812, 1992.
- Reiter, E. R., Stratospheric-tropospheric exchange processes, *Rev. of Geophys.*, 13, 459-474, 1975.
- Shea, D. J., Surface air temperature, precipitation, sea level pressure, and sea surface temperature. (45 deg. S- 90 deg. N), Boulder, Colorado. NCAR Technical Note, 269, 1986.
- Todd, J. F., G. T. F. Wong, C. R. Olsen, I. L. Larsen, Atmospheric depositional characteristics of Beryllium 7 and lead 210 along the southeastern Virginia coast, *J. of Geophys. Res.*, 94(D8), 11,106-11116, 1989.
- Toumi, R., S. Bekki, K. S. Law, Indirect influence of ozone depletion on climate forcing by clouds, *Nature*, 372, 348-351, 1994.
- Turekian, K. K., Y. Nozaki, and L. K. Beninger, Geochemistry of atmospheric radon and radon products, *Annu. Rev. Earth Planet. Sci.*, 5, 227-255, 1977.
- Turekian, K. K., L. K. Beninger, and E. P. Dion, <sup>7</sup>Be and <sup>210</sup>Pb total deposition fluxes at New Haven, Connecticut, and at Bermuda, *J. of Geophys. Res.*, 88, 5411-5415, 1983.
- Viezee, W., and H. B. Singh, The distribution of beryllium-7 in the troposphere: Implications on stratospheric/tropospheric air exchange, *Geophys. Res. Lett.*, 7, 805-808, 1980.
- Walton, A, and R. E. Fried, The deposition of <sup>7</sup>Be and <sup>32</sup>P in precipitation at north temperate latitudes, *J. of Geophys. Res.* 67(13), 5335-5340, 1962.
- Waser, N. A. D., and M. P. Bacon, Wet deposition fluxes of cosmogenic <sup>32</sup>P and <sup>33</sup>P and variations in the <sup>33</sup>P/<sup>32</sup>P ratios at Bermuda, *Earth and Planet. Sci. Lett.*, 133, 71-80, 1995.
- Wilkening, M. H. and W. E. Clements, Radon-222 from the ocean surface, *J. Geophys. Res.*, 80, 3828-3830, 1975.
- WMO, Scientific Assessment of Ozone Depletion: 1994, *WMO 37*, Geneva, Switzerland, 1995.

**Table 3.1** Rainfall and specific activities of  $^{32}\text{P}$ ,  $^{33}\text{P}$ ,  $^7\text{Be}$ , and  $^{210}\text{Pb}$  measured in individual rain events at Clark Laboratory at Woods Hole, MA (41°32' N, 70°39'W). ND = No Data. BD = Below Detection.

Sample	Rainfall (cm)	$^{32}\text{P}$ (dpm L <sup>-1</sup> )	± error	$^{33}\text{P}$ (dpm L <sup>-1</sup> )	± error	$^7\text{Be}$ (dpm L <sup>-1</sup> )	± error	$^{210}\text{Pb}$ (dpm L <sup>-1</sup> )	± error
15-Mar-96	ND	1.61	0.41	1.20	0.60	ND		ND	
18-Mar-96	ND	1.42	0.06	1.44	0.11	ND		ND	
02-Apr-96	2.62	1.55	0.04	1.17	0.03	ND		ND	
06-Apr-96	1.67	3.51	0.30	2.21	0.17	ND		ND	
07-Apr-96	ND	1.65	0.23	1.19	0.15	ND		ND	
10-Apr-96	1.73	11.53	0.92	9.24	0.72	ND		ND	
12-Apr-96	0.31	4.53	0.90	4.96	0.25	ND		ND	
15-Apr-96	2.10	3.77	0.80	3.45	0.30	ND		ND	
23-Apr-96	0.20	1.60	0.52	1.68	0.06	ND		ND	
27-Apr-96	0.08	2.36	0.44	2.20	0.31	ND		ND	
29-Apr-96	0.22	3.31	0.24	2.20	0.07	ND		ND	
30-Apr-96	0.90	1.90	0.42	1.78	0.12	ND		ND	
08-May-96	0.41	1.45	0.43	1.55	0.88	ND		ND	
10-May-96	0.53	4.54	1.42	2.82	0.61	ND		ND	
17-May-96	0.87	3.11	0.52	3.47	0.20	88	4	12.3	0.9
21-May-96	0.14	4.93	0.35	3.33	0.17	283	13	96.4	4.5
30-May-96	1.72	ND		ND		60	4	24.9	1.5
04-Jun-96	0.97	3.05	0.24	2.42	0.47	ND		ND	
10-Jun-96	0.77	1.42	0.23	1.10	0.32	119	8	8.2	1.1
17-Jun-96	0.79	3.86	0.12	3.27	0.17	288	13	28.9	1.3
20-Jun-96	0.40	1.63	0.08	1.12	0.11	ND		ND	
22-Jun-96	0.05	4.10	0.18	3.87	0.10	425	19	36.9	1.7
01-Jul-96	0.35	3.09	0.10	2.42	0.12	111	6	10.8	0.7
12-Jul-96	0.07	0.61	0.06	0.54	0.05	99	5	46.5	2.2

**Table 3.1 Continued.**

Sample	Rainfall (cm)	<sup>32</sup> P (dpm L <sup>-1</sup> )	± error	<sup>33</sup> P (dpm L <sup>-1</sup> )	± error	<sup>7</sup> Be (dpm L <sup>-1</sup> )	± error	<sup>210</sup> Pb (dpm L <sup>-1</sup> )	± error
15-Jul-96	0.51	0.74	0.04	0.58	0.05	115	5	20.4	1.0
19-Jul-96	0.20	2.01	0.09	1.38	0.05	183	8	27.2	1.3
02-Aug-96	3.28	3.06	0.14	2.69	0.10	260	11	54.5	2.5
12-Aug-96	1.27	ND		ND		116	5	7.3	0.6
13-Aug-96	2.57	3.60	0.44	2.28	0.28	12	1	2.4	0.2
29-Aug-96	1.65	ND		ND		128	6	14.1	0.7
01-Sep-96	5.88	0.91	0.08	1.33	0.08	110	5	14.4	0.9
08-Sep-96	5.56	0.47	0.02	0.66	0.05	108	5	22.2	1.1
13-Sep-96	0.33	1.26	0.16	1.06	0.04	48	2	5.8	0.4
14-Sep-96	4.15	1.42	0.09	2.01	0.18	143	6	4.6	0.3
23-Sep-96	1.12	ND		ND		244	11	12.6	0.7
25-Sep-96	0.36	0.87	0.04	0.88	0.23	332	14	50.4	2.3
28-Sep-96	0.63	3.39	0.17	2.88	0.11	399	17	13.4	0.8
29-Sep-96	0.18	ND		ND		229	10	11.1	0.7
08-Oct-96	4.91	ND		ND		74	3	8.0	0.5
19-Oct-96	2.72	ND		ND		69	3	4.2	0.4
20-Oct-96	4.29	2.73	0.73	2.79	0.61	38	2	13.3	0.8
21-Oct-96	0.07	ND		ND		469	21	125.2	5.9
23-Oct-96	1.98	ND		ND		222	10	26.6	1.2
28-Oct-96	0.51	ND		ND		160	7	42.2	2.1
30-Oct-96	0.21	2.86	0.18	3.00	0.16	261	11	54.0	2.6
01-Nov-96	0.23	7.11	0.26	5.20	0.29	273	12	24.0	1.4
07-Nov-96	0.15	3.10	0.09	3.96	0.13	370	16	39.8	1.9
09-Nov-96	0.60	3.61	0.13	3.42	0.20	150	7	16.4	1.0
19-Nov-96	0.08	9.08	0.35	8.03	0.52	717	31	127.1	5.7
25-Nov-96	0.51	13.61	1.17	9.42	0.24	555	24	83.7	3.7



**Table 3.1 Continued.**

Sample	Rainfall (cm)	<sup>32</sup> P		<sup>33</sup> P		<sup>7</sup> Be		<sup>210</sup> Pb	
		(dpm L <sup>-1</sup> )	± error	(dpm L <sup>-1</sup> )	± error	(dpm L <sup>-1</sup> )	± error	(dpm L <sup>-1</sup> )	± error
26-Nov-96	0.80	1.72	0.05	1.69	0.06	84	4	7.8	0.8
27-Nov-96	0.55	2.57	0.12	3.06	0.18	224	10	29.9	1.4
01-Dec-96	1.04	1.79	0.05	1.46	0.22	143	6	12.0	0.9
12-Dec-96	0.29	2.34	0.08	3.36	0.54	309	13	64.2	2.9
14-Dec-96	0.08	0.84	0.04	1.10	0.06	221	10	15.7	0.9
18-Dec-96	0.51	2.47	0.14	3.21	0.19	99	5	6.9	0.4
19-Dec-96	1.47	1.50	0.13	2.16	0.30	90	4	3.6	0.3
01-Jan-97	0.03	1.49	0.34	1.53	0.18	292	13	34.5	1.6
05-Jan-97	0.13	8.03	0.41	9.79	0.77	350	16	94.5	4.4
09-Jan-97	0.28	1.92	0.05	1.50	0.35	192	8	23.1	1.2
12-Jan-97	0.08	1.37	0.07	1.58	0.24	233	10	18.2	0.9
16-Jan-97	1.04	2.15	0.10	1.84	0.21	141	6	11.7	0.6
22-Jan-97	0.93	0.70	0.07	0.80	0.10	158	7	15.8	0.8
25-Jan-97	0.77	2.05	0.05	2.34	0.32	220	10	26.5	1.2
27-Jan-97	1.21	2.25	0.05	2.87	0.40	334	15	16.7	0.8
28-Jan-97	1.07	0.82	0.02	0.54	0.06	69	3	4.4	0.3
01-Feb-97	0.26	3.17	0.38	2.89	0.80	544	24	42.4	1.9
04-Feb-97	1.20	1.19	0.09	1.30	0.25	74	3	9.7	0.5
05-Feb-97	0.54	1.45	0.03	1.14	0.11	143	6	9.8	0.5
14-Feb-97	0.99	3.67	0.26	3.81	0.33	242	10	29.3	1.3
17-Feb-97	0.68	0.64	0.04	0.56	0.09	65	3	11.7	0.6
26-Feb-97	0.57	2.07	0.14	1.67	0.14	202	10	26.5	1.9
02-Mar-97	0.10	2.20	0.19	1.65	0.18	246	12	21.6	1.4
09-Mar-97	0.77	3.38	0.08	2.91	0.15	138	6	10.1	0.6
14-Mar-97	1.74	2.74	0.08	2.13	0.14	197	9	24.2	1.2
22-Mar-97	0.95	4.81	0.31	4.82	0.16	820	36	91.5	4.2

**Table 3.1 Continued.**

Sample	Rainfall (cm)	<sup>32</sup> P		<sup>33</sup> P		<sup>7</sup> Be		<sup>210</sup> Pb	
		(dpm L <sup>-1</sup> )	± error	(dpm L <sup>-1</sup> )	± error	(dpm L <sup>-1</sup> )	± error	(dpm L <sup>-1</sup> )	± error
25-Mar-97	1.28	4.72	0.25	4.78	0.20	277	12	18.2	0.9
28-Mar-97	5.17	3.48	0.17	2.99	0.07	190	8	14.4	0.9
31-Mar-97	4.48	0.70	0.10	0.59	0.07	143	6	11.9	0.6
01-Apr-97	4.27	1.67	0.07	1.63	0.14	37	2	2.5	0.4
13-Apr-97	1.49	3.96	0.10	3.71	0.09	264	11	10.5	0.6
17-Apr-97	0.51	2.59	0.20	2.82	0.12	515	22	24.2	1.2
24-Apr-97	0.14	2.20	0.06	1.87	0.07	232	10	32.4	1.5
27-Apr-97	0.18	4.52	0.13	3.83	0.13	237	10	28.8	1.5
28-Apr-97	0.81	1.72	0.08	1.58	0.05	72	3	5.4	0.5
01-May-97	0.79	2.36	0.09	1.87	0.08	150	7	27.0	1.3
9-May-97	0.63	6.38	0.47	6.28	0.33	301	13	31.6	1.6
10-May-97	0.13	2.22	0.10	1.75	0.15	491	22	26.8	4.0
13-May-97	0.19	4.35	0.11	4.28	0.13	173	8	21.1	1.1
16-May-97	1.33	4.52	0.25	4.23	0.23	210	9	24.9	1.1
18-May-97	1.21	3.57	0.11	3.40	0.09	228	10	30.9	1.4
19-May-97	0.38	7.51	0.22	6.84	0.22	380	17	46.4	2.1
20-May-97	0.09	7.46	0.38	7.22	0.30	284	14	23.9	1.5
26-May-97	2.03	0.43	0.06	0.34	0.05	36	2	14.8	0.7
31-May-97	2.27	0.89	0.04	0.84	0.02	88	4	26.2	1.2
01-Jun-97	0.24	3.38	0.12	3.13	0.09	69	3	3.9	0.4
02-Jun-97	0.23	4.34	0.15	3.90	0.13	183	8	8.4	0.6
13-Jun-97	0.13	2.68	0.08	2.76	0.11	348	16	56.7	2.7
18-Jun-97	0.66	1.76	0.06	1.43	0.06	120	6	30.6	1.7
19-Jun-97	0.08	2.55	0.11	2.32	0.16	399	20	63.3	4.0
22-Jun-97	0.76	2.16	0.05	1.84	0.05	210	9	31.4	1.5
26-Jun-97	0.48	2.16	0.06	1.63	0.09	164	7	41.3	1.9

**Table 3.1 Continued.**

Sample	Rainfall (cm)	<sup>32</sup> P (dpm L <sup>-1</sup> )	± error	<sup>33</sup> P (dpm L <sup>-1</sup> )	± error	<sup>7</sup> Be (dpm L <sup>-1</sup> )	± error	<sup>210</sup> Pb (dpm L <sup>-1</sup> )	± error
03-Jul-97	0.66	1.75	0.19	1.18	0.11	ND		ND	
18-Jul-97	0.13	9.04	0.38	7.61	0.32	313	16	113.9	5.1
03-Aug-97	0.47	3.85	0.13	3.18	0.10	47	2	5.5	0.6
04-Aug-97	0.62	2.51	0.07	2.27	0.06	210	9	32.1	1.9
05-Aug-97	0.06	2.17	0.20	2.03	0.46	145	7	29.9	2.1
09-Aug-97	0.74	1.19	0.03	0.98	0.03	ND		ND	
13-Aug-97	1.23	1.24	0.06	1.18	0.08	ND		ND	
17-Aug-97	2.66	0.57	0.03	0.45	0.03	21	1	6.5	0.5
18-Aug-97	0.13	0.46	0.07	0.30	0.06	20	5	3.2	0.2
29-Aug-97	2.36	1.39	0.07	1.36	0.05	149	7	6.4	0.5
03-Sep-97	0.71	2.56	0.13	2.49	0.10	191	8	25.3	1.2
12-Sep-97	0.44	2.94	0.12	2.97	0.08	209	9	15.8	0.9
20-Sep-97	0.15	0.62	0.07	0.60	0.07	259	12	25.7	1.3
25-Sep-97	0.08	1.55	0.18	1.31	0.08	657	29	72.3	3.5
29-Sep-97	0.57	1.17	0.05	0.83	0.03	54	3	14.1	0.9
03-Oct-97	0.23	2.96	0.13	2.47	0.15	ND		28.6	1.5
05-Oct-97	0.04	4.05	0.81	3.44	0.43	1347	63	144.2	7.2
20-Oct-97	0.18	2.57	0.07	2.27	0.07	122	6	15.8	1.1
25-Oct-97	1.88	0.88	0.06	0.86	0.06	52	3	26.1	1.3
26-Oct-97	1.69	0.31	0.03	0.28	0.02	17	2	4.9	0.7
01-Nov-97	3.80	1.24	0.05	1.14	0.06	118	5	15.4	0.8
02-Nov-97	0.05	1.59	0.15	1.29	0.14	99	6	10.6	1.4
04-Nov-97	0.30	4.36	0.09	3.83	0.36	170	8	4.7	0.5
08-Nov-97	2.83	3.10	0.32	3.78	0.39	60	3	5.1	0.8
15-Nov-97	0.11	3.61	0.13	3.83	0.28	1442	64	29.5	1.8
22-Nov-97	2.08	0.91	0.06	0.75	0.04	291	13	14.7	0.9

**Table 3.1 Continued.**

Sample	Rainfall (cm)	<sup>32</sup> P (dpm L <sup>-1</sup> )	± error	<sup>33</sup> P (dpm L <sup>-1</sup> )	± error	<sup>7</sup> Be (dpm L <sup>-1</sup> )	± error	<sup>210</sup> Pb (dpm L <sup>-1</sup> )	± error
30-Nov-97	1.05	0.68	0.01	0.46	0.02	24	2	6.9	0.7
01-Dec-97	0.21	1.97	0.12	1.69	0.18	408	48	11.4	0.5
03-Dec-97	0.11	1.39	0.14	1.26	0.19	504	22	27.5	1.5
06-Dec-97	0.46	0.98	0.10	1.07	0.05	215	17	28.0	2.4
13-Dec-97	0.85	1.80	0.06	2.20	0.08	365	18	59.0	3.0
24-Dec-97	0.64	0.63	0.12	0.58	0.10	123	7	3.8	0.5
25-Dec-97	0.07	0.53	0.01	0.55	0.14	173	8	4.7	0.4
27-Dec-97	1.03	0.18	0.04	0.22	0.03	59	4	9.9	0.8
29-Dec-97	1.65	2.74	0.24	2.09	0.85	237	15	16.7	1.7
06-Jan-98	0.57	2.61	0.11	2.42	0.18	154	8	22.1	1.3
07-Jan-98	0.32	0.92	0.05	0.76	0.07	83	4	4.0	0.4
08-Jan-98	0.99	3.28	0.15	2.69	0.19	53	3	1.6	0.4
09-Jan-98	0.52	1.66	0.08	1.52	0.16	119	8	5.9	0.8
10-Jun-98	0.89	2.48	0.12	2.27	0.07	140	7	5.5	0.5
13-Jan-98	0.52	1.70	0.07	1.54	0.06	307	15	17.4	1.2
16-Jan-98	1.27	0.98	0.06	0.83	0.03	35	2	14.6	1.2
17-Jan-98	1.36	1.32	0.11	1.24	0.06	129	6	3.6	0.4
18-Jan-98	1.71	2.39	0.10	2.39	0.10	178	10	10.9	1.3
19-Jan-98	0.04	1.21	0.09	1.06	0.04	54	3	6.1	0.7
20-Jan-98	0.11	0.92	0.03	1.07	0.06	189	13	10.2	1.5
24-Jan-98	3.84	2.17	0.06	1.89	0.23	134	8	9.5	0.8
25-Jan-98	0.84	1.54	0.04	1.50	0.18	221	13	5.3	0.8
29-Jan-98	1.85	2.02	0.06	2.08	0.07	78	5	12.8	0.7
31-Jan-98	0.20	3.96	0.12	3.82	0.13	394	18	38.4	1.9

**Table 3.1 Continued.**

<b>Sample</b>	<b>Rainfall (cm)</b>	<b><sup>32</sup>P (dpm L<sup>-1</sup>)</b>	<b>± error</b>	<b><sup>33</sup>P (dpm L<sup>-1</sup>)</b>	<b>± error</b>	<b><sup>7</sup>Be (dpm L<sup>-1</sup>)</b>	<b>± error</b>	<b><sup>210</sup>Pb (dpm L<sup>-1</sup>)</b>	<b>± error</b>
04-Feb-98	1.23	4.00	0.39	3.26	0.24	126	12	7.1	0.3
05-Feb-98	0.61	2.59	0.23	1.95	0.17	77	4	3.6	0.3
06-Feb-98	0.86	1.86	0.11	1.42	0.09	235	10	7.7	0.5

**Table 3.2** Rainfall and specific activities of  $^{32}\text{P}$ ,  $^{33}\text{P}$ ,  $^7\text{Be}$ , and  $^{210}\text{Pb}$  measured during integrated periods at the U.S. Coast Guard Station, Portsmouth, NH (43°04' N, 70°42' W). Samples are decay corrected to the midpoint of collection. ND = No Data. BD = Below Detection.

Sample	Rainfall (cm)	$^{32}\text{P}$ (dpm L <sup>-1</sup> )	± error	$^{33}\text{P}$ (dpm L <sup>-1</sup> )	± error	$^7\text{Be}$ (dpm L <sup>-1</sup> )	± error	$^{210}\text{Pb}$ (dpm L <sup>-1</sup> )	± error
05-Mar-97	2.98*	1.31	0.04	0.99	0.12	141	6	15.7	0.8
17-Mar-97	2.80	1.32	0.05	1.30	0.26	206	10	16.7	1.1
26-Mar-97	2.56	1.34	0.12	0.94	0.11	127	6	7.0	0.6
07-Apr-97	3.40	1.40	0.45	0.92	0.12	126	6	10.1	0.6
16-Apr-97	4.96	7.61	0.29	6.66	0.44	187	8	5.6	0.3
19-Apr-97	5.02	1.36	0.07	1.50	0.05	118	6	8.2	0.7
24-Apr-97	1.68	2.15	0.19	1.34	0.18	158	8	4.9	0.4
06-May-97	2.40	3.63	0.84	2.79	0.26	375	17	25.8	1.3
17-May-97	2.68	3.10	0.29	2.56	0.25	255	12	9.2	0.7
02-Jun-97	2.06	3.02	0.23	2.96	0.17	256	12	20.3	1.0
16-Jun-97	2.40	3.25	0.73	1.79	0.25	149	7	9.4	0.6
30-Jun-97	3.44	2.26	0.15	2.00	0.15	197	9	8.1	0.6
14-Jul-97	3.02	3.40	0.55	2.63	0.31	166	7	15.5	0.8
30-Jul-97	4.51	1.76	0.08	1.36	0.07	138	6	9.5	0.5
08-Aug-97	6.20	1.04	0.09	0.66	0.09	100	5	5.4	0.4
02-Sep-97	2.22	2.17	0.18	1.98	0.18	263	13	17.6	1.1
24-Sep-97	3.14	BD		BD		262	19	12.8	1.3
19-Oct-97	6.00	1.50	0.12	1.16	0.11	132	4	4.6	0.4
08-Nov-97	3.02	0.81	0.14	1.08	0.09	196	6	4.1	0.6

\* Rainfall may be underestimated due to snowfall.

**Table 3.3** Rainfall and specific activities  $^{32}\text{P}$ ,  $^{33}\text{P}$ ,  $^7\text{Be}$ , and  $^{210}\text{Pb}$  measured sequentially during single rainfall events lasting 6-12 hours at Woods Hole, MA. BD = Below Detection.

Sample	Rainfall (cm)	$^{32}\text{P}$ (dpm L <sup>-1</sup> )	± error	$^{33}\text{P}$ (dpm L <sup>-1</sup> )	± error	$^7\text{Be}$ (dpm L <sup>-1</sup> )	± error	$^{210}\text{Pb}$ (dpm L <sup>-1</sup> )	± error
<i>6-Dec-96</i>									
1	0.70	1.56	0.20	2.48	0.23	134	6	12.4	0.8
2	0.72	3.26	0.14	3.24	0.10	206	11	20.0	1.7
3	0.39	0.75	0.08	0.94	0.07	67	4	7.2	0.8
4	0.51	2.19	0.35	3.00	0.57	216	9	25.5	1.3
5	0.22	0.96	0.09	1.10	0.20	157	8	15.7	1.2
<i>25-Jul-97</i>									
1	1.35	1.89	0.18	1.61	0.21	47	3	11.5	1.1
2	0.44	3.04	0.16	3.23	0.26	136	6	11.1	1.9
3	0.68	0.82	0.14	0.69	0.12	21	1	1.7	0.5
4	0.49	1.21	0.16	0.94	0.16	62	3	4.4	0.7
5	0.51	1.43	0.03	1.15	0.19	62	3	5.7	0.7
6	0.68	ND		ND		47	2	5.5	0.6
<i>8-Aug-97</i>									
1	0.88	0.40	0.05	0.32	0.03	27	1	4.1	0.4
2	0.91	0.47	0.02	0.28	0.03	27	2	3.2	0.6
3	0.25	1.40	0.12	1.05	0.09	84	4	7.6	0.7
4	1.33	0.94	0.07	0.67	0.08	55	3	6.5	0.8
5	0.05	1.81	0.07	1.49	0.04	68	4	7.7	0.9
<i>14-Nov-97</i>									
1	0.33	2.80	0.11	2.50	0.11	167	7	5.0	0.5
2	0.50	1.89	0.06	1.63	0.07	77	4	2.4	0.5
3	0.06	1.07	0.05	0.99	0.06	43	2	2.0	0.3
4	0.30	2.33	0.05	2.15	0.12	57	3	2.3	0.5

**Table 3.3 Continued.**

<b>Sample</b>	<b>Rainfall (cm)</b>	<b><sup>32</sup>P (dpm L<sup>-1</sup>)</b>	<b>± error</b>	<b><sup>33</sup>P (dpm L<sup>-1</sup>)</b>	<b>± error</b>	<b><sup>7</sup>Be (dpm L<sup>-1</sup>)</b>	<b>± error</b>	<b><sup>210</sup>Pb (dpm L<sup>-1</sup>)</b>	<b>± error</b>
<i>23-Dec-97</i>									
1	0.15	0.81	0.17	0.79	0.13	99	8	18.4	1.6
2	0.20	0.70	0.13	0.72	0.07	58	3	3.0	0.3
3	0.75	0.66	0.15	0.69	0.12	23	1	1.1	0.2
4	1.37	0.25	0.07	0.24	0.06	44	2	2.4	0.2
5	1.68	BD		BD		38	3	1.5	0.3
6	1.74	BD		BD		55	3	3.0	0.6



## Chapter 4

### Temporal variability of inorganic and organic phosphorus cycling in the coastal ocean

#### ABSTRACT

Study of the temporal variations of nutrient uptake, regeneration and export are important for understanding the mechanisms which control plankton distributions, particulate export, and the biological cycling of marine organic matter. In this study, we have developed a new technique which has enabled the determination of *in situ* phosphorus turnover rates in a coastal marine environment using the naturally occurring radionuclides, phosphorus-32 ( $t_{1/2} = 14.3$  d) and phosphorus-33 ( $t_{1/2} = 25.3$  d). Both  $^{32}\text{P}$  and  $^{33}\text{P}$  were determined in dissolved inorganic, organic, and particulate phosphorus pools over a seasonal cycle. Here we present the first evidence of the temporal variability in the residence time of dissolved organic and inorganic phosphorus. Our results suggest that bacteria and picoplankton utilize phosphorus on rapid timescales and play an important role in the remineralization of dissolved organic phosphorus and in the uptake of dissolved inorganic phosphorus during the late summer.

## INTRODUCTION

The radionuclides  $^{32}\text{P}$  and  $^{33}\text{P}$  are produced primarily by cosmic ray interactions with atmospheric argon and enter the oceans predominantly in rain (Waser and Bacon, 1995; Benitez-Nelson and Buesseler, 1998a). If the ratio of  $^{33}\text{P}/^{32}\text{P}$  in rain is known, then one can determine the relative 'age' of cosmogenic P by measuring the  $^{33}\text{P}/^{32}\text{P}$  ratio in various biological pools. The higher the ratio, the older the P pool. The inventories of  $^{32}\text{P}$  and  $^{33}\text{P}$  in the ocean are quite low, ranging from just tens to hundreds of d.p.m. (disintegrations per minute)  $\text{m}^{-2}$  (Lal and Lee, 1988; Lee *et al.*, 1991;1992; Waser *et al.*, 1995) Thus,  $^{32}\text{P}$  and  $^{33}\text{P}$  measurements require several thousand liters of seawater and extensive purification. Previous investigations which sought to utilize these isotopes were hampered by a lack of known input fluxes, possible contamination, and the inability to measure the low energy beta emitter  $^{33}\text{P}$ , especially in high P coastal environments (Lal and Lee, 1988; Lee *et al.*, 1991; Waser *et al.*, 1995). This study is the first to constrain the  $^{32}\text{P}$  and  $^{33}\text{P}$  input flux (Benitez-Nelson and Buesseler, 1998a) *and* to simultaneously measure both these isotopes in dissolved inorganic, organic and particulate pools.

## STUDY AREA

Sampling was conducted in Wilkinson Basin, in the Gulf of Maine ( $42^{\circ}29.41'\text{N}$   $69^{\circ}45.02'\text{W}$ ) during four cruises in March, April, July and August of 1997 (Fig. 4.1). This area was chosen for a number of reasons which include the large seasonality in plankton production, relatively low horizontal advection and diffusion, and its proximity to the Woods Hole Oceanographic Institution. More importantly, however, is that elucidating nutrient cycling within this area will have a tremendous impact on current understanding of the Gulf of Maine ecosystem.

The Gulf of Maine is a highly productive region which supports one of the largest fisheries in North America (O'Reilly and Busch, 1984). Measurements of inorganic nutrients, while limited, indicate that this regime is predominantly nitrogen limited, as nitrate and nitrite concentrations decrease to levels which are below detection while

inorganic phosphate and silicate do not (Benway and Loder, 1996; Christensen *et al.*, 1996; Loder *et al.*, 1996). In addition, during the summer the ratio of dissolved inorganic nitrogen (nitrate + nitrite + ammonium) to dissolved inorganic phosphate appears to be over an order of magnitude lower than the expected Redfield N:P ratios of 16:1 (Loder *et al.*, 1996).

There is a large range of estimates of new and recycled production within the Gulf of Maine (O'Reilly and Busch, 1984; Campbell, 1986; Schlitz and Cohen, 1984; Townsend, 1991; Christensen *et al.*, 1991; Charette *et al.*, 1996; Pilskaln *et al.*, 1996; Townsend, 1998). This lack of consensus is largely due to the limited set of integrated time-series measurements of nutrient cycling in this basin. As a result, it is not entirely clear what the effects of increasing anthropogenic nitrogen inputs are on the Gulf of Maine ecosystem. Other limiting nutrients, particularly phosphorus, may become essential for primary production within future years (Hecky and Kilham, 1988). In any case, greater understanding of phosphorus cycling is of prominent importance, since the deviation of dissolved inorganic nutrient concentrations from Redfield ratios may result in both coastal eutrophication and more frequent blooms of harmful plankton (Hecky and Kilham, 1988; Smayda, 1991; Gulf of Maine Research Plan, 1992). Phosphorus has been studied to a significantly lesser extent than nitrogen in the Gulf of Maine, therefore, it is difficult to describe its role in food web dynamics with any degree of confidence.

Water circulation within the Gulf of Maine is complex. Within Wilkinson Basin, surface waters generally flow in a cyclonic pattern and are separated from the southwesterly flowing coastal current and the more nutrient rich slope waters which enter Jordan Basin, NE of Wilkinson Basin (Brooks, 1991; Christensen *et al.*, 1991). The specific sampling site is located in the center, where advective water flow is at a minimum and where subsurface sediment traps were placed continuously during 1995 and 1996 (Pilskaln *et al.*, 1996). Increasing vertical stratification initiates an intense spring bloom in early March to late April (Townsend and Spinrad, 1986). During the summer, nutrient depletion within the euphotic zone causes a shift in food web structure to phytoplanktonic

assemblages consisting of smaller, more efficient picoplankton and bacteria (O'Reilly and Busch, 1984; Walsh *et al.*, 1987). Zooplankton, consisting primarily of copepods, peak in concentration and biomass in late summer (Meise and O'Reilly, 1996).

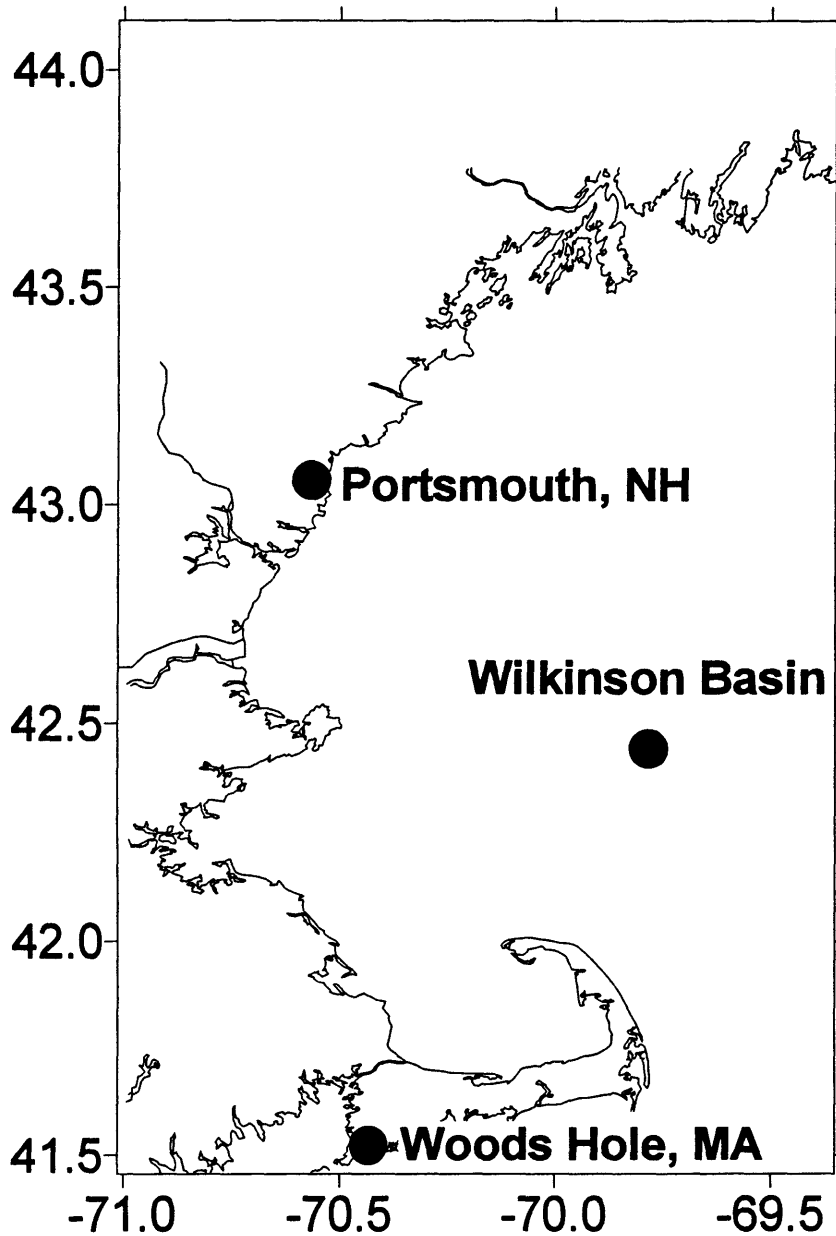


**Figure 4.1** Map of rain collection and Wilkinson Basin stations.

## METHODS

Surface and deep particulate and total dissolved phosphorus (TDP) samples were collected by passing 4000-6000 L of seawater sequentially through a series of 10, 1.0, and 0.2  $\mu\text{m}$  cartridge prefilters followed by cartridges packed with iron impregnated polypropylene filters. These filters have been demonstrated to collect TDP with close to 100% efficiency (see **Chapter 2**, Benitez-Nelson and Buesseler, 1998b). Separate surface samples were collected for soluble reactive phosphorus (SRP), as defined by the molybdenum blue method (Koroleff, 1983), using acrilan filters and the technique developed by Lee *et al.* (1992).

Briefly, this technique involves the collection of over 1000 Liters of 0.2  $\mu\text{m}$  filtered seawater into an acid cleaned polyethylene lined container. The Koroleff (1983) reagents which form the phosphomolybdate complex were added to the sample in reduced concentrations (50% of the required Koroleff mixed reagent and 25% of the ascorbic acid reagent) in order to decrease possible hydrolysis of any labile organic phosphorus compounds. The reduction in reagents does not affect the complexation, but rather the color development of the phosphomolybdate complex (Lee *et al.*, 1992). The final solution was thoroughly mixed and passed through three 61 cm long, 7.6 diameter PVC pipes (vol. = 2.7 L) packed with acrilan filters. The acrilan filters were prepared by impregnating the material with sodium hydroxide (see **Chapter 2**). This extraction method was found to collect SRP with greater than 98% efficiency (Lee *et al.*, 1992). TDP and SRP concentrations were measured in the filtrate during sample filtration. Results found that all of the SRP (complexed as phosphomolybdate) was absorbed onto the acrilan filters, while all of the dissolved organic phosphorus remained in the filtrate.

Plankton tows (>102  $\mu\text{m}$ ) were integrated over the depth of the mixed layer in March (MLD = 100 m) and April (MLD = 110 m) and at specific depths in July and August. All plankton tow samples were then sieved through a 335  $\mu\text{m}$  screen to collect different size classes. The biological composition of each plankton tow was first elucidated by visual inspection without magnification. Large zooplankton, such as

euphausiids, were immediately identified. Aliquots of each plankton tow were fixed with 2% formaldehyde and were further examined under a high powered microscope.

All samples were extensively purified to remove all other  $\beta$  emitting radionuclides using a series of P-specific precipitation and ion-exchange columns (see **Chapter 2**). Activities were measured via an ultra-low level liquid scintillation counter, Packard Tri-Carb 2770TR/SL, which allowed for the separation and simultaneous measurement of both  $^{32}\text{P}$  and  $^{33}\text{P}$  with greater than 50% efficiency (see **Chapter 2**, Benitez-Nelson and Buesseler, 1998b).

All ancillary samples were collected using Niskin bottles. Nutrient samples were filtered through combusted GF/F filters into acid cleaned polypropylene bottles and immediately frozen for analysis in the laboratory (Table 4.1). Suspended particulate matter (SPM) samples were collected by filtering onto pre-weighed 1  $\mu\text{m}$  polycarbonate filters. Particulate organic carbon, nitrogen and separate pigment samples were collected via low pressure (< 5 psi) filtration onto combusted GF/F filters. Dissolved (< 0.7  $\mu\text{m}$ ) nitrate, nitrite and silicate were analyzed by the Analytical Service Center at the Virginia Institute of Marine Science according to the methods described by Pollard *et al.* (1996). SRP and DOP were determined according to the molybdenum-blue and acid-persulfate methods described by Koroleff (1983). Dissolved organic carbon (DOC) measurements were made in triplicate and according to Peltzer and Hayward (1996). Chl *a* in the greater than 0.7  $\mu\text{m}$  size class was determined using HPLC according to Zapata *et al.* (1987). Particulate organic carbon and nitrogen were determined using CHN and all CHN samples were processed according to Gunderson *et al.* (1993), the same procedure utilized at the JGOFS Bermuda Atlantic Time Series.

**Table 4.1.** Ancillary measurements taken at Wilkinson Basin.

<b>Sample Depth (m)</b>	<b>NO<sub>3</sub> + NO<sub>2</sub> (<math>\mu\text{M}</math>)</b>	<b>SRP (<math>\mu\text{M}</math>)</b>	<b>TDP (<math>\mu\text{M}</math>)</b>	<b>Silicate (<math>\mu\text{M}</math>)</b>	<b>Chl a (<math>\mu\text{g L}^{-1}</math>)</b>	<b>DOC (<math>\mu\text{M}</math>)</b>	<b>POC (<math>\text{mg L}^{-1}</math>)</b>	<b>SPM (<math>\text{mg L}^{-1}</math>)</b>
<b><i>March</i></b>								
5	7.035	0.86	0.86	5.6	0.64	N.D.	0.060	0.24
20	6.967	0.86	0.86	5.9	0.75	N.D.	0.084	0.41
35	7.348	0.90	0.90	6.6	1.44	N.D.	0.134	0.39
50	6.671	0.82	0.82	5.8	0.86	N.D.	0.110	1.23
72	7.100	0.89	0.89	7.4	0.86	N.D.	0.077	0.35
<b><i>April</i></b>								
5	5.011	0.60	0.56	3.86	1.26	N.D.	0.090	0.44
30	7.386	0.91	0.91	5.73	0.78	N.D.	0.093	0.27
60	7.917	0.98	0.98	5.96	N.D.	N.D.	0.166	0.49
90	7.518	0.91	0.91	5.86	1.15	N.D.	0.080	1.23
110	10.324	1.09	1.09	10.88	0.57	N.D.	0.067	0.38
<b><i>July</i></b>								
5	0.079	0.26	0.46	1.11	0.19	78.2	0.083	1.64
15	0.157	0.34	0.59	1.79	0.38	90.5	0.065	0.31
37	3.496	0.70	0.78	2.67	1.17	74.6	0.120	0.45
50	7.394	0.92	0.86	4.63	0.37	N.D.	0.657	0.34
65	8.762	1.02	0.95	5.93	0.10	67.2	0.048	0.12
<b><i>August</i></b>								
5	0.137	0.32	0.52	4.96	0.19	64.5	0.102	0.89
15	0.116	0.39	0.61	1.83	0.27	58.2	0.107	0.16
30	0.785	0.56	0.69	2.80	2.98	196.9	0.130	0.41
45	9.176	1.04	1.01	6.79	0.08	52.1	0.057	1.82
65	7.506	0.95	0.95	4.43	0.18	144.1	0.068	1.71

## RESULTS

Results from the ancillary measurements are given in Table 4.1. As expected,  $\text{NO}_3 + \text{NO}_2$  concentrations were highest in March and April and lowest during July and August (see Fig. 5.4 in Chapter 5). TDP concentrations decreased as well, but not to the same extent. Rather, SRP concentrations decreased in concurrence with an increase in DOP in July and August. The inorganic N:P ratio in surface waters also decreased from a high of 8-8.4 in spring to a low of 0.3-4 in summer, indicating possible nitrogen limitation of phytoplankton. Large subsurface chl *a* maximums were observed in March, July and August. In April, chl *a* concentrations were high throughout the water column and showed no clear trend. Particulate organic carbon (POC) increased at the depth of the chl *a* maximum and was typically 20% of the measured total suspended particulate matter (SPM). Although it should be noted that overestimation of SPM can easily occur if filters are not rinsed properly of salts.

The results of the  $^{32}\text{P}$  and  $^{33}\text{P}$  activity in dissolved ( $< 0.2 \mu\text{m}$ ) and in small (1-10  $\mu\text{m}$ , 10 -102  $\mu\text{m}$ ) and large particulate size classes (102-335  $\mu\text{m}$ ,  $>335 \mu\text{m}$ ) are presented in Table 4.2. Those samples which are not shown had  $^{32}\text{P}$  and  $^{33}\text{P}$  activities below detection. DOP was found by the difference between TDP and SRP. In March and April, plankton tows were integrated over the depth of the mixed layer which was 100 and 110 m, respectively. In July and August, plankton tows were taken at specific depth intervals. Replicate plankton tow samples were taken in July, at 37 and 65 m. Plankton tow activities are reported in both d.p.m.  $\text{g P}^{-1}$  and in d.p.m.  $\text{m}^{-3}$  (Table 4.2). Results reported in d.p.m.  $\text{m}^{-3}$  will enable comparisons with plankton tow  $^{32}\text{P}$  and  $^{33}\text{P}$  measurements from other regimes, whereas results reported in d.p.m  $\text{g P}^{-1}$  do not.

Filtration volumes were determined using the area of the plankton tow, the speed of the ship and assuming that plankton tows were 100% efficient in collection. The largest difficulty in the volume calculation is the assumption of 100% efficiency. Numerous researchers have shown that such factors as wire angle, plankton biomass, mesh size and net shape can significantly change the filtration efficiency of a plankton tow (Smith *et al.*,



**Table 4.2** Specific activity of  $^{32}\text{P}$  and  $^{33}\text{P}$  in various total dissolved phosphorus (TDP), soluble reactive phosphorus (SRP), dissolved organic phosphorus (DOP), and small (0.2- 1.0  $\mu\text{m}$ , 1.0- 10  $\mu\text{m}$ ) and large particulate pools (10-102  $\mu\text{m}$ ) from Wilkinson Basin, Gulf of Maine. Plankton tow (PT) activities given in parenthesis are in in d.p.m.  $\text{P}^{-1}$ . Those samples which are not shown were below detection.  $\tau$  was determined using the 'age' model described in the text. Error bars are  $2\sigma$ .

Sample	$^{32}\text{P}$ (dpm $\text{m}^{-3}$ )	$^{33}\text{P}$ (dpm $\text{m}^{-3}$ )	$^{33}\text{P}/^{32}\text{P}$	$\tau$ (days)
<i>March, 1997</i>				
0.2-1.0 $\mu\text{m}$ , 5 m	$0.44 \pm 0.04$	$0.43 \pm 0.04$	$0.98 \pm 0.13$	9
10-102 $\mu\text{m}$ , 5 m	$0.70 \pm 0.18$	$0.51 \pm 0.13$	$0.73 \pm 0.26$	< 1
TDP, 5 m	$5.60 \pm 0.97$	$4.56 \pm 0.79$	$0.81 \pm 0.20$	8
0.2-1.0 $\mu\text{m}$ , 72 m	$0.51 \pm 0.12$	$0.43 \pm 0.10$	$0.84 \pm 0.28$	2
TDP, 72 m	$0.86 \pm 0.07$	$1.86 \pm 0.10$	$2.16 \pm 0.21$	54
PT1 102-335 $\mu\text{m}$ , integ. 0-100 m	$0.0031 \pm 0.0002$ (124 $\pm$ 9)	$0.00242 \pm 0.0002$ (98 $\pm$ 9)	$0.79 \pm 0.08$	< 1
>335 $\mu\text{m}$ , integ. 0-100 m	$0.07269 \pm 0.0067$ (246 $\pm$ 23)	$0.08411 \pm 0.0067$ (285 $\pm$ 24)	$1.16 \pm 0.14$	17
<i>April, 1997</i>				
0.2-10 $\mu\text{m}$ , 5 m	$0.14 \pm 0.01$	$0.15 \pm 0.01$	$1.07 \pm 0.10$	10
TDP, 5 m	$3.61 \pm 0.57$	$3.11 \pm 0.47$	$0.86 \pm 0.19$	10
0.2-10 $\mu\text{m}$ , 110 m	$0.28 \pm 0.02$	$0.21 \pm 0.02$	$0.75 \pm 0.09$	< 1
10-102 $\mu\text{m}$ , 110 m	$0.31 \pm 0.02$	$0.26 \pm 0.02$	$0.84 \pm 0.08$	< 1
TDP, 110 m	$1.06 \pm 0.03$	$1.26 \pm 0.06$	$1.19 \pm 0.23$	26
PT1 102-335 $\mu\text{m}$ , integ. 0-110 m	$0.0125 \pm 0.0016$ (358 $\pm$ 45)	$0.0111 \pm 0.0013$ (318 $\pm$ 39)	$0.89 \pm 0.15$	< 2
>335 $\mu\text{m}$ , integ. 0-110 m	$0.0961 \pm 0.0063$ (219 $\pm$ 14)	$0.1182 \pm 0.0080$ (269 $\pm$ 18)	$1.23 \pm 0.12$	17

Table 4.2 Continued.

Sample	$^{32}\text{P}$ (dpm m <sup>-3</sup> )	$^{33}\text{P}$ (dpm m <sup>-3</sup> )	$^{33}\text{P}/^{32}\text{P}$	$\tau$ (days)
<i>July 1997</i>				
0.2-1.0 $\mu$ , 5 m	0.41 $\pm$ 0.02	0.33 $\pm$ 0.02	0.80 $\pm$ 0.06	< 1
1-10 $\mu$ , 5 m	0.10 $\pm$ 0.02	0.08 $\pm$ 0.01	0.80 $\pm$ 0.19	< 1
10-102 $\mu$ , 5 m	0.66 $\pm$ 0.10	0.45 $\pm$ 0.10	0.68 $\pm$ 0.18	< 1
TDP, 5 m	4.16 $\pm$ 0.27	4.48 $\pm$ 0.22	1.08 $\pm$ 0.11	17
SRP, 5 m	2.14 $\pm$ 0.08	2.15 $\pm$ 0.07	1.00 $\pm$ 0.05	21
DOP*, 5 m	2.02 $\pm$ 0.01	2.33 $\pm$ 0.12	1.47 $\pm$ 0.26	32
0.2-1.0 $\mu$ , 65 m	0.22 $\pm$ 0.02	0.17 $\pm$ 0.01	0.77 $\pm$ 0.08	< 1
1-10 $\mu$ , 65 m	0.22 $\pm$ 0.03	0.18 $\pm$ 0.02	0.82 $\pm$ 0.14	< 1
10-102 $\mu$ , 65 m	0.42 $\pm$ 0.06	0.27 $\pm$ 0.04	0.64 $\pm$ 0.13	< 1
TDP, 65 m	0.51 $\pm$ 0.12	0.98 $\pm$ 0.10	1.92 $\pm$ 0.39	45
PT5/6 102-335 $\mu$ , 5 m	0.025 $\pm$ 0.001 (141 $\pm$ 6)	0.037 $\pm$ 0.001 (208 $\pm$ 8)	1.48 $\pm$ 0.07	37
>335 $\mu$ , 5 m	0.0013 $\pm$ 0.001 (11 $\pm$ 4)	0.0017 $\pm$ 0.001 (15 $\pm$ 4)	1.37 $\pm$ 0.26	33
PT4 102-335 $\mu$ , 37 m	0.037 $\pm$ 0.001 (24 $\pm$ 1)	0.043 $\pm$ 0.001 (28 $\pm$ 1)	1.16 $\pm$ 0.04	25
>335 $\mu$ , 37 m	0.008 $\pm$ 0.001 (10 $\pm$ 1)	0.012 $\pm$ 0.001 (15 $\pm$ 1)	1.50 $\pm$ 0.23	37
PT3 102-335 $\mu$ , 37 m	0.0063 $\pm$ 0.001 (9 $\pm$ 1)	0.0078 $\pm$ 0.001 (11 $\pm$ 1)	1.24 $\pm$ 0.25	28
>335 $\mu$ , 37 m	0.022 $\pm$ 0.001 (64 $\pm$ 3)	0.028 $\pm$ 0.001 (81 $\pm$ 3)	1.27 $\pm$ 0.07	30
PT2 102-335 $\mu$ , 65 m	0.0030 $\pm$ 0.001 (51 $\pm$ 17)	0.0027 $\pm$ 0.001 (46 $\pm$ 17)	1.09 $\pm$ 0.28	22
>335 $\mu$ , 65 m	0.009 $\pm$ 0.001 (16 $\pm$ 2)	0.021 $\pm$ 0.001 (37 $\pm$ 2)	2.33 $\pm$ 0.28	58
PT1 102-335 $\mu$ , 65 m	0.006 $\pm$ 0.001 (28 $\pm$ 5)	0.004 $\pm$ 0.001 (19 $\pm$ 5)	1.23 $\pm$ 0.16	28
>335 $\mu$ , 65 m	0.0112 $\pm$ 0.001 (11 $\pm$ 1)	0.0273 $\pm$ 0.001 (27 $\pm$ 1)	2.44 $\pm$ 0.24	60

\* DOP = TDP - SRP

Table 4.2 Continued.

Sample	$^{32}\text{P}$ (dpm m <sup>-3</sup> )	$^{33}\text{P}$ (dpm m <sup>-3</sup> )	$^{33}\text{P}/^{32}\text{P}$	$\tau$ (days)
<i>August, 1997</i>				
0.2-1.0 $\mu$ , 5 m	1.64 $\pm$ 0.15	1.44 $\pm$ 0.14	0.88 $\pm$ 0.05	2
1-10 $\mu$ , 5 m	0.24 $\pm$ 0.03	0.23 $\pm$ 0.03	0.96 $\pm$ 0.17	6
10-102 $\mu$ , 5 m	0.14 $\pm$ 0.04	0.14 $\pm$ 0.04	1.00 $\pm$ 0.40	8
TDP, 5 m	5.44 $\pm$ 0.30	4.65 $\pm$ 0.26	0.85 $\pm$ 0.07	10
SRP, 5 m	5.16 $\pm$ 0.22	4.34 $\pm$ 0.25	0.84 $\pm$ 0.06	9
DOP*, 5 m	0.28 $\pm$ 0.37	0.32 $\pm$ 0.36	1.14 $\pm$ 2.30	--
PT5/6 102-335 $\mu$ , 5 m	0.0103 $\pm$ 0.001 (139 $\pm$ 35)	0.0097 $\pm$ 0.001 (179 $\pm$ 45)	0.94 $\pm$ 0.13	< 1
>335 $\mu$ , 5 m	0.0587 $\pm$ 0.001 (89 $\pm$ 6)	0.09103 $\pm$ 0.001 (127 $\pm$ 6)	1.55 $\pm$ 0.03	21
PT3/4 102-335 $\mu$ , 37 m	0.0044 $\pm$ 0.001 (90 $\pm$ 10)	0.0065 $\pm$ 0.001 (133 $\pm$ 10)	1.49 $\pm$ 0.38	19
>335 $\mu$ , 37 m	0.0154 $\pm$ 0.001 (111 $\pm$ 7)	0.0285 $\pm$ 0.001 (206 $\pm$ 7)	1.85 $\pm$ 0.10	29
PT1/2 102-335 $\mu$ , 65 m	0.00213 $\pm$ 0.001 (353 $\pm$ 34)	0.00274 $\pm$ 0.001 (332 $\pm$ 34)	1.28 $\pm$ 0.52	12
>335 $\mu$ , 65 m	0.0144 $\pm$ 0.001 (264 $\pm$ 5)	0.0206 $\pm$ 0.001 (409 $\pm$ 5)	1.43 $\pm$ 0.11	17

\* DOP = TDP -SRP

1968; Omori and Ikeda, 1984; Wiebe *et al.*, 1985). One measure of the collection efficiency within an environment is the open area ratio,  $R$ , which can be expressed in high plankton density coastal waters by:

$$\log R = 0.38 \log(V/A) - 0.17$$

where  $V$  is the volume filtered ( $\text{m}^3$ ) and  $A$  is the mouth area ( $\text{m}^2$ ) of the plankton net (Smith *et al.*, 1968). In this study, the estimated volume of water filtered per tow was  $500 \text{ m}^3$  and the mouth area of the plankton net was  $0.785 \text{ m}^2$ . This gives an open area ratio of 7.9. Using a  $333 \mu\text{m}$  plankton net of similar design to the one used in this study, Smith *et al.* (1968) found that between 300 and  $2600 \text{ m}^3$  of water could be filtered with greater than 85% efficiency. The amount of water filtered was completely dependent on the plankton biomass. The plankton net mesh used in this study was significantly lower,  $102 \mu\text{m}$ . However the plankton biomass within Wilkinson Basin is also most likely lower than the near shore waters off of San Pedro, CA tested by Smith *et al.* (1968). Furthermore, plankton tows never appeared to be clogged. Thus, the assumption of 100% efficiency is considered to be reasonable.

## DISCUSSION

Rain samples were collected at two coastal stations, Woods Hole, MA and Portsmouth, NH, at least 20 days prior to and during each cruise (Benitez-Nelson and Buesseler, 1998a) (Fig. 4.1). The ratio of  $^{33}\text{P}/^{32}\text{P}$  measured in rain at the two coastal stations prior to each cruise averaged  $0.69 \pm 0.05$ . Any ratio in seawater higher than this value must be due to radioactive decay, and indicates an 'aging' of material. Assuming that there is no isotopic fractionation during uptake and that all of the radioactive phosphorus which enters the oceans is equally bioavailable,  $^{32}\text{P}$  and  $^{33}\text{P}$  can be used to determine the residence time of phosphorus within the upper ocean.

Although fractionation may occur, it is unlikely that the magnitude of such a process would significantly effect the  $^{33}\text{P}/^{32}\text{P}$  ratio. For example, an improbable fractionation of 100% between  $^{32}\text{P}$  and stable P results in only a 10% change in the ratio

of  $^{32}\text{P}$  to stable P (20% for  $^{33}\text{P}$  to stable P) (Waser *et al.*, 1996). This is well within the error of many of the  $^{33}\text{P}/^{32}\text{P}$  ratio measurements.

The assumption that all of the radioactive phosphorus which enters the ocean is available for biological uptake is difficult to test. There are few studies which have examined atmospheric P deposition in any detail (Graham and Duce, 1979; 1981; 1982). According to Duce and Graham (1982), 20-50% of the total phosphorus present in aerosol particles is soluble in seawater. The remaining fraction appears to be of both anthropogenic and marine origin, and is dominated by polyphosphates and organic phosphorus compounds (Duce *et al.*, 1981; 1982). Although there have been no direct measurements of the solubility of radioactive P in seawater, the above studies suggest that the majority of  $^{32}\text{P}$  and  $^{33}\text{P}$  which enters the ocean is labile, especially given the mechanism by which these isotopes are created. Once formed, these isotopes oxidize and scavenge onto aerosol surfaces (Lal and Peters, 1967). Thus, it is hypothesized that most, if not all, radioactive P which enters the oceans can desorb as phosphate. It should be noted, however, that aerosols can have significant differences in their composition, which in turn may effect the rate of P desorption. Furthermore, aerosol composition may change from one rain event to the next as different air masses are scavenged (See Chapter 3).

With the above caveats kept in mind, there are two simple models that can be used to determine the residence time of phosphorus. The first model assumes steady state and is used to depict continuous P uptake. For example, the residence time of phosphorus within zooplankton can be described as the balance between phytoplankton ingestion and loss via radioactive decay, excretion and mortality. The zooplankton mass balance equation for  $^{32}\text{P}$  is given by the following equation (Waser *et al.*, 1996):

$$g \ ^{32}\text{P}_{\text{phy}} = ^{32}\text{P}_{\text{zoo}} (\lambda_{32} + \varepsilon + s)$$

where  $^{32}\text{P}_{\text{phy}}$  and  $^{32}\text{P}_{\text{zoo}}$  are the activities of  $^{32}\text{P}$  in phytoplankton and zooplankton, respectively;  $g$  is the zooplankton grazing rate;  $\lambda_{32}$  is the radioactive decay constant for  $^{32}\text{P}$ ;  $\varepsilon$  is the rate of zooplankton excretion; and  $s$  is the zooplankton mortality rate. A

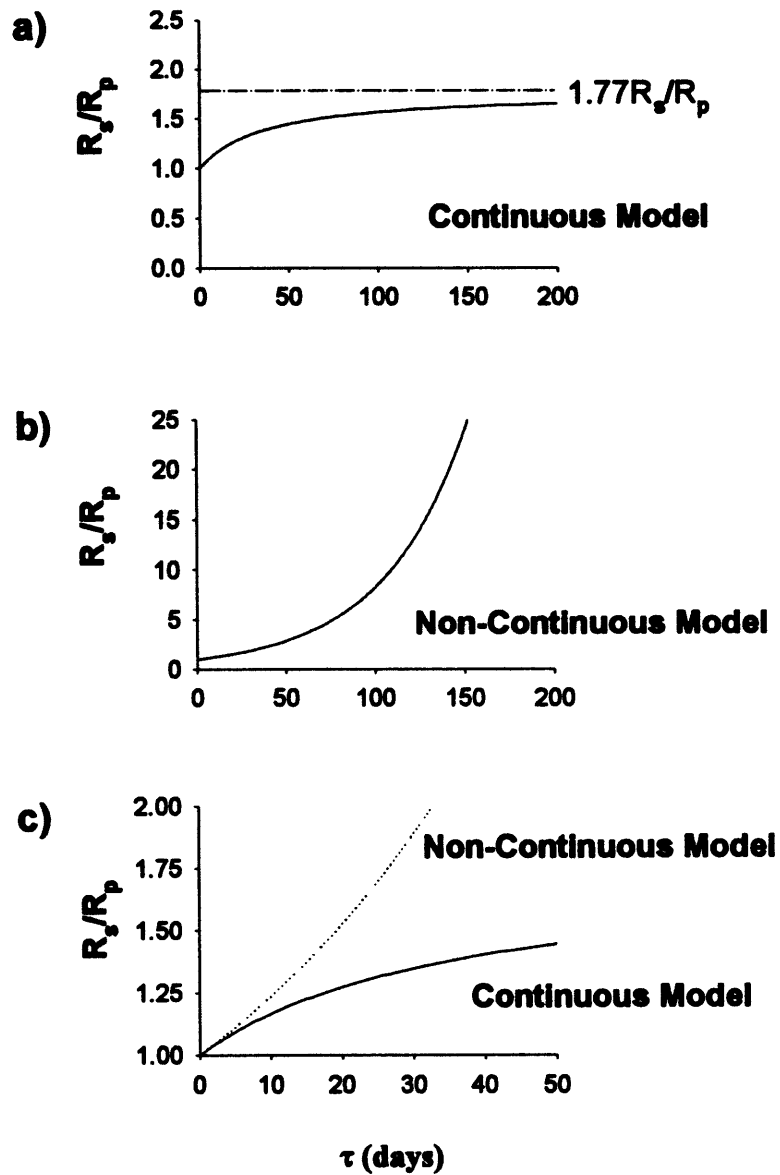


**Figure 4.2** Schematic of a) continuous, b) non-continuous and c) both models.  $R_s$  is the ratio of  $^{33}\text{P}/^{32}\text{P}$  within the source material and  $R_p$  is the ratio of  $^{33}\text{P}/^{32}\text{P}$  in the product material.

similar equation can be written for  $^{33}\text{P}$  such that the phosphorus residence time in zooplankton,  $\tau$ , can then be given by (Waser *et al.*, 1996):

$$\tau_{\text{zoo}} = [(R_{\text{zoo}}/R_{\text{phy}})-1] / [\lambda_{32} - \lambda_{33}(R_{\text{zoo}}/R_{\text{phy}})]$$

where  $\tau_{\text{zoo}}$  is defined as  $1/(\epsilon + s)$  and  $R_{\text{zoo}}$  and  $R_{\text{phy}}$  are the activity ratios of  $^{33}\text{P}/^{32}\text{P}$  in zooplankton and phytoplankton, respectively. This continuous model predicts that the ratio of  $^{33}\text{P}/^{32}\text{P}$  in zooplankton,  $R_{\text{zoo}}$ , will range from an initial  $^{33}\text{P}/^{32}\text{P}$  ratio in phytoplankton,  $R_{\text{phy}}$ , to a maximum ratio of  $1.77R_{\text{phy}}$  (Fig. 4.2a). As  $R_{\text{zoo}}$  approaches  $1.77R_{\text{phy}}$  small changes in  $R_{\text{zoo}}$  result in large differences in  $\tau$ .

The second model depicts phosphorus uptake as a discontinuous process, such that the relative 'age' of phosphorus can be described by radioactive decay alone. The radioactive decay of a  $^{32}\text{P}$  can be described by:

$$^{32}\text{P}_{\text{zoo}} = ^{32}\text{P}_{\text{phy}}e^{-\lambda\tau}$$

where  $^{32}\text{P}_{\text{zoo}}$  is the activity of  $^{32}\text{P}$  in zooplankton time  $\tau$  after ingestion and  $^{32}\text{P}_{\text{phy}}$  is the  $^{32}\text{P}$  activity in phytoplankton. A similar equation can be written for  $^{33}\text{P}$  such that the relative age of zooplankton is given by:

$$\tau_{\text{zoo}} = [\ln (R_{\text{zoo}}/R_{\text{phy}})] / (\lambda_{32} - \lambda_{33})$$

where  $\tau_{\text{zoo}}$  is now the age of zooplankton compared to phytoplankton. In contrast to the continuous model,  $R_{\text{zoo}}$  is allowed to increase indefinitely (Fig. 4.2b) such that beyond  $R_{\text{zoo}}/R_{\text{phy}} \approx 5$ , large differences in  $R_{\text{zoo}}/R_{\text{phy}}$  result in small differences in  $\tau$ .

It should be noted that both of these models assume that there is no heterogeneity of radioactive phosphorus within the phytoplankton and zooplankton pools. In other words, zooplankton are ingesting all of the phytoplankton, as opposed to a younger more labile fraction. Zooplankton excretion is also assumed to be representative of the entire zooplankton radioactive P pool.

Comparable equations for both models can be written for the residence time of P within dissolved and small and large particulate size classes. For the purposes of this discussion, only one source at a time was chosen for the supply of P to a particular pool. Increasing the number of sources would have added complexity beyond the scope of this

discussion. As a result, care was taken when choosing the source material of phosphorus for a specific size class as differences in the  $^{33}\text{P}/^{32}\text{P}$  ratio of the chosen source could significantly affect results. When possible SRP was chosen as the source material for the small particulate size classes. Larger particulates were assumed to consume the smaller particles. Regardless, with the exception of July, the above issue was minor as  $^{33}\text{P}/^{32}\text{P}$  ratios between surface dissolved and small particulate pools ( $<102\ \mu\text{m}$ ) were not significantly different from one another.

Both models assume that the rain input of  $^{32}\text{P}$  and  $^{33}\text{P}$  is continuous. However, it is clear from Figure 3.2 in Chapter 3 that the input of radioactive phosphorus can vary dramatically from season to season. As a result, the initial ratio of  $^{33}\text{P}/^{32}\text{P}$  in dissolved phosphorus pools, particularly SRP, can increase due to lack of rain rather than due to changes in biological activity. Furthermore, changes in the magnitude and timing between events may 'reset' dissolved  $^{33}\text{P}/^{32}\text{P}$  ratios to different degrees. Confidence in our approach is gained from closer inspection of the atmospheric deposition of radioactive phosphorus measured prior to each cruise. With the exception of April, the average atmospheric fluxes of  $^{32}\text{P}$  and  $^{33}\text{P}$  were the same, within error, in March, July, and August (Table 4.3).

In this study, a significant number of the  $^{33}\text{P}/^{32}\text{P}$  ratios, especially within the larger size classes in July and August ( $>102\ \mu\text{m}$ ) did not fall within the range required by the continuous model formulation ( $R_*$  to  $1.77R_*$ ; Fig. 4.2a). Thus, the 'age' or non-continuous model was chosen for discussing the data. The large range in observed  $^{33}\text{P}/^{32}\text{P}$  ratios is not surprising given that biological uptake is known to occur in a non-continuous fashion. However, the non-continuous model is also an over simplification as P consumption does not completely cease. Rather, P consumption may begin again after some given time interval which can range from several days to weeks. The non-continuous model does not account for this process. It should further be noted that the residence times of P derived from the non-continuous model are shorter than that found



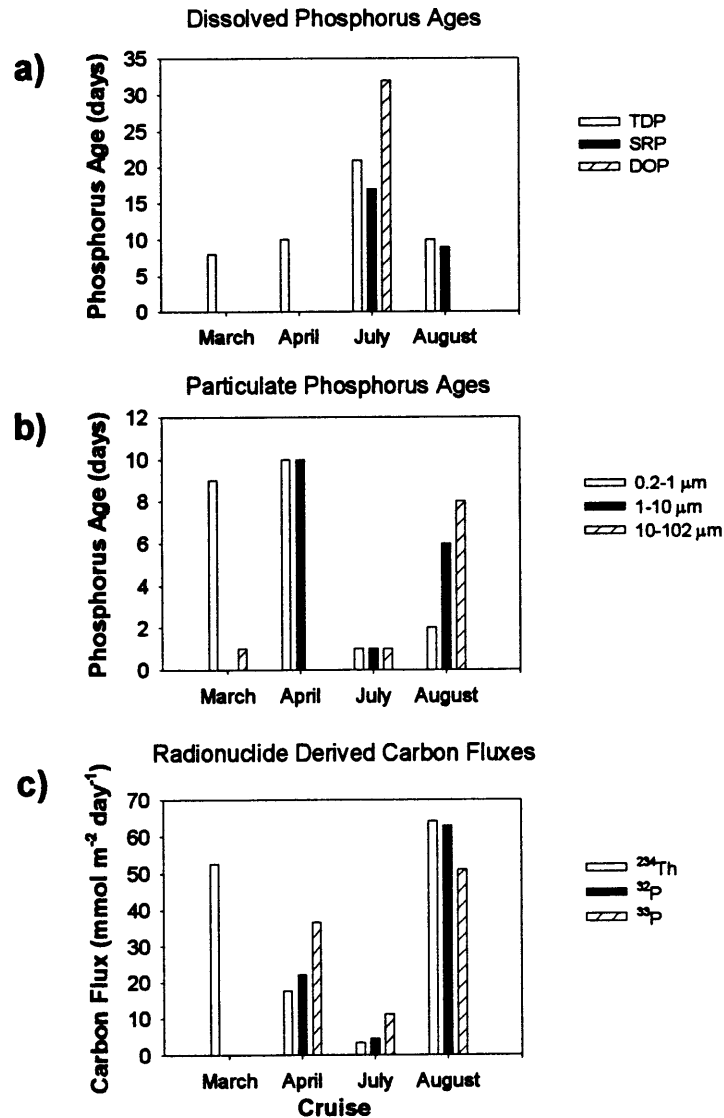


**Figure 4.3.** Phosphorus ages and radionuclide derived carbon export. a) Phosphorus ages derived using the non-continuous model in TDP, SRP and DOP pools. Separate SRP samples were not taken during the March and April cruises. In August, a DOP age could not be determined due to the large errors associated with the P activity measurements. b) Phosphorus ages in small particulate size classes. Bars not shown had P activities below detection. c) Radionuclide derived carbon fluxes over the upper 50 m.

from the continuous model (Fig. 4.2c). Nonetheless, regardless of the model used, the trends in P residence time ages between size classes will remain similar.

$^{33}\text{P}/^{32}\text{P}$  ratios in total dissolved and small particulate matter ( $< 102 \mu\text{m}$ ) in surface waters in March, April and August were similar to those found in the rain, denoting rapid turnover rates on timescales of less than a few days to just over a week (Table 4.2, Figs. 4.3 -4.7). In July, however, the ratio of  $^{33}\text{P}/^{32}\text{P}$  within TDP was significantly higher and resulted in a P residence time of three weeks (Figs. 4.3 and 4.6). Given the low phosphorus activities observed at depth, it is highly unlikely that diffusion from high  $^{33}\text{P}/^{32}\text{P}$  ratio deep waters will significantly effect the  $^{33}\text{P}/^{32}\text{P}$  ratio measured in TDP. In July, a vertical eddy diffusivity of  $1.5 \text{ cm}^2 \text{ sec}^{-1}$  was determined using  $^7\text{Be}$  (see Chapter 5). Assuming that P activities decrease exponentially with depth, a flux of 0.21 and 0.22 d.p.m.  $\text{m}^{-2} \text{ day}^{-1}$  of  $^{32}\text{P}$  and  $^{33}\text{P}$ , respectively, diffuses into the upper 10 m. This is less than 6% of the rain input of both  $^{32}\text{P}$  and  $^{33}\text{P}$  (see Chapter 3 and Table 4.3).

Also in July, the  $^{33}\text{P}/^{32}\text{P}$  ratios measured in the small particulate size classes were less than that measured in either the SRP, DOP, or large particulate size classes. The most likely source of radioactive P to the small particulate size classes is SRP. This suggests that there must be a fraction of radioactive containing SRP which is not only younger than the bulk radioactive SRP pool, but is also more bio-available. Such a feature may be the result of differences in the strength of adsorption of radioactive P to various types of aerosol particles.

In March and April, dissolved deep water  $^{32}\text{P}$  and  $^{33}\text{P}$  activities measured above the base of the mixed layer (defined by  $\Delta p/\Delta z \geq 0.125$ ) were significantly lower than that found at the surface and dissolved  $^{33}\text{P}/^{32}\text{P}$  ratios, significantly higher. This indicates that incomplete mixing of radioactive P had occurred within the mixed layer. Increases in TDP deep activity and a decrease in the deep water  $^{33}\text{P}/^{32}\text{P}$  ratio from March to April were most likely due to a large storm which struck the Wilkinson Basin station between the two cruises, deepening the mixed layer from 100 m to 110 m. By July, deep water dissolved  $^{33}\text{P}/^{32}\text{P}$  ratios had again increased. Assuming that the majority of radioactive P supplied to

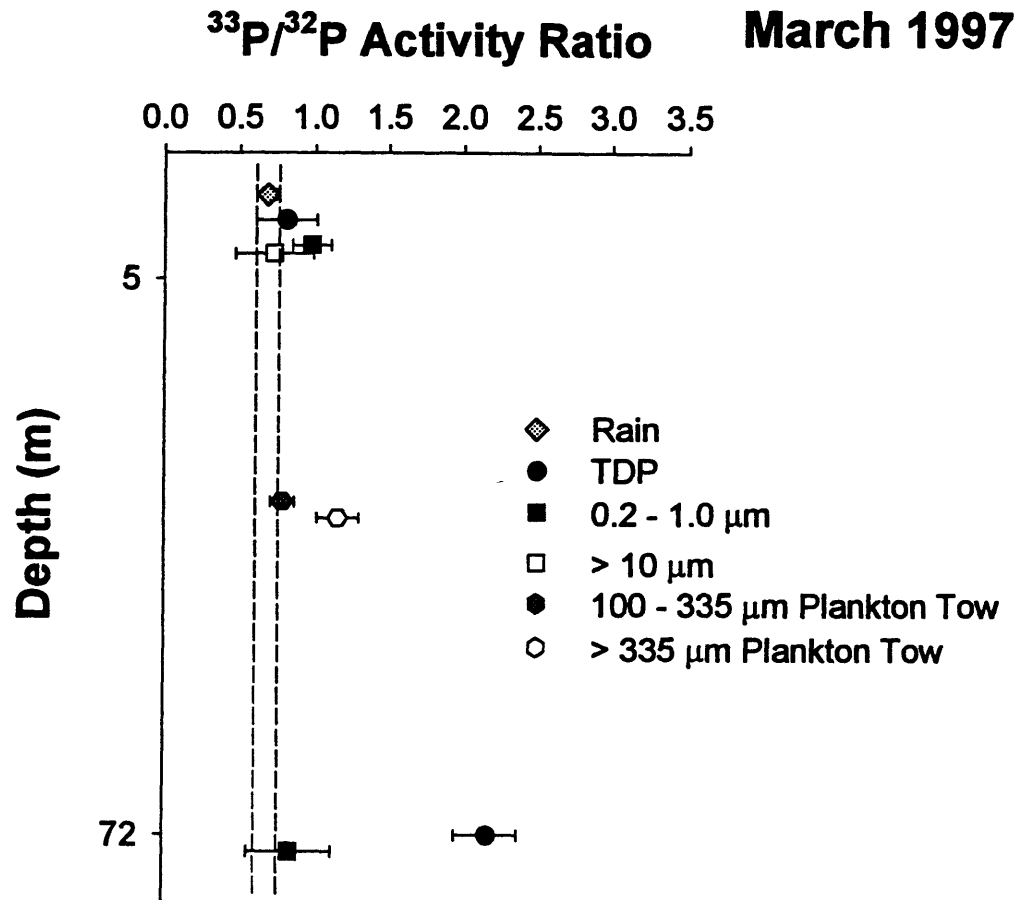


**Figure 4.4** Ratio of  $^{33}\text{P}/^{32}\text{P}$  in dissolved and in small and large particulate pools for March, 1997. All samples, with the exception of the plankton tows, were taken at the specific depth listed along the y axis. Vertical separation is for clarity only. Dotted lines represent the error associated with the  $^{33}\text{P}/^{32}\text{P}$  ratio of rain. Plankton tows were integrated over the depth of the mixed layer and are thus shown at the midpoint between the surface and deep samples.

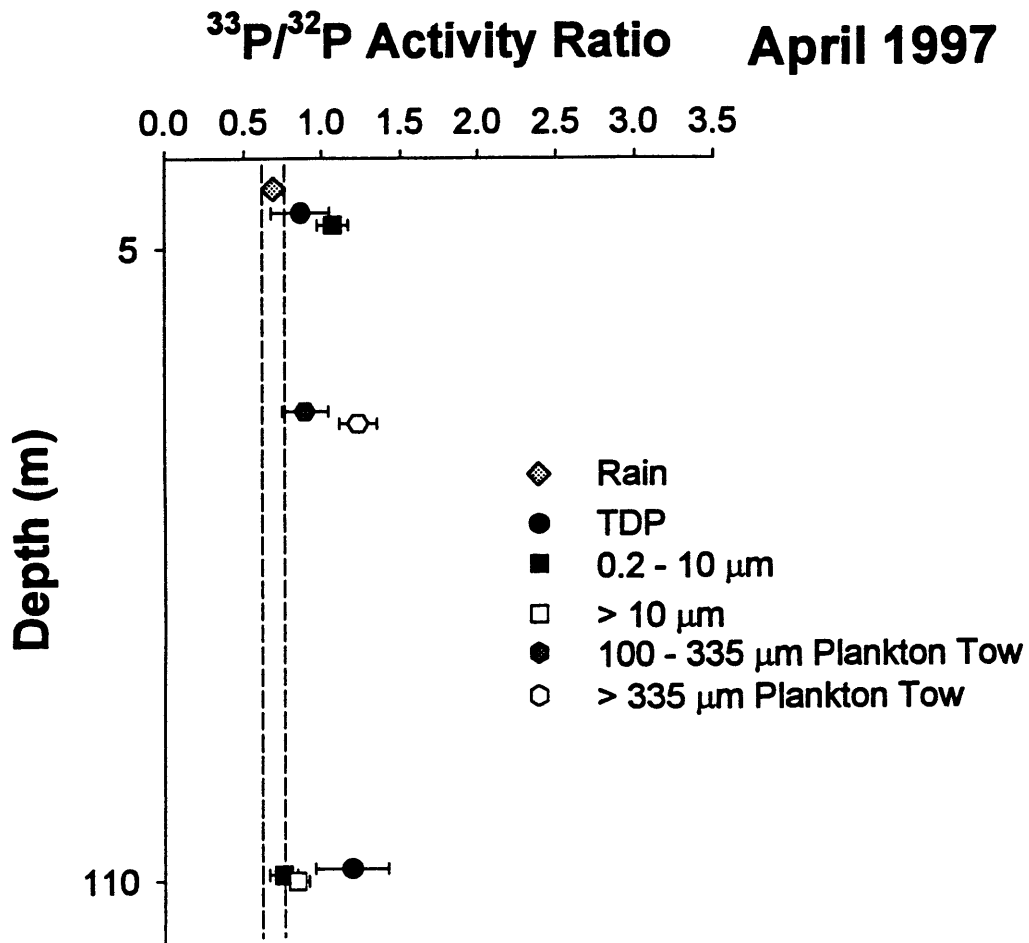


**Figure 4.5** Ratio of  $^{33}\text{P}/^{32}\text{P}$  in dissolved and in small and large particulate pools for April, 1997. All samples, with the exception of the plankton tows, were taken at the specific depth listed along the y axis. Vertical separation is for clarity only. Dotted lines represent the error associated with the  $^{33}\text{P}/^{32}\text{P}$  ratio of rain. Plankton tows were integrated over the depth of the mixed layer and are thus shown at the midpoint between the surface and deep samples.

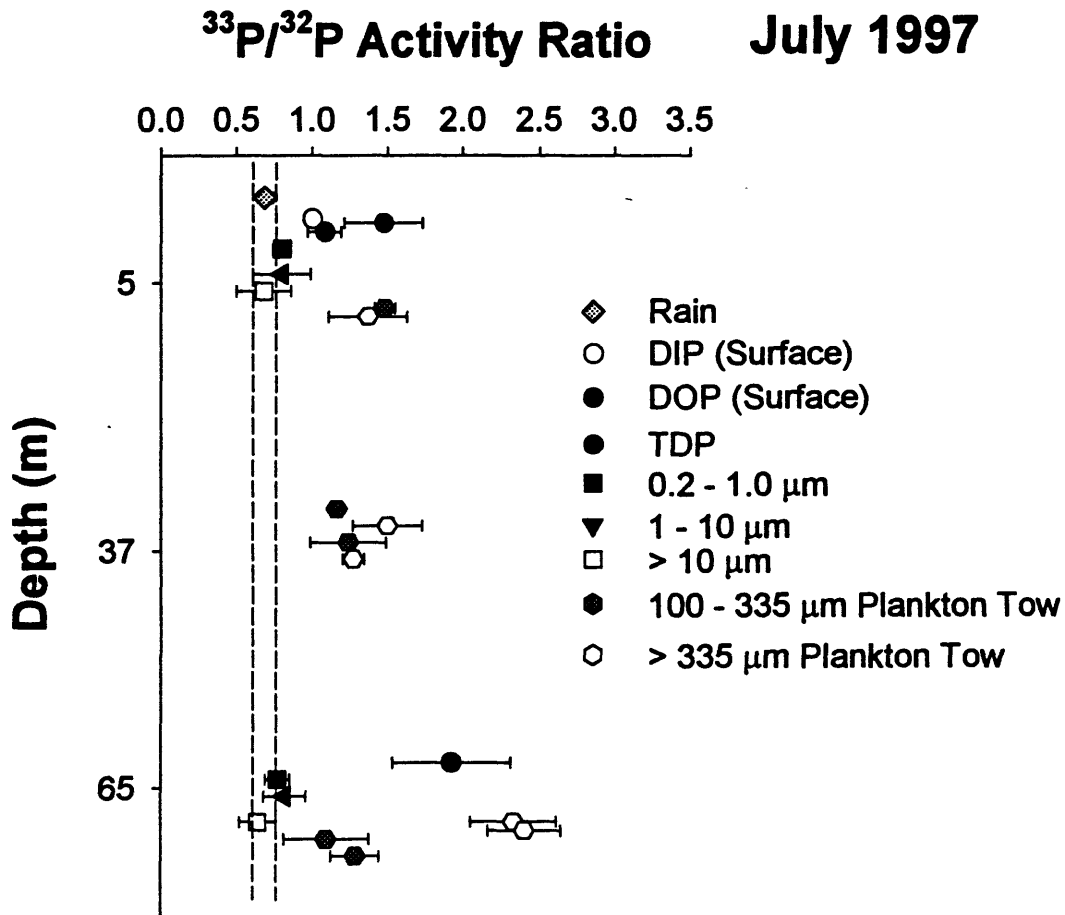


**Figure 4.7** Ratio of  $^{33}\text{P}/^{32}\text{P}$  in dissolved and in small and large particulate pools for August, 1997. All samples, *including* plankton tows, were taken at the specific depth listed along the y axis. Vertical separation is for clarity only. Dotted lines represent the error associated with the  $^{33}\text{P}/^{32}\text{P}$  ratio of rain.

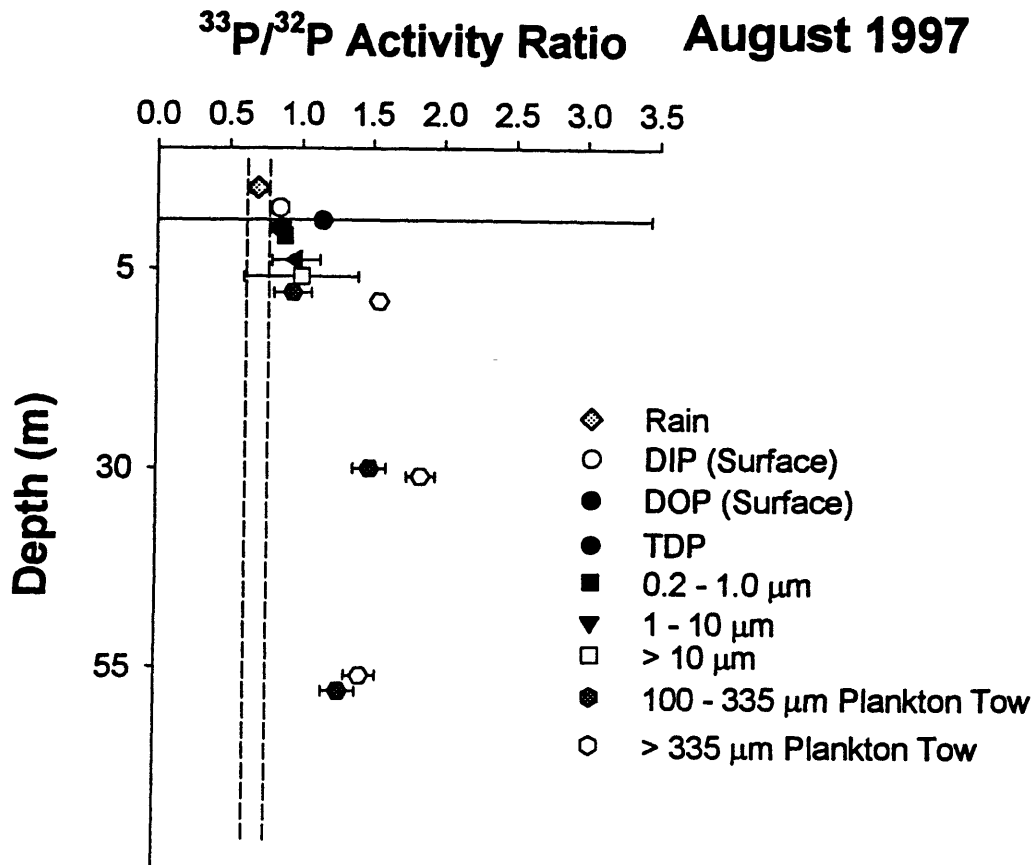


**Figure 4.6** Ratio of  $^{33}\text{P}/^{32}\text{P}$  in dissolved and in small and large particulate pools for July, 1997. All samples, *including* plankton tows, were taken at the specific depth listed along the y axis. Plankton tows taken at 37 and 65 m are replicate samples. Vertical separation is for clarity only. Dotted lines represent the error associated with the  $^{33}\text{P}/^{32}\text{P}$  ratio of rain.

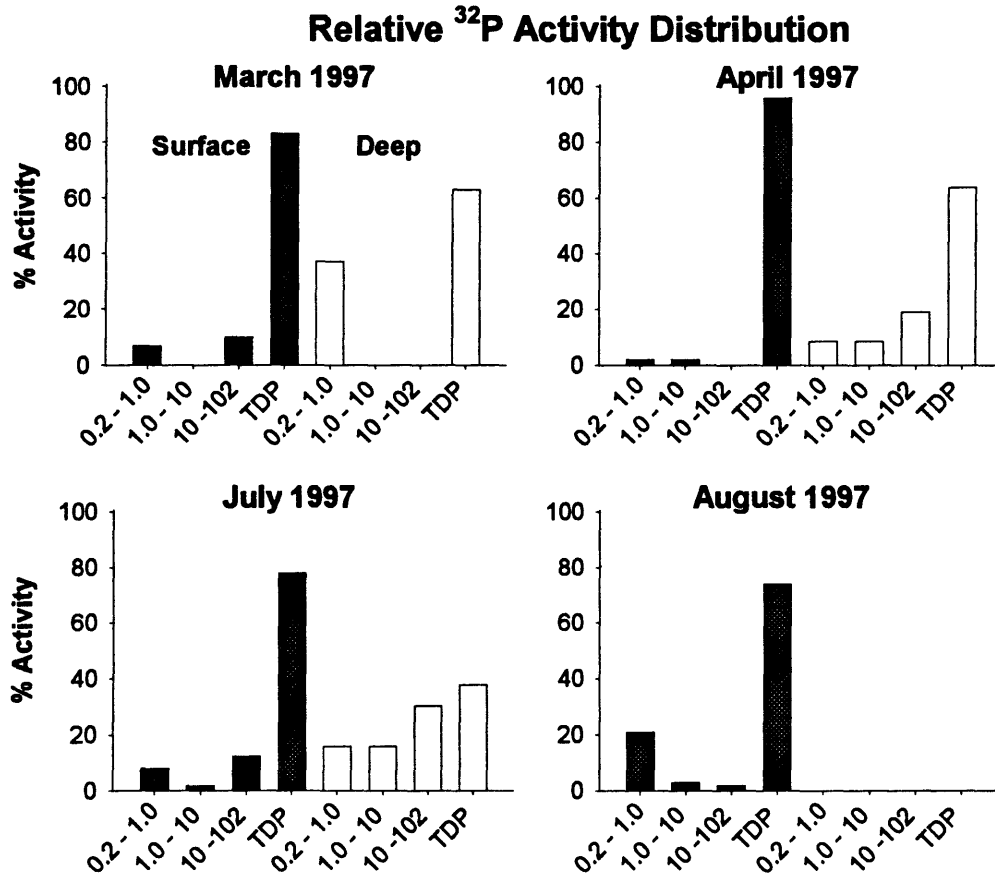


**Figure 4.8** Relative distribution of  $^{32}\text{P}$  activity found among the measured size classes at that water depth. The same pattern is observed for  $^{33}\text{P}$ . Deep water activities were typically three times lower than that found at surface. Surface and deep percentages are denoted by black and white bars, respectively. Bars not shown were below detection.

deep waters was by remineralization of sinking particulate material (0.2 - 10  $\mu\text{m}$  avg.  $^{33}\text{P}/^{32}\text{P}$  ratio = 0.76), a deep water TDP residence time of 6 weeks was determined. In all cruises, ratios of  $^{33}\text{P}/^{32}\text{P}$  in particulate matter were similar between surface and deep waters indicating that transport of sinking particulate material from the euphotic zone to depth occurred over time periods of less than a few days. Only in August were activities in total dissolved and all particulate samples retrieved from deep waters below detection, indicating that the source of sinking particulates had decreased (Fig. 4.7).

One of the biggest differences between the four cruises was the large change in the relative activity of  $^{32}\text{P}$  (and  $^{33}\text{P}$ ) within the bacterial and picoplankton (0.2-1.0  $\mu\text{m}$ ) size class (Fig. 4.8). Phosphorus activities increased by over a factor of 2 between the July and August cruises. Assuming all the P uptake of the 0.2 -1.0  $\mu\text{m}$  size class was derived from the TDP pool, a P turnover rate of approximately 2 days can be determined for the late summer. This is comparable to the bacterial P residence time of several hours to several days found by previous investigations using incubation techniques (Orrett and Karl, 1987; Cotner *et al.*, 1997).

The separation of TDP and SRP pools has allowed for an estimation of the  $^{33}\text{P}/^{32}\text{P}$  ratio in DOP (= TDP-SRP). DOP is operationally defined as that fraction which does not react to form a molybdenum blue complex as defined by Koroleff (1983). Thus, DOP contains a complex mixture of both biotic (e.g. sugars and nucleotides) and abiotic components (e.g. pyrophosphate and inorganic polyphosphates) while SRP may contain some easily hydrolyzed DOP such as phosphosugars (e.g. Strickland and Parsons, 1972; Karl and Yanagi, 1997). A recent study by Monaghan and Ruttanburg (1998), however found that less than 5% of a wide range of DOP compounds was hydrolyzed after the addition of Koroleff (1983) reagents. This finding, in addition to the reduced Koroleff (1983) reagents used in this study, suggest that the measured SRP fraction consists predominantly of phosphate and not the more easily hydrolyzed fractions of DOP.

Surface DOP concentrations increased from a low of 0.04  $\mu\text{M}$  in April to 0.20  $\mu\text{M}$  in July, whereas DIP concentrations decreased from 0.56 to 0.26  $\mu\text{M}$ . In July, the activity



of  $^{33}\text{P}$  and  $^{32}\text{P}$  in the DOP pool was close to 50% of the TDP activity, and the residence times of the SRP and TDP pools were 17 and 21 days, respectively (Fig. 3a). The residence time of the July DOP pool was significantly longer: 32 days. In contrast, the August TDP and SRP pools had residence times of less than 10 days (Table 4.2, Fig. 3a). The relative fraction of  $^{32}\text{P}$  and  $^{33}\text{P}$  activity in the August DOP pool also decreased by over a factor of two compared to July, whereas DOP concentrations decreased by less than 5%. The measured decrease in August DOP activity, however, could not be accounted for by radioactive decay alone. This implies that there was preferential remineralization of a more labile fraction of DOP, which was younger than the bulk DOP pool.

This labile fraction of DOP is difficult to identify given the few studies, which have sought to elucidate the composition of DOP in seawater. In Wilkinson Basin, DOP is below detection in the spring. This suggests that the principal fraction of DOP measured in the summer was of biological origin. Phosphorus is an essential nutrient, which is utilized by all organisms. As such, it is incorporated into a vast variety of compounds within the cell. These compounds include lipids, sugars, nucleotides and nucleic acids (Karl and Yanagi, 1997). Several studies have found that monophosphate esters are an important component (10-50%) of DOP (Taft *et al.*, 1977; Koboru and Taga, 1979; Karl and Yanagi, 1997). The second major DOP component appears to be comprised of nucleotides, such as adenosine tri-phosphate (ATP) (Karl and Yanagi, 1997). The rest, is most likely a mixture of such compounds as nucleic acids, polyphosphates and phosphonates (Strickland and Parsons, 1972).

Remineralization of DOP primarily occurs through enzymatic reactions at the cell surface of organisms within *Bacteria* and *Eucarya* (Ducklow, 1983; Ammerman and Azam, 1985, 1991; Azam, 1998). These organisms predominantly use two classes of enzymes, alkaline phosphatase and 5' nucleotidase (Karl and Craven, 1980; Ammerman and Azam, 1985, 1991; Ammerman, 1991; Karl and Yanagi, 1997). These enzymes enable organisms, such as bacteria, to consume both monophosphate esters and

nucleotides (Taft *et al.*, 1977; Koboru and Taga, 1979; Ammerman and Azam, 1985). The enzyme, alkaline phosphatase has been found to be inhibited in the presence of orthophosphate, whereas 5' nucleotidase is not (Perry, 1972; Ammerman and Azam, 1985). Given that SRP concentrations do not fall below 0.26  $\mu\text{M}$  in this study, the most likely mechanism of DOP remineralization is through enzymatic activity of 5' nucleotidase. As a result, the DOP fraction which is most available for remineralization (labile) is most likely comprised of nucleotides. Further evidence for this hypothesis is given by Ammerman and Azam (1985), who found that bacterial plankton hydrolyzed ATP at rates which exceeded 100% per hour. In fact, their study found that picoplankton could supply up to 50% of the orthophosphate required by larger plankton of California coast waters.

The relatively high  $^{32}\text{P}$  and  $^{33}\text{P}$  activities and low  $^{33}\text{P}/^{32}\text{P}$  ratio found within the August bacteria and picoplankton (0.2-1.0  $\mu\text{m}$ ) size class indicates that the dominant source of P was from the SRP pool. These results are similar to other investigations which have also suggested dissolved inorganic nutrient uptake by bacteria (Currie and Kalff, 1984; Wheeler and Kirchman, 1986; Tupas and Koike, 1991). Furthermore, most of the P released from the 0.2-1.0  $\mu\text{m}$  size class must have also occurred as SRP, given the low  $^{33}\text{P}$  and  $^{32}\text{P}$  activities found in the August DOP pool. Thus, bacteria and picoplankton were a large factor not only in the remineralization of dissolved organic matter, but also in the utilization of inorganic nutrients.

Ratios of  $^{33}\text{P}/^{32}\text{P}$  provide a unique tool with which to investigate phosphorus residence times within the larger micro- and mesoplanktonic pools as well. In general, larger zooplankton will consume both phytoplankton and zooplankton within the smaller size classes. Due to the large sample requirements necessary for  $^{32}\text{P}$  and  $^{33}\text{P}$  measurement, it was not possible to separate phytoplankton from zooplankton assemblages. As a result, the plankton tows contain mixtures of both. As expected,  $^{32}\text{P}$  and  $^{33}\text{P}$  activities (in d.p.m.  $\text{m}^{-3}$ ) within the 100-335 and >335  $\mu\text{m}$  size fractions were over a factor of two lower than those found in the smaller particles (<102  $\mu\text{m}$ ).  $^{33}\text{P}/^{32}\text{P}$  ratios ranged from  $0.79 \pm 0.08$  to as high as  $2.44 \pm 0.24$  on the 100-335 and >335  $\mu\text{m}$  fractions (Table 1). In March and

April, 100-335  $\mu\text{m}$  size class consisted predominantly of the phytoplankton, *Seratium* and *Coscinodiscus*. Assuming that the dominant P source to these pools was from TDP, we can calculate a P turnover rate of less than 2 days. In July and August, however, the 102-335  $\mu\text{m}$  size class contained mixed assemblages of copepods, such as *Calanus finmarchicus*, and to a lesser extent, dinoflagellates *Seratium*. These mixtures of phytoplankton and zooplankton had longer P turnover rates of typically two to four weeks assuming that the zooplankton were grazing phytoplankton within the smaller 10-102  $\mu\text{m}$  size class.

In the >335  $\mu\text{m}$  size class, residence times were longer. In March and April, the >335  $\mu\text{m}$  plankton tows were again dominated by the phytoplankton *Seratium* and *Coscinodiscus*, and P residence times averaged two weeks. In July and August residence times in this size class were generally longer, ranging from three to seven weeks (source material = 10-102  $\mu\text{m}$ ), and were dominated by mature copepods, such as *Calanus finmarchicus*, and some developmental stages of euphausiids. Our estimates of in situ meso-planktonic P turnover rates are similar to the 19 days found by laboratory studies which fed copepods with  $^{32}\text{P}$ -labeled phytoplankton (Marshall *et al.*, 1961). Furthermore, our estimates are within the 30-80 day range found using *in situ* measurements of  $^{32}\text{P}$  and  $^{33}\text{P}$  (with both continuous and non-continuous models) at Bermuda and off the coast of Southern California (Lal and Lee, 1988; Lee *et al.*, 1991; Waser *et al.*, 1995).

The measured seawater inventory of  $^{32}\text{P}$  and  $^{33}\text{P}$  was directly compared to that measured in rain to derive a nutrient export flux. While the ratio of  $^{33}\text{P}/^{32}\text{P}$  was the same,  $^{32}\text{P}$  and  $^{33}\text{P}$  fluxes differed between the two coastal sites: 1781 and 1653 d.p.m.  $\text{m}^{-2} \text{yr}^{-1}$  at Woods Hole versus 2123 and 1752 d.p.m.  $\text{m}^{-2} \text{yr}^{-1}$  at Portsmouth (Benitez-Nelson and Buesseler, 1998a). The flux of radioactive P out of surface waters can be determined assuming steady state and negligible advection and diffusion using the following equation:

$$P = (I - A_z)\lambda$$

where P is the flux (d.p.m.  $\text{m}^{-2} \text{d}^{-1}$ ) of  $^{32}\text{P}$  or  $^{33}\text{P}$  out of the depth interval of interest, I is the measured inventory of  $^{32}\text{P}$  or  $^{33}\text{P}$  from rain (d.p.m.  $\text{m}^{-2}$ ),  $A_z$  is the

**Table 4.3** Particulate organic carbon fluxes derived from  $^{32}\text{P}$ ,  $^{33}\text{P}$ , and  $^{234}\text{Th}$  radionuclide inventories.  $^{32}\text{P}$  and  $^{33}\text{P}$  inventories in March and April were determined by fitting an exponential curve to the activity depth distribution of  $^{32}\text{P}$  and  $^{33}\text{P}$ . In July and August,  $^{32}\text{P}$  and  $^{33}\text{P}$  inventories were determined by assuming constant activities over the 8 m mixed layer depth, and constant activities below. Fluxes were integrated over the upper 50 m. Organic carbon measurements used in the flux determination were measured on GF/F filters collected simultaneously from the same depths.

Sample	Rain Input ( $\text{dpm m}^{-2}$ )		$^{234}\text{Th}$ Flux ( $\text{dpm m}^{-2} \text{d}^{-1}$ )	$^{32}\text{P}$ Flux ( $\text{dpm m}^{-2} \text{d}^{-1}$ )	$^{33}\text{P}$ Flux ( $\text{dpm m}^{-2} \text{d}^{-1}$ )	Radionuclide Derived Carbon Fluxes		
	$^{32}\text{P}$	$^{33}\text{P}$				$^{234}\text{Th}$ ( $\text{mmol C m}^{-2} \text{d}^{-1}$ )	$^{32}\text{P}$ ( $\text{mmol C m}^{-2} \text{d}^{-1}$ )	$^{33}\text{P}$ ( $\text{mmol C m}^{-2} \text{d}^{-1}$ )
<i>March</i>	107	133	1460	--	--	52.6	--	--
<i>April</i>	205	254	821	2.31	3.07	17.7	22.0	36.7
<i>July</i>	111	135	574	0.52	0.93	3.4	4.4	11.3
<i>August</i>	117	133	1141	2.82	2.23	64.2	63.0	51.1

inventory of  $^{32}\text{P}$  or  $^{33}\text{P}$  (d.p.m.  $\text{m}^{-2}$ ) within the depth interval of interest, and  $\lambda$  is the radioactive decay constant for  $^{32}\text{P}$  or  $^{33}\text{P}$ . One of the largest errors associated with the flux calculation stem from the determination of the seawater  $^{32}\text{P}$  and  $^{33}\text{P}$  inventory, as sampling was only conducted at two depths. In March and April,  $^{32}\text{P}$  and  $^{33}\text{P}$  activities were assumed to decay exponentially with depth. In July and August,  $^{32}\text{P}$  and  $^{33}\text{P}$  inventories were determined by assuming complete mixing within the mixed layer (MLD = 8 m) and constant phosphorus activities, equivalent to deep waters, below.

The average  $^{32}\text{P}$  and  $^{33}\text{P}$  rain input flux between Woods Hole and Portsmouth was used to calculate the upper ocean radioactive phosphorus export flux over the upper 50 m. The flux of particulate organic carbon was then determined by multiplying the calculated  $^{32}\text{P}$  and  $^{33}\text{P}$  fluxes by the ratio of  $^{32}\text{P}$  (and  $^{33}\text{P}$ ) to carbon on sinking particles (Table 4.3) (e.g. Buesseler, 1998). It should be noted that  $^{32}\text{P}$  and  $^{33}\text{P}$  particulate activities were measured on a 1  $\mu\text{m}$  cartridge, while particulate organic carbon was measured on a GF/F ( $\sim 0.7 \mu\text{m}$ ).

The  $^{32}\text{P}$  and  $^{33}\text{P}$  derived organic carbon export fluxes were compared to those derived from  $^{234}\text{Th}$  fluxes measured during the same cruise and under similar assumptions (see Table 4.3 and see Chapter 5). Unlike  $^{32}\text{P}$  and  $^{33}\text{P}$ , the input of  $^{234}\text{Th}$  to the oceans is due to production from its soluble parent,  $^{238}\text{U}$ , a conservative element in seawater ( $^{238}\text{U}$  (d.p.m.  $\text{L}^{-1}$ ) = 0.0686 salinity; Chen *et al.*, 1986). In addition, while  $^{32}\text{P}$  and  $^{33}\text{P}$  export fluxes were expected to be dominated by biological removal,  $^{234}\text{Th}$  is a very particle reactive nuclide whose distribution can be expected to reflect the sum of both abiotic and biotic particle formation and export processes (Buesseler, 1998). It should be noted that particulate  $^{234}\text{Th}$  activities were also measured on a 1  $\mu\text{m}$  cartridge.

The organic carbon fluxes derived from the three isotopes were similar, with the exception of March, when measured  $^{32}\text{P}$  and  $^{33}\text{P}$  inventories were the same, within error, as that expected from rain measurements (Table 4.3). Export fluxes varied seasonally and ranged from 3.4 to 64.2  $\text{mmols C m}^{-2} \text{d}^{-1}$ . High carbon export rates in March were most likely the result of the spring bloom. In August, zooplankton grazing and mortality in late

summer led to high export rates as well. Differences between the carbon fluxes derived from the three radionuclides may be due to differences in the radionuclides half life, as fluxes integrate over the mean lives of each isotope. For example, because  $^{33}\text{P}$  is longer lived than  $^{32}\text{P}$ , it was probably more affected by downward advective mixing and diffusion in April and July. In August, stratification minimizes these processes. Furthermore, differences in the radioactive P source function, i.e. surface input versus constant production with depth, may also play a role in the above carbon flux estimates. Using primary production estimates of  $66.2 \text{ mmols C m}^{-2} \text{ d}^{-1}$  in the Gulf of Maine (O'Reilly and Busch, 1984) allows one to calculate an average 'export' ratio ( $ThE = \text{export/primary production}$ ; Buesseler, 1998) of 0.52, a number typical of many coastal environments (Dugdale and Goering, 1967; Eppley and Peterson, 1979). It is encouraging that the estimates of carbon export from simple models and isotopes of differing half-lives and source functions are so similar.

The dynamic nature and *in situ* temporal variability of P turnover within small particulate, SRP and DOP pools has never before been shown. Dissolved inorganic and organic P turnover rates have been inferred in the past using tracer studies of radiolabeled carbon, nitrogen, and phosphate as well as with specific organic phosphorus compounds which may or may not be representative of the DOP pool (Perry and Eppley, 1981; Bjorkman and Karl, 1994; Karl and Yanagi, 1997). These studies have found phosphorus turnover rates ranging from 1 to 80 days. The only other *in situ* study of TDP turnover rates using both  $^{32}\text{P}$  and  $^{33}\text{P}$  was conducted by Lal and Lee (1988) off the coast of California in September of 1987. However this study did not constrain the input ratio of  $^{33}\text{P}/^{32}\text{P}$  in rain. Nonetheless, their TDP residence time estimate of 20 days is similar to that found during July of this study.

## CONCLUSIONS

Our results are the first to show *in situ* evidence of the residence time of DOP, and the relative importance of bacterial and picoplankton activity within the biological food web. Phosphorus residence times ranged from less than a few days within the smaller size classes to greater than several weeks in the larger plankton. Further measurements of these isotopes, especially at open ocean and phosphorus limited sites, will help to provide new constraints on models which seek to emulate rates of nutrient uptake and remineralization. It is already clear that  $^{32}\text{P}$  and  $^{33}\text{P}$  have the unique ability to pinpoint the most biologically 'active' pools of dissolved inorganic, organic, and particulate phosphorus pools.

## REFERENCES

- Azam, F. (1998) Microbial control of oceanic carbon flux: The plot thickens. *Science*, **280**, 694-696.
- Ammerman, J. W. (1991) Role of eco-phosphohydrolases in phosphorus regeneration in estuarine and coastal ecosystems. In: *Microbial enzymes in aquatic environments*. R. J. Frost (Ed.), Springer-Verlag, New York, pp. 165-186.
- Ammerman, J. W. and F. Azam (1991) Bacterial 5'-nucleotidase activity in estuarine and coastal marine waters: Characterization of enzyme activity. *Limnol. Oceanogr.*, **36**, 1427-1436.
- Ammerman, J. W. and F. Azam (1985) Bacterial 5'-nucleotidase in aquatic ecosystems: A novel mechanism of phosphorus regeneration. *Science*, **227**, 1338-1340.
- Benitez-Nelson, C. R. and K. O. Buesseler (1998) Measurement of cosmogenic  $^{32}\text{P}$  and  $^{33}\text{P}$  activities in rainwater and seawater. *Anal. Chem.* **70**, 64-72.
- Benitez-Nelson, C. R. and K. O. Buesseler (1998)  $^{32}\text{P}$ ,  $^{33}\text{P}$ ,  $^7\text{Be}$ , and  $^{210}\text{Pb}$ : Atmospheric fluxes and utility in tracing Stratosphere/Troposphere exchange. *J. of Geophys. Res.* Submitted.
- Benway, H and T. Loder (1996) An investigation of the nutrient dynamics of Jeffreys Basin: A potential nutrient trap. Poster presented at the Gulf of Maine Ecosystem Dynamics: A Scientific Symposium and Workshop, St. Andrews, NB, September, 1996.
- Bjorkman, K. and D. M. Karl (1994) Bioavailability of inorganic and organic phosphorus compounds to natural assemblages of microorganisms in Hawaiian coastal waters. *Mar. Ecol. Prog. Ser.*, **111**, 265-273.
- Brooks, D. A., (1991) A brief overview of the physical oceanography of the Gulf of Maine. In: *Proceedings of the Gulf Of Maine Scientific Workshop, Woods Hole*, T. Wiggen and C. N. K. Mooers, Eds., pp. 51-74.
- Buesseler, K. O. (1998) The decoupling of production and particle export in the surface ocean. *Glob. Biogeochem. Cycles*, **12**, 297-310.
- Campbell, D. E., (1986) Process variability in the Gulf of Maine - a macroestuarine environment. In: *Estuarine Variability*, D. A. Wolfe, Ed., Academic Press., pp. 261-275.
- Chen, J. H., R. L. Edwards and G. J. Wasserburg (1986)  $^{238}\text{U}$ ,  $^{234}\text{U}$  and  $^{232}\text{Th}$  in seawater. *Earth and Planet. Sci. Lett.* **80**, 241-251.
- Charette, M. A., S. B. Moran and C. H. Pilskaln (1996) Particulate organic carbon export fluxes in the central Gulf of Maine estimated from  $^{234}\text{Th}/^{238}\text{U}$  disequilibria. Poster presented at the Gulf of Maine Ecosystem Dynamics: A Scientific Symposium and Workshop, St. Andrews, NB, September, 1996.
- Christensen, J. P., D. B. Smith and L. M. Mayer, (1991) The nitrogen budget of the Gulf of Maine and climate change. In: *Proceedings of the Gulf Of Maine Scientific Workshop, Woods Hole*, T. Wiggen and C. N. K. Mooers, Eds., p. 75-90.



- Christensen, J. P., D. W. Townsend and J. P. Montoya (1996) Water column nutrients and sedimentary denitrification in the Gulf of Maine. *Cont. Shelf Res.*, **16**, 489-515.
- Cotner, J. B., J. W. Ammerman, E. R. Peele and E. Bentzen (1997) Phosphorus limited bacterioplankton growth in the Sargasso Sea. *Aquatic Microb. Biol.*, **13**, 141-149 (1997).
- Currie, D. J. and J. Kalff (1984) The relative importance of bacterioplankton and phytoplankton in phosphorus uptake in freshwater. *Limnol. Oceanogr.* **29**, 311-321.
- Ducklow, H. W. (1983) Production and fate of bacteria in the oceans. *Bioscience*, **33**, 494-501.
- Dugdale, R. C. and J. J. Goering (1967) Uptake of new and regenerated forms of nitrogen in primary productivity. *Limnol. Oceanogr.*, **12**, 196-206.
- Eppley, R. W. and B. J. Peterson (1978) Particulate organic matter flux and planktonic new production in the deep ocean. *Nature* **282**, 677-680 (1978).
- Graham, W. F. and R. A. Duce (1979) Atmospheric pathways of the phosphorus cycle. *Geochimica et Cosmochimica Acta*, **43**, 1195-1208.
- Graham, W. F. and R. A. Duce (1981) Atmospheric input of phosphorus to remote tropical islands. *Pacific Science*, **35**, 241-255.
- Graham, W. F. and R. A. Duce (1982) The atmospheric transport of phosphorus to the Western North Atlantic. *Atmospheric Environment*, **16**, 1089-1092.
- Gulf of Maine Research Plan (1992). Prepared by: The Gulf of Maine Regional Marine Research Program, Orono, ME, 35 pp.
- Gunderson, K., A. Michaels, and N. Bates (1993) Determination of particulate organic carbon and nitrogen. In: *Bats Method Manual, Version 3*. Bermuda Biological Station for Research, Inc., Bermuda, 108 pp.
- Hecky, R. E. and P. Kilham (1988). Nutrient limitation of phytoplankton in freshwater and marine environments: A review of recent evidence on the effects of enrichment. *Limnology Oceanography*, **33**, 796-822.
- Karl, D. M. and K. Yanagi (1997) Partial characterization of the dissolved organic phosphorus pool in the oligotrophic North Pacific Ocean. *Limnol. Oceanogr.*, **42**, 1398-1405.
- Karl, D. M. and D. B. Craven (1980) Effects of alkaline phosphatase activity on nucleotide measurements in aquatic microbial communities. *Appl. Environ. Microbiol.*, **40**, 549-561.
- Kobori, H. and N. Taga (1979) Phosphatase activity and its role in the mineralization of organic phosphorus in coastal seawater. *J. exp. mar. Biol. Ecol.*, **36**, 23-39.
- Koroleff, F. (1983) Determination of nutrients, in *Methods of seawater analysis, 2<sup>nd</sup> ed.*, edited by K. Grasshoff, M. Ehrherd, and K. Kremling, pp. 125-135, Verlag Chemie, Weinheim.
- Lal, D. and T. Lee (1988) Cosmogenic <sup>32</sup>P and <sup>33</sup>P as tracers to study phosphorus recycling in the upper ocean. *Nature* **333**, 752-754.

- Lee, T, E. Barg and D. Lal(1991) Studies of vertical mixing in the Southern California Bight with cosmogenic radionuclides  $^{32}\text{P}$  and  $^7\text{Be}$ . *Limnol. Oceanogr.*, **36**, 1044-1053.
- Lee, T, E. Barg, E. and D. Lal (1992) Techniques for extraction of dissolved inorganic and organic phosphorus from large volumes of seawater. *Anal. Chim. Acta* **260**, 113-121.
- Loder, T., R. Boudrow, C. Coniaris, H. Benway, and C. Martorano (1996) Seasonal changes in nutrients and nutrient ratios in Massachusetts Bay during 1995. Poster presented at the Gulf of Maine Ecosystem Dynamics: A Scientific Symposium and Workshop, St. Andrews, NB, September, 1996.
- Marshall, S. M., R. J. Conover, and A. P. Orr (1961) On the biology of *Calanus finmarchicus*. XII. The phosphorus cycle: excretion, egg production, and autolysis. The turnover of phosphorus by *Calanus finmarchicus*. *J. of Marine Biol. Assoc. U. K.*, **41**, 463-488.
- Meise, C. J. and J. E. O'Reilly (1996) Spatial and seasonal patterns in abundance and age-composition of *Calanus finmarchicus* in the Gulf of Maine and on Georges Bank: 1977-1987. *Deep-Sea Res. II*, **43**, 1473-1501.
- Michaels, A. F. and M. W. Silver (1988) Primary production, sinking fluxes and the microbial food web. *Deep-Sea Res.*, **35**, 473-490.
- Monaghan, E. J. and k. C. Ruttenburg (1998) measurement of dissolved phosphorus in the coastal ocean: A reassessment of available methods and an examination of seasonal water column phosphorus profiles from the eel river shelf. *Limnol. Oceanogr.*, submitted.
- Omori, M. and T. Ikeda (1984) Chapter 5: Processing and Measurements. In: *Methods in Marine Zooplankton Ecology*. John Wiley and Sons, New York, pp. 79-104.
- Orrett, K. & Karl, D. M. (1987) Dissolved organic phosphorus production and turnover in surface waters. *Limnol. Oceanogr.*, **32**, 383-395.
- O'Reilly, J. E. and D. A. Busch (1984) Phytoplankton primary production on the northwestern Atlantic Shelf. *Rapp. P.-v. Reun. Cons. Int. Explor. Mer.*, **183**, 255-268.
- Peltzer, E. T. and N. A. Hayward (1996) Spatial and temporal variability of total organic carbon along 140°W in the equatorial Pacific Ocean in 1992. *Deep-Sea Research II*, **43**, 155-1180.
- Perry, M. J. and R. W. Eppley (1981) Phosphate uptake by phytoplankton in the central North Pacific Ocean. *Deep-Sea Res.*, **28**, 39-49.
- Pilskaln, C. H., W. Arnold, C. Lehmann and L. E. Watling (1996) Particulate flux dynamics in Jordan and Wilkinson Basins: Seasonal POC export and particle resuspension. Poster presented at the Gulf of Maine Ecosystem Dynamics: A Scientific Symposium and Workshop, St. Andrews, NB, September, 1996.
- Pollard, C., G. Battisto, E. Keese and B. J. Rutan (1996) Analytical service center procedure summaries. Virginia Institute of Marine Science/School of Marine Science, College of William and Mary, Gloucester Point, VA, February, 1996, 35 pp.

- Schlitz, R. J. and E. B. Cohen, (1984) A nitrogen budget for the Gulf of Maine and Georges Bank. *Biology Oceanography*, **3**, 203-221.
- Smayda, T. J. (1991). Global epidemic of noxious phytoplankton blooms and food chain consequences. In: Food Chains, Yields, Models and Management of Large Marine Ecosystems. AAAS Symp. Vol., K. Sherman and V. Alexander (Eds.).
- Smith, P. E., R. C. Counts and R. I. Clutter (1968) Changes in filtering efficiency of plankton nets due to clogging under tow. *J. Cons. perm. Int. Explor. Mer*, **32**, 232-248.
- Strickland, J. D. H and T. R. Parsons (1972) A practical handbook of seawater analysis. Fisheries Research Board of Canada, Ottawa, pp. 45-64.
- Taft, J. L., M. E. Loftus and W. R. Taylor (1977) Phosphate uptake from phosphomonoesters by phytoplankton in the Chesapeake Bay. *Limnol. Oceanogr.*, **22**, 1012-1021.
- Townsend, D. W., (1998) Sources and cycling of nitrogen in the Gulf of Maine. *Journal of Marine Systems*, accepted.
- Townsend, D. W. and R. W. Spinrad (1986). Early spring phytoplankton blooms in the Gulf of Maine. *Cont. Shelf Res.*, **6**, 515-529.
- Tupas, L. and I. Koike (1991) Simultaneous uptake and regeneration of ammonium by mixed assemblages of heterotrophic marine bacteria. *Mar. Ecol. Prog. Ser.* **70**, 273-282.
- Walsh, J. J., T. E. Whitley, J. E. O'Reilly, W. C. Phoel, and A. E. Draxler, (1987) Nitrogen cycling on Georges Bank and the New York Shelf: comparison between well-mixed and seasonally stratified waters. In: *Georges Bank*. (ed. Backus, R. H.) 234-246 (MIT Press, Cambridge).
- Waser, N. A. D. and M. P. Bacon (1995) Wet deposition fluxes of cosmogenic  $^{32}\text{P}$  and  $^{33}\text{P}$  and variations in the  $^{33}\text{P}/^{32}\text{P}$  ratios at Bermuda. *Earth and Planet. Sci. Lett.* **133**, 71-80 (1995).
- Waser, N. A. D., M. P. Bacon and A. P. Michaels, (1996) Natural activities of  $^{32}\text{P}$  and  $^{33}\text{P}$  and the  $^{33}\text{P}/^{32}\text{P}$  ratio in suspended particulate matter and plankton in the Sargasso Sea. *Deep-Sea Res.* **43(2-3)**, 421-436.
- Wheeler, P. A. and D. Kirchman, D. (1986) Utilization of inorganic and organic nitrogen by bacteria in marine systems. *Limnol. Oceanogr.*, **31**, 998-1009.
- Wiebe, P. H., A. W. Morton, A. M. Bradley, R. H. Backus, J. E. Braddock, V. Barber, T.J. Cowles and G. R. Flierl (1985) New developments in the MOCNESS, an apparatus for sampling zooplankton and micronekton. *Marine Biol.*, **87**, 313-323.
- Zapata, M., A. M. Ayala, J. M. Franco, J. L. Garrido (1987) Separation of chlorophylls and their degradation products in marine phytoplankton by reversed-phase high performance liquid chromatography. *Chromatographia*, **23**, 26-30.



## Chapter 5

### **Carbon export, eddy diffusivity and horizontal transport in the southwestern Gulf of Maine**

#### **ABSTRACT**

The radionuclides  $^{234}\text{Th}$  and  $^7\text{Be}$  were used to investigate the magnitude of particulate organic carbon export and the rate of vertical eddy diffusion in the southwestern Gulf of Maine. Sampling took place during March, April, July and August of 1997. Total surface  $^{234}\text{Th}$  activities varied both temporally and spatially: increasing with greater distance from shore and decreasing during the spring bloom and late summer. In contrast,  $^7\text{Be}$  distributions showed only minor offshore gradients during all four cruises.

Both non-steady state and horizontal transport models were assessed and found to be important for the accurate determination of  $^{234}\text{Th}$  derived particulate export. Our measurements demonstrate that the southwestern Gulf of Maine is typical of many coastal regimes and has an average organic carbon export ratio (particulate export/primary production) between 0.11 and 0.37. Estimates of vertical eddy diffusivity from  $^7\text{Be}$  in July and August range from 1.5 to 0.5  $\text{cm}^2 \text{sec}^{-1}$ , and show that this mechanism is sufficient to support the amount of 'new' nitrogen required for the measured particulate carbon export.

## INTRODUCTION

The Gulf of Maine is a highly productive continental shelf sea situated along the northeastern coast of the United States and southwestern Nova Scotia. This semi-enclosed water mass is bordered by a heavily populated coastline and supports one of the largest fisheries industries in North America (O'Reilly and Busch, 1984). Unfortunately, increasing anthropogenic inputs from agricultural and industrial activities have placed this unique basin in jeopardy.

There are currently few direct measurements of particulate export in the Gulf of Maine (Moran and Buesseler, 1993; Charette *et al.*, 1996; Pilskaln *et al.*, 1996). Such knowledge has proven to be essential for predicting the fate of organically bound or biologically active contaminants, such as anthropogenically produced CO<sub>2</sub>, hydrocarbons and heavy metals (Wageman and Muir, 1984; Larsen *et al.*, 1985; Barrick and Prahl, 1987; U.S. JGOFS Rept. 11, 1990; Kennicutt, 1994). The predominant transfer of these contaminants from the upper ocean to underlying sediments is generally thought to be biologically mediated (Bacon *et al.*, 1985; Dymond and Collier, 1988; Buesseler *et al.*, 1992a; Thunell *et al.*, 1994).

Primary production within the Gulf of Maine varies on seasonal timescales (O'Reilly and Busch, 1984). In the winter, deep convective mixing limits the light available to phytoplankton. In the spring, the onset of thermal stratification initiates a spring bloom dominated by large, rapidly growing primary producers, such as diatoms (O'Reilly and Busch, 1984; Townsend and Spinrad, 1986). The presence of larger phytoplankton has been shown to be directly related to high particulate export rates in the upper ocean (Buesseler, 1998). In contrast, strong thermal stratification and nutrient depletion ( $\text{NO}_3 + \text{NO}_2 \approx 0$ ) in the summer reduces biomass, resulting in a change in food web structure to smaller phytoplankton and bacteria, which are more efficient at nutrient uptake and remineralization (Walsh *et al.*, 1987). A second period of high particulate export may occur in mid to late summer as result of grazing and mortality of dense populations of copepods (e.g. Meise and O'Reilly, 1996).

The extent of particulate carbon export which results from this seasonally changing community structure is unknown. Within the Gulf of Maine, there are a wide range of estimates of new and recycled production, of which many are inferred from limited data sets (O'Reilly and Busch, 1984; Campbell, 1986; Schlitz and Cohen, 1984; Townsend, 1991; Christensen *et al.*, 1991; Townsend, 1998). In a recent study, Townsend (1998) determined that the total flux of 'new' nitrogen into the Gulf of Maine, i.e. that which supports 'new production', corresponded to  $13.5 \text{ mmol C m}^{-2} \text{ day}^{-1}$ . When compared to estimated rates of total primary production of  $66.2 \text{ mmol C m}^{-2} \text{ day}^{-1}$  made by O'Reilly and Busch (1984), a Gulf wide export ratio (export versus total production) of 0.20 was determined. Townsend (1998), however, hypothesized that the actual export ratio was closer to 0.40 based on what had been found in other coastal environments. As a result, Townsend (1998) suggested that another possible source of new nitrogen to surface waters was via water column nitrification followed by upward diffusion *within* the Gulf of Maine. Unfortunately, there was little direct evidence to support this conclusion.

In this study we have examined the magnitude of particulate carbon export using the particle reactive radionuclide  $^{234}\text{Th}$  ( $t_{1/2} = 24.1 \text{ d}$ ) and the rate of vertical eddy diffusion using  $^7\text{Be}$  ( $t_{1/2} = 53.3 \text{ d}$ ). Seasonal sampling was conducted in Wilkinson Basin in the southwestern Gulf of Maine. One dimensional and three dimensional steady state and non-steady state  $^{234}\text{Th}$  scavenging models were tested. Our measurements demonstrate that the Gulf of Maine is typical of many coastal regimes and has an average export ratio which ranges between 0.11 and 0.37. Estimates of vertical eddy diffusivity in July and August also show that this mechanism is sufficient to support the amount of 'new' nitrogen required for the measured particulate carbon export.

## Station Locations

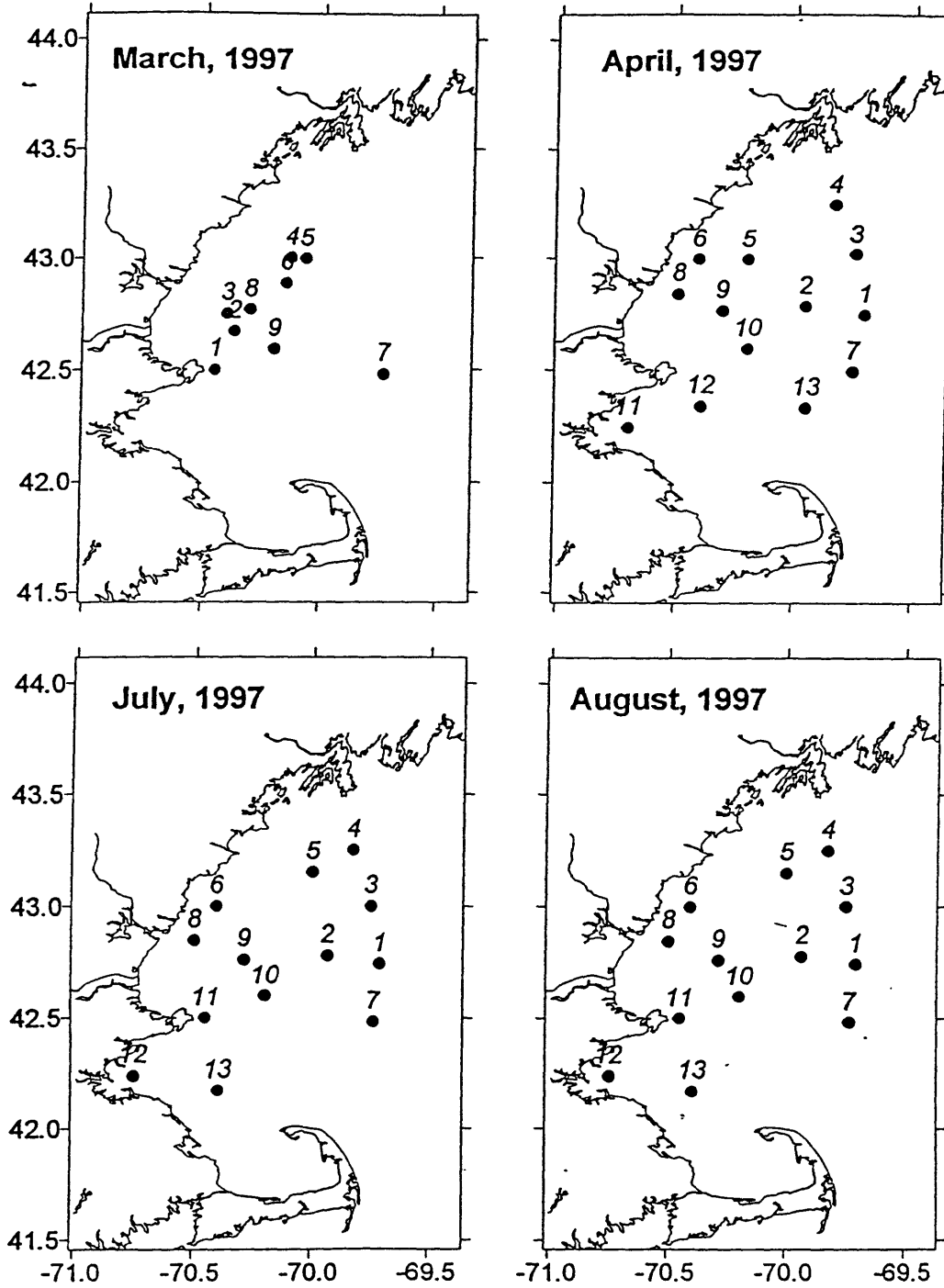


Figure 5.1 Station locations for all four cruises conducted in 1997.



## METHODS

Samples were collected during four cruises in the spring and summer of 1997 in Wilkinson Basin (depth = 275 m) in the Gulf of Maine (Fig. 1). This particular basin was chosen due to its relatively low advection and diffusion rates (Vermersch *et al.*, 1979; Brooks, 1985) and its close proximity to the Woods Hole Oceanographic Institution. Cruises were conducted in two paired sets, March and April, and July and August. A suite of surface samples and one depth profile (st. 7 in all cruises) were collected. The depth profile station was specifically chosen because it is the same site where subsurface sediment traps were placed continuously during 1995 and 1996 and because advection and diffusion are minimized (Pilskaln *et al.*, 1996). A large diameter hose was placed over the side of the ship and water pumped on deck using a large rotary bronze gear pump (Model: Teel, ¼ port). For  $^{234}\text{Th}$  and  $^7\text{Be}$ , between 200 and 400 L of seawater were passed sequentially through a 1  $\mu\text{m}$  polypropylene Hytrec filter followed by two 3 inch  $\text{MnO}_2$  impregnated Hytrec cartridges and a 1 L PVC pipe packed with iron impregnated polypropylene sheets. A flowmeter was placed on the end of the PVC pipe in order to monitor flow rate and volume.  $\text{MnO}_2$  adsorbers have been previously shown to efficiently collect dissolved  $^{234}\text{Th}$  (Buesseler *et al.*, 1992; 1995). The activity of  $^{234}\text{Th}$  can be quantified by determining the  $\text{MnO}_2$  collection efficiency from:

$$\text{Collection efficiency} = 1 - B/A$$

where A and B are the  $^{234}\text{Th}$  activities in disintegrations per minute (d.p.m.) on the first and second  $\text{MnO}_2$  cartridges in the series.  $^{234}\text{Th}$  collection efficiencies averaged  $0.86 \pm 0.08$  (n = 66).

While the  $\text{MnO}_2$  filters collect  $^{234}\text{Th}$ , these cartridges do not collect  $^7\text{Be}$ . Tests conducted by this laboratory found that less than 5% of the dissolved  $^7\text{Be}$  activity was collected on both the Mn A and Mn B  $^{234}\text{Th}$  cartridges. In contrast, previous investigations have found that  $^7\text{Be}$  is efficiently collected using iron oxide impregnated

materials (Lee *et al.*, 1991; Luo *et al.*, 1996). Although  $^{234}\text{Th}$  can also be collected using iron oxide, our tests found that variable amounts of the parent radionuclide,  $^{238}\text{U}$ , were adsorbed as well. Inconsistent adsorption of  $^{238}\text{U}$  results in variable ingrowth of  $^{234}\text{Th}$  with time and would compromise the  $^{234}\text{Th}$  data. Thus, two separate sets of radionuclide samples were collected:  $^7\text{Be}$  on  $\text{Fe}(\text{OH})_3$  and  $^{234}\text{Th}$  on  $\text{MnO}_2$ .  $^7\text{Be}$  collection efficiencies were determined in the same manner as with  $^{234}\text{Th}$ , by splitting the upper half of the cartridge into an A and the lower half into a B. Collection efficiencies were lower and more variable than that found with  $^{234}\text{Th}$  and averaged  $0.71 \pm 0.19$  ( $n = 49$ ). Variability in  $^7\text{Be}$  collection efficiencies was most likely the result of non-uniform iron impregnation of the polypropylene filters.

All ancillary samples were collected using Niskin bottles. Unfiltered and filtered (through a GF/F) nutrient samples were collected in acid cleaned polypropylene bottles and immediately frozen for analysis in the laboratory. Suspended particulate matter (SPM) samples were collected by filtering onto pre-weighed polycarbonate filters. Particulate organic carbon, nitrogen, and phosphorus and separate pigment samples were collected via low pressure ( $< 5$  psi) filtration onto combusted GFF filters. Integrated and depth specific 102  $\mu\text{m}$  plankton tows were also retrieved at the Wilkinson Basin station (st. 7). Plankton samples were split into two size classes via sieving through a 335  $\mu\text{m}$  mesh screen, and fixed with 2% formaldehyde.

Upon returning to the lab,  $^{234}\text{Th}$   $\text{MnO}_2$  cartridges were immediately acid digested, purified, and counted via low level beta counting according to the methods described by Buesseler *et al.* (1992b). Iron oxide and Hytrex prefilters were ashed and placed in clear pre-weighed polystyrene counting jars. Iron oxide filters were measured for  $^7\text{Be}$  and Hytrex prefilters for both  $^7\text{Be}$  and  $^{234}\text{Th}$  using CANBERRA 2000  $\text{mm}^2$  LEGe style gamma detectors.  $^{234}\text{Th}$  gamma ( $E_n = 63$  KeV) and low level beta efficiencies have been determined previously (Buesseler *et al.*, 1992b; 1995). For  $^7\text{Be}$  ( $E_n = 477$  KeV), gamma detectors were calibrated using standards of known activity (EPA Standard Pitchblend Ore). Standards of similar geometry and of differing heights were placed in the same

counting jars used for our samples.  $^7\text{Be}$  efficiencies and self absorption were then determined by interpolating between the gamma emissions of  $^{214}\text{Pb}$  (242, 295, 352 KeV) and  $^{214}\text{Bi}$  (609 KeV). An additional check of this interpolation procedure was conducted by directly comparing the interpolated efficiencies found for  $^{137}\text{Cs}$  (661 KeV) with those derived from counting a known activity  $^{137}\text{Cs}$  standard. Interpolated and measured  $^{137}\text{Cs}$  efficiencies were within 5% of each other.  $^{234}\text{Th}$  and  $^7\text{Be}$  activities were corrected to the midpoint of collection and reported in disintegrations per minute (d.p.m.). Activity errors were determined from the propagation of uncertainties derived from volume collection, detector calibration, and for  $^{234}\text{Th}$  chemical recoveries. All errors are  $1\sigma$ .

Ancillary measurements for total and dissolved ( $< 0.7 \mu\text{m}$ )  $\text{NO}_3 + \text{NO}_2$ , ammonia, silicate, and phosphorus were analyzed by the Analytical Service Center at the Virginia Institute of Marine Science according to the methods described by Pollard *et al.* (1996). Dissolved organic carbon measurements were made according to Peltzer and Hayward (1996). Pigments in the greater than  $0.7 \mu\text{m}$  size class were determined using HPLC according to Zapata *et al.* (1987). Particulate organic carbon and nitrogen were determined using CHN. All CHN samples were processed according to Gunderson *et al.* (1993), the same procedure utilized at the JGOFS Bermuda Atlantic Time Series. This method involves fuming with concentrated HCl for 24 hours to remove carbonate prior to measurement. Previous researchers have found that acid fuming is not sufficient for the removal of inorganic carbon in sediment trap and in sediment samples with high carbonate and dolomite concentrations (Hedges and Stern, 1984; Cowie and Hedges, 1991). It is unlikely that this is a problem in our study given the small sample sizes ( $< 50 \mu\text{g}$  of organic C per sample).

## RESULTS

Dissolved and particulate  $^{234}\text{Th}$  and  $^7\text{Be}$  surface water activities, decay corrected to the midpoint of collection, are shown in Table 1. Total  $^{234}\text{Th}$  and  $^7\text{Be}$  surface activity distributions are shown in Figures 2 and 3. Contour plots were constructed using a software package (SURFER<sup>TM</sup> by Golden Software), which utilizes a linear kriging technique to grid the data. Kriging is a technique which places irregularly spaced data on a regularly spaced grid. Each grid point or node is determined by an average value which is the result of weighting all of the data in accordance with their proximity to the actual grid point. In essence, the closer the data point, the higher the weighting factor in the determination of the concentration at that grid point. Station locations are shown for each cruise and grid scales are uniform in order to better demonstrate temporal and spatial trends in our radionuclide data.

In March at the start of the spring bloom, nutrients were high and the mixed layer depth at our vertical profile station (st. 7) was 100 m (Fig. 4). Total surface  $^{234}\text{Th}$  activities ranged from 0.6 to 1.5 d.p.m.  $\text{L}^{-1}$  and increased with increasing distance from the coast (Fig. 2a). Particulate  $^{234}\text{Th}$  ( $>1 \mu\text{m}$ ) ranged between 20 and 50% of the total measured activity. In contrast, total  $^7\text{Be}$  activities, with the exception of one station, had a narrow range, 91 - 381 d.p.m.  $\text{m}^{-3}$ , and showed no clear gradient between onshore and offshore waters (Fig 3a). In addition, particulate  $^7\text{Be}$  concentrations never exceeded 11% of the total measured activity.

In April, prior to our cruise, a large storm struck Wilkinson Basin. This resulted in an increase in the mixed layer depth at our vertical profile station from 100 to 110 m, and likely disrupted the spring bloom. Surface activities of  $^{234}\text{Th}$  were generally higher than in March and ranged from 0.6 to 1.8 d.p.m.  $\text{L}^{-1}$ , with a single offshore value above equilibrium values of 2.2 d.p.m.  $\text{L}^{-1}$ . (Fig. 2b). Total  $^{234}\text{Th}$  increased dramatically in the offshore waters. Particulate  $^{234}\text{Th}$  activities were still high and similar in range to those measured in March. Total  $^7\text{Be}$  concentrations, however, were significantly higher than in March, ranging from 180 to 512 d.p.m.  $\text{m}^{-3}$ , but there was no clear gradient in

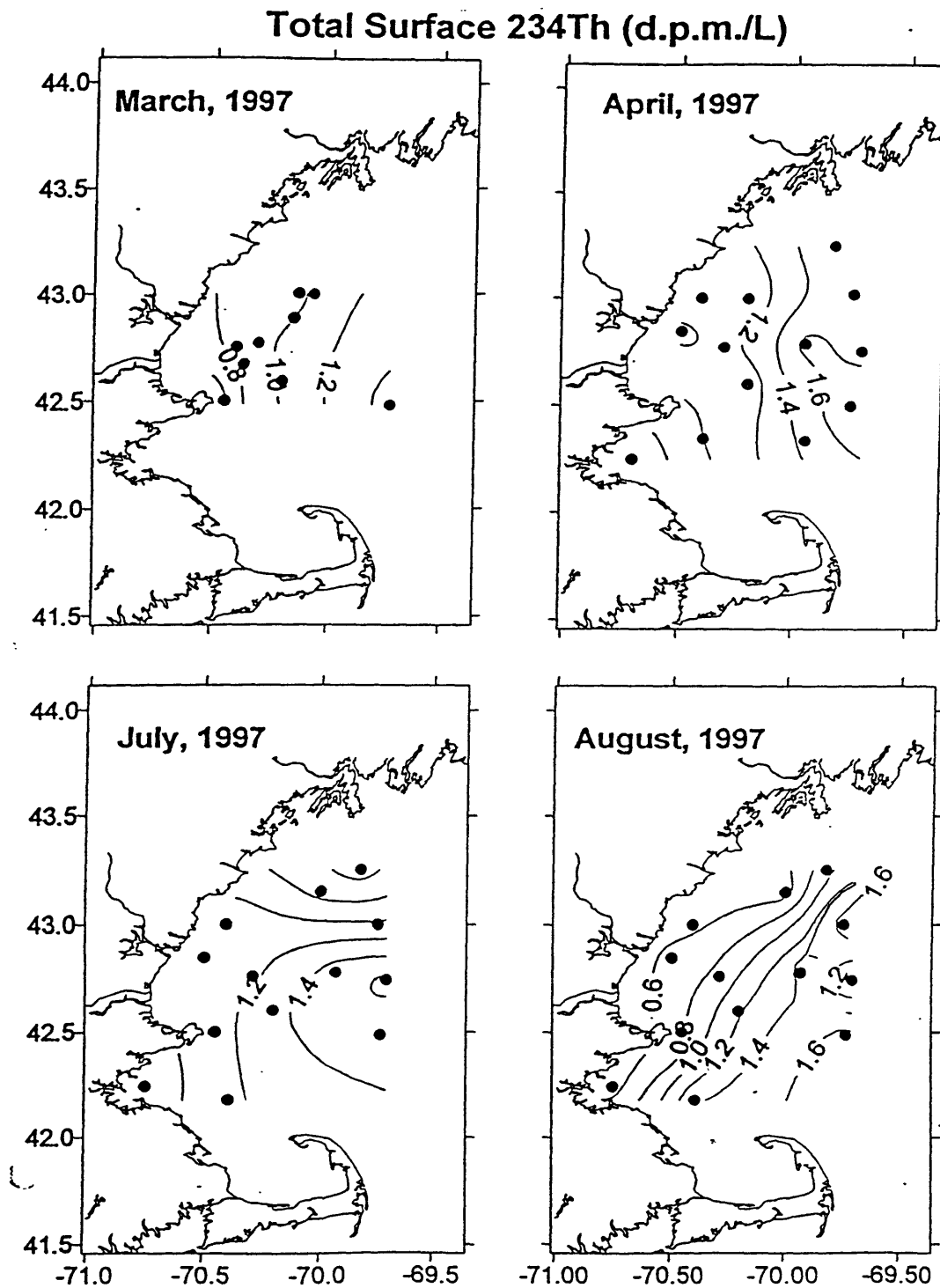


**Figure 5.2a-d** Contour plots of total  $^{234}\text{Th}$  surface activities in d.p.m.  $\text{L}^{-1}$  from all four cruises. Station locations are shown as black circles.

### Total Surface $^7\text{Be}$ (d.p.m./m<sup>3</sup>)

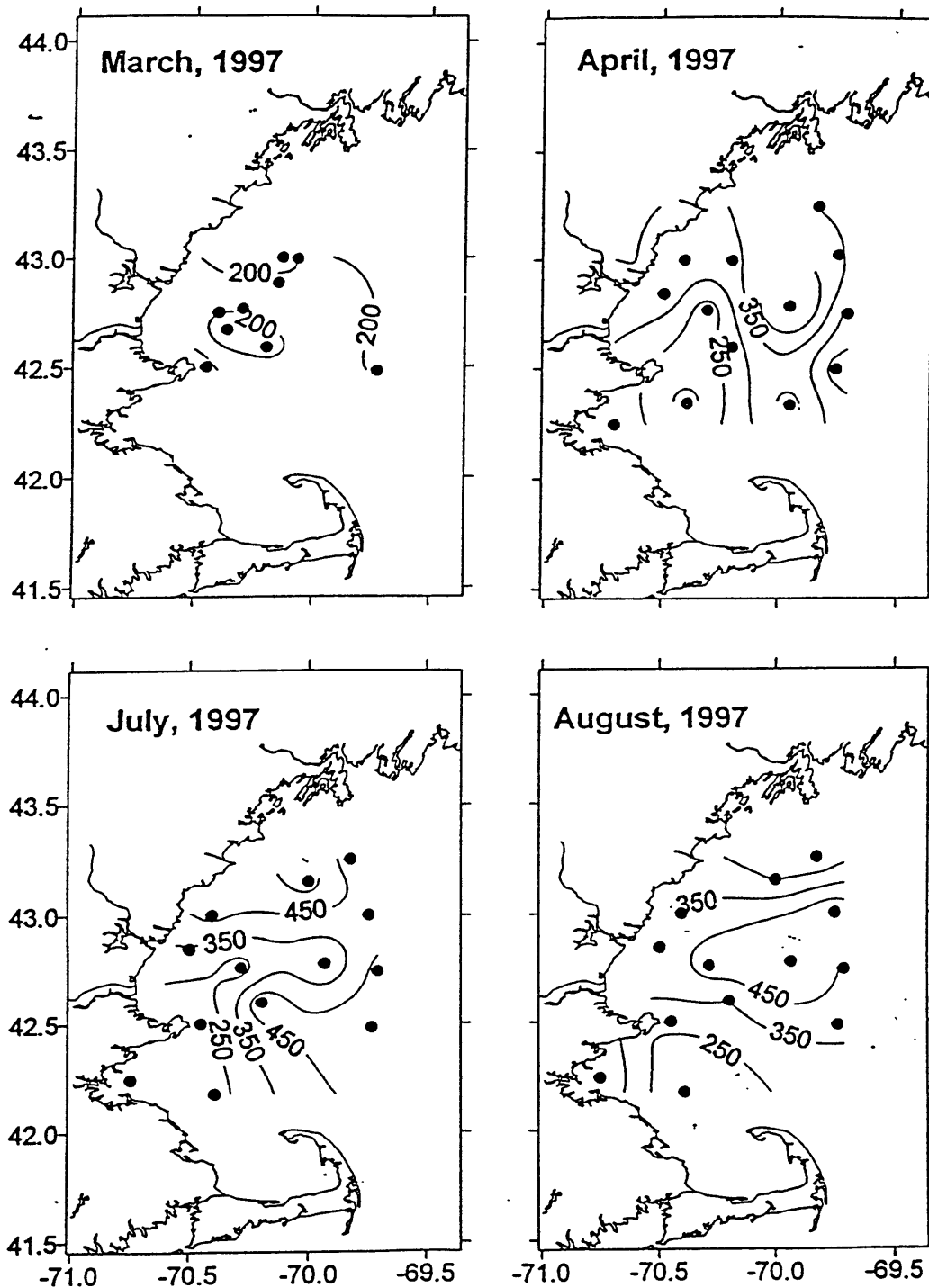


**Figure 5.3a-d** Contour plots of total  $^7\text{Be}$  surface activities in d.p.m. m<sup>-3</sup> from all four cruises. Station locations are shown as black circles.

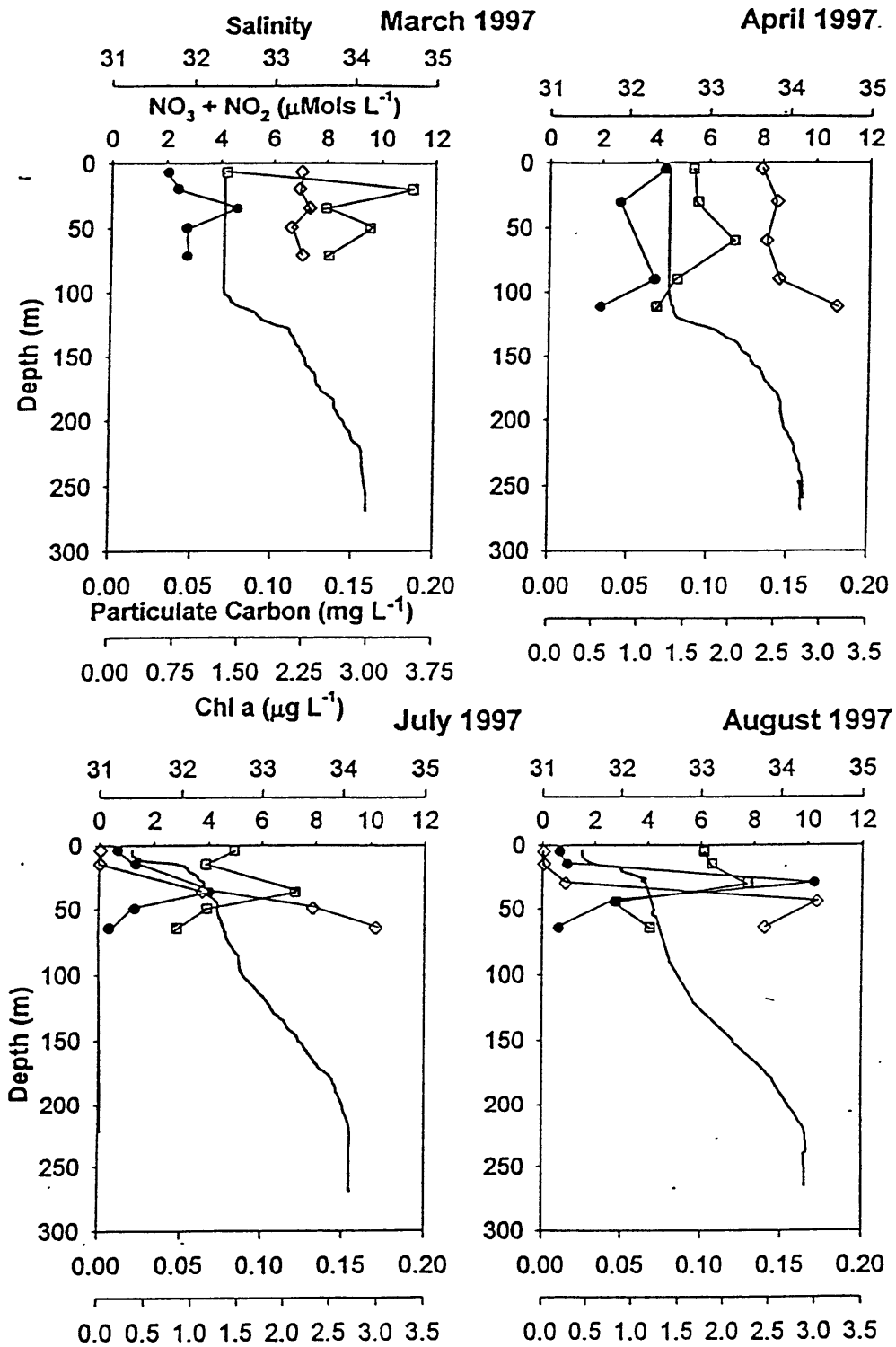


**Figure 5.4** Depth profiles of salinity (black line),  $\text{NO}_3 + \text{NO}_2$  (Diamonds), particulate organic carbon (squares) and chl *a* (circles). Note the decrease in mixed layer depth for March to August and the formation of a large subsurface chl *a* maximum.

concentration with increasing distance from the coast (Fig. 3b). Higher  $^7\text{Be}$  activities were the result of the substantial increase in rainfall which occurred during the large storm which struck the southwestern Gulf of Maine between the March and April cruises (Benitez-Nelson and Buesseler, 1998). Particulate  $^7\text{Be}$  concentrations were still less than 10% of the total  $^7\text{Be}$  measured activity.

In the early summer increasing thermal stratification and nutrient uptake following the spring bloom resulted in low nutrient waters, which persisted through the August cruise. In July, total surface water  $^{234}\text{Th}$  activities ranged from 0.5 to 1.65 d.p.m.  $\text{L}^{-1}$ , with particulate concentrations between 20 and 50% of the total (Fig. 2c). Although there was a large offshore gradient in total  $^{234}\text{Th}$  activity, the magnitude of this gradient was less than that found in April.  $^7\text{Be}$  activities ranged from 198 to 600 d.p.m.  $\text{m}^{-3}$ , generally increasing with increasing distance from shore (Fig. 3c). Particulate  $^7\text{Be}$  concentrations were again less than 10% of the total measured  $^7\text{Be}$  activity. In August, total surface water  $^{234}\text{Th}$  activities were similar in range to those found in July, yet offshore gradients were significantly larger (Fig. 2d). In addition, particulate  $^{234}\text{Th}$  activities decreased to values which were typically less than 20% of the total measured  $^{234}\text{Th}$  activity.  $^7\text{Be}$  concentrations and offshore distribution were also similar to those found in July (Fig. 3d). Particulate  $^7\text{Be}$  concentrations, however, decreased to less than 5% of the total measured  $^7\text{Be}$  activity.

Depth profiles of  $^{234}\text{Th}$  and  $^7\text{Be}$  activities at station 7 in Wilkinson Basin are given in Table 1 and Figures 5 and 6. In March and April, both dissolved and particulate  $^{234}\text{Th}$  and  $^7\text{Be}$  concentrations remained relatively constant with depth. Although in April, both total  $^{234}\text{Th}$  and  $^7\text{Be}$  activities increased by close to factor of 1.5 over the upper 75 m. In July, total  $^{234}\text{Th}$  activities increased with depth below the 8 m mixed layer, reaching equilibrium values at 65 m. In contrast, total  $^7\text{Be}$  activities decreased by a factor of two between the mixed layer and deeper waters. In August,  $^{234}\text{Th}$  activities actually decreased to a minimum at 30 m, the depth of the Chl  $a$  maximum, and remained low to 55 m.  $^7\text{Be}$  activities, on the other hand, were high only in the upper 30 m, decreasing rapidly to near



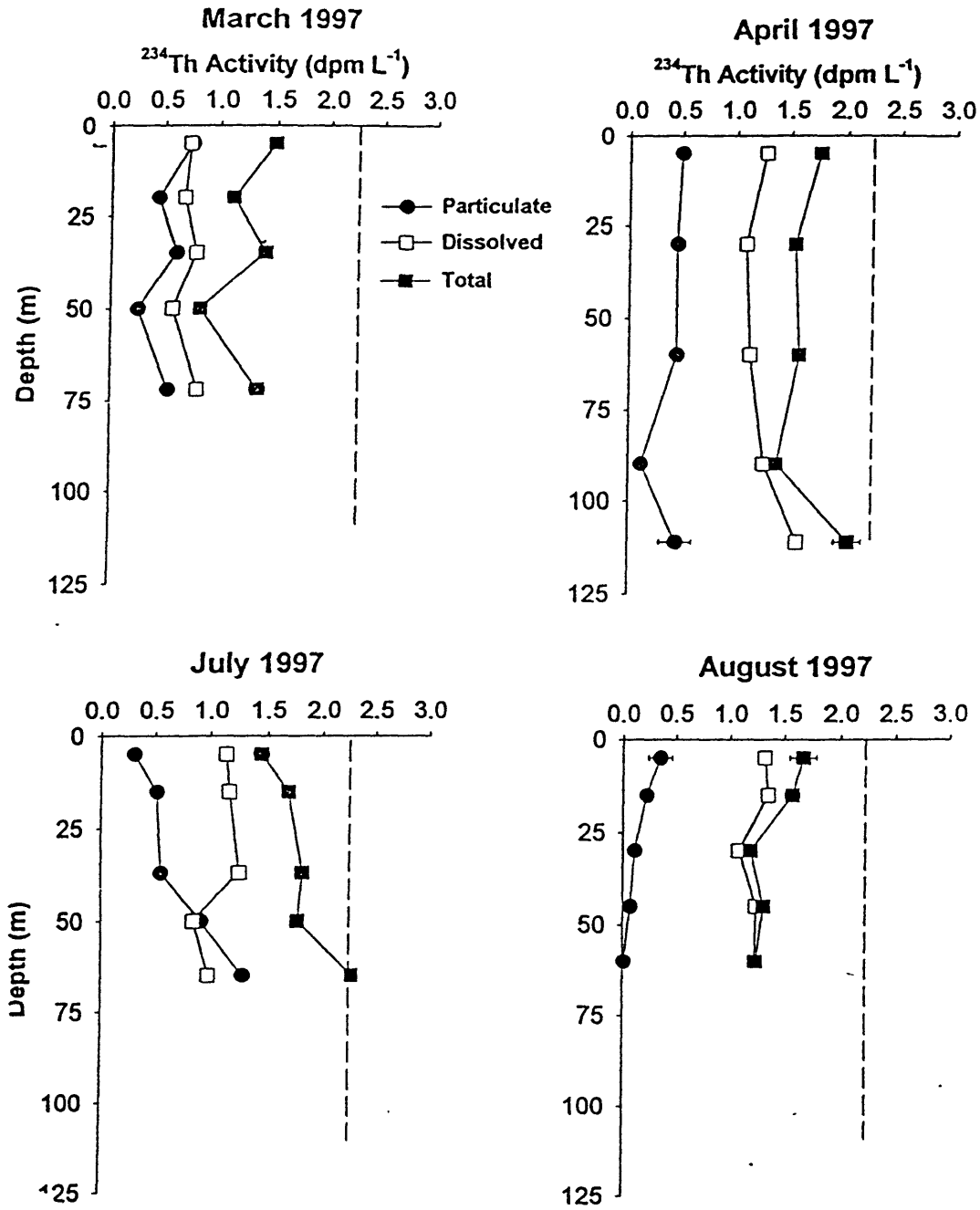


**Figure 5.5** Particulate (closed circles), dissolved (open squares), and total  $^{234}\text{Th}$  (closed squares) activities in d.p.m.  $\text{L}^{-1}$  with depth. Dashed lines are representative of  $^{238}\text{U}$  activities. Error bars are  $1\sigma$ .

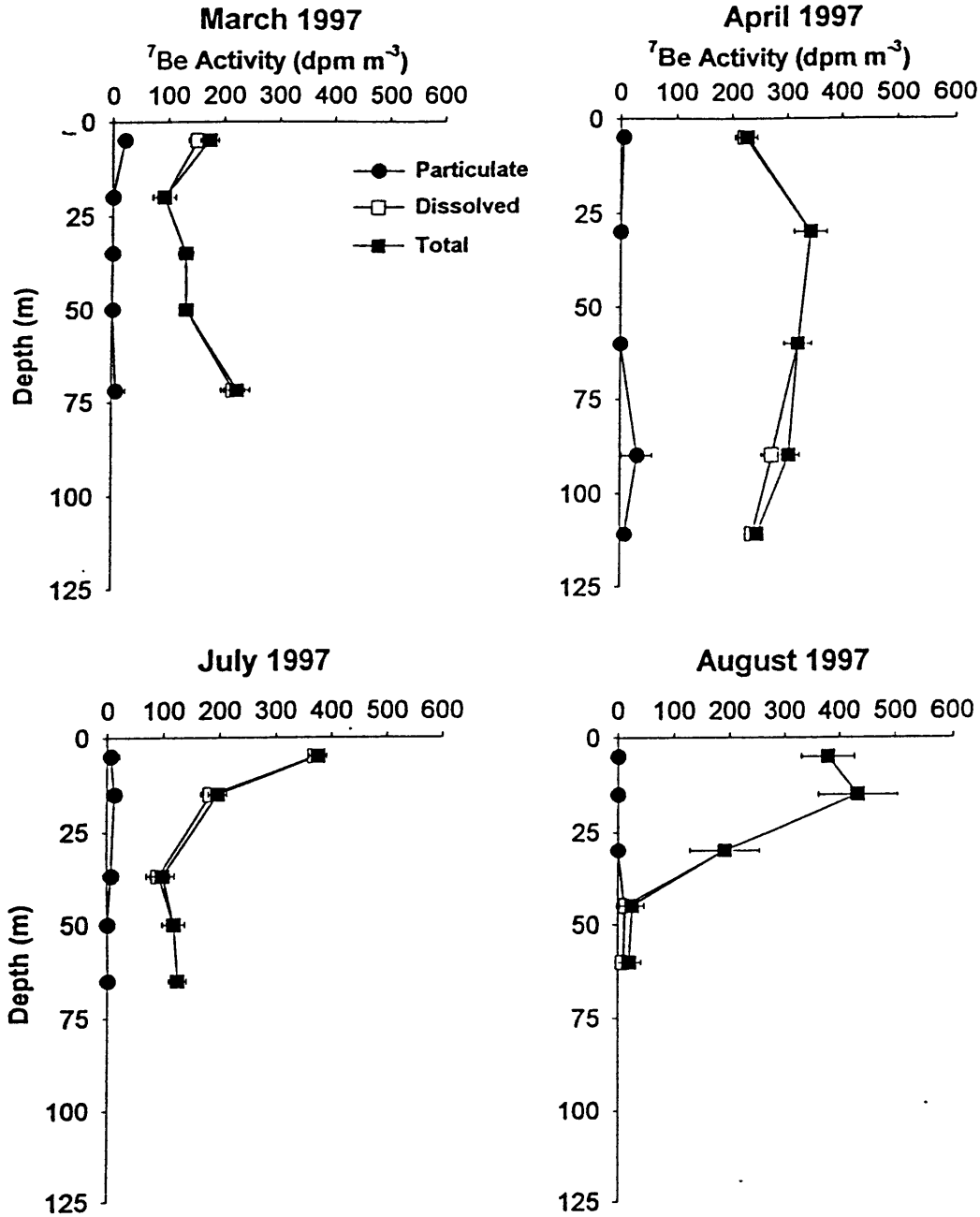


**Figure 5.6** Particulate (closed circles), dissolved (open squares), and total  $^7\text{Be}$  (closed squares) activities in d.p.m.  $\text{m}^{-3}$  with depth. Error bars are  $1\sigma$ .

zero levels at depth. Increased errors on  $^7\text{Be}$  activities in August are due to the longer time period between sample collection and measurement.

## DISCUSSION

### *$^{234}\text{Th}$ derived particle export*

$^{234}\text{Th}$  is a naturally occurring particle-reactive radionuclide which has been commonly used to study particle scavenging in the upper ocean (Santschi *et al.*, 1979; Kaufman *et al.*, 1981; Coale and Bruland, 1985, 1987; Murray *et al.*, 1989; Buesseler *et al.*, 1992; 1994; 1998). Since the half-life of  $^{234}\text{Th}$  is 24.1 days, the disequilibrium between its soluble conservative parent  $^{238}\text{U}$  and the measured  $^{234}\text{Th}$  activity reflects the net rate of particle export from the upper ocean on time scales of days to weeks. In the surface ocean, both the formation of fresh particle surfaces (proportional to primary production) and the packaging of particles into sinking aggregates (export or new production) are reflected in the observed  $^{234}\text{Th}$  distribution. The activity balance of  $^{234}\text{Th}$  can be described by the following equation:

$$dA_{\text{Th}}/dt = A_{\text{U}}\lambda - A_{\text{Th}}\lambda - P + V \quad (1)$$

where  $dA_{\text{Th}}/dt$  is the change in  $^{234}\text{Th}$  activity with time,  $A_{\text{U}}$  is the  $^{238}\text{U}$  activity ( $^{238}\text{U}$  (d.p.m.  $\text{L}^{-1}$ ) = 0.0686 salinity; Chen *et al.* 1986),  $A_{\text{Th}}$  is the total measured  $^{234}\text{Th}$  activity,  $\lambda$  is the decay constant for  $^{234}\text{Th}$  ( $= 0.0288 \text{ d}^{-1}$ ),  $P$  is the net removal flux of  $^{234}\text{Th}$  on particles, and  $V$  is the sum of advective and diffusive terms. The magnitude of the export flux is most often driven by the extent of the  $^{234}\text{Th}/^{238}\text{U}$  disequilibrium. Steady state is often assumed ( $dA_{\text{Th}}/dt = 0$ ) and physical processes ignored. However, non steady state effects (Buesseler *et al.*, 1992a, 1998) and physical processes (Buesseler *et al.*, 1995) can be substantial.

The use of non-steady state  $^{234}\text{Th}$  formulations appears to be important during plankton blooms, when significant  $^{234}\text{Th}$  removal can occur (Buesseler *et al.*, 1992a, 1998;

Cochran *et al.*, 1995;1997). More commonly, however, steady-state models are sufficient (Tanaka *et al.*, 1983; Moran and Buesseler, 1993). Vertical advection,  $V$  in equation (1), has been shown to be significant in areas of intense upwelling, such as in the Equatorial Pacific and along the coast of the Arabian Sea during the SW Monsoon (Buesseler *et al.*, 1995, 1998; Bacon *et al.*, 1996). In addition, horizontal  $^{234}\text{Th}$  transport can be important in coastal regions, especially in bays, where large horizontal gradients in  $^{234}\text{Th}$  scavenging can occur (McKee *et al.*, 1984; Wei and Murray, 1992; Gustaffson *et al.*, 1998).

The general circulation of the Gulf of Maine is complex and driven by a combination of processes such as wind stress, strong tidal forcing, and spring riverine discharge (Brooks, 1991). Because of the seasonality expected in physical transport and biological processes and the near-shore nature of our sampling sites, we have sought to understand the relative effects of non-steady state and physical processes, such as horizontal advection, on the measured  $^{234}\text{Th}$  budgets.

#### ***Steady State and Non-Steady State 1D $^{234}\text{Th}$ Flux model***

$^{234}\text{Th}$  fluxes, integrated over the upper 10 m, were first determined using a one dimensional (1D) model, which assumes steady state (SS,  $dA_{\text{Th}}/dt = 0$  in equation 1) and ignores physical processes ( $V = 0$  in equation 1). Results are shown in Table 2 and Figure 7. As expected,  $^{234}\text{Th}$  fluxes tended to decrease with increasing distance from shore within the southwestern Gulf of Maine, reflecting a reduction in particulate export. In April, July, and August  $^{234}\text{Th}$  fluxes were over a factor of two smaller within Wilkinson Basin than at the coast. At station 7,  $^{234}\text{Th}$  activity profiles further allowed the determination of 1D  $^{234}\text{Th}$  fluxes over the upper 50 m, the depth of the euphotic zone. Fluxes ranged from 352 to 1460 dpm  $\text{m}^{-2} \text{d}^{-1}$  (Table 3), peaking in March and August. The difference in the total  $^{234}\text{Th}$  activity from equilibrium values drives the magnitude of the  $^{234}\text{Th}$  particulate export flux, such that the greater the deficit, the larger the particulate export. Equilibrium is generally reached with increasing depth, below the euphotic zone. However, in this study, total  $^{234}\text{Th}$  activities do not. Thus, integrating  $^{234}\text{Th}$  inventories to

Steady State  $^{234}\text{Th}$  Flux integrated over the upper 10 m  
(d.p.m./m<sup>2</sup>/day)

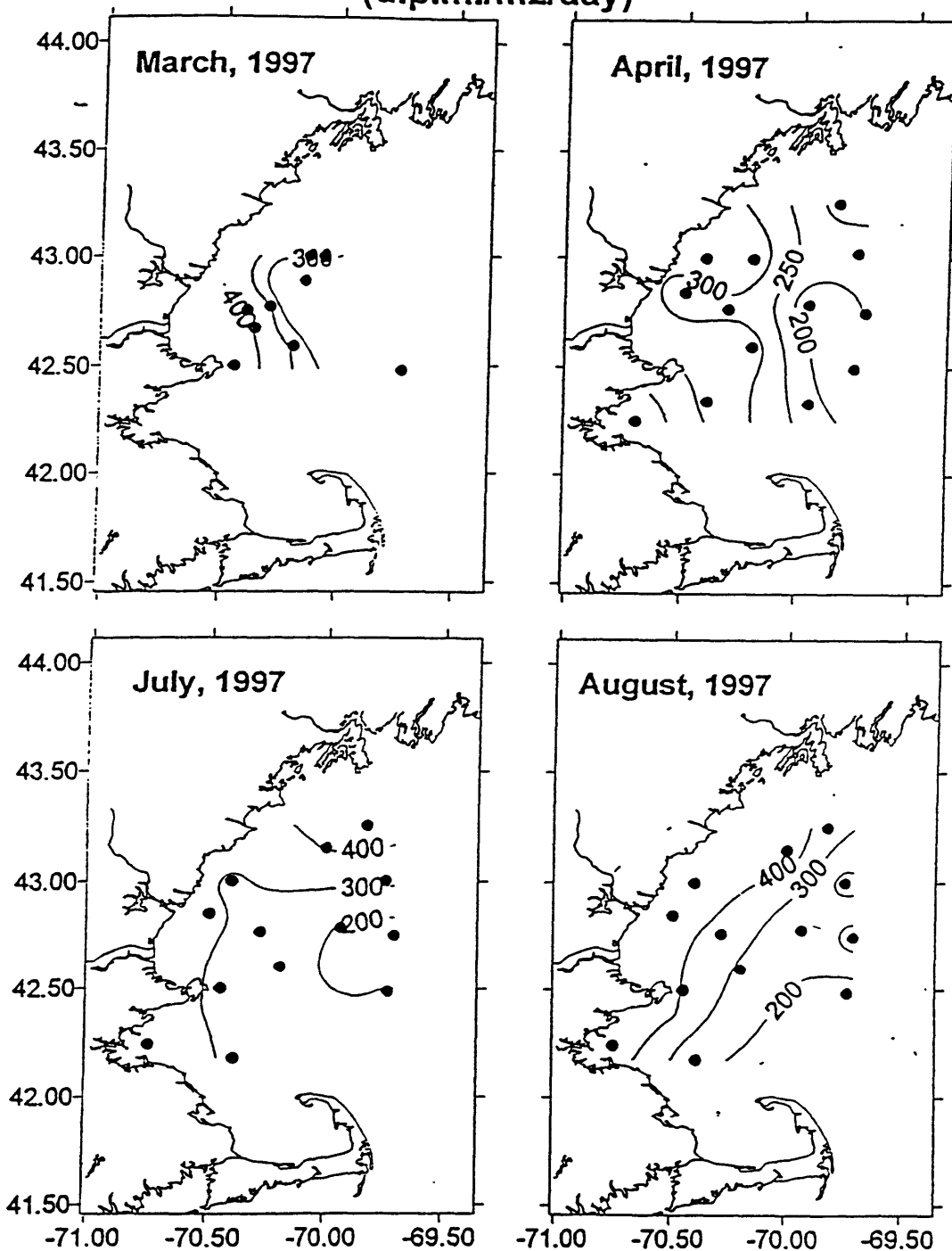


**Figure 5.7** Contour plots of steady state determinations of the upper 10 m particulate  $^{234}\text{Th}$  flux in d.p.m. m<sup>-2</sup> day<sup>-1</sup>. Station locations are shown as black circles.

deeper depths where  $^{234}\text{Th} < ^{238}\text{U}$ , especially within the euphotic zone, will tend to increase particulate export fluxes.

The above  $^{234}\text{Th}$  flux calculations, however, all assume steady state. Although at first glance there appears to be little seasonality in the upper 10 m  $^{234}\text{Th}$  activities, closer examination reveals that the non-steady state term (NSS),  $dA_{\text{Tm}}/dt$  in equation (1), can be substantial (physical processes,  $V$ , in equation 1 are still assumed to be zero). In general, decreasing  $^{234}\text{Th}$  inventories with time (i.e. due to increased scavenging intensity) will result in a calculated steady state (SS) particulate export which is too low. In contrast, increasing the  $^{234}\text{Th}$  inventory (i.e. due to decreased scavenging intensities) results in steady state particulate export estimates which are too high.

The change in activity with time,  $dA_{\text{Tm}}/dt$  (equation 1), was determined for April, using March data, and for August using data taken in July. This determination assumes a single water mass. We maintain that this is appropriate for the month long interval separating our spring and summer cruises, given the  $^{234}\text{Th}$  mean-life of 35 days. However, we do not use this assumption for the longer 3 month time period between the April and July Cruises.  $^{234}\text{Th}$  activities used in the non-steady state calculation were occasionally interpolated from the stations closest in proximity to the station of interest from the preceding cruise. Results are shown in Table 2. Inclusion of the non-steady state term in the upper 10 m  $^{234}\text{Th}$  flux calculation for the April cruise decreased particulate fluxes from a SS average of 271 d.p.m.  $\text{m}^{-2} \text{day}^{-1}$  to 170 d.p.m.  $\text{m}^{-2} \text{day}^{-1}$ . In contrast, in August, NSS  $^{234}\text{Th}$  particulate export fluxes were 378 d.p.m.  $\text{m}^{-2} \text{day}^{-1}$ , less than 15% greater than the August SS average of 334 d.p.m.  $\text{m}^{-2} \text{day}^{-1}$ .

The magnitude of the NSS term in the 50 m integrated  $^{234}\text{Th}$  flux calculation at station 7 was quite significant (Table 3). NSS, 50 m integrated particulate export fluxes determined for the April cruise were over an order of magnitude smaller than that of the steady state determination. This is due to the increase in  $^{234}\text{Th}$  activities between March and April. In August, however, inclusion of the non-steady state term increased  $^{234}\text{Th}$

particulate fluxes by only 30%. This was probably due to an increase in subsurface production as evident by higher chl *a* concentrations (Fig. 4).

Our results demonstrate that non-steady state effects were significant in these export calculations within the southwestern Gulf of Maine during the spring. Whether this was due to the spring phytoplankton bloom or to the large storm which struck Wilkinson Basin between the March and April cruises is unclear. Regardless, these results indicate that temporal variability at individual stations can be quite important when using  $^{234}\text{Th}$  as an export tracer. This is in contrast to many open ocean regimes (e.g. Buesseler, 1998). Since the spring bloom plays such an important role in annual particulate export within coastal regimes, utilization of  $^{234}\text{Th}$  to derive particulate export should include temporal measurements of  $^{234}\text{Th}$  concentrations.

#### ***Non-Steady State Multi-dimensional $^{234}\text{Th}$ Flux model***

Physical processes such as horizontal advection and diffusion should also be considered in estimating  $^{234}\text{Th}$  derived particulate export fluxes, especially in coastal areas (Gustaffson *et al.*, 1998). Such processes are often ignored in calculating  $^{234}\text{Th}$  particulate export due to the difficulty associated with estimating the magnitude of horizontal transport fluxes. In addition, calculations require good spatial coverage of the  $^{234}\text{Th}$  activity distribution within a study site. In many cases, time and budget constraints do not allow for such measurements to be made.

In this study, the effect of horizontal advection and diffusion on our  $^{234}\text{Th}$  budget was evaluated using a multi-dimensional model for several boxes located in the center of our suite of stations (Fig. 8). Physical processes such as advection and diffusion,  $V$  in

equation (1), can be rewritten as:

$$V = -u \frac{dA_{\text{Th}}}{dx} - v \frac{dA_{\text{Th}}}{dy} + K_x \frac{d^2 A_{\text{Th}}}{dx^2} + K_y \frac{d^2 A_{\text{Th}}}{dy^2} \quad (2)$$

where  $u$  and  $v$  are the velocities in the chosen  $x$  and  $y$  direction, respectively,  $dA_{\text{Th}}/dx$  is the activity gradient along the  $x$  axis,  $dA_{\text{Th}}/dy$  is the activity gradient along the chosen  $y$  axis,  $K_x$  and  $K_y$  are the  $x$  and  $y$  horizontal diffusivities, respectively, and  $d^2 A_{\text{Th}}/dx^2$  and  $d^2 A_{\text{Th}}/dy^2$ , the second derivative of the activity distribution. Note that this formulation does not consider upwelling of higher activity  $^{234}\text{Th}$  from deep waters.

Horizontal advection directions and rates were not measured during our cruises. Therefore, historical measurements derived from surface current meter measurements in close proximity to our stations were used in conjunction with current simulations. Two sets of current meter data were used. The first set consists of data taken during November 1974 to December 1975 at a depth of 33 m (Vermersch *et al.*, 1978). The second set consists of data taken from June to August of 1983 and 1984 at a depth of 25 m (Brooks, 1985; Gottlieb and Brooks, 1986). Both data sets show that the dominant water flow at our study site is along the coast to the South or Southwest. Drifter track model simulations and actual drifter track measurements made in the spring of 1993 and 1994 further support this alongshore direction (R. Geyer. Personal communication; Namie, 1996).

The day to day intensity of the alongshore and offshore current is highly variable. However, 1-3 month long integrated current measurements taken from different years are similar, and indicate an average alongshore current velocity of 5 to 13  $\text{cm sec}^{-1}$  and an average offshore current velocity of -2 to 4  $\text{cm sec}^{-1}$  (Gottlieb and Brooks, 1986; Vermersch *et al.* 1985; R. Geyer, personal communication). It should be noted that the activity distribution of  $^{234}\text{Th}$  at any particular point in time reflects the net  $^{234}\text{Th}$  source and/or sink over the mean life ( $1/\lambda \approx 35$  days) of  $^{234}\text{Th}$ . Thus, while horizontal advective velocities may vary significantly over day to several week long time scales, it is necessary



to use the *average* current velocity integrated over longer, month long time periods. In this study, a current velocity of  $1 \text{ cm sec}^{-1}$  moving directly offshore was used ( $\sim 135^\circ$  from true North). A coordinate system was set such that  $v \, dA_{\text{Th}}/dy$  in equation (2) was zero.

Surface  $^{234}\text{Th}$  distributions show north/south patterns which for the most part follow the coastline along the dominant direction of water flow during each cruise (based on drogue simulations; Naimie, 1996). Thus, alongshore gradients in the  $^{234}\text{Th}$  activity tended to be small, resulting in low net  $^{234}\text{Th}$  transport parallel to the coast. In contrast, significantly larger gradients in  $^{234}\text{Th}$  activity occurred with increasing distance from shore. This is not surprising given that particulate concentrations also decrease away from the coast. Similar  $^{234}\text{Th}$  distributions both alongshore and offshore have been found in the Arabian Sea and Casco Bay in the Gulf of Maine (Buesseler *et al.*, 1998; Gustafson *et al.*, 1998)

Horizontal diffusion estimates were obtained using Okubo's (1971) empirically derived oceanic diffusion diagrams. Confidence in these estimates arises from the fact that our study site is similar in nature to those (i.e. New York Bight) used to develop Okubo's empirically derived diffusion estimates. The distance, or 'length scale' between each station ranged from 10 to 40 Km. This yielded an apparent diffusivity of  $0.8 \times 10^5$  to  $4.0 \times 10^5 \text{ cm}^2 \text{ sec}^{-1}$ . These estimates are significantly lower than those used by Gustaffson *et al.* (1998) in nearby Casco Bay. The Casco Bay study differs from ours as it was conducted at sites closer inshore and within a tidal strait, where tidally induced high shear rates occur (Gustaffson *et al.*, 1998). Gustaffson *et al.* (1998) found that horizontal advective transport within inner and outer Casco Bay was insignificant relative to dispersion and particulate export. In addition, dispersive properties were substantial within inner Casco Bay only during one of the two cruises.

In order to determine  $^{234}\text{Th}$  activity gradients, data were first placed onto a regularly spaced 16 point grid using a linear kriging technique (Fig. 8; SURFER<sup>TM</sup>). These gridded points were then used to determine the effect of horizontal advection and diffusion during the April, July, and August cruises on both 'inshore' (#1 and #3) and

‘offshore’ boxes (#2 and #4) using the following box model equation (Fig. 8):

$$V = v (C_{y+1} - C_{y-1}) / (2\Delta y) + K_y (C_{y-1} - 2C_y + C_{y+1}) / \Delta y^2 \quad (3)$$

where:  $\Delta y$  is the distance between grid nodes,  $C_y$  is the  $^{234}\text{Th}$  concentration within the box, and  $C_{y+1}$  and  $C_{y-1}$  are the  $^{234}\text{Th}$  activities on either side of each box. In March, there were too few offshore data points to obtain a grid. Distances between grid nodes were 33.2 Km. This was equivalent to an Okubo (1971) derived apparent diffusivity of  $K_y = 3.2 \times 10^5 \text{ cm}^2 \text{ sec}^{-1}$ .

Results from the above analysis are shown in Figure 9. In this figure, we compare the magnitude of each term from equation (1). Note that equation (1) has the particulate export flux,  $P$ , as positive in the depth direction. The steady state term,  $(A_U\lambda - A_{Th}\lambda)$  depicts the difference between the  $^{234}\text{Th}$  activity expected from  $^{238}\text{U}$  decay and that actually measured. The non-steady state term  $(dA_{Th}/dt)$  takes into account that  $^{234}\text{Th}$  activities may change with time. A negative  $^{234}\text{Th}$  non-steady state flux simply implies that the  $^{234}\text{Th}$  inventory has decreased from one sampling period to another. As a result, there is actually more export occurring than what would have been found had steady state been assumed. Thus, the non-steady state term is assigned a positive value. In April, July, and August the advection/diffusion term ( $V$  in equation 3) reflects the transport of low  $^{234}\text{Th}$  activity waters to areas of higher activity. This low  $^{234}\text{Th}$  activity results in the ‘appearance’ of more particulate export than what has actually occurred. As a result, the advection/diffusion term is assigned a negative value.

The uncertainty associated with gridding was determined by taking the difference between the  $^{234}\text{Th}$  activity measured at a specific station with the  $^{234}\text{Th}$  activity interpolated from the gridded data at that station. Overall errors are determined from the average uncertainties associated with gridding and  $^{234}\text{Th}$  collection efficiencies and counting statistics. The inclusion of both advection and diffusion terms significantly reduced the  $^{234}\text{Th}$  export flux. In August, when  $^{234}\text{Th}$  gradients were largest,  $^{234}\text{Th}$  fluxes

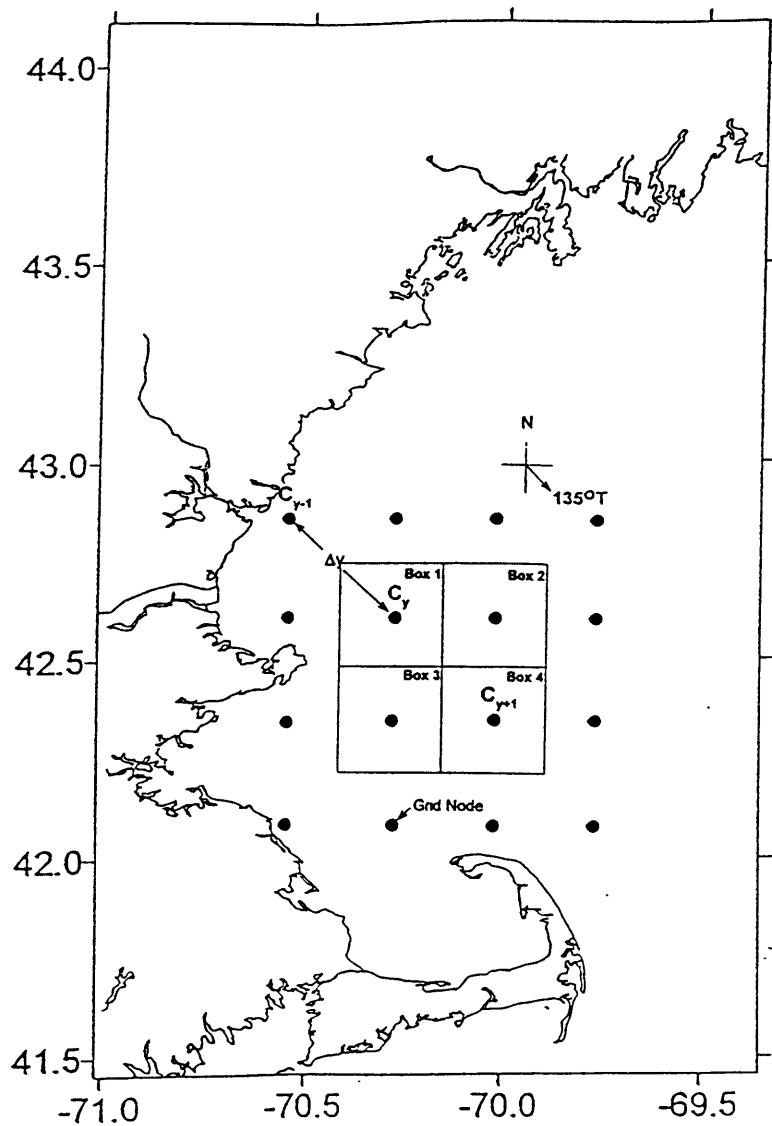


**Figure 5.8** Schematic of box model. Circles depict grid nodes. Boxes are numbered clockwise starting at the northwestern most box. Both advective and diffusive flow is to the south at  $135^\circ\text{T}$ .

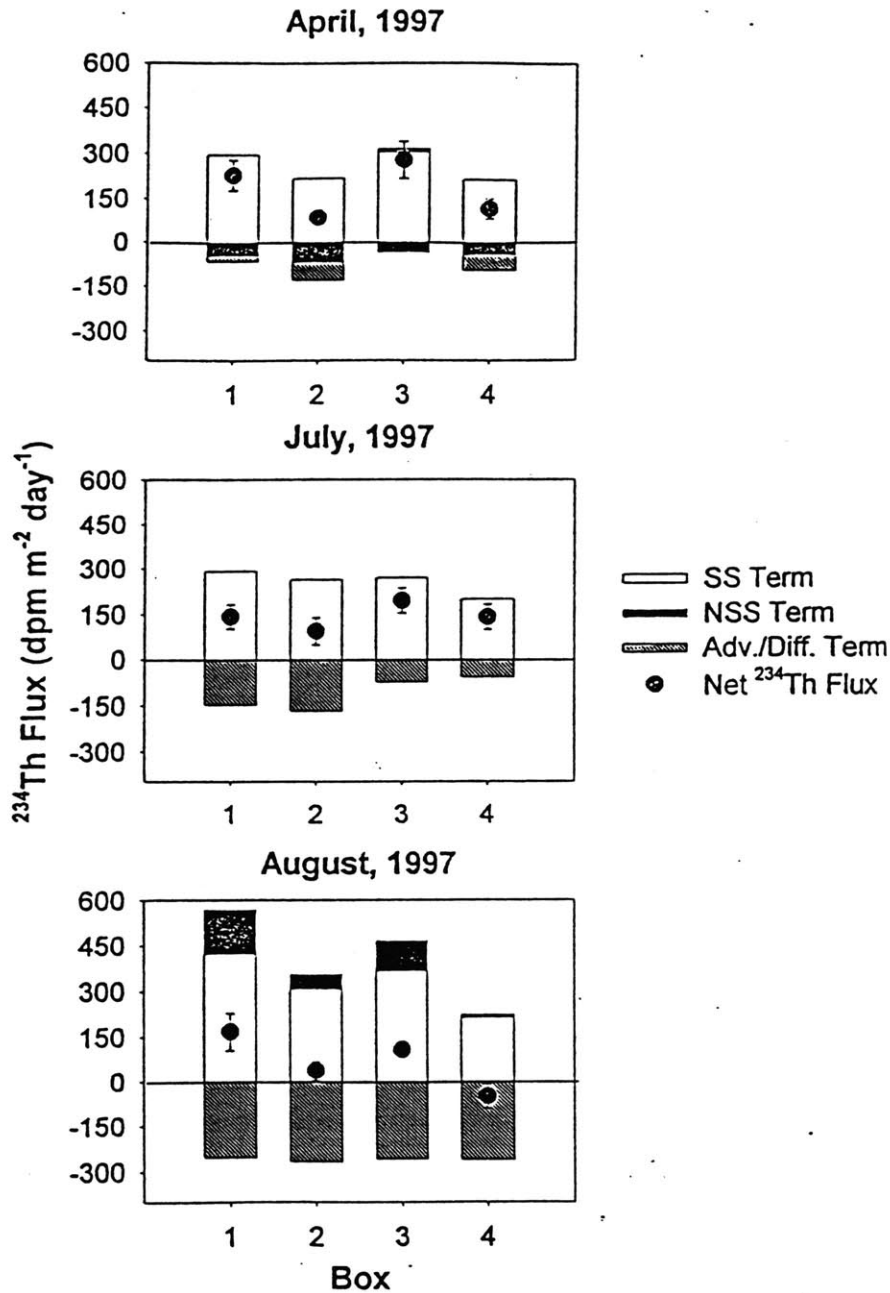


**Figure 5.9a-c**  $^{234}\text{Th}$  model flux results for the April, July and August cruises. Each stacked bar represents the magnitude of the steady state term ( $A_U\lambda - A_{Th}\lambda$ ; white), non-steady state term ( $dA_{Th}/dt$ ; black) and advection/diffusion term ( $V$ ; light gray). All fluxes were integrated over the upper 10 m and are in  $\text{d.p.m. m}^{-2} \text{day}^{-1}$ . The net  $^{234}\text{Th}$  flux (black circles) from the inclusion of all three terms is also shown.

decreased by >100% (Table 4).  $^{234}\text{Th}$  derived particulate export fluxes were always greater in the nearshore boxes (1, 3) than in the offshore boxes (2, 4). However, only in April was this due to the inclusion of the advective/diffusive term. In July and August, these differences appeared to be due mostly to variations in the SS term (Fig. 5.9).

In August, a negative  $^{234}\text{Th}$  flux was determined for the southeastern most box. Negative  $^{234}\text{Th}$  particulate export fluxes can be caused by two processes. Either there was upwelling of high  $^{234}\text{Th}$  concentrations from depth, i.e. from sub-surface remineralization, or the terms describing the  $^{234}\text{Th}$  budget at that box were not properly constrained. It is most likely the latter explanation.

The above calculation is highly dependent on the chosen current velocities, horizontal eddy diffusivities and measured  $^{234}\text{Th}$  activity gradients (e.g. equation (3)). Doubling the advective offshore current velocity,  $v$ , results in a decrease in the  $^{234}\text{Th}$  export flux by greater than 50% in April and July, and greater than 250% in August. In contrast, doubling the horizontal eddy diffusivity,  $K_y$ , increases the  $^{234}\text{Th}$  export flux by less than 30%. Increasing or decreasing the first and second order activity gradients (e.g.  $dA_{\text{Th}}/dx$  and  $d^2A_{\text{Th}}/dx^2$  in equation (2)) results in similar magnitude changes in the  $^{234}\text{Th}$  export for the April, July, and August cruises.

It should be noted that an underestimation of particulate export rates will occur if deep waters with higher  $^{234}\text{Th}$  activity are significantly transported into low activity surface waters. It is difficult to predict the extent of this effect on the 10 m integrated  $^{234}\text{Th}$  flux with only surface measurements of  $^{234}\text{Th}$ . Nonetheless, one can gauge the importance of this process by using the depth distribution of  $^{234}\text{Th}$  at station 7 and the vertical eddy diffusivity rates found from  $^7\text{Be}$  during the July and August cruises (see *Vertical Eddy Diffusivity, ( $K_v$ )*). In July, the flux of  $^{234}\text{Th}$  into the upper 10 m was determined to be 26 d.p.m  $\text{m}^{-2} \text{d}^{-1}$ . This would result in less than a 10% increase in the previously determined steady state  $^{234}\text{Th}$  export flux of 206 d.p.m  $\text{m}^{-2} \text{d}^{-1}$  (Table 2). In August, deep waters are

actually lower in  $^{234}\text{Th}$  activity than that observed at the surface. As a result, the upper 10 m non-steady state  $^{234}\text{Th}$  export flux is actually reduced by 14 d.p.m  $\text{m}^{-2} \text{d}^{-1}$  or 20%.

Our simple box model demonstrates the complexity involved in trying to evaluate the effect of physical processes, such as horizontal advection, in a coastal marine environment, especially when there are large gradients in  $^{234}\text{Th}$  activity over small spatial scales. It should be noted these physical processes do not pertain to  $^{234}\text{Th}$  alone and would be true for any mass balance of N, P, or even  $\text{O}_2$  within a coastal system.

Many open ocean regimes also have significant regional variability in  $^{234}\text{Th}$  activity, but this often occurs over much larger spatial scales, such that  $dA/dx$  and  $dA/dy$  (from equation (2)) are relatively small (Buesseler *et al.*, 1995; 1998). In addition, total  $^{234}\text{Th}$  activities are often integrated over depth intervals which are much larger than that used in the above calculations (100 versus 10 m). This requires the use of depth integrated horizontal current velocities which are substantially smaller than those at the surface. As a result, the  $V$  term in equation (1) is substantially reduced in the open ocean as opposed to coastal environments. Our study in Wilkinson Basin indicates that understanding the magnitude and direction of coastal currents is a major issue for accurately determining  $^{234}\text{Th}$  particulate export fluxes in coastal waters. Future work in coastal regimes must consider these processes.

### ***Particulate Organic Carbon Export derived from $^{234}\text{Th}$***

The use of  $^{234}\text{Th}$  data to calculate the export fluxes of particulate organic C and N is based upon work conducted over the last thirty years (e.g. Buesseler, 1998). In these studies, it has been found that one can use the predicted  $^{234}\text{Th}$  flux and the site and time specific measurements of particulate  $^{234}\text{Th}$  to organic C and N, to estimate POC and PON fluxes. Confidence in this approach has been obtained by the close agreement between the  $^{234}\text{Th}$ -derived flux estimates, and export determined by a variety of independent techniques (tCO<sub>2</sub> decrease, N-budgeting, DOC balances, etc.- Buesseler *et al.*, 1992a; 1995).

*ThE* ratios are defined as the ratio of  $^{234}\text{Th}$  derived export production to primary production (Buesseler, 1998). While distinct, these ratios are similar in nature to *f* and *e* ratios commonly used in previous studies in that it is a measure of the productivity of the regime (Eppley and Peterson, 1979; Downs, 1989; Buesseler, 1998). Primary production estimates are commonly derived from  $^{14}\text{C}$  incubation techniques. The *f* ratio, is defined as the ratio of 'new' to total primary production, where new production is determined from the uptake of  $^{15}\text{N}$  labelled substrates and is the amount of primary production supported by nutrients from outside the euphotic zone, i.e. from upwelling (Eppley and Peterson, 1979). Conversely, regenerated production is often defined as the amount of primary production supported by nutrients recycled within the euphotic zone. The *e*-ratio is defined as the ratio of upper ocean sediment trap derived export to primary production (Downs, 1989). Thus, it should be noted that all of these definitions are highly dependent on the integration depth and time scale of interest.

The only assumption in estimating POC export from  $^{234}\text{Th}$  is that the filtration techniques utilized are collecting material representative of the sinking particulate flux and hence, have the correct POC/ $^{234}\text{Th}$  ratio. It has been found the POC/ $^{234}\text{Th}$  ratio is best determined from the exact same filter in order to remove differences associated with the filter collection efficiency. However, our large volume sampling requirements did not enable the use of conventional filter media. The 10 inch cartridge filters used in this study could not be reproducibly sectioned for POC analysis prior to  $^{234}\text{Th}$  measurement. Thus, POC measurements were made on separate GF/F samples taken during  $^{234}\text{Th}$  filtration.

The POC/ $^{234}\text{Th}$  ratio has been found to vary between small ( $> 1 \mu\text{m}$ ) and large ( $> 53 \mu\text{m}$ ) particulate size classes (Buesseler *et al.*, 1995; Bacon *et al.*, 1996; Buesseler *et al.*, 1998). On the one hand, if  $^{234}\text{Th}$  is related to surface area and POC to volume, one would expect an increase in the POC/ $^{234}\text{Th}$  ratio with increasing particle size. On the other hand, the opposite phenomena might be expected if organic carbon is preferentially remineralized relative to particulate  $^{234}\text{Th}$  as larger particles are formed via aggegation or biological processes. In general, size related differences in POC/ $^{234}\text{Th}$  ratios are smaller

within a study area than between different regimes, among seasons and with depth (Buesseler, 1998). Within the upper 10 m, the ratio of POC/<sup>234</sup>Th had a wide range: from 8 to 66  $\mu\text{mol/d.p.m.}$  in March to 14 to 135  $\mu\text{mol/d.p.m.}$  in August (Table 1). Values greater than 135  $\mu\text{mol/d.p.m.}$  in August have large associated errors ( $\pm 100\%$ ) due to very low particulate <sup>234</sup>Th. Seasonal differences in the POC/<sup>234</sup>Th were almost entirely due to changes in the measured particulate <sup>234</sup>Th distribution.

POC export fluxes were determined for the upper 10 m gridded <sup>234</sup>Th April and August data using the results from the steady state 1D and non-steady state multi-dimensional <sup>234</sup>Th flux models (Table 4). In July, 1D SS and multi-dimensional SS <sup>234</sup>Th flux models were compared. POC/<sup>234</sup>Th ratios with errors less than 50% were gridded in the same manner as for <sup>234</sup>Th. POC export fluxes integrated over the upper 10 m are shown in Table 4. Errors are determined from the propagation of uncertainties associated with gridding (similar to <sup>234</sup>Th, see above) and measurement of <sup>234</sup>Th activities and POC/<sup>234</sup>Th ratios.

In April there was no difference among the three models in the calculated POC export, which ranged from 1.7 to 8.6  $\text{mmol C m}^{-2} \text{ day}^{-1}$ . POC export fluxes were similar in July. However, there was a difference between the 1D and the multi-dimensional SS models within the northernmost boxes, where POC export decreased by 50%. August showed the largest differences in the upper 10 m integrated POC export among the three models. While POC export fluxes were the same within error between the 1D SS and the 1D NSS models, inclusion of physical processes decreased the POC export in all four boxes by greater than 50% to between 0 and 19.3  $\text{mmol C m}^{-2} \text{ day}^{-1}$ . As expected, POC export was higher within the inshore boxes than in the offshore boxes during the April, July and August cruises. However, differences were most apparent in April and in August. In August, inshore POC export was almost an order of magnitude greater, whereas in April, POC export was only two times higher than in the offshore boxes.

At station 7, depth profiles of <sup>234</sup>Th enabled 1D NSS (SS for March) estimates of particulate carbon export over the depth of the euphotic zone ( $\sim 50$  m; Table 3).



Increasing the depth interval enables the inclusion of subsurface production, such as indicated by subsurface chl *a* maximums, which generally also results in an increase in  $^{234}\text{Th}$  scavenging. POC/ $^{234}\text{Th}$  ratios generally decrease with depth due to preferential remineralization of particulate organic carbon (Bacon *et al.*, 1996; Buesseler, 1998). As a result, the  $^{234}\text{Th}$  derived particulate carbon export can be very sensitive to the chosen depth of integration. However, in this study, only in July are there obvious gradients in POC/ $^{234}\text{Th}$  ratios with depth (Table 1). As a result, an average POC/ $^{234}\text{Th}$  ratio over the upper 50 m was used to determine POC fluxes. Regardless, only in March was there a significant difference between the 50 m and the 0-50 m average POC/ $^{234}\text{Th}$  ratio, 36 versus 15  $\mu\text{mol d.p.m.}^{-1}$ , respectively.

Particulate carbon export rates, integrated over the upper 50 m, were determined assuming SS in March and July, and NSS in April and August. It should be noted that the steady state assumption is most likely incorrect, given the advent of the spring bloom in March and the substantial decrease in mixed layer depth between April and July. Both processes most likely result in a decrease in  $^{234}\text{Th}$  export, however, the limited data do not allow for an evaluation of the extent of this reduction. POC fluxes were high in March and most likely the result of the spring bloom (Table 3). Similar occurrences have also been seen during the North Atlantic Bloom Experiment and at high latitudes, such as in the Arctic (Cochran *et al.*, 1995;1997). A second large peak in particulate organic carbon export occurred in August. Speciation analyses of plankton tows collected in August indicated that the water column was dominated by a large assemblage of copepods in various stages of their life cycle. Abundances were substantially larger than those found during the July cruise. Thus, the increased particulate export in August was most likely the result of increased zooplankton grazing and mortality within the euphotic zone.

The 50 m integrated POC export estimates given above are considered to be minimum estimates for the southwestern Gulf of Maine. The utilization of 1  $\mu\text{m}$  POC/ $^{234}\text{Th}$  ratios most likely result in an underestimation of particulate organic carbon flux within the Gulf of Maine. Previous measurements of  $^{234}\text{Th}$  on larger particles (>53

$\mu\text{m}$ ) have POC/ $^{234}\text{Th}$  ratios approximately two times higher (M. Charette, unpublished data). In addition, the majority of our determinations were made only within the upper 10 m of the water column. Integrating to deeper depths will further increase the particulate export by including subsurface productivity, such as that associated with the base of the mixed layer during the summer. Nonetheless, our estimates provide a starting point for determining the average particulate organic carbon export rate within the southwestern Gulf of Maine. The integrated 10 m  $^{234}\text{Th}$  derived multi-dimensional NSS (1D SS for March and multi-dimensional SS for July) POC export rate was  $7.0 \pm 2.6 \text{ mmol C m}^{-2} \text{ d}^{-1}$ . Using an annual Gulf of Maine primary production estimate of  $66.2 \text{ mMols C m}^{-2} \text{ d}^{-1}$  (determined by O'Reilly and Busch from 1978-1980) allows one to calculate an average *ThE* ratio of  $0.11 \pm 0.04$ .

Although the effects of advective and diffusive mixing were not determined for our depth profile station (st. 7), it is expected that these processes are significantly smaller in magnitude than that determined for the upper 10 m. Especially since only August showed substantial advective/diffusive effects in all of the inshore and offshore boxes. Furthermore, offshore gradients in  $^{234}\text{Th}$  integrated over the depth of the euphotic zone as well as horizontal current velocities are reduced when compared to that at the surface. Similar results have been found in the Arabian Sea and in the Equatorial Pacific (Buesseler *et al.*, 1995;1998). Current meter readings taken at various depths close to our study site also show an exponential decrease in offshore current speed with increasing water depth (to 50 m; W. R. Geyer, personal communication). Nonetheless, future coastal investigations should include these physical processes.

The average particulate organic carbon NSS (SS for March) export rate averaged over the upper 50 m at station 7 was  $24.7 \pm 8.5 \text{ mmol C m}^{-2} \text{ d}^{-1}$ , over an order of magnitude greater than that found at this station for the upper 10 m alone. This results in an average *ThE* ratio of  $0.37 \pm 0.13$  when compared to basin wide primary production rates (O'Reilly and Busch, 1984). Our results are similar to the 50 m integrated particulate organic carbon export rates of  $21.9 \text{ mmol C m}^{-2} \text{ day}^{-1}$  found previously in the

central Gulf of Maine using  $^{234}\text{Th}$  (Charette *et al.*, 1996). However, our fluxes are substantially higher than the  $3.3 \text{ mmol C m}^{-2} \text{ day}^{-1}$  measured at 150 m using sediment traps during March and April of 1995 (Pilska *et al.*, 1996). Whether this is due to differences in timing, integration depth or difficulties associated with increased hydrodynamic problems found when using conical sediment traps in shallow waters (e.g. Gardner and Walsh, 1990; Buesseler *et al.*, 1994) is unclear. The *ThE* ratio found in the Gulf of Maine is also similar to that found in other productive regimes such as the Arabian Sea during the late SW Monsoon (Table 5). Care must be taken to note the depth of integration when comparing *ThE* ratios from other regimes as increasing the depth of integration generally results in higher export ratios.

Our measurements support the supposition of Townsend (1998) that export ratios are relatively high over the upper 50 m in the southwestern Gulf of Maine. This leads to the next question, however, of how nutrients are made available to support the measured POC export rates. As suggested by Townsend (1998), one such mechanism is water column nitrification within the Gulf of Maine followed by diffusion into surface waters. However, it is not clear whether diffusion alone is large enough to support the required flux of nutrients into the upper waters. One way to further examine this problem would be to investigate the magnitude of vertical eddy diffusivity using  $^7\text{Be}$ .

### ***Vertical Eddy Diffusivity ( $K_z$ )***

Several researchers have demonstrated that  $^7\text{Be}$ , a weakly particle reactive nuclide can be used to estimate vertical eddy diffusivity ( $K_z$ ) (Silker, 1972; Young and Silker, 1974, Lee *et al.*, 1991). This technique proves particularly useful in that  $^7\text{Be}$  integrates the net rate of vertical mixing over several weeks, given its relatively long half-life of 53.3 days. Previous measurements conducted by Silker (1972) and Young and Silker (1974) have found vertical eddy diffusivities on the order of  $0.1$  to  $0.9 \text{ cm}^2 \text{ sec}^{-1}$  at depths of 30-60 m in waters west of California and east of Barbados. In comparison, Lee *et al.* (1991) have found vertical eddy diffusivities to be an order of magnitude greater,  $> 7 \text{ cm}^2 \text{ sec}^{-1}$ , in

nearshore sites off the coast of California. In the Gulf of Maine, a wide range of  $K_z$ 's have been estimated depending on the area and season ( $0.3\text{--}4\text{ cm}^2\text{ sec}^{-1}$ : Townsend, 1992). Methods of determining  $K_z$  within the Gulf are varied and include those derived from empirically based models to extrapolation from areas of similar physical processes (Garside, 1985; Loder and Platt, 1985; Townsend, 1992).

The predominant method for determination of  $K_z$  using  $^7\text{Be}$  is based on the model first described by Silker (1972). Briefly, if the input from rain is constant and the radionuclides are not removed by settling, then the radionuclide concentration as a function of depth can be characterized by:

$$C_2 = C_1 \exp[-z (\lambda/K_z)^{0.5}] \quad (4)$$

where  $C_1$  and  $C_2$  are the measured concentrations at a depth interval,  $z$ , apart,  $\lambda$  is the known decay constant, and  $K_z$  is the coefficient of vertical eddy diffusion. It should be noted that this calculation requires that there be gradients in  $^7\text{Be}$  activities with depth. As a result, vertical eddy diffusivities were determined only for the two summer cruises, July and August, due to an inability to sample below the mixed layer during cruises conducted in the spring.

Measurements of the atmospheric deposition of  $^7\text{Be}$  were made several weeks prior to and during each cruise at Woods Hole, MA (south of the study area:  $41^\circ 32'$  N,  $70^\circ 39'$  W) and Portsmouth, NH (west of the sampling site:  $43^\circ 04'$  N,  $70^\circ 42'$  W) (Benitez-Nelson and Buesseler, 1998). The average flux between the two measurement sites was used to evaluate the seasonal fluctuation in  $^7\text{Be}$  deposition at Wilkinson Basin in the Gulf of Maine. The average  $^7\text{Be}$  flux was remarkably constant prior to and during the July and August cruises. Total expected  $^7\text{Be}$  inventories averaged  $11,640 \pm 118\text{ d.p.m. m}^{-2}$ , matching within error measured  $^7\text{Be}$  inventories of  $11,220 \pm 1930$  and  $11,906 \pm 1890\text{ d.p.m. m}^{-2}$  for July and August, respectively.

Our measurements of  $^7\text{Be}$  in the Gulf of Maine have shown typically less than 10% of the total  $^7\text{Be}$  activity was found on particulate material (Table 1). In addition, although surface measurements of  $^7\text{Be}$  activity increased slightly with increasing distance from shore, there were no clear seasonal trends (Fig. 3). Such temporal patterns would have been expected if a significant fraction of  $^7\text{Be}$  was being removed on settling particulate material (e.g.  $^{234}\text{Th}$ ). Small offshore and alongshore gradients in  $^7\text{Be}$  activity further suggest that horizontal advection and diffusion of  $^7\text{Be}$  is small.

An additional check on the particulate removal of  $^7\text{Be}$  was determined using  $^{234}\text{Th}$ . The flux of  $^7\text{Be}$  out of the upper 50 m can be determined in the same manner as the flux of particulate organic carbon, by multiplying the ratio of  $^7\text{Be}/^{234}\text{Th}$  by the measured steady state export flux of  $^{234}\text{Th}$ . In July,  $^7\text{Be}$  particulate activities were detectable in the upper 37 m only. Thus, only the average  $^7\text{Be}/^{234}\text{Th}$  ratio over the upper 37 m was used. Results indicate that 830 d.p.m.  $\text{m}^{-2}$  of  $^7\text{Be}$ , less than 8% of the expected inventory, is removed on sinking particles. A similar calculation was made for August using the average particulate  $^7\text{Be}/^{234}\text{Th}$  activity ratio over the upper 45 m. In August, the flux of particulate  $^7\text{Be}$  was over three times greater, 2880 d.p.m.  $\text{m}^{-2}$  or 25% of the expected inventory. However, this is most likely a substantial overestimation since the particulate  $^7\text{Be}$  activity in the upper 30 m was below detection and the  $^{234}\text{Th}$  particulate activities extremely low. Our results demonstrate that particulate removal of  $^7\text{Be}$  was minor during July and August.

Using equation (4), a vertical eddy diffusivity of  $1.5 \pm 0.4 \text{ cm}^2 \text{ sec}^{-1}$  was found for July, and  $0.5 \pm 0.2 \text{ cm}^2 \text{ sec}^{-1}$  for August for the flux of dissolved material into the upper 15 m (Figs. 4, 6). Although uncertainties are large,  $^7\text{Be}$  provides a good estimate of vertical eddy diffusivity integrated over the mean life of  $^7\text{Be}$  (76 days). Using this information coupled with vertical profiles of  $\text{NO}_3 + \text{NO}_2$ , it was possible to determine a 'new' nitrogen flux into the upper 10 m of the water column of 1.4 and 0.2  $\text{mmols N m}^{-2} \text{ d}^{-1}$  for July and August, respectively. Assuming a Redfield ratio of 6.6, the flux of new nitrogen was sufficient, within errors, to support the 10 m integrated particulate organic carbon export

flux of  $4.7 \pm 1.5$  mmols and  $1.6 \pm 0.7$  mmols C m<sup>-2</sup> d<sup>-1</sup> which occurred during the July and August cruises (Table 2).

The model, unfortunately, ignores the cycle of mixed layer shoaling and deepening which occurs throughout the seasons. Thus, vertical eddy diffusion rates derived from equation (4) can be substantially overestimated during the spring and early summer (Kadko and Olson, 1998). However, this effect would be expected to be important only for the July cruise, when shoaling of the mixed layer in early May sequesters dissolved <sup>7</sup>Be below the mixed layer. The depth of the mixed layer does not change between the July and August cruises (Fig. 4). Given the low calculated K<sub>z</sub> values and the time interval between the development of the summer mixed layer and subsequent <sup>7</sup>Be measurement, it would appear that the effect of mixed layer shoaling was small.

Our measurements of vertical eddy diffusivity are similar to the estimates of 0.3 cm<sup>2</sup> sec<sup>-1</sup> found previously in Wilkinson Basin during the stratified summer and are well within the range of the 0.1 to 7 cm<sup>2</sup> sec<sup>-1</sup> found in other areas of the Gulf of Maine and in different coastal regimes (e.g. Townsend, 1992; Lee *et al.*, 1991). It should be noted that the previous vertical eddy diffusivity estimates found for Wilkinson Basin were determined in a completely different manner, by using an empirical relationship based on temperature (e.g. Devol and King, 1979). In contrast, our estimates of the 'new' nitrogen flux into the upper 10 m are over 50% less than those determined by Townsend (1992). The discrepancy is most likely due to differences in the chosen depth interval of interest as well as real differences between NO<sub>3</sub> + NO<sub>2</sub> profiles. Nonetheless, our measurements of vertical eddy diffusivity provide additional evidence that upward diffusion of nitrogen is adequate to support the measured organic carbon export from the upper 10 m in central Wilkinson Basin.

## CONCLUSION

Our measurements provide some of the first direct estimates of particulate organic carbon export in the southwestern Gulf of Maine. Carbon export rates varied both seasonally and spatially. Fluxes were largest nearshore and decreased with increasing distance from land, indicating the importance of the coast on  $^{234}\text{Th}$  activity distributions. In March, high particulate export occurred during the spring phytoplankton bloom, whereas high rates in August were most likely the result of zooplankton grazing and mortality. The average annual export ranged between 7.0 and 24.7 mmol C m<sup>-2</sup> d<sup>-1</sup>, depending on the depth of integration. The average export ratio, based on primary productivity measurements of O'Reilly and Busch (1984), ranged between 0.11 and 0.37, similar to that found in many coastal environments. Accurate determinations of  $^{234}\text{Th}$  derived particulate export, however, necessitated the inclusion of both non-steady state and horizontal mixing. Omission of these processes generally resulted in substantial under predictions of particulate organic carbon export. Our study provides additional support for the incorporation of such processes in modelling  $^{234}\text{Th}$  in coastal regimes.

In contrast to  $^{234}\text{Th}$ , our measurements of the weakly particle reactive radionuclide  $^7\text{Be}$ , showed no seasonality in its distribution and only minor offshore gradients in activity. Vertical eddy diffusion rates into the upper 15 m of the water column were 1.5 and 0.5 cm<sup>2</sup> sec<sup>-1</sup>. These estimates coupled with NO<sub>3</sub>+NO<sub>2</sub> profiles suggest that the transport of 'new' nitrogen into surface waters was sufficient to support the export flux of particulate organic carbon. Thus, as initially suggested by Townsend (1998), nitrification followed by upwards diffusion is a viable mechanism by which high organic carbon export rates can be maintained.

**ACKNOWLEDGEMENTS**

The authors wish to thank J. E. Andrews, L. A. Ball, C. Tarr, R. Belastock and the crew of the R/V *Cape Hatteras* for their help in sample collection and B. Benitez-Nelson and Drs. D. Glover and W. Jenkins for comments pertaining to the manuscript. In addition, we wish to thank J. MacFarlane for the map of the Gulf of Maine. This work was supported by the STAR Environmental Protection Agency Fellowship Program, the Office of Naval Research Fellowship Program and the National Science Foundation (Grant OCE-9633240). This is contribution 9777 from the Woods Hole Oceanographic Institution.



## REFERENCES

- Barrick, R. C and F. G. Prahl, (1987) Hydrocarbon geochemistry of the Puget Sound Region-III. Polycyclic aromatic hydrocarbons in sediments. *Estuarine Coastal and Shelf Science*, **25**, 175-191.
- Bacon, M. P., C.-A. Huh, A. P. Fleer and W. G. Deuser, (1985) Seasonality in the flux of natural radionuclides and Plutonium in the deep sea. *Deep-Sea Research I*, **32**, 273-286.
- Bacon, M. P., J. K. Cochran, D. Hirschberg, T. R. Hammar and A. P. Fleer (1996) Export flux of carbon at the equator during the EqPac. time-series cruises estimated from  $^{234}\text{Th}$  measurements. *Deep-Sea Research II*, **43**, 1133-1154.
- Benitez-Nelson, C. R. and K. O. Buesseler, (1998)  $^{32}\text{P}$ ,  $^{33}\text{P}$ ,  $^7\text{Be}$ , and  $^{210}\text{Pb}$ : Atmospheric fluxes and utility in tracing Stratosphere/Troposphere exchange. *Journal of Geophysical Research*, submitted.
- Brooks, D. A., (1985) Vernal circulation in the Gulf of Maine. *Journal of Geophysical Research*, **90**, 4687-4705.
- Brooks, D. A., (1991) A brief overview of the physical oceanography of the Gulf of Maine. In: *Proceedings of the Gulf Of Maine Scientific Workshop, Woods Hole*, T. Wigen and C. N. K. Mooers, Eds., pp. 51-74.
- Buesseler, K. O., (1998) The decoupling of production and particle export in the surface ocean. *Glob. Biogeochem. Cycles*, **12**, 297-310.
- Buesseler, K. O., M. P. Bacon, J. K. Cochran and H. D. Livingston, (1992a) Carbon and nitrogen export during the JGOFS North Atlantic Bloom Experiment estimated from  $^{234}\text{Th}$ - $^{238}\text{U}$  disequilibria. *Deep-Sea Research*, **39**, 1115-1137.
- Buesseler, K. O., J. K. Cochran, M. P. Bacon, H. D. Livingston, S. A. Casso, D. Hirschberg, M. C. Hartman and A. P. Fleer (1992b) Determination of thorium isotopes in seawater by non-destructive and radiochemical procedures. *Deep-Sea Research*, **39**, 1103-1114.
- Buesseler, K. O., A. F. Michaels, D. A. Seigel and A. H. Knap (1994) A three-dimensional time-dependent approach to calibrating sediment trap fluxes. *Global Biogeochemical Cycles*, **8**, 179-193.
- Buesseler, K. O., J. A. Andrews, M. C. Hartman, R. Belostock and F. Chai, (1995) Regional estimates of the export flux of particulate organic carbon derived from thorium-234 during the JGOFS EQPAC program. *Deep-Sea Research II*, **42**, 777-804.
- Buesseler, K. O., L. Ball, J. Andrews, C. Benitez-Nelson, C., R. Belostock, F. Chai and Y. Chao, (1998) Upper ocean export of particulate organic carbon in the Arabian Sea derived from Thorium-234. *Deep-Sea Research II, Special Arabian Sea Issue*, accepted.

- Campbell, D. E., (1986) Process variability in the Gulf of Maine - a macroestuarine environment. In: *Estuarine Variability*, D. A. Wolfe, Ed., Academic Press., pp. 261-275.
- Charette, M. A., S. B. Moran and C. H. Pilskaln (1996) Particulate organic carbon export fluxes in the central Gulf of Maine estimated from  $^{234}\text{Th}/^{238}\text{U}$  disequilibria. Poster presented at the Gulf of Maine Ecosystem Dynamics: A Scientific Symposium and Workshop, St. Andrews, NB, September, 1996.
- Chen, J. H., R. L. Edwards and G. J. Wasserburg, (1986)  $^{238}\text{U}$ ,  $^{234}\text{U}$  and  $^{232}\text{Th}$  in seawater. *Earth and Planetary Science Letters*, **80**, 241-251.
- Christensen, J. P., D. B. Smith and L. M. Mayer, (1991) The nitrogen budget of the Gulf of Maine and climate change. In: *Proceedings of the Gulf Of Maine Scientific Workshop, Woods Hole*, T. Wiggen and C. N. K. Mooers, Eds., p. 75-90.
- Coale, K. H. and K. W. Bruland, (1985)  $^{234}\text{Th}$ . $^{238}\text{U}$  disequilibria within the California current. *Limnology and Oceanography*, **30**, 22-33.
- Coale, K. H. and K. W. Bruland, (1987) Ocean stratified euphotic zone as elucidated by  $^{234}\text{Th}$ . $^{238}\text{U}$  disequilibria. *Limnology and Oceanography*, **32**, 189-200.
- Cochran, J. K., C. Barnes, and D. Achman, (1995) Thorium-234/Uranium-238 disequilibrium as an indicator of scavenging rates and particulate organic carbon fluxes in the northeast polynya, Grrenland. *Journal of Geophysical Research*, **100**, 4399-4410.
- Cochran, J. K., K. A. Roberts, C. Barnes, and D. Achman, (1997) Radionuclides as indicators of particle and carbon dynamics on the East Greenland Shelf, in *Radioprotection-colloques*, **32(C2)**, *Proceedings of RADOX 96-97 "Radionuclides in the Oceans,"* edited by P. Germain, et al., pp. 129-136, Institut de Protection et de Surete nucleaire, Cherbourg, France.
- Cowie, G. L. and J. I. Hedges (1984) Organic carbon and nitrogen geochemistry of Black Sea surface sediments from stations spanning the oxic:anoxic boundary. In: *Black Sea Oceanography*, E. Izdar and J. W. Murrad, eds., NATO ASI Series, Kluwer, pp 343-359.
- Downs, J. N. (1989) Export of production in oceanic systems: Information from phaeopigment, carbon and nitrogen analyses, Ph.D. thesis, University of Washington, Seattle.
- Dugdale, R. C. and J. J. Goering, (1967) Uptake of new and regenerated forms of nitrogen in primary productivity. *Limnology and Oceanography*, **12**, 196-206.
- Dymond, J. and R. Collier, (1989) *U.S. JGOFS Planning Report*, **10**, 84-85.
- Eppley, R. W. and B. J. Peterson, (1978) Particulate organic matter flux and planktonic new production in the deep ocean. *Nature*, **282**, 677-680.
- Gardner, W. D. and I. D. Walsh (1990) Distribution of macroaggregates and fine-grained particles across a continental margin and their potential role in fluxes. *Deep Sea Research II*, **42**, 365-386, 1995.

- Garside, C., (1985) The vertical distribution of nitrate in open ocean surface water. *Deep Sea Research*, **32**, 723-732.
- Gottlieb, E. S. and D. A. Brooks, (1986) Current meter and atmospheric data from the Gulf of Maine: 1982-1985. *Tech. Rept. 86-3-T*, Texas A&M University, 80 pp.
- Gunderson, K., A. Michaels, and N. Bates (1993) Determination of particulate organic carbon and nitrogen. In: *Bats Method Manual, Version 3*. Bermuda Biological Station for Research, Inc., Bermuda, 108 pp.
- Gustafsson, Ö., K. O. Buesseler, W. R. Geyer, S. B. Moran, and P.M. Gschwend, (1998) An assessment of the relative importance of horizontal and vertical transport of particle-reactive chemicals in the coastal ocean: Two-dimensional Th-234 modeling. *Journal of Marine Research*, accepted.
- Hedges, J. I and J. H. Stern (1984) Carbon and nitrogen determinations of carbonate-containing solids. *Limnological Oceanography*, **29**, 657-663.
- Kadko, D. and D. Olson, (1996) Be-7 as a tracer of surface water subduction and mixed layer history. *Deep-Sea Research I*, **43**, 89-116.
- Kaufman, A., Y.-H. Li and K. K. Turekian, (1981) The removal rates of  $^{234}\text{Th}$  and  $^{228}\text{Th}$  from waters of the New York Bight. *Earth and Planetary Science Letters*, **54**, 385-392.
- Kennicutt II, M. C., T. R. Wade, B. J. Presley, A. G. Requejo, J. M. Brooks and G. J. Denoux, (1994) Sediment contaminants in Casco Bay, Maine: Inventories, sources, and potential for biological impact. *Environmental Science Technology*, **28**, 1-15.
- Jochem, F. J., S. Mathot, and B. Queginer, (1995) Size fractionated primary production in the open Southern Ocean during the austral spring. *Polar Biology*, **15**, 381-392.
- Larsen, P.F., D. F. Gadbois and A. C. Johnson, (1985) Observations on the distribution of PCBs in the deep water sediments of the Gulf of Maine. *Marine Pollution Bulletin*, **16**, 439-442.
- Lee, T, Barg, E. and D. Lal, (1991) Studies of vertical mixing in the Southern California Bight with cosmogenic radionuclides  $^{32}\text{P}$  and  $^7\text{Be}$ . *Limnology and Oceanography*, **36**, 1044-1053 (1991).
- Loder, J. W. and T. Platt, (1985) Physical controls on phytoplankton production at tidal fronts. In: *Proceedings of the Nineteenth European Marine Biology Symposium*, P. E. Gibbs, ed., Cambridge Univ. Press, 541 pp.
- Luo, S., Ku, T.-L., M. Kusakabe, J. K. B. Bishop and Y.-L. Yang, (1995) Tracing particle cycling in the upper ocean with  $^{230}\text{Th}$  and  $^{228}\text{Th}$ - An investigation in the equatorial Pacific along  $140^\circ\text{W}$ . *Deep-Sea Research*, **42**, 805-829.
- McKee, B. A., D. J. DeMaster and C. A. Nittrouer, (1984) The use of  $^{234}\text{Th}/^{238}\text{U}$  disequilibrium to examine the fate of particle-reactive species on the Yangtze continental shelf. *Earth and Planetary Science Letters*, **68**, 431-442.
- Meise, C. J. and J. E. O'Reilly, (1996) Spatial and seasonal patterns in abundance and age-composition of *Calanus finmarchicus* in the Gulf of Maine and on Georges Bank: 1977-1987. *Deep-Sea Research II*, **43**, 1473-1501.

- Moran, S.B. and K.O. Buesseler, (1993) Size-Fractionated  $^{234}\text{Th}$  in Continental Shelf Waters off New England: Implications for the Role of Colloids in Oceanic Trace Metal Scavenging. *Journal of Marine Research*, **51**, 893-922.
- Murray, J. W., J. N. Downs, S. Strom, C.-L. Wei and H. W. Jannasch, (1989) Nutrient assimilation, export production and  $^{234}\text{Th}$  scavenging in the eastern equatorial Pacific. *Deep-Sea Research I*, **36**, 1471-1489.
- Naimie, C., (1996) Georges Bank residual circulation during weak and strong stratification periods: prognostic numerical model results. *Journal of Geophysical Research*, **101**, 6469-6486.
- Okubo, A., (1971) Oceanic diffusion diagrams. *Deep-Sea Research*, **18**, 789-802.
- O'Reilly, J. E. and D. A. Busch, (1984) Phytoplankton primary production on the northwestern Atlantic Shelf. *Rapport P.-v. Reun. Cons. Int. Explor. Mer.*, **183**, 255-268.
- Peltzer, E. T. and N. A. Hayward (1996) Spatial and temporal variability of total organic carbon along  $140^\circ\text{W}$  in the equatorial Pacific Ocean in 1992. *Deep-Sea Research II*, **43**, 155-1180.
- Pilskaln, C. H., W. Arnold, C. Lehmann and L. E. Watling (1996) Particulate flux dynamics in Jordan and Wilkinson Basins: Seasonal POC export and particle resuspension. Poster presented at the Gulf of Maine Ecosystem Dynamics: A Scientific Symposium and Workshop, St. Andrews, NB, September, 1996.
- Pollard, C., G. Battisto, E. Keese and B. J. Rutan (1996) Analytical service center procedure summaries. Virginia Institute of Marine Science/School of Marine Science, College of William and Mary, Gloucester Point, VA, February, 1996, 35 pp.
- Rutgers van der Loeff, M. M., J. Friedrich and U. V. Bathmann (1997) Carbon export during the spring bloom at the southern polar front determined with the natural tracer  $^{234}\text{Th}$ . *Deep Sea Research II*, **44**, 457-478.
- Santchi, P. H., Y.-H. Li., and J Bell, (1979) Natural radionuclides in the water of Narragansett Bay. *Earth and Planetary Science Letters*, **45**, 201-213.
- Schlitz, R. J. and E. B. Cohen, (1984) A nitrogen budget for the Gulf of Maine and Georges Bank. *Biology Oceanography*, **3**, 203-221.
- Shimmield, G. B. and G. R. Ritchie (1995) The impact of marginal ice zone processes on the distribution of  $^{210}\text{Pb}$ ,  $^{210}\text{Po}$  and  $^{234}\text{Th}$  and implications for new production in the Bellingshausen Sea, Antarctica. *Deep Sea-Research II*, **42**, 1313-1335.
- Silker, W. B., (1972) Horizontal and vertical distributions of radionuclides in the north Pacific Ocean. *Journal of Geophysical Research*, **77**, 1061-1070.
- Tanaka, N., Y. Takeda and S. Tsunogai, (1983) Biological effect on removal of Th-234, Po-210 and Pb-210 from surface water in Funaka Bay, Japan. *Geochimica et Cosmochimica Acta.*, **47**, 1783-1790.
- Thunell, R. C., W. S. Moore, J. Dymond and C. Pilskain, (1994) Elemental and isotopic fluxes in the Southern California Bight: A time-series sediment trap study in the San Pedro Basin. *Journal of Geophysical Research*, **99**, 875-889.

- Townsend, D. W., (1991) Influences of oceanographic processes on the biological productivity of the Gulf of Maine. *Review of Aquatic Sciences*, **4**, 1-20.
- Townsend, D. W., (1992) An overview of oceanography and biological productivity in the Gulf of Maine. *The Gulf of Maine, NOAA Coastal Ocean Program Regional Synthesis Series*, **1**, 5-26.
- Townsend, D. W., (1998) Sources and cycling of nitrogen in the Gulf of Maine. *Journal of Marine Systems*, accepted.
- Townsend, D. W. and R. W. Spinrad (1986) Early spring phytoplankton blooms in the Gulf of Maine. *Continental Shelf Research*, **6**, 515-529.
- Vermersch, J. A., R. C. Beardsley, W. S. Brown, (1979) Winter circulation in the Western Gulf of Maine: Part 2. Current and pressure Observations. *Journal of Physical Oceanography*, **9**, 768-784.
- Walsh, J. J., T. E. Whitley, J. E. O'Reilly, W. C. Phoel, and A. E. Draxler (1987) Nitrogen cycling on Georges Bank and the New York Shelf: comparison between well-mixed and seasonally stratified waters. In: *Georges Bank*. (ed. Backus, R. H.), 234-246 (MIT Press, Cambridge, 1987).
- Wageman, R. and D. C. G. Muir, (1994) Concentrations of heavy metals and organochlorides in marine mammals of northern waters: Overview and evaluation. *Canadian Technical Report Fisheries Aquatic Science*, No. 1279, pp. 97.
- Wei, C.-L. and J. W. Murray, (1992) Temporal variations of  $^{234}\text{Th}$  activity in the water column of Dabob Bay: Particle scavenging. *Limnology and Oceanography*, **37**, 296-314.
- U.S. JGOFS Planning Report 11, (1990) U.S. Joint Global Ocean Flux Study Long Range Plan, The Role of Biogeochemical Cycles in Climate Change, U.S. JGOFS Steering Committee. U.S. JGOFS Planning office, Woods Hole, MA, 216 pp.
- Young, J. A. and W. B. Silker, (1974) The determination of air-sea exchange and oceanic mixing rates using  $^7\text{Be}$  during the bomex experiment. *Journal of Geophysical Research*, **79**, 4481-4489.
- Zapata, M., A. M. Ayala, J. M. Franco, J. L. Garrido (1987) Separation of chlorophylls and their degradation products in marine phytoplankton by reversed-phase high performance liquid chromatography. *Chromatographia*, **23**, 26-30.

**Table 5.1** Radionuclide data from samples collected in the southwestern Gulf of Maine. All data, with the exception of station 7 depth profiles, were collected at 5 m. Error bars are  $1\sigma$ . B.D. = Below Detection.

Station	Lat. (N)	Long. (W)	Part. $^7\text{Be}$ (d.p.m. $\text{m}^{-3}$ )	Diss. $^7\text{Be}$ (d.p.m. $\text{m}^{-3}$ )	Part. $^{234}\text{Th}$ (d.p.m. $\text{L}^{-1}$ )	Diss. $^{234}\text{Th}$ (d.p.m. $\text{L}^{-1}$ )	POC/ $^{234}\text{Th}$ ( $\mu\text{mols d.p.m.}^{-1}$ )
<i>Mar., 1997</i>							
1	42°30.0	70°29.9	7.8 ± 8.4	373 ± 28	0.24 ± 0.01	0.40 ± 0.01	67 ± 6
2	42°40.2	70°22.1	3.8 ± 7.5	109 ± 2	0.34 ± 0.01	0.49 ± 0.01	32 ± 4
3	42°51.0	70°29.8	9.6 ± 7.0	199 ± 18	0.36 ± 0.02	0.52 ± 0.01	24 ± 4
4	43°00.0	70°24.4	4.3 ± 8.7	86 ± 15	0.27 ± 0.01	0.65 ± 0.02	45 ± 5
5	42°59.7	70°12.0	4.7 ± 4.4	200 ± 22	0.49 ± 0.02	0.58 ± 0.02	22 ± 3
6	42°53.1	70°09.2	6.6 ± 9.2	247 ± 19	0.39 ± 0.01	0.61 ± 0.02	22 ± 3
7, 5 m	42°29.1	69°43.7	21.2 ± 12.6	174 ± 21	0.75 ± 0.02	0.73 ± 0.02	7 ± 2
20 m			B.D.	152 ± 16	0.44 ± 0.01	0.68 ± 0.02	7 ± 1
35 m			B.D.	93 ± 20	0.61 ± 0.02	0.79 ± 0.02	9 ± 1
50 m			0.7 ± 6.4	132 ± 13	0.25 ± 0.01	0.58 ± 0.01	36 ± 5
72 m			6.9 ± 17.7	133 ± 7	0.53 ± 0.01	0.81 ± 0.02	12 ± 2
8	42°46.0	70°18.2	6.6 ± 9.9	218 ± 22	0.35 ± 0.01	0.61 ± 0.02	22 ± 4
9	42°35.9	70°12.1	14.5 ± 19.2	171 ± 16	0.36 ± 0.01	0.67 ± 0.02	14 ± 4

**Table 5.1 Continued.**

Station	Lat. (N)	Long. (W)	Part. <sup>7</sup> Be (d.p.m. m <sup>-3</sup> )	Diss. <sup>7</sup> Be (d.p.m. m <sup>-3</sup> )	Part. <sup>234</sup> Th (d.p.m. L <sup>-1</sup> )	Diss. <sup>234</sup> Th (d.p.m. L <sup>-1</sup> )	POC/ <sup>234</sup> Th (μmols d.p.m. <sup>-1</sup> )
<i>April, 1997</i>							
1	42°46.0	69°43.5	19.4 7.1	268 ± 12	0.41 ± 0.02	1.11 ± 0.03	61 ± 4
2	42°47.2	69°57.3	16.3 5.5	495 ± 22	0.49 ± 0.02	1.17 ± 0.03	17 ± 3
3	43°01.0	69°44.8	16.2 7.1	341 ± 20	0.47 ± 0.02	0.95 ± 0.03	38 ± 3
4	43°15.0	69°50.0	21.2 6.5	326 ± 20	0.48 ± 0.02	1.11 ± 0.03	17 ± 3
5	42°59.8	70°12.1	26.5 8.0	307 ± 18	0.40 ± 0.02	0.62 ± 0.02	29 ± 3
6	42°60.0	70°24.5	23.3 6.8	305 ± 15	0.29 ± 0.02	0.71 ± 0.02	39 ± 5
7, 5 m	42°29.9	69°45.1	5.1 4.9	222 ± 17	0.49 ± 0.04	1.27 ± 0.03	15 ± 3
30 m			B.D.	343 ± 30	0.45 ± 0.04	1.09 ± 0.03	17 ± 3
60 m			B.D.	320 ± 25	0.45 ± 0.03	1.13 ± 0.03	21 ± 3
90 m			30.5 ± 27.7	273 ± 19	0.12 ± 0.05	1.26 ± 0.04	55 ± 24
111 m			8.2 ± 7.3	238 ± 11	0.45 ± 0.15	1.57 ± 0.05	12 ± 5
8	42°50.6	70°29.7	23.8 ± 13.5	327 ± 30	0.34 ± 0.05	0.92 ± 0.03	32 ± 6
9	42°46.1	70°18.4	7.5 ± 17.6	210 ± 29	0.27 ± 0.04	0.92 ± 0.02	51 ± 10
10	42°35.8	70°12.0	15.0 ± 2.1	258 ± 20	0.27 ± 0.04	0.80 ± 0.02	36 ± 7
11	42°24.9	70°47.9	80.9 ± 20.0	214 ± 9	0.19 ± 0.05	0.43 ± 0.01	126 ± 32
12	42°20.7	70°23.6	B.D.	180 ± 30	0.43 ± 0.08	0.57 ± 0.01	40 ± 8
13	42°20.1	69°57.0	31.5 ± 18.8	341 ± 25	0.65 ± 0.07	2.09 ± 0.04	67 ± 7

**Table 5.1 Continued**

Station	Lat. (N)	Long. (W)	Part. <sup>7</sup> Be (d.p.m. m <sup>-3</sup> )	Diss. <sup>7</sup> Be (d.p.m. m <sup>-3</sup> )	Part. <sup>234</sup> Th (d.p.m. L <sup>-1</sup> )	Diss. <sup>234</sup> Th (d.p.m. L <sup>-1</sup> )	POC/ <sup>234</sup> Th (μmols d.p.m. <sup>-1</sup> )
<i>July, 1997</i>							
1	42°44.8	69°42.5	3.9 ± 9.4	478 ± 31	0.49 0.02	1.15 ± 0.03	18 ± 3
2	42°46.9	69°57.2	B.D.	245 ± 19	0.30 0.02	1.20 ± 0.03	26 ± 5
3	43°15.0	69°49.9	16.2 ± 11.7	413 ± 29	0.30 0.02	0.72 ± 0.02	42 ± 5
4	43°09.0	70°00.5	6.3 ± 5.6	390 ± 19	0.16 0.01	0.36 ± 0.01	75 ± 10
5	43°00.1	70°24.4	B.D.	600 ± 22	0.19 0.02	0.54 ± 0.01	32 ± 8
6	42°28.7	69°44.1	B.D.	479 ± 24	0.22 0.01	0.91 ± 0.02	36 ± 6
7, 5 m	42°29.1	69°44.1	5.8 ± 16.3	370 ± 5	0.30 0.06	1.14 ± 0.04	23 ± 6
15 m			12.7 ± 7.6	184 ± 16	0.51 0.04	1.17 ± 0.03	11 ± 3
37 m			7.2 ± 3.4	92 ± 21	0.55 0.04	1.26 ± 0.04	18 ± 3
50 m			B.D.	119 ± 20	0.92 0.05	0.85 ± 0.03	6 ± 1
65 m			B.D.	125 ± 16	1.29 0.05	0.99 ± 0.03	3 ± 1
8	42°50.9	70°29.9	B.D.	340 ± 24	0.23 0.03	0.83 ± 0.02	48 ± 8
9	42°45.8	70°17.8	1.8 ± 5.4	226 ± 20	0.26 0.02	0.90 ± 0.02	24 ± 5
10	42°36.0	70°12.0	31.6 ± 21.2	504 ± 23	0.41 0.04	0.95 ± 0.02	35 ± 5
11	42°33.9	70°30.1	10.7 ± 7.4	146 ± 19	0.36 0.03	0.76 ± 0.02	30 ± 4
12	42°25.7	70°44.9	9.6 ± 8.8	205 ± 22	0.50 0.04	0.35 ± 0.01	47 ± 4
13	42°10.5	70°23.6	B.D.	212 ± 23	0.44 0.07	0.70 ± 0.02	28 ± 6



**Table 5.1 Continued**

Station	Lat. (N)	Long. (W)	Part. <sup>7</sup> Be (d.p.m. m <sup>-3</sup> )	Diss. <sup>7</sup> Be (d.p.m. m <sup>-3</sup> )	Part. <sup>234</sup> Th (d.p.m. L <sup>-1</sup> )	Diss. <sup>234</sup> Th (d.p.m. L <sup>-1</sup> )	POC/ <sup>234</sup> Th (μmols d.p.m. <sup>-1</sup> )
<i>Aug., 1997</i>							
1	42°44.5	69°42.2	B.D.	436 ± 46	0.15 ± 0.04	0.80 ± 0.02	117 ± 16
2	42°47.0	69°57.0	B.D.	627 ± 51	0.40 ± 0.02	1.03 ± 0.03	20 ± 10
3	43°01.0	69°43.9	2.1 ± 4.6	541 ± 81	0.07 ± 0.03	1.54 ± 0.04	134 ± 44
4	43°15.0	69°50.1	B.D.	145 ± 45	0.13 ± 0.02	0.80 ± 0.02	139 ± 258
5	43°09.2	70°05.2	B.D.	243 ± 52	0.05 ± 0.02	0.46 ± 0.01	210 ± 91
6	42°60.0	70°24.5	B.D.	361 ± 54	0.02 ± 0.02	0.54 ± 0.01	623 ± 783
7, 5 m	42°29.5	69°42.8	B.D.	379 ± 49	0.35 ± 0.11	1.32 ± 0.03	24 ± 4
15 m			B.D.	433 ± 71	0.22 ± 0.06	1.35 ± 0.04	39 ± 17
30 m			B.D.	191 ± 63	0.11 ± 0.05	1.08 ± 0.03	95 ± 50
45 m			11.5 ± 3.5	14 ± 12	0.07 ± 0.03	1.24 ± 0.04	57 ± 25
60 m			11.3 ± 3.9	9 ± 9	0.01 ± 0.01	1.23 ± 0.04	658 ± 980
8	42°51.0	70°30.0	B.D.	393 ± 67	0.03 ± 0.04	0.63 ± 0.02	449 ± 615
9	42°46.1	70°18.0	6.8 ± 4.4	496 ± 55	0.04 ± 0.03	0.82 ± 0.03	270 ± 193
10	42°36.0	70°12.3	10.2 ± 6.7	342 ± 51	0.37 ± 0.09	0.80 ± 0.02	32 ± 8
11	42°30.0	70°30.0	B.D.	232 ± 50	0.09 ± 0.02	0.59 ± 0.02	135 ± 31
12	42°25.1	70°47.9	13.4 ± 2.8	451 ± 88	0.23 ± 0.01	0.29 ± 0.01	67 ± 6
13	42°10.6	70°23.3	B.D.	142 ± 27	0.95 ± 0.27	0.43 ± 0.02	14 ± 4

**Table 5.2** Steady state and non-steady state surface model results. Error bars are 1 $\sigma$ .

Station	SS Particulate Export at 10m (d.p.m. m <sup>-2</sup> day <sup>-1</sup> )	NSS Particulate Export at 10m (d.p.m. m <sup>-2</sup> day <sup>-1</sup> )
<b>March</b>		
1	444 ± 13	--
2	397 ± 12	--
3	391 ± 12	--
4	372 ± 11	--
5	330 ± 10	--
6	351 ± 11	--
7	215 ± 4	--
8	362 ± 11	--
9	341 ± 10	--
<b>April</b>		
1	202 ± 9	24 ± 1
2	161 ± 7	--
3	228 ± 10	126 ± 6
4	180 ± 8	--
5	339 ± 16	314 ± 15
6	341 ± 18	285 ± 15
7	136 ± 12	31 ± 1
8	268 ± 38	59 ± 8
9	293 ± 48	174 ± 29
10	327 ± 45	301 ± 41
11	446 ± 110	476 ± 118
12	336 ± 64	262 ± 50
13	-151 ± 15	--

Table 5.2 Continued

Station	SS Particulate Export at 10m (d.p.m. m <sup>-2</sup> day <sup>-1</sup> )	NSS Particulate Export at 10m (d.p.m. m <sup>-2</sup> day <sup>-1</sup> )
<b>July</b>		
1	147 ± 7	--
2	191 ± 11	--
3	321 ± 21	--
4	465 ± 39	--
5	406 ± 43	--
6	289 ± 15	--
7	206 ± 38	--
8	313 ± 37	--
9	285 ± 28	--
10	226 ± 24	--
11	294 ± 26	--
12	372 ± 26	--
13	286 ± 48	--
<b>August</b>		
1	352 ± 18	547 ± 27
2	213 ± 28	233 ± 31
3	161 ± 5	--
4	357 ± 93	216 ± 56
5	469 ± 21	542 ± 24
6	457 ± 21	651 ± 30
7	144 ± 10	67 ± 5
8	428 ± 27	558 ± 36
9	376 ± 16	477 ± 20
10	283 ± 22	345 ± 27
11	420 ± 16	565 ± 22
12	465 ± 10	578 ± 12
13	216 ± 42	139 ± 27

**Table 3.** Depth integrated steady state and non-steady state model results. Particulate organic carbon export rates from the upper 50 m were obtained for the April and August cruises by multiplying the non-steady state  $^{234}\text{Th}$  particulate flux by the ratio of  $\text{POC}/^{234}\text{Th}$  at ~50 m (from Table 1). In March and July, particulate organic carbon fluxes were determined using the steady state model only. Error bars are  $1\sigma$ .

Cruise	SS Particulate Export at 50m (d.p.m. $\text{m}^{-2} \text{day}^{-1}$ )	NSS Particulate Export at 50m (d.p.m. $\text{m}^{-2} \text{day}^{-1}$ )	POC Export at 50m ( $\text{mmol m}^{-2} \text{day}^{-1}$ )
<i>March, Station 7</i>	$1460 \pm 4$	--	$22 \pm 2$
<i>April, Station 7</i>	$821 \pm 12$	$17.5 \pm 0.2$	$0.3 \pm 0.03$
<i>July, Station 7</i>	$574 \pm 38$	--	$8.3 \pm 1$
<i>August, Station 7</i>	$1141 \pm 10$	$1689 \pm 117$	$68 \pm 20$

**Table 4.** Steady state, non-steady state, and advection/diffusion model results. <sup>234</sup>Th derived POC export rates were determined over the upper 10 m only.

Box	SS Particulate Export at 10m (d.p.m. m <sup>-2</sup> day <sup>-1</sup> )	SS POC Export at 10m (mmol m <sup>-2</sup> day <sup>-1</sup> )	NSS Particulate Export at 10m (d.p.m. m <sup>-2</sup> day <sup>-1</sup> )	NSS POC Export at 10m (mmol m <sup>-2</sup> day <sup>-1</sup> )	NSS + Adv./Diff. At 10 m (d.p.m. m <sup>-2</sup> day <sup>-1</sup> )	NSS+ Adv./Diff. POC Export at 10m (mmol m <sup>-2</sup> day <sup>-1</sup> )
<i>April</i> , 1	295 ± 33	7.7 ± 1.2	246 ± 39	6.4 ± 1.3	227 ± 51	5.9 ± 1.5
2	216 ± 29	4.4 ± 0.9	143 ± 23	2.9 ± 0.6	83 ± 19	1.7 ± 0.5
3	303 ± 32	9.4 ± 1.6	264 ± 44	8.2 ± 1.7	276 ± 62	8.6 ± 2.2
4	212 ± 30	7.0 ± 1.3	167 ± 37	5.5 ± 1.4	113 ± 35	3.7 ± 1.2
<i>July</i> , 1	290 ± 28	11 ± 2	--		144 ± 40	5.3 ± 1.8
2	262 ± 32	7.1 ± 1.8	--		73 ± 45	2.0 ± 1.3
3	269 ± 30	8.3 ± 1.6	--		209 ± 42	6.4 ± 1.7
4	199 ± 29	5.7 ± 1.5	--		146 ± 41	4.2 ± 1.5
<i>August</i> , 1	419 ± 48	48 ± 16	568 ± 75	66 ± 22	166 ± 62	19 ± 7
2	305 ± 40	18 ± 7	355 ± 33	21 ± 7	36 ± 32	2.1 ± 1.2
3	364 ± 26	35 ± 12	475 ± 32	46 ± 16	106 ± 22	10 ± 4
4	211 ± 24	3.2 ± 1.3	224 ± 67	3.4 ± 1.7	-51 ± 42	--

**Table 5.** Comparison of *ThE* ratios found in the Gulf of Maine with those of other regimes.

Site	<sup>234</sup> Th derived POC Flux (mmol C m <sup>-2</sup> day <sup>-1</sup> )	Primary Production (mmol C m <sup>-2</sup> day <sup>-1</sup> )	<i>ThE</i> Ratio, %	References
<i>Arabian Sea 0-100 m; 1995</i>				
NE Monsoon	1 - 7	50 - 120	1 -6	Buesseler <i>et al.</i> , 1998
Spring Intermonsoon	1 - 6	65 - 100	1 -9	
Mid SW Monsoon	2 - 17	15 - 130	1 - 10	
Late SW Monsoon	11 -26	50 - 145	17 -27	
<i>Weddell Sea/Polar Front 0-100 m; 1992</i>				
Polar Front - Fall bloom	29	110	26	Jochem <i>et al.</i> , 1995
Marginal Ice Zone - Fall bloom	4-26	25	16-100	Rutgers van der Loeff <i>et al.</i> , 1997
<i>Bellingshausen Sea; 0-100 m</i>				
	22	60 ± 5	37	Shimmield and Ritchie, 1995
<i>NE Polynya, Greenland; 0-50 m</i>				
1992	13	20	65	Cochran <i>et al.</i> , 1995;
1993	33-70	80	41-88	1997
<i>BATS 0-150 m; 1993-1995 mean</i>				
	2.6	36	11	Buesseler, 1998

## Chapter 6

### Application of Cosmogenic $^{32}\text{P}$ and $^{33}\text{P}$ in Numerical Modelling Studies

#### ABSTRACT

Two different types of numerical models, inverse and prognostic, were investigated using the cosmogenically produced radioisotopes, phosphorus-32 and phosphorus-33. These isotopes were measured in dissolved and in small and large particulate size classes during March, April, July and August of 1997 within Wilkinson Basin in the Gulf of Maine. Inverse model results indicated that the residence time of phosphorus within dissolved, planktonic and detrital pools varied dramatically with season, ranging from less than 1 day to greater than a 100 days. In addition, there were substantial differences among inverse model formulations, demonstrating that compartment linkages played a crucial role in the determination of phosphorus residence times.

A 4 box prognostic model was also utilized to elucidate the temporal cycling of stable P. The model was first run with parameters deemed appropriate for the Gulf of Maine ecosystem. Initial model runs were then compared to those determined using parameters constrained by  $^{32}\text{P}$  and  $^{33}\text{P}$ . Results suggest that  $^{32}\text{P}$  and  $^{33}\text{P}$  can help to identify weaknesses within prognostic models and have the potential for 'tuning' parameters in future ecosystem modelling efforts.

## INTRODUCTION

Diagnostic models can provide powerful insight into a variety of oceanographic processes ranging from nutrient uptake to removal of anthropogenically produced contaminants (Fasham *et al.*, 1990;1993; Sarmiento *et al.*, 1993; Doney *et al.*, 1996; Cais *et al.*, 1995; Keeling *et al.*, 1996; Mosian and Hoffman, 1996; Cao and Woodward, 1998). Prognostic models have been used to help elucidate both past and future and natural and man-made impacts on an ecosystem (Fasham *et al.*, 1990; 1993; Houghton *et al.*, 1992; Keeling *et al.*, 1996; Cao and Woodward, 1998). However, one of the biggest obstacles in correctly formulating numerical models in ocean sciences is a lack of knowledge concerning food web interactions within the upper ocean.

In the past, many models approached this problem by treating the upper ocean as a 'black box', focusing on emulating observed nutrient and plankton distributions rather than on elucidating how and why such patterns occurred (Eppley and Peterson, 1979). More sophisticated models have attempted to take into account how nutrients are utilized within an ecosystem as well as the temporal interactions of phytoplankton with zooplankton (Evans and Parslow, 1985; Frost, 1987; Glover *et al.*, 1994; Doney *et al.*, 1996; Mosian and Hoffman, 1996). The most recent models now include microbial processes, as evidence has pointed to the importance of bacteria in detrital remineralization (Ducklow, 1983; Cho and Azam, 1988; Fasham *et al.* 1990; 1993; Sarmiento *et al.*, 1993; Azam, 1998).

This leads to one of the greatest difficulties in numerical modelling of ocean nutrient cycling: sampling the appropriate biological pools and the relationships between them. On the most basic level, this implies knowledge of not only how nutrients are made available to the system of interest, but *what* nutrients are controlling primary production. Most ecosystem models tend to focus on only one nutrient, namely nitrogen, as limiting primary production (Fasham *et al.*, 1990;1993; Doney *et al.*, 1996). However, a number of recent studies have found that the magnitude of phytoplankton production in both open ocean and coastal systems can be significantly affected by other macro-nutrients and trace



elements such as phosphorus, silica, and iron (Hecky and Kilham, 1988; Karl *et al.*, 1992; Lohrenz *et al.*, 1992; Martin *et al.*, 1994; Dugdale and Wilkerson, 1997; Hutchins and Bruland, 1998; Takeda, 1998). Furthermore, it has been postulated that the nutrients which limit primary production may change as a function of season (Karl *et al.*, 1992; Lohrenz *et al.*, 1992).

Unfortunately, as models become more complex, an increasing number of free parameters are introduced. Thus, while more detailed models may be more realistic, interpreting solutions becomes more difficult as models are often quite sensitive to the chosen parameter values. Even the most fundamental of parameters are not well constrained. For example, maximum phytoplankton and zooplankton growth rates used in biological models are based on either laboratory studies, which may not apply in the 'real world', or inferred from sparse data sets (Eppley, 1972; Evans and Parslow, 1985; Franks *et al.*, 1986; Fasham *et al.*, 1990; Prezelin *et al.*, 1991; Glover *et al.*, 1994; Doney *et al.*, 1996). As a result, one of the greatest needs in the development of ecosystem models is determining the uptake and regeneration of nutrients among biota.

The Gulf of Maine is a highly productive coastal regime which supports one of the largest fisheries in North America (O'Reilly and Busch, 1984). However, increasing populations along the shore have placed this region in jeopardy. In this study, an attempt was made to evaluate those processes which are the most important in the cycling of nutrients within Gulf of Maine surface waters. Two types of models, inverse and prognostic, were investigated using the cosmogenically produced radioisotopes phosphorus-32 ( $t_{1/2} = 14.3$  days) and phosphorus-33 ( $t_{1/2} = 25.3$  days). Our results suggest that these isotopes can help pinpoint model weaknesses as well as those biological processes which are important within an ecosystem. Future uses of these isotopes in ecosystem modelling efforts are also discussed.

## THE DATA

The radioisotopes  $^{32}\text{P}$  and  $^{33}\text{P}$  enter the oceans predominantly in rain (Waser and Bacon, 1995). If the input of these isotopes is known, and the activities of  $^{32}\text{P}$  and  $^{33}\text{P}$  are measured within various biological pools, then the uptake and regeneration rate of phosphorus between biological components can be determined. In essence, the ratio of  $^{33}\text{P}/^{32}\text{P}$  will increase with increasing 'age' of a particular biological reservoir.

There are several distinct advantages to using  $^{32}\text{P}$  and  $^{33}\text{P}$  to trace biological interactions. The utilization of an *in situ* tracer allows for temporal and spatial integration over the mean-life of the radionuclide. These isotopes in particular have mean-lives ( $1/\lambda$ :  $^{32}\text{P} = 20.5$  days and  $^{33}\text{P} = 36.5$  days) which are very relevant to biologically driven processes. Furthermore, *in situ* isotopic measurements avoid many of the difficulties associated with laboratory and/or incubation methods, which may be compromised due to bottle-related artifacts.

Seawater samples were collected within Wilkinson Basin (~ 275 m) in the southwestern Gulf of Maine during March, April, July and August of 1997. This coastal region is dominated by deep mixed layer depths during the winter. Increasing vertical stratification in the early spring results in a spring bloom which causes nutrient depletion during the summer (Townsend and Spinrad, 1986). Details regarding collection and measurement of  $^{32}\text{P}$  and  $^{33}\text{P}$  are found in Benitez-Nelson and Buesseler (1998a,b; **Chapter 4**). Stable and radioactive phosphorus were measured in total dissolved ( $< 0.2 \mu\text{m}$ ), small ( $0.2\text{-}1 \mu\text{m}$ ,  $1\text{-}10 \mu\text{m}$  and  $10\text{-}102 \mu\text{m}$ ) and large particulate pools, including plankton tows ( $> 102 \mu\text{m}$ ) (Table 1). Ancillary measurements included CTD profiles, pigments, and dissolved and sinking particulate concentrations. Atmospheric deposition of  $^{32}\text{P}$  and  $^{33}\text{P}$  was measured at two coastal sites, Portsmouth, NH and Woods Hole, MA, prior to and during each cruise (See **Chapter 3**; Benitez-Nelson and Buesseler, 1998c) (Table 6.1).

**Table 6.1** Radioactive and stable phosphorus data from surface waters of Wilkinson Basin in the Gulf of Maine (42°29.41'N 69°45.02'W) used in the inverse and prognostic models. Error bars are 1 $\sigma$ . N.D. = No Data

Cruise (at 5 m)	Stable P ( $\mu\text{mol m}^{-3}$ )	$^{32}\text{P}$ (d.p.m. $\text{m}^{-3}$ )	$^{32}\text{P}$ (d.p.m. $\text{m}^{-3}$ )
<i>March</i>			
Rain	N. D.	107	133
Dissolved (< 0.2 $\mu\text{m}$ )	720	5.60 $\pm$ 0.97	4.56 $\pm$ 0.79
Phytoplankton (10-102 $\mu\text{m}$ )	29	0.70 $\pm$ 0.18	0.51 $\pm$ 0.13
Zooplankton (>102 $\mu\text{m}$ )**	10	0.0758 $\pm$ 0.007	0.0865 $\pm$ 0.007
Detritus (0.2 -10 $\mu\text{m}$ )	60	0.44 $\pm$ 0.04	0.43 $\pm$ 0.04
<i>April</i>			
Rain	N. D.	205	254
Dissolved (< 0.2 $\mu\text{m}$ )	1233	3.61 $\pm$ 0.60	3.11 $\pm$ 0.47
Phytoplankton (10-102 $\mu\text{m}$ )*	9	0.31 $\pm$ 0.02	0.26 $\pm$ 0.02
Zooplankton (>102 $\mu\text{m}$ )***	15	0.109 $\pm$ 0.007	0.129 $\pm$ 0.008
Detritus (0.2 -10 $\mu\text{m}$ )	33	0.14 $\pm$ 0.01	0.15 $\pm$ 0.01
<i>July</i>			
Rain	N. D.	111	135
Dissolved (< 0.2 $\mu\text{m}$ )	458	4.16 $\pm$ 0.27	4.48 $\pm$ 0.22
Phytoplankton (10-102 $\mu\text{m}$ )	8	0.66 $\pm$ 0.10	0.45 $\pm$ 0.10
Zooplankton (>102 $\mu\text{m}$ )	2	0.026 $\pm$ 0.0065	0.129 $\pm$ 0.008
Detritus (0.2 -10 $\mu\text{m}$ )	27	0.51 $\pm$ 0.02	0.41 $\pm$ 0.02
<i>August</i>			
Rain	N. D.	117	133
Dissolved (< 0.2 $\mu\text{m}$ )	527	5.44 $\pm$ 0.30	4.65 $\pm$ 0.26
Phytoplankton (10-102 $\mu\text{m}$ )	6	0.14 $\pm$ 0.04	0.14 $\pm$ 0.04
Zooplankton (>102 $\mu\text{m}$ )	8	0.069 $\pm$ 0.001	0.101 $\pm$ 0.001
Detritus (0.2 -10 $\mu\text{m}$ )	36	1.88 $\pm$ 0.16	1.67 $\pm$ 0.15

\* Surface activities were below detection. Data is taken from a depth of 100 m

\*\* Integrated from 0 - 100 m

\*\*\* Integrated from 0 - 110 m

## THE MODELS

In order to use  $^{32}\text{P}$  and  $^{33}\text{P}$  in modelling studies, the following assumptions must hold: 1) no fractionation occurs during uptake and remineralization, 2) all of the radioactive P which enters the ocean is bioavailable and 3) the chosen boxes and exchanges between them are appropriate. The first and second assumptions have been discussed in detail in **Chapter 4**. Briefly, although fractionation may occur to some extent, it is unlikely that the magnitude of such a process would significantly effect results. For example, an improbable fractionation of 100‰ between  $^{32}\text{P}$  and stable P results in only a 10% change in the ratio of  $^{32}\text{P}$  and stable P (20% for  $^{33}\text{P}$  to stable P) (Waser *et al.*, 1996). This is well within the error of many of our  $^{33}\text{P}/^{32}\text{P}$  ratio measurements. However, it is probable that organisms are heterogeneous in their phosphorus activities. For example, zooplankton may ingest only the most labile or youngest fraction of the organism during plankton grazing.

The second assumption is harder to quantify given the limited number of studies which have examined atmospheric P deposition (Graham and Duce, 1979; 1981; 1982). It is highly likely that once formed,  $^{32}\text{P}$  and  $^{33}\text{P}$  oxidize and scavenge onto aerosol surfaces (Lal and Peters, 1967). Thus, it is hypothesized that most, if not all, radioactive P which enters the oceans can desorb as phosphate. However, the rate of desorption may be dependent on the composition of the aerosol particle, as different minerals vary in their affinity for phosphate. The distribution of aerosol types may change depending on the season and rain source. This aspect will have the greatest affect on the dissolved phosphorus pool as dissolved nutrients are at the bottom of the food-web.

The third assumption, that the chosen boxes are representative of specific biological components, is the biggest difficulty in this study. The low activities of  $^{32}\text{P}$  and  $^{33}\text{P}$  in marine systems necessitated the collection of large volumes of seawater. As a result, various biological pools are defined by specific size classes. In the following two models, 4 boxes are used to describe the biological cycling of P in the Gulf of Maine: <0.2  $\mu\text{m}$  (Nutrients), 10-102  $\mu\text{m}$  (Phytoplankton), >102  $\mu\text{m}$  (Zooplankton) and 0.2-10

$\mu\text{m}$  (Detritus). Thus, with the exception of the nutrient box, each box contained a mixture of more than one class of organisms. For example, the Phytoplankton box (10-102  $\mu\text{m}$ ) probably contained a significant fraction of micro-zooplankton, especially during the summer cruises. Speciation analyses of March and April plankton tows indicated that the 'Zooplankton' box (>102  $\mu\text{m}$ ) was actually dominated by diatoms. In addition, in July and August, the 'Zooplankton' box, although dominated by copepods, also contained a small percentage (10-20%) of dinoflagellates, such as *Seratium*. Finally, it has been shown in Chapter 4 that the Detritus box (0.2-10  $\mu\text{m}$ ) contains a significant fraction of bacteria and picoplankton, which not only play an important role in remineralization but in the uptake of inorganic phosphorus as well.

### *Inverse models*

The goal of the inverse box model was to estimate the residence time of phosphorus within various biological pools. Four different boxes were defined using size cutoffs: Nutrients (<0.2  $\mu\text{m}$ ), Phytoplankton (10-102  $\mu\text{m}$ ), Zooplankton (>102  $\mu\text{m}$ ), Detritus (0.2-10  $\mu\text{m}$ ) (Fig. 6.1). Bacterial remineralization was modeled implicitly rather than explicitly in the system.

Transfer between boxes was assumed to be linear with each arrow in Figure 6.1 representing the net flux between each box (Appendix 1). For example the 'Detritus' box is described by the following equation:

$$dD/dt = +k_3P + k_4Z - (k_5 + k_6)D - \lambda D$$

where  $dD/dt$  is the change in 'Detritus'  $^{32}\text{P}$  (or  $^{33}\text{P}$ ) activity with time; P is the  $^{32}\text{P}$  (or  $^{33}\text{P}$ ) activity in the 'Phytoplankton' Box; Z is the  $^{32}\text{P}$  (or  $^{33}\text{P}$ ) activity in the 'Zooplankton' Box;  $k_3$  through  $k_6$  represents the net exchange between boxes in days<sup>-1</sup>; and  $\lambda D$  is the removal of 'Detritus' activity via radioactive decay.

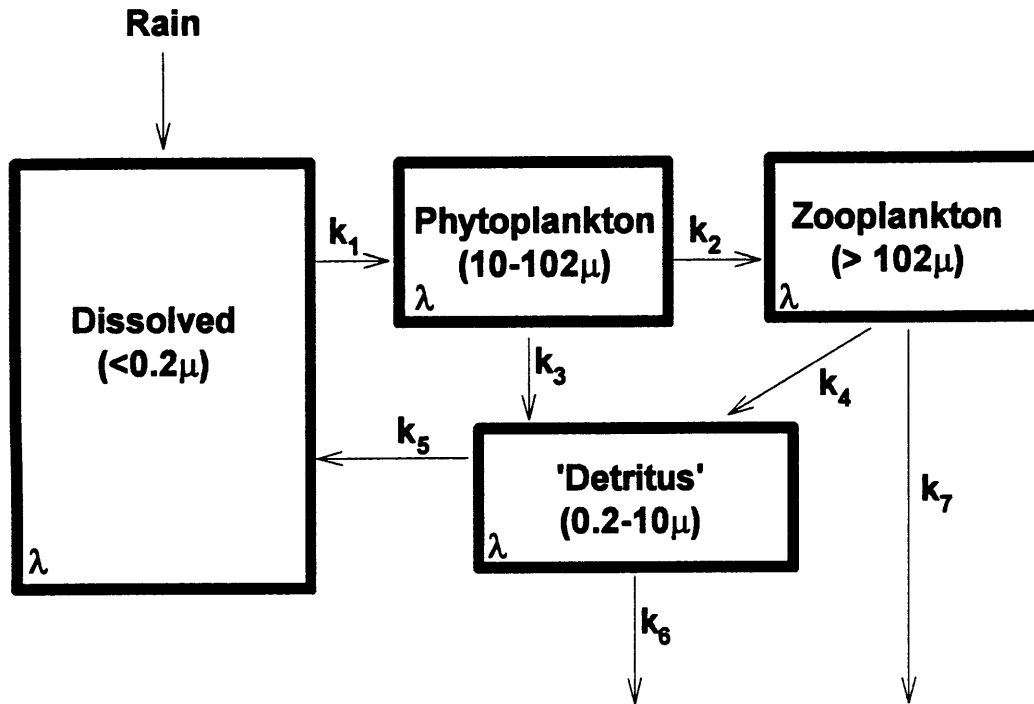


**Figure 6.1.** Schematic of Inverse Box Model

The linear simplification allowed for an over- rather than under-determined system. The model was then solved separately for each cruise using singular value decomposition and assuming steady state ( $dD/dt = 0$ ) (Appendix I). Singular value decomposition is a least squares fitting technique which uses an integrative process to provide the best solution to a series of linear inverse equations. Several different box model formulations were used. In the first case, a term ( $k_7$ ) is included which allows for the sinking of zooplankton directly from the euphotic zone. In the second case, all zooplankton removal goes through the detrital pool, such that  $k_7$  is zero. In the third scenario, the 'Zooplankton' box is redefined as 'Phytoplankton II' during the March and April cruises, such that uptake ( $k_2$ ) is from the 'Nutrient' box only. The fourth scenario is similar, however, direct particulate export ( $k_7$ ) is again zero.

### *Prognostic model*

The goal of the prognostic model was to further current understanding of the important processes controlling the distribution of P within Gulf of Maine surface waters during the spring and summer. The lack of data does not allow for complete emulation of the annual cycle within the Gulf of Maine. Again, only four boxes are used and all are described by using size cutoffs: Nutrients ( $<0.2 \mu\text{m}$ ), Phytoplankton ( $10\text{-}102 \mu\text{m}$ ), Zooplankton ( $>102 \mu\text{m}$ ), Detritus ( $0.2\text{-}10 \mu\text{m}$ ) (Fig. 6.2). The model is essentially the same as the nitrogen based formulation of Doney *et al.* (1996) hereafter referred to as Doney, who used the model to describe the biological cycling at the U.S. JGOFS Bermuda Atlantic Time-series Study (BATS). Although the two sites are dissimilar, the model can be applied to either region due to the simplicity of the model structure. A brief schematic of the four box model is given in Figure 6.2.

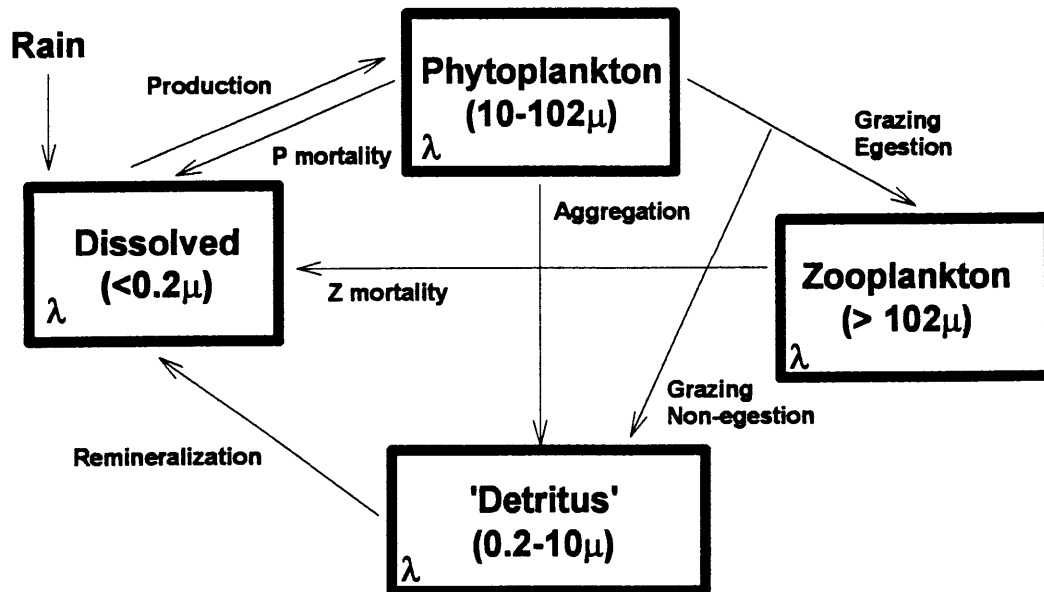


**Figure 6.2** Schematic of the Prognostic Model (from Doney *et al.*, 1996)

This particular model formulation was utilized for several reasons. First and foremost, the Doney model was found to maintain stability over a range of initial conditions. In addition, the number of parameters used in the model were relatively small and the chosen parameter values surprisingly appropriate for the Gulf of Maine (Table 6.2, see below). Furthermore, the model sought to emulate basic food web interactions, such as nutrient and light limitation, grazing, and remineralization. Although not explicitly modelled, bacterial activity is discerned implicitly via phytoplankton mortality and detrital remineralization.

The key difference between Doney's formulation and the initial one utilized in this study is the conversion of some of the biological parameters from mmols of nitrogen to mmols of phosphorus. Many of the studies which have sought to understand such processes as phytoplankton growth and zooplankton grazing have been conducted in terms of nitrogen cycling. Although limnological studies have examined such processes in relatively more detail for phosphorus, it is not appropriate to use parameters derived from freshwater systems when modelling marine systems. As a result, parameter conversion from Doney's model was achieved assuming Redfield ratios. This form of conversion has been utilized in the past in similar models of upper ocean phosphorus cycling (Six and Maier-Reimer, 1996). Further support for this conversion is found by the N:P ratios measured on GF/F (0.7  $\mu\text{m}$ ) in Gulf of Maine surface waters at the Wilkinson Basin site. Particulate N:P ratios averaged 15.4. It should be mentioned, however, that this value is greater than the inorganic N:P ( $\text{NO}_3 + \text{NO}_2/\text{PO}_4$ ) ratio of 4 measured in dissolved samples (see Table 4.1 in Chapter 4).

The biological formulations and parameters used to describe the transfer of P between each biological compartment is described in detail by Doney *et al.*, 1996 (Table 6.2). The uptake of nutrients by phytoplankton (Appendix II) was simplified from the original Doney model in that photoadaptation, the ability of phytoplankton to alter the efficiency at which photosynthesis occurs, is ignored. Phytoplankton production is



modeled using the following Michaelis-Menten equation:

$$\text{Production} = \mu_p NP f_h / (N + K_n)$$

where: N and P are the phosphate concentrations within the Nutrient and Phytoplankton boxes, respectively,  $\mu_p$  is the maximum phytoplankton growth rate,  $f_h$  is the light parameterization, and  $K_n$  is the nutrient half-saturation constant. The maximum phytoplankton growth rate,  $\mu_p$ , is based on a temperature dependent function of Eppley (1972) developed for phytoplankton biomass. The highest surface water temperature, 20°C, observed in our data occurred in the summer. This is equivalent to a  $\mu_p$  of 2.1 day<sup>-1</sup>. The light parameterization,  $f_h$ , simulates the depth of light penetration and is primarily dependent on the depth of mixed layer. Observed mixed layer depths (MLD) were duplicated using a simple sine curve formulation, which emulated the observed MLD. The light field was determined by using a simple exponential decay with depth. (see Appendix II).  $K_n$ , the nutrient half-saturation constant, is more difficult to quantify. Marra *et al.* (1990), determined a  $K_n$  value of 0.2 mmol N m<sup>-3</sup> for the Sargasso Sea using <sup>14</sup>C incubation techniques. Mosian and Hofman (1996), however, used values as high as of 0.6 mmol N m<sup>-3</sup> for the California coastal transition zone. This  $K_n$  was again based on culture studies of natural phytoplankton assemblages (MacIsaac and Dugdale, 1969). An average value of 0.4 mmol N m<sup>-3</sup> (0.025 mmol P m<sup>-3</sup>) was used in this formulation.

Zooplankton grazing is determined using a modified form of the Ivlev equation:

$$\text{Grazing} = (1-\gamma)\mu_z \Lambda PZ (1-\exp^{-\Lambda P})$$

where:  $\gamma$  is the non-egested fraction,  $\mu_z$  is the maximum zooplankton growth rate,  $\Lambda$  is the Ivlev constant, and P and Z are the concentrations of phytoplankton and zooplankton, respectively. The non-egested fraction,  $\gamma$ , of 0.3 is similar to that used in a number of different regimes (Wroblewski *et al.*, 1988; Fasham *et al.*, 1990; Glover *et al.*, 1994). This value is also similar to the maximum non-assimilation efficiencies observed for copepods by Landry *et al.* (1984). The maximum zooplankton growth rate,  $\mu_z$ , ranges from 0.5-1.5 day<sup>-1</sup> based on laboratory measurements and previous modelling studies (Franks *et al.*, 1986; Anderson and Nival, 1988; Wroblewski, 1989; Fasham *et al.*, 1990).

An average value of  $1.0 \text{ day}^{-1}$  was chosen for this investigation. The Ivlev parameter,  $\Lambda$ , is the most difficult to estimate, and has been found to range from  $0.33 - 2.0 \text{ m}^3 \text{ mmol N}^{-1}$ . Doney used the highest observed value of  $2.0 \text{ m}^3 \text{ mmol N}^{-1}$  ( $32 \text{ m}^3 \text{ mmol P}^{-1}$ ) based on observed grazing rates and zooplankton biomass estimates in the Sargasso Sea. The Gulf of Maine would be expected to have a higher Ivlev constant given that it is a highly productive coastal region (O'Reilly and Busch, 1984). Thus, the maximum  $\Lambda$  value found in the literature was used for this study.

Phytoplankton and Zooplankton mortality were parameterized using the same formulations as those in Doney (Appendix II). The constants  $\eta$ ,  $\epsilon_1$  and  $\epsilon_2$  each fall within a narrow range and are similar to those used in previous models (Franks *et al.*, 1996; Wroblewski, 1989, Fasham *et al.*, 1990; Doney *et al.*, 1996). The phytoplankton aggregation coefficient,  $w$ , is more difficult to quantify because it is a function of both phytoplankton size and species. In the Gulf of Maine, phytoplankton assemblage undergo a shift from larger faster growing phytoplankton to smaller more efficient species. As a result, an average value of  $0.1 \text{ m}^3 \text{ mmol N}^{-1} \text{ day}^{-1}$  ( $1.6 \text{ m}^3 \text{ mmol P}^{-1} \text{ day}^{-1}$ ) was chosen. The removal of P from surface waters, however, is modeled implicitly through the detrital pool.

The detrital remineralization rate,  $\delta$ , is one of the least constrained parameters in the model. This parameter is a function of the detrital sinking velocity and the depth scale of remineralization. Sinking velocities of marine snow and fecal material are on the order of  $100 \text{ m day}^{-1}$  (Fowler and Knauer, 1986; Alldredge and Silver, 1988). However, the 'Detritus' box is also expected to contain a significant fraction of suspended particulate matter. As a result, previous modelling efforts have used more moderate sinking rates which range from  $1-10 \text{ m day}^{-1}$ . The remineralization depth of sinking material at the Wilkinson Basin station in the Gulf of Maine is on the order of a 100 m based on sediment trap data (Pilskaln *et al.*, 1996). Thus, using an intermediate value for sinking material of  $10 \text{ m day}^{-1}$  gives a remineralization rate,  $\delta$ , of  $0.1 \text{ day}^{-1}$ . A list of all of the parameter values used in this study are given in the second row of Table 6.2.

**Table 6.2** Biological Parameter Values after Doney *et al.* (1996)

	Initial Value	Tuned Value	Units	Parameter
k	0.1		m <sup>-1</sup>	Avg. extinction coefficient for PAR*
K <sub>n</sub>	0.025		mmol P m <sup>-3</sup>	Nutrient half-saturation constant
γ	0.3			Non-egested fraction
δ	0.10	1.5	day <sup>-1</sup>	Detrital remineralization rate
ε <sub>1</sub>	0.03		day <sup>-1</sup>	Linear zooplankton mortality
ε <sub>2</sub>	2.88		m <sup>3</sup> mmol P <sup>-1</sup> day <sup>-1</sup>	Quadratic zooplankton mortality
λ	32	11.9	m <sup>3</sup> mmol P <sup>-1</sup>	Ivlev grazing coefficient
μ <sub>p</sub>	2.1		day <sup>-1</sup>	Max. phytoplankton growth rate
μ <sub>z</sub>	1.0		day <sup>-1</sup>	Max. zooplankton growth rate
η	0.075		day <sup>-1</sup>	Phytoplankton mortality rate
w	1.6	37	m <sup>3</sup> mmol P <sup>-1</sup> day <sup>-1</sup>	Phytoplankton aggregation coefficient

\* Photosynthetically available radiation

## RESULTS AND DISCUSSION

### *Inverse models*

Results from the inverse model analyses are shown in Table 6.3. Although each box is not comprised entirely of distinct biological components, these inverse models have allowed some insight into the temporal variation of the residence time of phosphorus and the processes which control the distribution of P within the Gulf of Maine. In addition, these models have a distinct advantage over the simple two box models used in prior investigations of <sup>32</sup>P and <sup>33</sup>P (Waser *et al.*, 1996; Benitez-Nelson and Buesseler, 1998c) in that exchange rates are the result of *all* of the compartments within the model. For example, exchange rates between the 'Phytoplankton' and 'Zooplankton' boxes are also dependent on the exchange rates between 'Detritus' and 'Nutrients'.

**Table 6.3** Stable phosphorus residence times derived from the inversion and two box models of the  $^{32}\text{P}$  and  $^{33}\text{P}$  data.

<b>Model</b>	<b>Nutrients</b>	<b>Phytoplankton</b>	<b>Zooplankton</b>	<b>Detritus</b>	<b>*Cond. #</b>
<i>Inversion 1</i>					
March	> 100 d	> 100 d	> 100 d	> 100 d	7000
April	> 100 d	6 d	> 100 d	5 d	431
July	1 d	2 d	8 d	< 1 d	400
August	5 d	< 1 d	< 1 d	< 1 d	1000
<i>Inversion 2</i>					
March	> 100 d	> 100 d	> 100 d	> 100 d	185
April	> 100 d	6 d	> 100 d	5 d	431
July	24 d	27 d	> 100 d	> 100 d	310
August	40 d	42 d	> 100 d	> 100 d	710
<i>Inversion 3</i>					
March	87 d	> 100 d	> 100 d	> 100 d	4200
April	25 d	25 d	> 100 d	> 100 d	3160
<i>Inversion 4</i>					
March	87 d	> 100 d	> 100 d	> 100 d	185
April	25 d	25 d	> 100 d	> 100 d	373
<i>2 box model</i>					
March	8 d	< 1 d	97 d	--	--
April	25 d	< 1 d	40 d	--	--
July	37 d	< 1 d	100 d	--	--
August	3 d	10 d	54 d	--	--

\* See text for definition

The model inversion #1 allowed for direct removal of 'Zooplankton' from the upper ocean via sinking ( $k_7$ ). Whereas the model inversion #2 did not ( $k_7 = 0$ ). Model inversions #3 and #4 were developed in order to better represent the observed speciation (predominantly diatoms and dinoflagellates) within the 'Zooplankton' box ( $>102 \mu\text{m}$ ) during the spring cruises. In this formulation, both  $k_1$  and  $k_2$  represented nutrient uptake, such that the 'Zooplankton' was redefined as 'Phytoplankton II' (Appendix I and Fig. 6.1). In inversion #3 direct sinking of the larger 'Phytoplankton II' pool was again allowed, while in inversion #4 it was not ( $k_7 = 0$ ).

For each model a condition number was determined (Table 6.3). The condition number, in a sense, is a measure of the robustness of the inverse calculation and is the ratio of the largest to the smallest rate constants (eigenvalues) determined from the model inversion. The larger the condition number, the more uncertain are the results (Press *et al.*, 1992). The inverse calculations were conducted in MATLAB™ and with double precision. Thus, condition numbers greater than  $10^{14}$  are beyond machine precision. There is no set definition as to what is an acceptable condition number and opinions can vary widely. However, it is sufficient to say that condition numbers greater than 100,000 are indicative of highly unconstrained systems.

Not surprisingly, the residence time of phosphorus among the various defined biological pools varied substantially throughout the spring and summer and between the different inverse models. In March, all four inverse models showed similar results with phosphorus residence times typically greater than 100 days: beyond the resolution of  $^{32}\text{P}$  and  $^{33}\text{P}$ . This was most likely due to the fact that the March cruise occurred just prior to the start of the spring bloom, when biological activity within the Gulf of Maine is relatively low (Walsh *et al.*, 1987). The lack of any significant differences in phosphorus residence times between the models in March suggests that direct removal of larger plankton from the euphotic zone is minor.

In April phosphorus residence times changed substantially. All four models showed a significant reduction in the phosphorus residence time of phytoplankton (6-25

days). This was most likely due to the advent of the spring bloom. Disagreement in the P residence times within the 'Nutrient', 'Zooplankton', and 'Detrital' compartments were most likely due to an incorrect assumption in the first two inversions. Model inversion #1 and #2 assumed that the 'Zooplankton' box was dominated by zooplankton rather than by the diatoms and dinoflagellates that were actually observed. Thus, models #3 and #4 are considered to be the most appropriate. Surprisingly, however, the residence time of phosphorus within the  $>102 \mu\text{m}$  (Zooplankton) fraction is greater than 100 days, regardless of the model formulation. Again, the reduction in P residence time from  $>100$  days to 25 days in the 'Nutrients' box was probably due to the spring bloom. In addition, the similarity between those models which had direct sinking of the larger plankton with those that did not, suggest that this particular removal mechanism was again small.

In July and August only model inversions #1 and #2 were conducted. Unlike March and April, there was a substantial difference between the two model types. In the first formulation, phosphorus residence times decreased to a week or less in all of the compartments. In contrast, in the second formulation, phosphorus residence times were substantially longer, ranging from a month in the 'Nutrients' and 'Phytoplankton' compartments to greater than 100 days in the 'Zooplankton' and 'Detrital' boxes. Closer inspection of the calculated exchange rates, however, revealed some important weaknesses in model inversion #1.

In both July and August the inclusion of direct 'Zooplankton' removal from the upper ocean causes many of the exchange rates ( $k_1$  through  $k_7$ ) to become negative. While it is possible to imagine that zooplankton may graze on detritus ( $k_4$ ) or that bacteria within the 'Detritus' box may directly uptake nutrients ( $k_6$ ), it is not reasonable for the biota within the 'Phytoplankton' box to ingest the larger 'Zooplankton'. While model #2 ( $k_7 = 0$ ) did not encounter these same difficulties, the calculated P residence times are unreasonable given the low  $^{33}\text{P}/^{32}\text{P}$  ratios and the high  $^{32}\text{P}$  and  $^{33}\text{P}$  activities observed in the 'Nutrient' and 'Detrital' pools (see **Chapter 4**).

It is interesting to compare the inverse model results of P residence times with those determined using simple two box models. In a two box model, the determination of the phosphorus residence time is similar to that of the inverse model. In addition, all boxes are defined by the same size class cutoffs. However, the exchange rates between boxes are solved independently of the rest of the system. For example, the 'Nutrients' Box is described by the following for  $^{32}\text{P}$  and  $^{33}\text{P}$ :

$$dN/dt = I - k_1P - \lambda N$$

where  $dN/dt (= 0)$  is the change in 'Nutrients' with time,  $I$  is the input of  $^{32}\text{P}$  or  $^{33}\text{P}$  in rain,  $k_1$  is the uptake of 'Nutrients' by P, 'Phytoplankton', and  $\lambda$  is the radioactive decay constant of  $^{32}\text{P}$  or  $^{33}\text{P}$ . Note that in this formulation, the exchange is between 'Nutrients' and 'Phytoplankton' only. There is no additional input from the 'Detritus' box ( $k_5 = 0$ ; Fig. 6.1). Similar equations can be written for the 'Phytoplankton' and 'Zooplankton' boxes. Results are shown in Table 6.3. It is not possible to determine similar residence time estimates for the 'Detritus' pool given the number of detrital sources.

In general, the calculated phosphorus residence times using the simple two box model were quite different from those of the inversion models, regardless of the cruise. The two box model phosphorus residence times were significantly less variable on seasonal time scales. In addition, there were no clear increasing or decreasing trends in residence times relative to the inverse models. Residence times in the two box models ranged from 3 to 37 days within the 'Nutrients' and from less than a day to 10 days within the 'Phytoplankton'. 'Zooplankton' had longer residence times, ranging from 40 to 100 days.

The differences in model results indicate that all of the compartments within the inversion models exert a substantial influence on the exchange rates. Thus, it appears that in this regime, four box models cannot be reduced to simple two-box models in the description of upper ocean phosphorus cycling. It should be noted, however, that all the above modelling efforts assume steady state. Non-steady state models of  $^{32}\text{P}$  and  $^{33}\text{P}$  can also result in significantly different phosphorus residence times (Waser *et al.*, 1996;

Benitez-Nelson *et al.*, 1998). Thus, care must be taken when comparing phosphorus residence times derived from  $^{32}\text{P}$  and  $^{33}\text{P}$ .

The difficulties associated with the 4 box inverse models are probably due in part to the manner in which the different biological pools were separated. The above exercise, however, has also shown that one of the processes which are essential in the cycling of P within Gulf of Maine surface waters is bacterial remineralization. A significant improvement in the model would be to include distinct bacterial and inorganic and organic phosphorus pools. Unfortunately, inclusion of these compartments results in an under-determined system which is not uniquely solvable. Conversely, direct sinking of the larger plankton ( $> 102 \mu\text{m}$ ) is not an important process during the spring. Furthermore, it appears that all of the biological P pools exert a substantial influence on one another, regardless of whether it is spring or summer. These findings have direct implications for those studies which seek to understand mechanisms of particulate matter export in the Gulf of Maine.

### ***Prognostic model***

The results from the forward time-stepping model are shown in Figures 6.3-6.5. One can immediately observe two distinct differences between the model output and the stable P data. Model detritus concentrations are over 2 times greater, while zooplankton are over an order of magnitude greater than that measured. Nutrient and Phytoplankton concentrations, however, are similar to what was measured.

The Doney model is easily adjusted to radioactive P by simply adding an input term to the nutrient box, a decay term to each equation, and a conversion factor which modifies those parameters in atoms of stable P to atoms of radioactive P. The conversion factor is based on the average measured ratio of stable P to radioactive P in each defined box (see Appendix II). It should be noted that there will be differences between the measured results and the model output simply due to the manner in which the model mixes concentrations with depth. Radioactive P enters the oceans at the surface and, given the



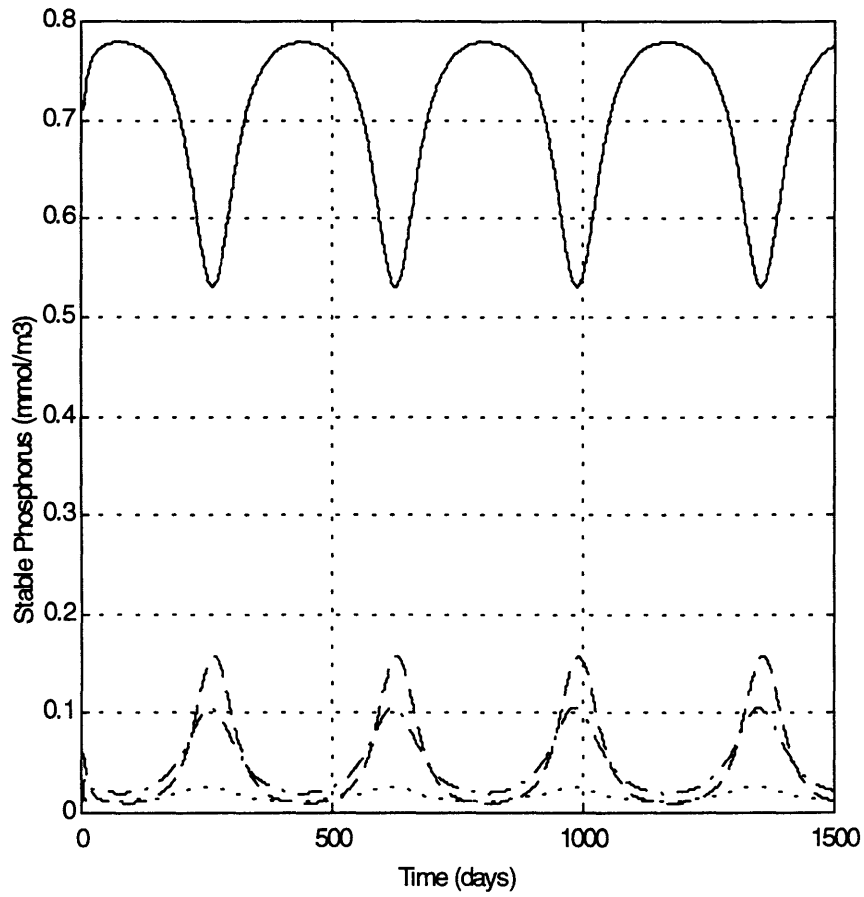


**Figure 6.3.** Doney's model for stable phosphorus using original parameters. The 'Nutrients' box is depicted by the solid line, 'Phytoplankton' by the dotted line, 'Zooplankton' by the dash dot line and 'Detritus' by the dashed line. Filled circles represent the actual data.

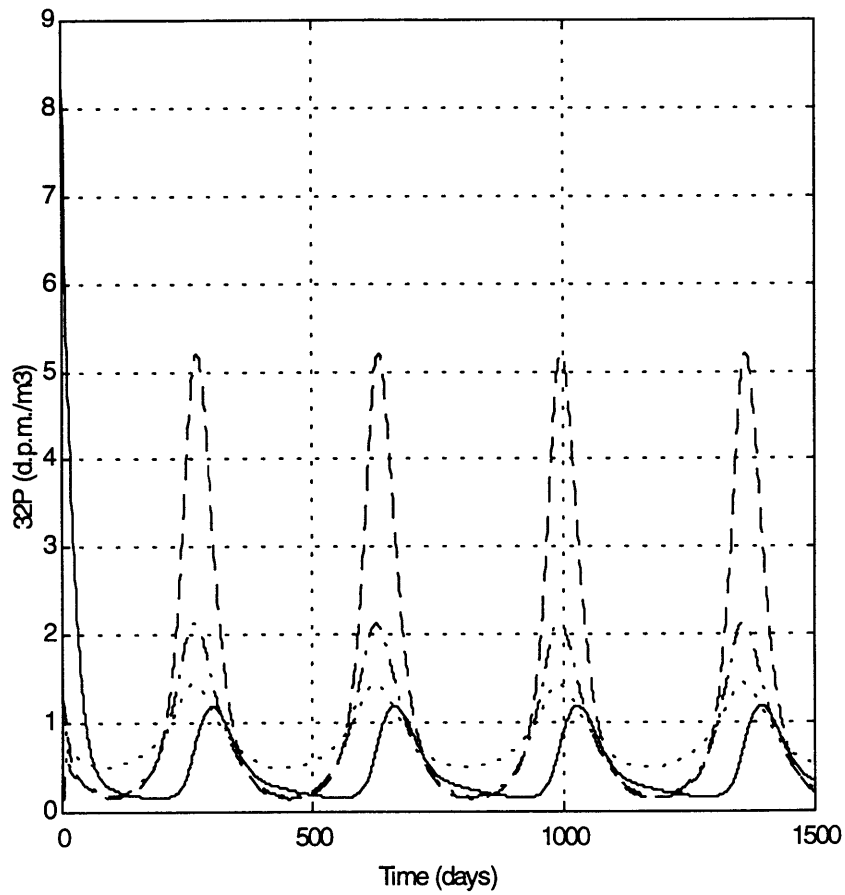


**Figure 6.4.** Doney's model for  $^{32}\text{P}$  using original parameters. The 'Nutrients' box is depicted by the solid line, 'Phytoplankton' by the dotted line, 'Zooplankton' by the dash dot line and 'Detritus' by the dashed line. Filled circles represent the actual data.

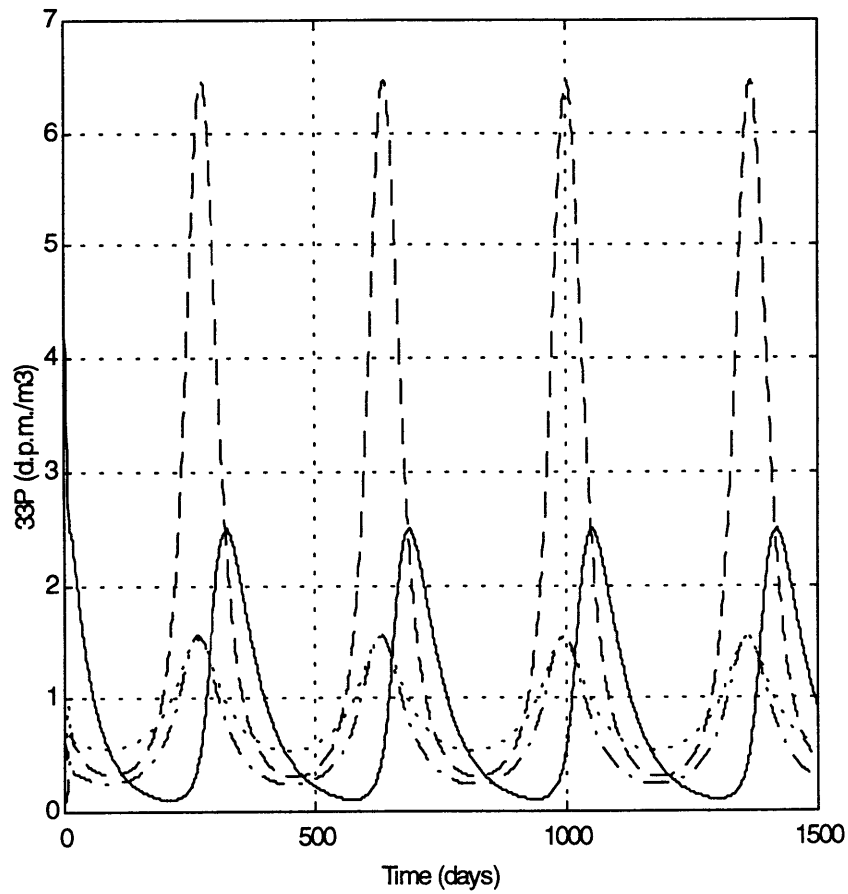


**Figure 6.5.** Doney's model for  $^{33}\text{P}$  using original parameters. The 'Nutrients' box is depicted by the solid line, 'Phytoplankton' by the dotted line, 'Zooplankton' by the dash dot line and 'Detritus' by the dashed line. Filled circles represent the actual data.

differences in  $^{32}\text{P}$  and  $^{33}\text{P}$  activity within the mixed layer, does not mix immediately to deeper depths (Benitez-Nelson and Buesseler, 1998b). The model, however, mixes constituents instantaneously to depth, such that box concentrations of radioactive  $^{32}\text{P}$  and  $^{33}\text{P}$  will be lower than that observed in the data.

Results are shown in Figures 6.3-6.5. Similar to stable P, several discrepancies between the model and the real data are apparent. Nutrient activities are a factor of two lower than the measured results. In addition, the Detritus pool is over three times higher than expected and phytoplankton concentrations, over a factor of two too high. Zooplankton concentrations are over an order of magnitude too large.

The differences between the modeled stable and radioactive phosphorus concentrations with the observed data are most likely due to the manner in which each biological pool was described. Size fractionated samples simply do not represent the well defined trophic levels described by the model. Another problem with the model is the inclusion of bacteria and picoplankton within the 'Detrital' pool. This alone is the most probable cause of the mis-match between observed and modeled 'Detritus' concentrations. Nonetheless, it is interesting to try and use the radioactive phosphorus data to both 'tune' the model and pinpoint where some of the *additional* difficulties in the numerical model lie.

From the previous discussion, there are several model parameters which are highly unconstrained, the Ivlev grazing coefficient, the detrital remineralization rate and the phytoplankton aggregation term. The Doney model can be broken down and simplified into discrete exchanges between boxes. These exchange rates can then be solved

individually assuming steady state. For example, the Zooplankton box can be described by grazing and mortality such that:

$$dZ/dt = (1-\gamma)\mu_z\Lambda ZP(1-e^{-\Lambda P}) - kZ - \lambda Z$$

where  $dZ/dt$  is the change in zooplankton concentrations with time (at steady state  $dZ/dt = 0$ ) and  $Z$  and  $P$  are the zooplankton and phytoplankton concentrations, respectively. The parameters  $\gamma$ ,  $\lambda$ ,  $\mu_z$  and  $\Lambda$  are described in Table 2. Unlike the original Doney formulation, the removal flux is described by a simple linear term,  $kZ$ . In order to solve this equation using  $^{32}\text{P}$  and  $^{33}\text{P}$  it is necessary to reduce the equation to two unknowns. In this case, it is assumed that both  $\gamma$ , the non-egested fraction, and  $\mu_z$ , the maximum growth rate, are reasonably well constrained.

The above equation was then solved for the Ivlev grazing coefficient,  $\Lambda$ , for the two summer cruises (when zooplankton were dominant in the  $>102 \mu\text{m}$  size class). An average value of  $11.9 \text{ m}^3 (\text{mmol P})^{-1}$  was determined (Table 6.2). This is within the  $5.3$  to  $32 \text{ m}^3 \text{ mmol P day}^{-1}$  range (converted from  $\text{N}$  using Redfield) used in previous modelling efforts (Franks *et al.*, 1986; Anderson and Nival, 1988; Wroblewski, 1989; Fasham *et al.*, 1990; Doney *et al.*, 1996). Although a full scale sensitivity test of this procedure was not conducted, it was found that  $\Lambda$  was very sensitive to both the chosen  $\gamma$  and  $\mu_z$ . Increasing or decreasing either resulted in a similar change in  $\Lambda$ .

Similar procedures were conducted for the determination of  $\delta$ , the detrital remineralization rate and for  $w$ , the phytoplankton aggregation coefficient. For the determination of  $\delta$ , the equation for the 'Nutrient' box was used (Appendix II). Steady state was again assumed, and the parameters,  $\mu_p$ ,  $k_n$ ,  $\eta$ ,  $\epsilon_1$  and  $\epsilon_2$  were taken to be correct. It should be noted that increasing or decreasing  $k_n$ ,  $\eta$ ,  $\epsilon_1$  and  $\epsilon_2$  by as much as a factor of 2 has only a small effect on the calculated detrital remineralization rate. Solving for each cruise, with the exception of April, resulted in a wide range of  $\delta$  from a high of  $3.3 \text{ day}^{-1}$  in March, to a low of  $0.1$  in August. The April data was ignored for this exercise

due to a large storm which struck the Wilkinson Basin site just prior to the April cruise. An intermediate value of  $1.5 \text{ day}^{-1}$  was chosen.

The phytoplankton aggregation coefficient,  $w$ , was determined by solving the equation for the 'Detritus' box and assuming steady state (Appendix II). The average detrital remineralization rate of  $1.5 \text{ day}^{-1}$  determined from above was used to calculate  $w$  for the March, July, and August cruises. Values ranged over two orders of magnitude, from 37 to  $4700 \text{ m}^3 \text{ mmol P day}^{-1}$ . These values are much larger than that utilized in previous modelling efforts. The minimum value alone is over 4 times higher than that used in the Doney model. The highest value of  $4700 \text{ m}^3 \text{ mmol P day}^{-1}$  is simply not possible. For this exercise, the minimum value of  $37 \text{ m}^3 \text{ mmol P day}^{-1}$  was used.

The results from using the new parameters are shown in Figures 6.6-6.8. It is immediately evident that the relative distributions of stable P,  $^{32}\text{P}$  and  $^{33}\text{P}$  among the 4 compartments is comparable to that seen in the data. For stable P, 'Zooplankton' and 'Detritus' concentrations are now more similar to levels which were observed in the Gulf of Maine. The seasonal cycle of the 'Nutrients' box, however, is worse. For  $^{32}\text{P}$  and  $^{33}\text{P}$ , 'Nutrient' concentrations are now overestimated by 30 to 50%. 'Detritus' concentrations on the other hand, are similar to that observed for both  $^{32}\text{P}$  and  $^{33}\text{P}$ . In addition, 'Phytoplankton' concentrations are still over an order of magnitude greater than that observed for  $^{32}\text{P}$  and  $^{33}\text{P}$  data. However, both  $^{32}\text{P}$  and  $^{33}\text{P}$  'Zooplankton' activities fall to zero. However, increasing the Ivlev constant by 20%, to  $14.8 \text{ m}^3 \text{ mmol P day}^{-1}$ , brings 'Zooplankton' activities back to  $^{32}\text{P}$  and  $^{33}\text{P}$  activity levels observed in the data set.

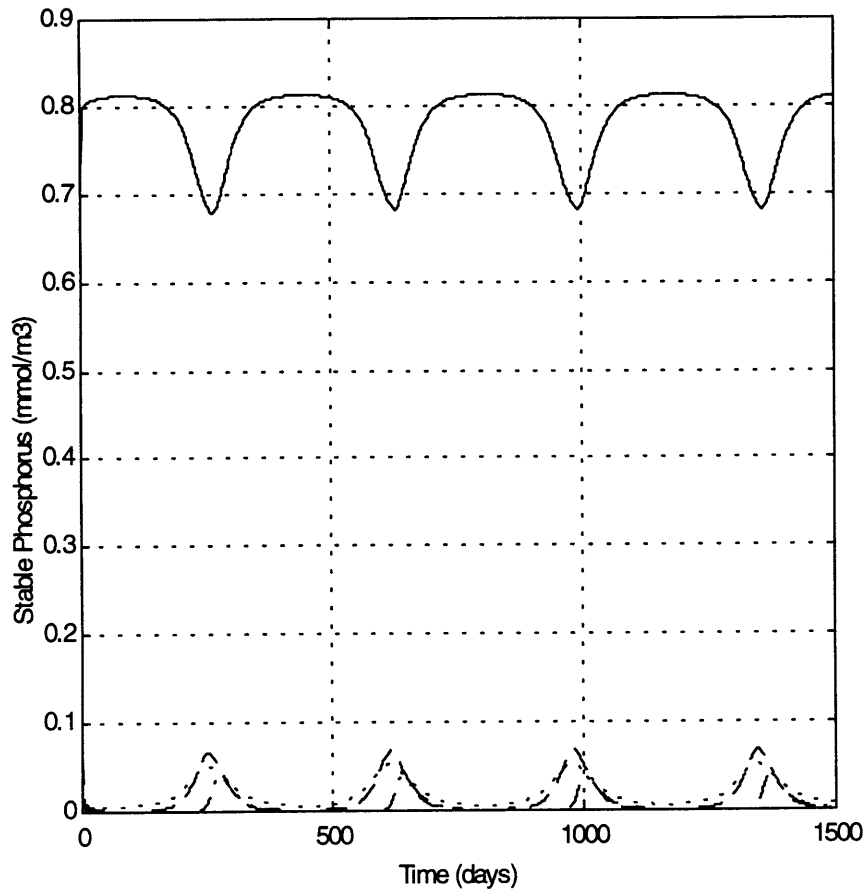


**Figure 6.6** Doney's model for stable phosphorus using the new parameters derived from  $^{32}\text{P}$  and  $^{33}\text{P}$  data in the Gulf of Maine. The 'Nutrients' box is depicted by the solid line, 'Phytoplankton' by the dotted line, 'Zooplankton' by the dash dot line and 'Detritus' by the dashed line. Filled circles represent the actual data.

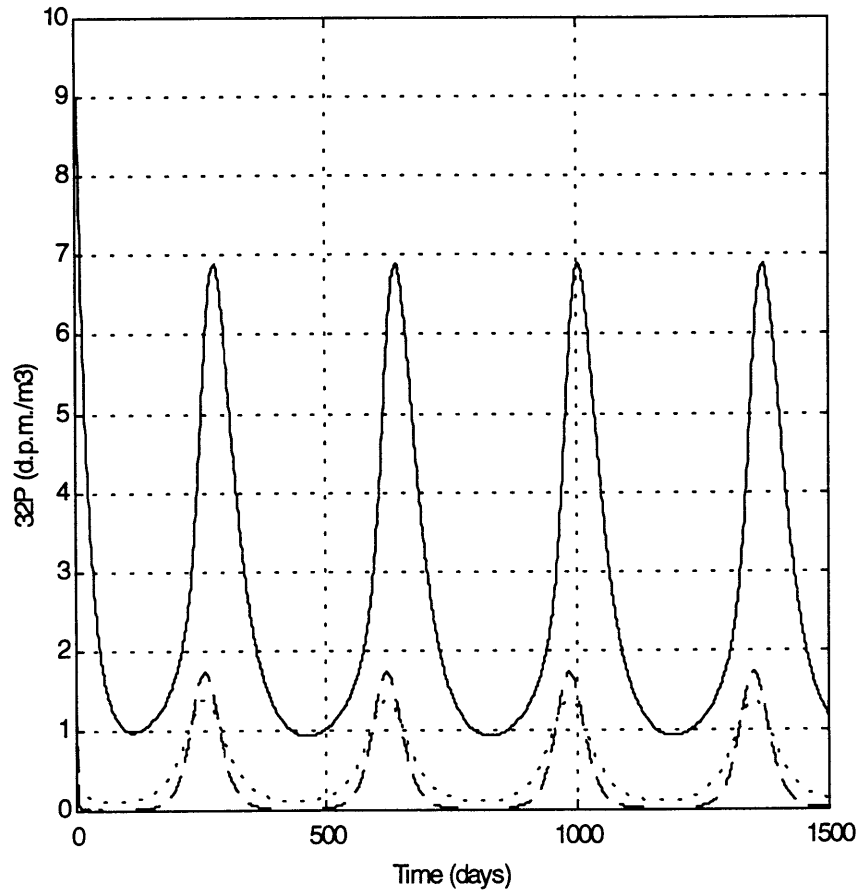


**Figure 6.7** Doney's model for  $^{32}\text{P}$  using 'tuned' parameters derived from  $^{32}\text{P}$  and  $^{33}\text{P}$  data in the Gulf of Maine. The 'Nutrients' box is depicted by the solid line, 'Phytoplankton' by the dotted line, 'Zooplankton' by the dash dot line and 'Detritus' by the dashed line. Filled circles represent the actual data.



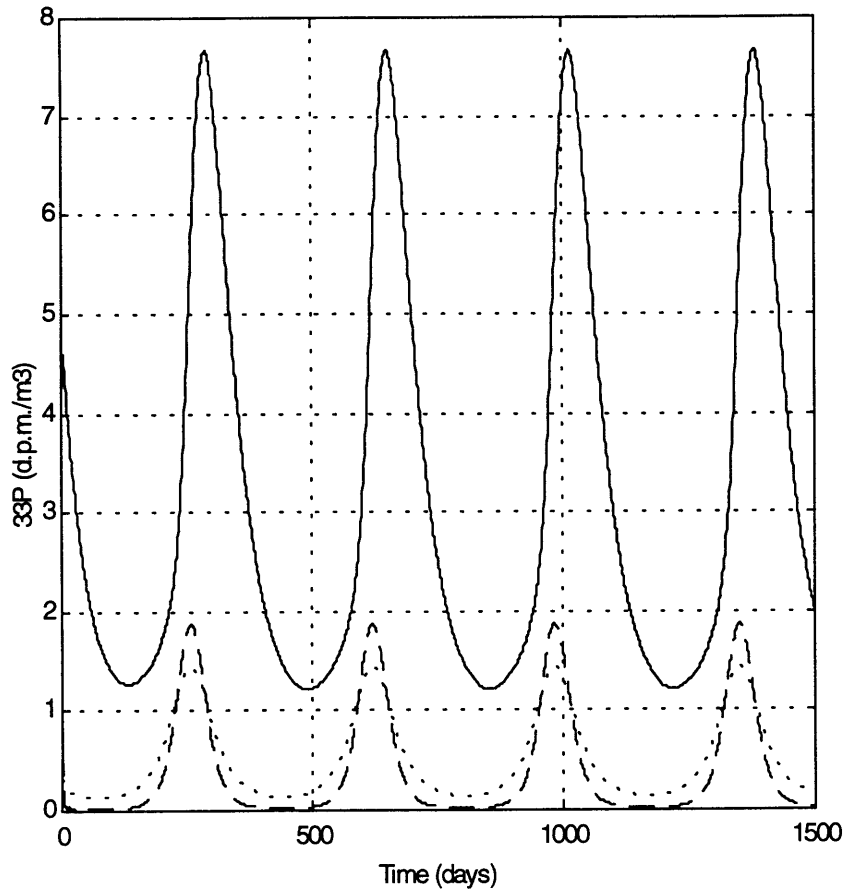


**Figure 6.8** Doney's model for  $^{33}\text{P}$  using the new parameters derived from  $^{32}\text{P}$  and  $^{33}\text{P}$  data in the Gulf of Maine. The 'Nutrients' box is depicted by the solid line, 'Phytoplankton' by the dotted line, 'Zooplankton' by the dash dot line and 'Detritus' by the dashed line. Filled circles represent the actual data.

The above results suggest that  $^{32}\text{P}$  and  $^{33}\text{P}$  can be used to 'tune' prognostic models. Although, it should be stressed that the new parameters derived from using  $^{32}\text{P}$  and  $^{33}\text{P}$  are based on biological compartments which have been distinguished by size, rather than trophic level. One of the problems already identified in the Doney model is the lack of an explicit bacterial and picoplankton pool. Closer inspection of the  $^{32}\text{P}$  and  $^{33}\text{P}$  derived parameters, however, can further pinpoint some of the additional inadequacies of the prognostic model.

The  $^{32}\text{P}$  and  $^{33}\text{P}$  derived Ivlev grazing coefficient of  $11.9 \text{ m}^3 (\text{mmol P})^{-1}$  derived from the two summer cruises is almost three times lower than that used initially in the Doney model. The low derived value is surprising given that the initial Doney estimate of  $32 \text{ m}^3 (\text{mmol P})^{-1}$ , converted from nitrogen, was used for the Sargasso Sea, an area with relatively low primary production rates and zooplankton biomass (Lohrenz *et al.*, 1992; Roman *et al.*, 1993). It is possible that the decrease in the Ivlev grazing parameter is due to the inclusion of phytoplankton in the operationally defined 'Zooplankton' box. However, speciation analyses of the  $> 102 \mu\text{m}$  fraction found that it consisted of more than 80% zooplankton. All of the grazing parameters used in this study were the same as in Doney, which suggests that the grazing formulation used by Doney is inappropriate for coastal systems.

Further evidence for this conclusion is found from the large range in the phytoplankton aggregation coefficient, 37 to  $4700 \text{ m}^3 \text{ mmol P day}^{-1}$ . Even the smallest value is over an order of magnitude higher than the original Doney estimate. The inclusion of zooplankton in the 'Phytoplankton' pool would not be expected to effect this coefficient to such a great extent. Thus, it appears that the Doney model does not adequately resolve the cycling of phytoplankton within the Gulf of Maine. It appears that either additional uptake and removal mechanisms and/or more 'Phytoplankton' and 'Zooplankton' boxes are necessary.

This new detrital remineralization rate of  $1.5 \text{ day}^{-1}$  is also over an order of magnitude higher than that used in the Doney model. However, using a particle

rem mineralization depth of 100 m (Pilska et al., 1996), one can calculate a new particulate sinking rate that is only slightly higher than typical sinking velocities of 100 m day<sup>-1</sup> for fecal material and marine snow (Fowler and Knauer, 1986; Doney *et al.*, 1996). A higher detrital remineralization rate also seems reasonable given that the Gulf of Maine is a highly productive coastal environment with significantly higher particulate export rates than that found at Bermuda (see **Chapter 5**; Michaels *et al.*, 1994; Benitez-Nelson *et al.*, 1998).

<sup>32</sup>P and <sup>33</sup>P have provided insight into the inadequacies of the Doney model in depicting stable and radioactive P concentrations in the Gulf of Maine. Although size fractionated data do not represent the explicitly defined biological pools of the Doney model, our results suggest that the modeled phytoplankton/zooplankton interactions are inappropriate for coastal ecosystems. These results, however, have been based on only four series of measurements made in the spring and summer. It is possible that the Doney model better emulates phytoplankton zooplankton interactions during other seasons or in other years.

## **FUTURE MODELLING EFFORTS**

The biggest difficulty in using <sup>32</sup>P and <sup>33</sup>P in modelling studies is the requirement of large sample volumes. The lack of activity measurements in specific biological pools will certainly hinder the use of <sup>32</sup>P and <sup>33</sup>P in future modelling efforts. Nonetheless, the above exercises have provided evidence that <sup>32</sup>P and <sup>33</sup>P can give a new perspective to prognostic ecosystem models. The potential for using these isotopes in 'tuning' specific biological parameters and in identifying those model formulations which are inadequate, are substantial.

It is likely that the inclusion of a separate bacteria and picoplankton pool (0.2-1.0 µm) would have greatly improved the Doney model. In fact, <sup>32</sup>P and <sup>33</sup>P data are available within this size class (see **Chapter 4**). The increase in the number of unconstrained parameters, however, makes the addition of another biological box difficult. The biggest

problem in building ecosystem models is stability. Interactions between various chosen parameters exponentially increase with the addition of each box. Determining those parameters which have the most influence on model stability are sometimes unclear. As a result, models tend to be under- rather than over-simplified. Furthermore, model parameters formulations tend to be chosen for stability reasons rather than that which is actually observed.

Future work involves the addition of a fifth box to the Doney model which describes the bacteria and picoplankton size class. In addition an adjoint model will be built in order to determine model sensitivity. Only then can the other failings (phytoplankton/zooplankton interaction) of the Doney model be investigated.

## CONCLUSIONS

The radioisotopes,  $^{32}\text{P}$  and  $^{33}\text{P}$ , were used in both inverse and prognostic models in order to obtain information on the utilization of phosphorus in the upper ocean. Inverse model results have shown that the residence time of phosphorus within various biological pools can vary dramatically with season, ranging from < 1 day to > 100days. In March and April, no difference was found between those models which had direct removal of zooplankton and those that did not. In contrast, in July and August inclusion of a direct removal term had a substantial effect on the residence time of P. Residence times were typically less than a week with direct zooplankton removal and greater than a month when this mechanism was removed. These inverse models also demonstrated that care must be taken when compartmentalizing biota into discrete size classes, as incorrect results could be obtained by linking compartments inappropriately.

The radioisotopes  $^{32}\text{P}$  and  $^{33}\text{P}$  were used to constrain parameters within a simple prognostic model of stable phosphorus within the Gulf of Maine. Although it was not expected that this model would perfectly emulate the Gulf of Maine ecosystem, our results have helped to identify specific inadequacies of the numerical model. For example, our results suggest that within Wilkinson Basin during the spring and summer, the prognostic model does not adequately depict zooplankton grazing or the cycling of phytoplankton.

The results from the above models demonstrate the utility of  $^{32}\text{P}$  and  $^{33}\text{P}$  in various modelling investigations. A full sensitivity analysis of the prognostic model is beyond the scope of this discussion. However, such analyses should be conducted in order to pinpoint which model parameters are the most sensitive to change. Future efforts should also include the development of more sophisticated models, where bacterial pools are directly expressed and nutrients divided into separate organic and inorganic compartments. Although the development of such models is much more difficult and results in greater numbers of free parameters, this study has demonstrated that measurement of  $^{32}\text{P}$  and  $^{33}\text{P}$  can help pinpoint where weaknesses in these future models lie.

## REFERENCES

- Anderson, V. and P. Nival (1988) A pelagic ecosystem model simulating production and sedimentation of biogenic particles: role of salps and copepods. *Marine Ecology Progress Series*, **44**, 37-50.
- Azam, F. (1998) Microbial control of oceanic carbon flux: The plot thickens. *Nature*, **280**, 694-696.
- Benitez-Nelson, C. R. and K. O. Buesseler (1998a) Measurement of cosmogenic  $^{32}\text{P}$  and  $^{33}\text{P}$  activities in rainwater and seawater. *Analytical Chemistry* **70**, 64-72.
- Benitez-Nelson, C. R. and K. O. Buesseler (1998b)  $^{32}\text{P}$ ,  $^{33}\text{P}$ ,  $^7\text{Be}$ , and  $^{210}\text{Pb}$  as tracers of aerosol residence times and Stratosphere/Troposphere exchange. *Journal of Geophysical Research* submitted.
- Benitez-Nelson, C. R. and K. O. Buesseler (1998c) In situ temporal variability of inorganic and organic phosphorus cycling in the coastal ocean. *Nature*, submitted.
- Benitez-Nelson, C. R., K. O. Buesseler and G. Crossin (1998) Carbon export, eddy diffusivity and horizontal transport in the southwestern Gulf of Maine. *Continental Shelf Research*, submitted.
- Cais, P., P. P. Tan, M. Trolier, J. W. C. White and R. J. Francy (1995) A large northern hemisphere terrestrial  $\text{CO}_2$  sink indicated by  $^{13}\text{C}/^{12}\text{C}$  of atmospheric  $\text{CO}_2$ . *Science*, **269**, 1098-1102.
- Cao, C. and F. I. Woodward (1998) Dynamic responses of terrestrial ecosystem carbon cycling to global climate change. *Nature*, **393**, 249-252.
- Cho, B. C. and F. Azam (1988) Major role of bacteria in biogeochemical fluxes in the oceans interior. *Nature*, **332**, 41-443.
- Doney, S. C., D. M. Glover, and R. G. Najjar (1996) A new-coupled, one-dimensional biological-physical model for the upper ocean: Applications to the JGOFS Bermuda Atlantic Time-Series Study (BATS) site. *Deep-Sea Research II*, **43**, 591-624.
- Ducklow, H. W. (1983) Production and fate of bacteria in the oceans. *Bioscience*, **33**, 494-501.
- Dugdale, R. C. and F. P. Wilkerson (1998) Silicate regulation of new production in the equatorial Pacific upwelling. *Nature*, **391**, 270-273.
- Eppley, R. W. (1972) Temperature and phytoplankton growth in the sea. *Fishery Bulletin*, **17**, 5-24.
- Eppley, R. W. and B. J. Peterson (1979) Particulate organic matter flux and planktonic new production in the deep ocean. *Nature*, **282**, 677-680.
- Evans, G. T. and J. S. Parslow (1985) A model of annual plankton cycles. *Biological Oceanography*, **3**, 327-347.
- Fasham, M. J. R., H. W. Ducklow, and S. M. McKelvie (1990) A nitrogen-based model of plankton dynamics in the oceanic mixed layer. *Journal of Marine Research*, **48**, 591-639.

- Fasham, M. J. R., J. L. Sarmiento, R. D. Slater, H. W. Ducklow and R. Williams (1993) Ecosystem behavior at Bermuda Station "S" and Weather Station "India": A general circulation and observational analysis. *Global Biogeochemical Cycles*, **7**, 379-415.
- Fowler, S. W. and G. A. Knauer (1986). Role of large particles in the transport of elements and organic compounds through the oceanic water column. *Progress in Oceanography*, **16**, 147-194.
- Franks, P. J. S, J. S. Wroblewski and G. R. Fliel (1986) Behavior in a simple plankton model with food-level acclimation by herbivores. *Marine Biology*, **91**, 121-129.
- Frost, B. W. (1987) Grazing control of phytoplankton stock in the open subarctic Pacific Ocean: a model assessing the role of mesozooplankton, particularly the large calanoid copepods *Neocalanus* spp. *Marine Ecology Progress Series*, **39**, 49-68.
- Glover, D. M., J. S. Wroblewski and C. R. McClain (1994) Dynamics of the transition zone in coastal zone color scanner-sensed ocean color in the North Pacific during oceanographic spring. *Journal of Geophysical Research*, **99**, 7501-7511.
- Graham, W. F. and R. A. Duce (1979) Atmospheric pathways of the phosphorus cycle. *Geochimica et Cosmochimica Acta*, **43**, 1195-1208.
- Graham, W. F. and R. A. Duce (1981) Atmospheric input of phosphorus to remote tropical islands. *Pacific Science*, **35**, 241-255.
- Graham, W. F. and R. A. Duce (1982) The atmospheric transport of phosphorus to the Western North Atlantic. *Atmospheric Environment*, **16**, 1089-1092.
- Hecky, R. E. and P. Kilham (1988). Nutrient limitation of phytoplankton in freshwater and marine environments: A review of recent evidence on the effects of enrichment. *Limnology Oceanography*, **33**, 796-822.
- Houghton, J. T., B. A. Callender, and S. K. Varney (eds.) (1992) *Climate change 1992*. The supplementary report to the IPCC Scientific Assessment (Cambridge University Press).
- Hutchins, D. A. and K. W. Bruland (1998) Iron-limited diatom growth and Si:N ratios in a coastal upwelling regime. *Nature*, **393**, 561-564.
- Karl, D.M., R. Letelier, D.V. Hebel, D.F. Bird and C.D. Winn, (1992) E. J. Carpenter, D. G. Capone and J. G. Rueter (Eds.), In: *Marine Pelagic Cyanobacteria: Trichodesmium and Other Diazotrophs*, Kluwever Academic Publishers, Boston, 219-237.
- Keeling, R. F. S. C. Piper and M Heimann (1996) Global and hemispheric CO<sub>2</sub> sinks deduced from changes in atmospheric O<sub>2</sub> concentration. *Nature*, **381**, 218-221.
- Lal, D., and B. Peters (1967). Cosmic ray produced radioactivity on the Earth, K. Sitte (Eds.) In: *Handbuch der Physik 46/2*, , Springer Verlag, New York, 551-612.
- Landry, M. R., R. P. Hassett, V. Fagerness, J. Downs and C. J. Lorenzen (1984) Effect of food acclimation on assimilation efficiency of *Calanus Pacificus*. *Limnol. Oceanog.*, **29**, 361-364.

- Lohrenz, S. E., G. A. Knauer, V. L. Asper, M. Tuel, A. F. Micheals, and A. H. Knap (1992) Seasonal variability in primary production and particle flux in the northwestern Sargasso Sea: U.S. JGOFS Bermuda Atlantic Time-Series Study. *Deep-Sea Research*, **39**, 1373-1391.
- MacIsaac, J. J. and R. C. Dugdale (1969) The kinetics of nitrate and ammonia uptake by natural populations of marine phytoplankton. *Deep-Sea Res.*, **6**, 45-57.
- Marra, J., R. R. Bidigare and T. D. Dickey (1990) Nutrients and mixing, chlorophyll and phytoplankton growth. *Deep-Sea Res.*, **37**, 127-143.
- Martin, J.H., K.H. Coale, K.S. Johnson, S.E. Fitzwater, R.M. Gordon, S.J. Tanner, C.N. Hunter, V.A. Elrod, J.L. Nowicki, T.L. Coley, R.T. Barber, S. Lindley, A.J. Watson, K.V. Scoy, C.S. Law, M.I. Liddicoat, R. Ling, T. Stanton, J. Stockel, C. Collins, A. Anderson, R. Bidigare, M. Ondrusek, M. Latasa, F.J. Millero, K. Lee, W. Yao, J.Z. Zhang, G. Friederich, C. Sakamoto, F. Chavez, K. Buck, Z. Kolber, R. Greene, P. Falkowski, S.W. Chisholm, F. Hoge, R. Swift, J. Yungel, S. Turner, P. Nightingale, A. Hatton, P. Liss and N.W. Tindale (1994). Testing the Iron Hypothesis in Ecosystems of the Equatorial Pacific Ocean. *Nature*, **371**, 123-129.
- Michaels, A. F., N. R. Bates, K. O. Buesseler, C. A. Carlson and A. H. Knap (1994). Carbon-cycle imbalances in the Sargasso Sea. *Nature*, **372**, 537-540.
- Mosian, J. R. and E. E. Hoffman (1996) Modelling nutrient and plankton processes in the California coastal transition zone 1. A time- and depth-dependent model. *Journal of Geophysical Research*, **101**, 22,647-22,676.
- O'Reilly, J. E. and D. A. Busch (1984) Phytoplankton primary production on the northwestern Atlantic Shelf. *Rapp. P.-v. Reun. Cons. Int. Explor. Mer.*, **183**, 255-268.
- Pilskaln, C. H., W. Arnold, C. Lehmann and L. E. Watling (1996) Particulate flux dynamics in Jordan and Wilkinson Basins: Seasonal POC export and particle resuspension. Poster presented at the Gulf of Maine Ecosystem Dynamics: A Scientific Symposium and Workshop, St. Andrews, NB, September, 1996.
- Press, W. H., S. A. Teukolsky, W. T. Vetterling, B. P. Flannery (1992) In: *Numerical recipes in FORTRAN. The art of scientific computing, 2<sup>nd</sup> Edition*. Cambridge University Press.
- Prezelin, B. B., M. M. Tilzer, O. Schofield and C. Haese (1991) The control of the production process of phytoplankton by the physical structure of the aquatic environment with special reference to its optical properties. *Aquatic Science*, **53**, 136-186.
- Roman, M. R., H. G. Dam, A. L. Gauzens and J. M. Knapp (1993) Zooplankton biomass and grazing at the JGOFS Sargasso Sea time series station. *Deep-Sea Research*, **40**, 883-901.
- Sarmiento, J. L., R. D. Slater, M. J. R. Fasham, H. W. Ducklow, J. R. Toggweiler and G. T. Evans (1993) A seasonal three-dimensional ecosystem model of nitrogen cycling in the North Atlantic euphotic zone. *Global Biogeochemical Cycles*, **7**, 379-415.



- Six, K. D. and E. Maier-Reimer (1996) Effects of plankton dynamics on seasonal carbon fluxes in an ocean general circulation model. *Global Biogeochemical Cycles*, **10**, 559-583.
- Takeda, S. (1998) Influence of diatom availability on nutrient consumption ratio of diatoms in oceanic waters. *Nature*, **393**, 774-777.
- Townsend, D. W. and R. W. Spinrad (1986) Early spring phytoplankton blooms in the Gulf of Maine. *Continental Shelf Research*, **6**, 515-529.
- Waser, N. A. D., and M. P. Bacon (1995) Wet deposition fluxes of cosmogenic  $^{32}\text{P}$  and  $^{33}\text{P}$  and variations in the  $^{33}\text{P}/^{32}\text{P}$  ratios at Bermuda. *Earth and Planetary Science Letters*, **133**, 71-80.
- Waser, N. A. D., M. P. Bacon, M. P. and A. P. Michaels (1996) Natural activities of  $^{32}\text{P}$  and  $^{33}\text{P}$  and the  $^{33}\text{P}/^{32}\text{P}$  ratio in suspended particulate matter and plankton in the Sargasso Sea. *Deep-Sea Research*, **43(2-3)**, 421-436.
- Walsh, J. J., T. E. Whitledge, J. E. O'Reilly, W. C. Phoel and A. E. Draxler (1987) R. H. Backus (Ed.) In: *Georges Bank*. MIT Press, Cambridge, 234-246.
- Wroblewski, J. S. (1989) A model of the spring bloom in the North Atlantic and its impact on ocean optics. *Limnology and Oceanography*, **34**, 1563-1571.
- Wroblewski, J. S., J. L. Sarmiento and G. R. Flierl (1988) An ocean basin scale model of plankton dynamics in the North Atlantic 1. Solutions for the climatological oceanographic conditions in May. *Glob. Biogeochem. Cycles*, **2**, 199-218.

## Appendix I

Following are the model equations used in the first two inverse models, where the only difference between the first and the second inversion is that  $k_7 = 0$  (see Fig. 1).

N = 'Nutrient' activity

P = 'Phytoplankton' activity

Z (or PII) = 'Zooplankton' activity

D = 'Detritus' activity

$\lambda = {}^{32}\text{P}$  or  ${}^{33}\text{P}$  decay constant.

$$dN/dt = -k_1N + k_5D - \lambda N$$

$$dP/dt = +k_1N - (k_2 + k_3)P - \lambda P$$

$$dZ/dt = +k_2N - (k_4 + k_7)Z - \lambda Z$$

$$dD/dt = +k_3P + k_4Z - (k_5 + k_6)D - \lambda D$$

The third and fourth inverse models are described by the following, where the only difference between the third and fourth inversions is that  $k_7 = 0$  (see Fig. 1).

$$dN/dt = -(k_1 + k_2)N + k_5D - \lambda N$$

$$dP/dt = +k_1N - (k_2 + k_3)P - \lambda P$$

$$d\text{PII}/dt = +k_2N - (k_4 + k_7)\text{PII} - \lambda\text{PII}$$

$$dD/dt = +k_3P + K_4\text{PII} - (k_5 + k_6)D - \lambda D$$

## Appendix II

The following describes the equations used in the Doney model.

### *Mixed Layer Depth Oscillation*

$$\text{MLD} = 50$$

$$h = \text{MLD} \sin((2\pi t)/365 + (40\pi/365)) + (\text{MLD} + 10);$$

where the MLD is the midpoint of the range of mixed layer depths observed in the data.

### *Light Parameterization*

$$f_h = -((1 - \exp(-k h))/(-0.6321 k h))$$

### *Differential Equations*

$$dN/dt = -\mu_p N P f_h / (N + K_n) + \epsilon_1 Z + \epsilon_2 Z^2 + \delta D + \eta P$$

$$dP/dt = \mu_p N P f_h / (N + K_n) - \mu_z \Lambda P Z (1 - \exp^{-\Lambda P}) - \eta P - w P^2$$

$$dZ/dt = (1 - \gamma) \mu_z \Lambda P Z (1 - \exp^{-\Lambda P}) - \epsilon_1 Z - \epsilon_2 Z^2$$

$$dD/dt = \gamma \mu_z \Lambda P Z (1 - \exp^{-\Lambda P}) + w P^2 - \delta D$$

where: N = 'Nutrient' activity, P = 'Phytoplankton' activity, Z = 'Zooplankton' activity  
and D = 'Detritus' activity

Adjusting the equations for  $^{32}\text{P}$  and  $^{33}\text{P}$  involves the addition of an input term, I, to the nutrient equation. The I term is described by the following equation:

$$I = \text{Rain input} / h$$

**Appendix II cont.**

An additional decay term is also subtracted from each equation such that:

$$dN/dt = I \dots - \lambda N$$

$$dP/dt = \dots - \lambda P$$

$$dZ/dt = \dots - \lambda Z$$

$$dD/dt = \dots - \lambda D$$

where  $\lambda$  is the radioactive decay constant for  $^{32}\text{P} = 0.04853 \text{ d}^{-1}$  or  $^{33}\text{P} = 0.02739 \text{ d}^{-1}$

Parameters with units of mmol (or atoms) of stable P also needed to be converted to atoms of  $^{32}\text{P}$  and  $^{33}\text{P}$ . The conversion factor as determined from using the average ratio of stable P (in atoms) to  $^{32}\text{P}$  (or  $^{33}\text{P}$ , in atoms) for each compartment.

	<b>Avg. stable P/<math>^{32}\text{P}</math> (atom/atom)</b>	<b>Avg. stable P/<math>^{33}\text{P}</math> (atom/atom)</b>
Nutrients	$2.3 \times 10^{15}$	$2.2 \times 10^{15}$
Phytoplankton	$6.2 \times 10^{14}$	$4.3 \times 10^{14}$
Zooplankton	$2.2 \times 10^{15}$	$2.6 \times 10^{15}$

## Chapter 7

### SUMMARY

Some of the most important questions facing oceanographers today focus on the mechanisms by which nutrients are utilized within the upper ocean. Such knowledge has important implications for understanding not only carbon export, but also the removal of anthropogenically produced compounds like lead and chlorine containing hydrocarbons (PCB's) (Larsen *et al.*, 1985; Barrick and Prahl, 1987; Kennicutt, 1994, Gustaffson *et al.*, 1998). Many of the techniques available to prior researchers in this area, however, have proven unsatisfactory. Thus, new avenues have been pursued for the elucidation of the biogeochemical cycling of nutrients.

This thesis work has successfully utilized the cosmogenically produced radioisotopes, phosphorus-32 ( $t_{1/2} = 14.3$  days) and phosphorus-33 ( $t_{1/2} = 25.3$  days), to understand the biogeochemical cycling of phosphorus within Wilkinson Basin in the Gulf of Maine. Previous research has shown that radioisotopes can provide unique insight into many oceanic and atmospheric processes because they integrate over their mean life ( $\Lambda = 1/\lambda$ ). Phosphorus isotopes are especially powerful in oceanic studies in that: 1) there are two radioisotopes of phosphorus with mean lives ( $^{32}\text{P} = 20.6$  days,  $^{33}\text{P} = 36.5$  days) similar to many phytoplankton and zooplankton life cycles, and 2) phosphorus is an essential

macro-nutrient required for growth by primary producers. Briefly, if the input flux of  $^{33}\text{P}$  and  $^{32}\text{P}$  is known then the ratio of  $^{33}\text{P}/^{32}\text{P}$  can be used to determine the 'age' of phosphorus within a particular reservoir. In other words, the  $^{33}\text{P}/^{32}\text{P}$  ratio will increase with time.

Unfortunately,  $^{32}\text{P}$  and  $^{33}\text{P}$  activities are very low, ranging from a few disintegrations per minute (d.p.m.)  $\text{L}^{-1}$  in rain water to less than a d.p.m  $\text{m}^{-3}$  in seawater. Thus, measurement requires the collection of large amounts of rainwater and over several thousand liters of seawater. Not surprisingly, there have been difficulties associated with the collection and measurement of radioactive phosphorus in the past (Lal and Lee, 1988; Lal *et al.*, 1988; Lee *et al.*, 1991; 1992; Waser *et al.*, 1994; 1995). As a result, in this thesis, different collection and measurement techniques were explored.

In **Chapter 2**, new methods for the collection, purification, and measurement of  $^{32}\text{P}$  and  $^{33}\text{P}$  in rain and seawater were developed. The major difference between this and prior investigations was the use of a newly developed ultra low level liquid scintillation counter: Packard Tri-Carb 2770 TR/SL LSS. This instrument enabled the simultaneous measurement of both  $^{32}\text{P}$  and  $^{33}\text{P}$  with high efficiency (> 50%). Previous researchers were limited to use of anti-coincidence low level beta counting, a counting technique that measured  $^{33}\text{P}$  with an efficiency of often less than 10% (Waser, 1993; Waser *et al.*, 1994). In addition, a new material was used for the extraction of  $^{32}\text{P}$  and  $^{33}\text{P}$  from large volumes of rain and seawater. Iron oxide was impregnated onto polypropylene sheets rather than acrilan fibers. This allowed for: 1) more uniform iron oxide impregnation, 2) higher flow rates and 3) increased ease in purification. Modifications of past radiophosphorus purification methods (Lee *et al.*, 1992; Waser *et al.*, 1994) were also made in order to fully remove previously unidentified contaminants,  $^{210}\text{Pb}$  and  $^{210}\text{Bi}$ . It is not clear how these isotopes may have affected previous  $^{32}\text{P}$  and  $^{33}\text{P}$  measurements.

In order to use  $^{32}\text{P}$  and  $^{33}\text{P}$  in marine studies it was necessary to first constrain their input into the oceans. In previous studies, it had been hypothesized that although the absolute activity of  $^{32}\text{P}$  and  $^{33}\text{P}$  in rain may differ spatially, the ratio of  $^{33}\text{P}/^{32}\text{P}$  would not (Lal *et al.*, 1988; Lee *et al.*, 1991). However, there was few data to support this theory. Furthermore, most of the measurements that had been made were conducted at low

latitudes, and it was not clear, given the cosmogenic production mechanism of  $^{32}\text{P}$  and  $^{33}\text{P}$ , that the constant  $^{33}\text{P}/^{32}\text{P}$  ratio assumption would hold for the higher latitudes.

In **Chapter 3**, results from a two year study of  $^{32}\text{P}$ ,  $^{33}\text{P}$ ,  $^7\text{Be}$ , and  $^{210}\text{Pb}$  in rainwater are presented. Radionuclide activities were determined in individual rain events at Woods Hole, MA and in two week integrated rain samples from Portsmouth, NH. Although the absolute flux of  $^{32}\text{P}$  and  $^{33}\text{P}$  differed between the two sites, the average  $^{33}\text{P}/^{32}\text{P}$  ratio ( $0.88 \pm 0.14$ ) did not.

In addition to constraining the input flux, rain measurements of  $^{32}\text{P}$ ,  $^{33}\text{P}$ ,  $^7\text{Be}$ , and  $^{210}\text{Pb}$  were also used to investigate such atmospheric processes as aerosol residence times and troposphere stratosphere exchange. Results suggest that simple models of cosmogenic production and removal from within a single airmass were insufficient. In addition, it was demonstrated that fractionation occurs among phosphorus, beryllium and lead between production and atmospheric removal via precipitation. This indicates that chemistry, and not just physics, has a significant influence on atmospheric removal. Finally, the appearance of high  $^{33}\text{P}/^{32}\text{P}$  ratios during severe storm events suggests that these isotopes can trace stratosphere/troposphere exchange processes at ground level. Elucidation of such atmospheric mixing can provide much needed insight into the atmospheric cycling of many naturally and anthropogenically produced trace elements.

Four cruises were conducted in Wilkinson Basin in the southwest Gulf of Maine during the spring and summer of 1997. Results are discussed in **Chapters 4 and 5**. In **Chapter 4**, the in situ temporal variability in upper ocean nutrient cycling and particulate export was examined using  $^{32}\text{P}$  and  $^{33}\text{P}$ . These isotopes were simultaneously measured in dissolved inorganic (DIP), dissolved organic (DOP) and in small and large particulate pools. Phosphorus residence times varied between the spring and summer and ranged from less than one day to as long as 60 days. The separation of DIP and DOP further enabled the observation that these two pools have significantly different residence times. In the August cruise, a large increase was observed within the bacterial and picoplankton size class suggesting that these organisms were important in the uptake of *both* DIP and DOP. In addition, carbon export rates derived from  $^{32}\text{P}$  and  $^{33}\text{P}$  were found to match, within error, those rates determined by  $^{234}\text{Th}$ . This lends further credence to the  $^{234}\text{Th}$

approach in measuring carbon export, given that phosphorus, as an essential nutrient, is directly related to biological particle formation. The results of this thesis demonstrate the unique ability of  $^{32}\text{P}$  and  $^{33}\text{P}$  to increase current understanding of the *in situ* biogeochemical cycling of nutrients within the upper ocean.

During the April, March, July and August cruises dissolved and particulate surface samples were collected for  $^{234}\text{Th}$  and  $^7\text{Be}$  throughout the southwestern Gulf of Maine. One deep profile was also measured within Wilkinson Basin. In **Chapter 5**, these isotopes were used to determine the magnitude of particulate organic carbon export and the rate of vertical eddy diffusivity. Steady state, non-steady state, and horizontal advection/diffusion models were tested and compared. It was found that within coastal environments, the inclusion of both non-steady state and horizontal advection/diffusion processes was essential for the accurate determination of  $^{234}\text{Th}$  derived particulate organic carbon export. Our measurements indicate that the average organic carbon export ratio (particulate export/primary production) ranged from 0.11 to 0.37, a range typical of many coastal regimes. Estimates of  $^7\text{Be}$  derived vertical eddy diffusivity in July and August further demonstrated that this mechanism was sufficient to support the amount of 'new' nitrogen necessary for the observed particulate organic carbon export.

The last **Chapter 6** discusses the use of  $^{32}\text{P}$  and  $^{33}\text{P}$  in numerical modelling efforts. Several inverse and one prognostic model were explored. Substantial differences among the inverse model formulations demonstrated the importance of linkages among defined boxes in the determination of phosphorus residence times. In the prognostic model,  $^{32}\text{P}$  and  $^{33}\text{P}$  were used in order to identify weaknesses in the model formulation. Our results suggest that in the future,  $^{32}\text{P}$  and  $^{33}\text{P}$  could be used to 'tune' biological parameters within prognostic models.



## Suggestions for Future Work

As in all scientific studies, there are a number of questions which arise during the course of the investigation. This thesis work is no different and the results of the previous chapters have opened a number of avenues for future atmospheric and oceanic research. Although  $^{32}\text{P}$  and  $^{33}\text{P}$  have been measured in atmospheric studies since the late 1950's (Lal, 1959), their combined use in determining upper atmosphere mixing processes has only been recently discovered. One of the difficulties, however, in using these isotopes for such investigations is the limited number of atmospheric  $^{32}\text{P}$  and  $^{33}\text{P}$  measurements which have been made.

There are several questions which must be answered for the future use of these isotopes to help understand upper atmospheric mixing. One essential question is what is the cosmogenic production rate of  $^{32}\text{P}$  and  $^{33}\text{P}$ ? Estimates of the  $^{33}\text{P}/^{32}\text{P}$  production ratio have a wide range (Lal and Peters, 1967; Waser *et al.*, 1995). Thus, direct measurements of stratospheric  $^{32}\text{P}$  and  $^{33}\text{P}$  production from Argon nuclei need to be conducted. A second primary question is what is the distribution of  $^{33}\text{P}$  and  $^{32}\text{P}$  in the upper atmosphere. Are  $^{33}\text{P}/^{32}\text{P}$  ratios higher within the lower stratosphere than in the upper troposphere? Answering these queries will enable the use of  $^{33}\text{P}$  and  $^{32}\text{P}$  to investigate the magnitude and timing of stratosphere troposphere exchange. In addition, the atmospheric  $^{33}\text{P}/^{32}\text{P}$  ratio measurements will provide further insight into the processes which control horizontal lower stratospheric mixing.

From the measurement of  $^{32}\text{P}$ ,  $^{33}\text{P}$ ,  $^7\text{Be}$ , and  $^{210}\text{Pb}$  in rain, it has been found that aerosol scavenging of radionuclides is related in part to chemical reactivity. Little is currently known about radionuclide aerosol scavenging, and it is often assumed that it is an instantaneous, *physical* process. Measurement of these isotopes on different aerosol size classes, in addition to laboratory studies, may provide insight into how such scavenging processes occur. Such information would be very valuable in increasing the understanding of the atmospheric cycling of many naturally and anthropogenically produced compounds.

In general, the development of new extraction, purification and measurement techniques will greatly enhance the future application of  $^{32}\text{P}$  and  $^{33}\text{P}$  to study upper ocean phosphorus dynamics. There are two types of aquatic regimes where radioactive phosphorus measurements should be conducted in the immediate future: in freshwater lakes and in oceanic environments where phosphorus may limit primary production.

Lake studies would be ideal environments for the study of  $^{32}\text{P}$  and  $^{33}\text{P}$ . It is highly likely that radioactive phosphorus activities would be substantially higher in these environments, given the lower dilution of rain input. Higher activities coupled with better extraction efficiencies (due to lower anion concentrations) would enable much better precision in the study of nutrient and plankton interactions. In addition, phosphorus is often the limiting nutrient within lakes. So changes in dissolved inorganic and organic phosphorus residence times would be directly related to primary production rates.

In the open ocean, the potential for  $^{32}\text{P}$  and  $^{33}\text{P}$  studies is enormous, especially in areas such as the Sargasso Sea and the North Pacific gyre where phosphorus may limit primary production during certain times of the year (Lohrenz *et al.*, 1994; Karl *et al.*, 1997). Studies in the North Pacific would be of particularly high value given the recent observation that this area may be transitioning from a nitrogen based ecosystem to that of a phosphorus based ecosystem. This hypothesis is based on the increasing abundance of nitrogen fixing cyanobacteria, *Trichodesmium* (Karl *et al.*, 1995;1997). It has also been theorized that these organisms are themselves phosphorus limited and migrate to the surface ocean from depths of as much as 150m (Karl and Tien, 1997). Measurement of  $^{32}\text{P}$  and  $^{33}\text{P}$  within *Trichodesmium* as well as within other biological pools, such as DOP, will not only actively elucidate nutrient sources and mechanisms promoting *Trichodesmium* growth, but also how the biogeochemical cycling of phosphorus is changing with time.

Studies like the one outlined above can greatly increase current knowledge of phosphorus cycling and its effects on the environment. One of the newest applications of  $^{32}\text{P}$  and  $^{33}\text{P}$  is in numerical ecosystem modelling. Current development of advanced plankton dynamic models is hindered by a lack of known nutrient uptake and regeneration rates. It has been shown that radioactive phosphorus can be used to help tune even simple

models. Their use in more complex modelling efforts has yet to be determined. In reality, the use of  $^{32}\text{P}$  to  $^{33}\text{P}$  to understand both atmospheric and marine processes has only just begun.

## REFERENCES

- Barrick, R. C and F. G. Prahl (1987). Hydrocarbon geochemistry of the Puget Sound Region-III. Polycyclic aromatic hydrocarbons in sediments. *Estuarine Coastal and Shelf Science*, **25**, 175-191.
- Gustafsson, Ö., P.M. Gschwend, and K. O. Buesseler (1998). Using  $^{234}\text{Th}$  disequilibria to estimate the vertical removal rates of polycyclic aromatic hydrocarbons from the surface ocean. *Marine Chemistry*, accepted.
- Karl, D. M., Letelier, R., Hebel, D., Tupas, L., Dore, J., Christian, J., Winn, C. (1995). Ecosystem changes in the North Pacific subtropical gyre attributed to the 1991-1992 El Nino. *Nature*, **373**, 230-234.
- Karl, D. M. and Tien, G. (1997a) Temporal variability in dissolved phosphorus concentrations at station ALOHA (22 45'N, 158W). *Marine Chemistry*, **56**, 77-97.
- Karl, D. M., Letelier, R., Tupas, L., Christian, J., Hebel, D. (1997b) The role of nitrogen fixation in biogeochemical cycling in the subtropical North Pacific ocean. *Nature*, **388**, 533-538.
- Kennicutt II, M. C., T. R. Wade, B. J. Presley, A. G. Requejo, J. M. Brooks and G. J. Denoux, (1994) Sediment contaminants in Casco Bay, Maine: Inventories, sources, and potential for biological impact. *Environmental Science Technology*, **28**, 1-15.
- Lal, D., and B. Peters (1967). Cosmic ray produced radioactivity in the Earth. In: *Handbuch der Physik* 46/2, S. Flugge, ed., Springer-Verlag, Berlin, pp. 551-612.
- Lal, D. and T. Lee, 1988. Cosmogenic  $^{33}\text{P}$  and  $^{32}\text{P}$  Used as Tracers to Study Phosphorus Recycling in the Upper Ocean. *Nature*, **333**, 752-754.
- Lal, D., Y. Chung, T. Platt and T. Lee, 1988. Twin Cosmogenic Radiotracer Studies of Phosphorus Recycling and Chemical Fluxes in the Upper Ocean. *Limnology and Oceanography*, **33(6, part 2)**, 1559-1567.
- Larsen, P.F., D. F. Gadbois and A.C. Johnson (1985). Observations on the distribution of PCBs in the deepwater sediments of the Gulf of Maine. *Marine Pollution Bulletin*, **16**, 439-442.
- Lee, T., E. Barg, and D. Lal (1991). Studies of vertical mixing in the Southern California Bight with cosmogenic radionuclides  $^{32}\text{P}$  and  $^7\text{Be}$ . *Limnology Oceanography*, **36(5)**, 1044-1053.
- Lee, T., E. Barg, and D. Lal (1992). Techniques for extraction of dissolved inorganic and organic phosphorus from large volumes of sea water. *Analytica Chimica Acta*, **260**, 113-121.
- Lohrenz, S. E., G. A. Knauer, V. L. Asper, M. Tuel, A. F. Micheals, and A. H. Knap (1992) Seasonal variability in primary production and particle flux in the northwestern Sargasso Sea: U.S. JGOFS Bermuda Atlantic Time-Series Study. *Deep-Sea Research*, **39**, 1373-1391.
- Waser, N. A. D (1993). Cosmogenic  $^{32}\text{P}$  and  $^{33}\text{P}$  in the atmosphere and oligotrophic ocean and applications to the study of phosphorus cycling, Ph.D. Thesis, MIT/WHOI, Woods Hole, MA, 153 pp.

- Waser, N. A. D., A. P. Fleer, T. R. Hammer, K. O. Buesseler and M. P. Bacon (1994). Determination of natural  $^{32}\text{P}$  and  $^{33}\text{P}$  in rainwater, marine particles and plankton by low-level beta counting. *Nucl. Instr. and Meth. in Phys.*, **A388**, 560-567.
- Waser, N.A.D., M. P. Bacon and A. F. Michaels (1995). Natural Activities of  $^{32}\text{P}$  and  $^{33}\text{P}$  and the  $^{33}\text{P}/^{32}\text{P}$  Ratio in Suspended Particulate Matter and Plankton in the Sargasso Sea. *Deep-Sea Research II*, **43**, 421-436.

## Biographical Note

Claudia Benitez-Nelson was born on Mother's Day on May 14, 1972, in Waterbury, Connecticut. After living in New York City for seven years, the family moved to Seattle, Washington. She attended the University of Washington from 1987 to 1992 and graduated with a double degree in Chemistry and Oceanography. After spending the following year traveling in Europe, she returned to enter the MIT/WHOI Joint Program in Oceanography where she was an Office of Naval Research (1993-1996) and Environmental Protection Agency Fellow (1996-1998).

## Publications

- Buesseler, K. O. and C. R. Benitez (1994) Determination of mass accumulation rates and sediment inventories in the deep Black Sea. *Deep-Sea Res.*, **41**, 1605-1615.
- Benitez-Nelson, C. R. and K. O. Buesseler (1998) Measurement of cosmogenic  $^{32}\text{P}$  and  $^{33}\text{P}$  activities in rainwater and seawater. *Analytical Chemistry* **70**, 64-72.
- Benitez-Nelson, C. R. and K. O. Buesseler (1998)  $^{32}\text{P}$ ,  $^{33}\text{P}$ ,  $^7\text{Be}$ , and  $^{210}\text{Pb}$  as tracers of aerosol residence times and Stratosphere/Troposphere exchange. *Journal of Geophysical Research* submitted.
- Buesseler, K. O., Ball, L., Andrews, J.; Benitez-Nelson, C.; Belostock, R., Chai, F., and Chao, Y. Upper ocean export of particulate organic carbon in the Arabian Sea derived from Thorium-234. *Deep-Sea Research II, Special Arabian Sea Issue*, accepted.
- Benitez-Nelson, C. R. and K. O. Buesseler (1998) In situ temporal variability of inorganic and organic phosphorus cycling in the coastal ocean. *Nature*, submitted.
- Benitez-Nelson, C. R., K. O. Buesseler and G. Crossin (1998) Carbon export, eddy diffusivity and horizontal transport in the southwestern Gulf of Maine. *Continental Shelf Research*, submitted.